High resolution non-hydrostatic numerical simulations for wind energy assessment over Libya.

Author:
Alhawari, Ibrahim S. M.

Publication Date:
2009

DOI:
https://doi.org/10.26190/unsworks/22865

High Resolution Non-hydrostatic Numerical Simulations for Wind Energy Assessment over Libya.

A thesis submitted in fulfilment of the requirements for the degree of

(Master of Science)

By

IBRAHIM S. M. ALHAWARI

School of Mathematics and Statistics

Faculty of Science

University of New South Wales

Sydney, Australia

August 2009

THE UNIVERSITY OF NEW SOUTH WALES

Thesis/Dissertation Sheet

Surname or Family name: ALHAWARI

First name: IBRAHIM S. M. Other name/s:

Abbreviation for degree as given in the University calendar: MSc
School: Mathematics and Statistics
Faculty: Science

Title: High Resolution Non-hydrostatic Numerical Simulations for Wind Energy Assessment over Libya.

Abstract 350 words maximum

This research is aimed at understanding the national wind energy resource of Libya to examine the viability of obtaining wind-generated electricity in the country. High-resolution regional wind observations in Libya are not sufficient for wind resource assessments throughout the country. To overcome such a barrier, the wind conditions have been estimated utilising high-resolution 3-D nested numerical simulations by the Non-hydrostatic Mesoscale Model of the Weather Research and Forecasting system (WRF-NMM). Analysis 2007 data from the Global Forecast System (GFS) were used as initial conditions whereas the boundary conditions came from a combination of GFS analysis and forecast data, in all runs.

The coarse domain had a horizontal resolution of 15 km and a temporal resolution of 30 seconds while the fine domain had a horizontal resolution of 5 km and a temporal resolution of 10 seconds. 365 successive nested simulations were performed to produce hourly wind velocity data at 10 m above the ground along with at model sigma levels for both domains for the entire year. A cubic spline interpolation was used to interpolate wind velocity data between sigma levels and 10-m winds. Thus, wind velocity data at each grid point at six fixed heights (25, 50, 75, 100, 125, and 150 m above the ground) were obtained. Hourly power density data were computed at the seven mentioned heights. Wind power outputs were also estimated based on the power curves of commercial wind turbines of different sizes and designs.

Results have shown that Libya has a very good potential for wind power generation. Several areas have been identified to be promising for future wind farms. The eastern and western coastlines, the northwestern high-altitude regions, and the mountainous areas in the Sahara Desert, have great potentials of using wind-generated electricity. Summer experiences the highest wind power resource over most parts of Libya. Over most areas, vertical wind shear peaks in the atmospheric layer of 75-100m. The use of the standard value of wind shear exponent would underestimate the vertical wind speed and power changes on most parts of the nation, while it would overestimate them in a few areas.

Originality Statement

'I hereby declare that this submission is my own work and to the best of my knowledge it contains no materials previously published or written by another person, or substantial proportions of material which have been accepted for the award of any other degree or diploma at UNSW or any other educational institution, except where due acknowledgement is made in the thesis. Any contribution made to the research by others, with whom I have worked at UNSW or elsewhere, is explicitly acknowledged in the thesis. I also declare that the intellectual content of this thesis is the product of my own work, except to the extent that assistance from others in the project's design and conception or in style, presentation, and linguistic expression is acknowledged.'

Ibrahim S. M. Alhawari

Copyright Statement

Authenticity Statement

‘I certify that the Library deposit digital copy is a direct equivalent of the final officially approved version of my thesis. No emendation of content has occurred and if there are any minor variations in formatting, they are the result of the conversion to digital format.’

Ibrahim S. M. Alhawari

Dedication

To my parents who have supported me throughout my life, and who have given me a continual encouragement.

Acknowledgment

Firstly, a great gratitude goes to Mr Russel Morison without whom this dissertation would not have been possible. Many thanks go to him for his continual support, guidance, and dedication of much of his time throughout the research period.

I am deeply indebted to Mr Morison for his help in supervising me especially in the initial stages of my project, his advice, assistance with numerical weather prediction models, and with the provision of extra storage space for the huge data used in this project.

I consider myself lucky to undertake my research at the UNSW School of Mathematics and Statistics, which was ranked the world number 14 on the quality index. My gratitude goes towards this school for providing computing facilities that were required to perform extensive numerical model runs.

I would like to express gratitude to my family and friends for their ongoing emotional supports, which have allowed me to complete this project in an organised and above all enjoyable manner. I would also like to thank people who assisted me in facilitating my research at any stage even with one word.

Finally, I am deeply appreciative to the Libyan Government for the financial support throughout my study.

Ibrahim S. M. Alhawari

Contents

List of Tables

List of Figures

Table of Acronyms and Units

Acronyms/Units	Definition
A.D.	Anno Domini
AFWA	Department of Defence's Air Force Weather Agency
ARW	Advanced Research WRF model
AusAID	Australian Government's Overseas Aid Program
AWEA	American Wind Energy Association
B.C.	Before Christ
BMJ	Betts-Miller-Janjic convective scheme
BWEA	British Wind Energy Association
CAPS	Centre for Analysis and Prediction of Storms
CFD	Computational Fluid Dynamics
CO2	Carbon Dioxide
CSES	Centre for Solar Energy Studies
CPU	Central Processing Unit
DOE	USA Department Of Energy
DWIA	Danish Wind Industry Association
ECMWF	European Centre for Medium-range Weather Forecasting model
ECMWF	European Centre for Medium-range Weather Forecasts
EIA	Energy Information Administration
ESRL	Earth System Research Laboratory
FAA	Federal Aviation Administration
G1	Grid point 1
G2	Grid point 2
G3	Grid point 3
G4	Grid point 4

G5	Grid point 5
G6	Grid point 6
GASP	Global AnalysiS Prediction model
GB	Gigabyte
GECOL	General Electric Company Of Libya
GFS	Global Forecast System
GHG	Green House Gas
GSM	Global Spectral Model
GRIB	Gridded Binary
GWhr	Gigawatt-hours
HIRLAM	High Resolution Limited Area Model
hPa	Hectopascal
INL	Idaho National Laboratory
ITCZ	Inter-Tropical Convergence Zone
JMA	Japan Meteorological Agency
kg/m^3	Kilogram per cubic metre
km	Kilometre
km^2	Square Kilometre
kW	Kilowatt
kWhr	Kilowatt-hours
m	Metre
m/s	Metre per second
MMM	Mesoscale and Microscale Meteorology
MM5	PSU/NCAR Fifth-generation Mesoscale Model
mph	Mile per hour
MW	Megawatt
MWhr	Megawatt-hours
MYJ	Mellor-Yamada-Janjic PBL scheme
NCAR	National Centre for Atmospheric Research
NCEP	National Centres for Environmental Prediction
NOAA	National Oceanic and Atmospheric Administration

Noah-LSM	Noah Land Surface Model
NRL	Naval Research Laboratory
NWS	National Weather Service
NWP	Numerical Weather Prediction
OU	University of Oklahoma
PBL	Planetary Boundary Layer
PGI	Fortran, C and C++ compilers for High Performance Computing Systems from Portland Group
PSU	Pennsylvania State University
PWhr	Petawatt-hours
RAM	Random Access Memory
RRTM	Rapid Radiative Transfer Model scheme
TB	Terabyte
TW	Terawatt
TKE	Turbulent Kinetic Energy
UNSW	University of New South Wales
USA	United States of America
UTC	Coordinated Universal Time
W	Watt
W/m^2	Watt per square metre
WPS	WRF Pre-processing System
WPP	WRF Post-processor
WRF	Weather Research and Forecasting system
WRF-NMM	WRF Non-hydrostatic Mesoscale Mod
WWEA	World Wind Energy Association
3-D	Three-Dimensional

Abstract

This research is aimed at understanding the national wind energy resource of Libya to examine the viability of obtaining wind-generated electricity in the country. High-resolution regional wind observations in Libya are not sufficient for wind resource assessments throughout the country. To overcome such a barrier, the wind conditions have been estimated utilising high-resolution 3-D nested numerical simulations by the Non-hydrostatic Mesoscale Model of the Weather Research and Forecasting system (WRF-NMM). Analysis 2007 data from the Global Forecast System (GFS) were used as initial conditions whereas the boundary conditions came from a combination of GFS analysis and forecast data, in all runs.

The coarse domain had a horizontal resolution of 15 km and a temporal resolution of 30 seconds while the fine domain had a horizontal resolution of 5 km and a temporal resolution of 10 seconds. 365 successive nested simulations were performed to produce hourly wind velocity data at 10 m above the ground along with at model sigma levels for both domains for the entire year. A cubic spline interpolation was used to interpolate wind velocity data between sigma levels and 10-m winds. Thus, wind velocity data at each grid point at six fixed heights (25, 50, 75, 100, 125, and 150 m above the ground) were obtained. Hourly power density data were computed at the seven mentioned heights. Wind power outputs were also estimated based on the power curves of commercial wind turbines of different sizes and designs.

Results have shown that Libya has a very good potential for wind power generation. Several areas have been identified to be promising for future wind farms. The eastern and western coastlines, the northwestern high-altitude regions, and the mountainous areas in the Sahara Desert, have great potentials of using wind-generated electricity. Summer experiences the highest wind power resource over most parts of Libya. Over most areas, vertical wind shear peaks in the atmospheric layer of 75-100m. The use of the standard value of wind shear exponent would underestimate the vertical wind speed and power changes on most parts of the nation, while it would overestimate them in a few areas.

Chapter 1

Introduction

1.1 Background and Motivation

Libya is the region of interest in this dissertation. Libya is situated in the subtropics in the northern part of the Sahara Desert (the world's largest hot desert) in the middle of North Africa between Egypt and Tunisia on the southern coast of the Mediterranean Sea [Figure 1.1]. It stretches along about 1770 km of the coastline. The Mediterranean country extends from about 19° to 33° North latitude and from 9° to 25° East longitude. It occupies nearly 1,759,540 km^2 of area, more than 90% of which is either desert or semi-desert. The terrain is mostly arid, flat to rolling plains, and plateaus. Libya has a population of about 6 million, more than two-thirds of which live on the coast.

Over the past few years, there has been a sharp expansion in the electricity consumption in Libya. Statistics from the Energy Information Administration have indicated that the electricity consumption in Libya jumped from 13.2 million megawatt-hours (MWhr) in 2004 up to 20.7 million MWhr in 2006 (EIA, 2009b). This is an increase in the electricity demand of more than 55% within only two years. This substantial growth is attributed to the development of the economy, socioeconomic growth,

moderate expansion of the population, and life style improvement.

This improvement is a good sign for the country, but it would be more beneficial for its economy if part of the consumed electricity came from other renewable sources. Unfortunately, the production of electricity in Libya relies totally on fossil fuel reserves. Approximately 70% of the electricity consumption is satisfied by oil burning, and 30% is met by natural gas (EIA, 2009a). This means that without fossil fuels the economy of the country would substantially suffer as it depends heavily on oil and gas resources. The heavy dependency of Libya on fossil fuels for electricity generation does not secure its energy sector, and in turn disadvantages its economic development.

Serious problems caused by burning fossil fuels are the degradation of the environment, climate change, and global warming. Burning fossil fuels contribute to a large amount of green house gas (GHG) emissions, which lead to climate change. The total carbon dioxide (CO2) emitted due to the consumption of conventional electricity in Libya grew from 41.9 million metric tonnes in 2000 to 53.5 million metric tonnes in 2006 (EIA, 2009b).

Libya has signed and ratified the Kyoto Protocol, an international agreement aimed at stabilising GHGs emitted to the atmosphere. This worldwide treaty obliges every participating country, including Libya, to set some schemes to reduce its GHG emissions. One of the main policies is to reduce the country's reliance on conventional resources for electricity production and to diversify energy production by integrating renewable energy sources into the electricity grids. This can decrease the amount of fossil fuels being burned for power generation, and hence lessen GHG emissions.

It has become more and more evident that GHG emissions bring about global warming and rising sea levels. A Spanish-British project to estimate the effect of climate change on the Mediterranean Sea has found that most positive scenario demonstrates a sea temperature rise of 1 °C by the end of

21st century, while two negative scenarios show an increase of 2.5 °C, and the temperature rise will accelerate during this century (Marcos and Tsimplis, 2008). Marcos and Tsimplis have also stated that "the level of the whole Mediterranean will rise by between 3 cm and 61 cm* on average as a result of the effects of warming". Libya would be one of the most disadvantaged nations by rising sea level, because the bulk of its population inhabit along the Mediterranean coast. Indeed, this is a serious concern about the future climate of the country.

While the prices of oil and natural gas have been fluctuating, the long-term trend has seen a considerable rise. Rising fossil fuel prices are ultimately followed by an increase in the electricity generation costs. Libya is an oil-producing country. The availability of fossil fuel reserves may discourage the decision makers to seek alternative green power sources. Libya is a lucky nation to have good oil and natural gas reserves, but the question posed here is "which is more beneficial for the economy selling the oil or burning it to generate electricity?". It is obvious that exporting part of the fossil fuels that are being burned to generate electricity and replace them with renewable sources of energy would advantage the economy of Libya.

Another risk of being dependent on oil and natural gas for electricity production is that these reserves are exhaustible and finite. At present, it is great that oil and natural gas resources are available in the country and there is a definite desire that they are not terminated. Yet, the lifetime of these resources is not known. Not to be pessimistic but in the long term conventional resources will run out, simply because they are unrenewable resources.

In view of the above discussion, Libya should expand its electricity production sources to include alternative renewable sources. Wind energy offers good solutions for all issues related to burning fossil fuels for power production. "In light of the threefold global crises mankind is facing currently – the energy crisis, the finance crisis and the

environment/climate crisis – it is becoming more and more obvious that wind energy offers solutions to all of these huge challenges, offering a domestic, reliable, affordable and clean energy supply." (WWEA, 2009).

Increasing the share of wind power in the electricity grids can help in reducing the reliance on fossil fuels to generate electricity, reducing GHG emissions, and securing the future of the energy sector and hence the economy. Wind energy is renewable, inexhaustible, and sustainable. Unlike oil and natural gas reserves, the wind will never stop blowing. The long-term costs of wind power have gone down dramatically during the last few years. The use of wind power can assist to decrease the unemployment rate by creating many jobs. Furthermore, wind energy is regarded as one of the cleanest and most environmentally friendly power sources.

However, the most critical challenge encountering wind power technology is that the wind resource varies according to the weather conditions. The wind does not blow at speeds within the range sufficient for wind power generation during all the time. Hence, an accurate assessment of the wind resource of Libya should be performed before any plan for the construction of wind farms. Such an evaluation should include identifying potential areas with sufficient wind speeds in the range suitable for wind power generation.

Wind resource assessment is the process of collecting and obtaining wind velocity data throughout a site/district in order to examine the potential of utilising the energy in the wind. Understanding the national distribution of wind power resources allows wind energy manufacturers to implement site-specific detailed evaluations, in an attempt to select appropriate locations for wind farms or stand-alone turbines. Investing lots of money, effort, and time without gaining enough knowledge about the wind resource can result in economic losses whereas a good wind assessment can assist to optimise the use of wind power.

1.2 Aim and Approach of Study

The main objective of this research is to evaluate and understand the national wind resource of Libya, and to identify the potential of wind energy exploitation over the country. This study aims at a regional assessment of wind power resources over Libya at different heights, in order to determine weather there is a good prospective of integrating wind power to the electricity networks. If the feasibility of wind power utilisation is high, areas with good wind power potential will be highlighted. The wind resource and the power over the identified regions will be analysed and discussed further to examine the temporal, horizontal, and vertical variations of wind energy resources.

The data used in wind energy evaluation normally come from one of three sources, which are on-site wind observations, the synoptic meteorological stations, or numerical weather simulations. Wind resource evaluation throughout Libya requires wind velocity data with high spatial and temporal resolutions. However, it is extremely difficult to distribute sufficient synoptic stations throughout a big and desert region like Libya. Therefore, the horizontal resolution of wind observations is inadequate for assessing the feasibility of wind energy generation over the country. Even the available historical wind measurements were not collected for the purpose of wind energy development.

Thus, the wind conditions at different elevations will be estimated using three-dimensional (3-D) real-data high-resolution nested numerical simulations. The Non-hydrostatic Mesoscale Model dynamic core of the Weather Research and Forecasting system (WRF-NMM) will be employed to simulate the wind velocity over the country using 2007 data from the Global Forecast System (GFS) as initial and boundary conditions. The goal of wind energy assessment will be targeted through the following approaches:

- ❖ Modeling the wind conditions to estimate hourly wind speeds over the country, based on numerical simulations.
- ❖ Computing the theoretical corresponding power density available over the country at different heights.
- ❖ Hypothetically installing several commercial wind turbines at different heights throughout the country to estimate as accurately as possible the actual wind turbine power outputs that can be obtained.
- ❖ Identifying favorable areas that have good wind power resources, and may be suitable for additional detailed site-specific evaluations.
- ❖ Selecting several grid points for site-specific wind energy assessment.

1.3 Structure of Dissertation

The thesis has been organised in seven chapters. Chapter 2 will give information background that improves the understanding of wind energy technology. Chapter 3 will look at the meteorology of wind energy. It discusses global and local wind resources, wind resource assessment, the wind energy situation and potential in Libya, and wind power evaluation data. The discipline of Numerical Weather Prediction (NWP) and the WRF-NMM will be discussed in Chapter 4. Chapter 5 will illustrate and discuss the methodology followed in this study. The methodology chapter will include the model setup, input data, simulation runs, simulation result preparation for wind power assessment over Libya, and other implementations. In chapter 6, the simulation results will be presented and discussed. The conclusions of the study and some recommendations will be provided in Chapter 7. This chapter will provide the main findings of the study, and some future suggestions.

Figure 1.1: A Libyan map showing major city/town locations.

Table 1.1: The geographical location of some Libyan cities/towns.

PLACE	LATITUDE	LONGITUDE	PLACE	LATITUDE	LONGITUDE
Ajdabiya	30° 54'N	20° 04'E	Imsaad	31° 34′N	25° 2′E
Al Bayda	32° 50'N	21° 44'E	Jadu	31° 57′N	12° 1′E
Al Kufrah	24° 17'N	23° 15'E	Ghiryan	32° 10'N	13° 00'E
Al Kums	32° 66'N	14° 26'E	Ghat	24° 59'N	10° 11'E
Al Malaki	23° 20'N	15° 30'E	Murzuk	25° 53'N	13° 57'E
Al Marj	32° 25'N	20° 30'E	Misratah	32° 24'N	15° 03'E
Al Wigh	24° 17'N	14° 59'E	Tripoli	32° 49'N	13° 7'E
Awbari	26° 46'N	12° 57'E	Tobruk	32° 7'N	23° 55'E
Benghazi	32° 1'N	20° 03'E	Zuwarah	32° 56′N	12° 05′E
Dirj	30° 10'N	10° 28'E	Yifrin	32° 04′N	12° 32′E
Darnah	32° 45'N	22° 45'E			

Chapter 2

Wind Energy Background

2.1 Introduction

Wind energy is the kinetic energy available in moving air. It is significantly subject to the amount of solar energy that is received by the atmosphere. In fact, since the wind is constantly recharged from the sun, wind energy is regarded as an indirect form of solar energy. The power in the wind is the total available energy per a unit of time.

This chapter gives background information about the theory of wind energy. The goal of this chapter is to provide a good understanding of wind power technology.

Section 2.2 shows how the wind power technology has developed, and Section 2.3 discusses the advantages and disadvantages of wind power utilisation. Information of the machines extracting the energy from the wind is provided in Section 2.4. Section 2.5 gives the physics equations of wind power, and Section 2.6 explains the maximum energy extracted from the wind. Factors affecting the available wind power are identified in Section 2.7, and Section 2.8 depicts the vertical wind shear for wind power

applications. The concepts of power curve and the capacity factor of wind turbines are elucidated in Section 2.9 and Section 2.10, in that order. Section 2.11 provides a very brief summary for this chapter.

2.2 Historical Development of Wind Energy

Harnessing the energy in the wind is not a modern concept. Since the ancient era, the wind has played a significant role in the historical civilisation of human beings. It is believed that wind power was first exploited to propel small boats in the Nile River roughly 5000 years ago (Patel, 1999, Hepbasli and Ozgener, 2004). However, historical records suggest that the first appearance of vertical-axis windmills known now as wind turbines was in Afghanistan in the 7th century B.C., while horizontal-axis windmills were initially used in Persia, Tibet, and China in 1000 A.D. (Dodge, 2001, Ackermann and Soder, 2000). These windmills used to generate mechanical energy were utilised for various purposes, such as grain grinding and water pumping.

In spite of such a long historical record, the energy contained in the wind has been utilised for electricity production for only about a century, whereas the comprehensive wind-generated electricity has only recently become competitive to the conventional electricity. By the end of the 19th century, the Danish meteorologist Poul La Cour invented the first wind turbine used to generate electrical power rather than mechanical power (Ackermann and Soder, 2000, Ackermann, 2005). In 1926, the German physicist Albert Betz contributed to an important theoretical advancement when he discovered that a wind turbine could convert only up to 59.3% (Betz's law) of the energy in the wind into usable power (Betz, 1966, Patel, 1999).

During the second World War, some Danish engineers overcame the shortage of energy supply by developing a wind turbine with high performance, which was designed to produce extra power (Durak and Sen,

2002, Hepbasli and Ozgener, 2004). The following few decades did not see the wind as a feasible source of electricity in comparison to conventional resources because then fossil fuels were widespread and inexpensive.

Yet, interests in wind power reemerged in the early of 1970s (Ackermann and Soder, 2000, Ackermann, 2005). The scarcity of crude oil and natural gas reserves led many nations to recognise that these resources are exhaustible. The oil crisis forced many governments and private organisations to focus their attentions on wind power technology providing electrical power. The early 1980s saw major economic optimisations introduced to wind power technology when the Californian market contributed to commercialise the industry worldwide. In the mid-1980s, the size of a common wind turbine reached about 100 kW (Herberta et al., 2007). The annual growth of the installed capacity of wind power slowed down during the succeeding years. This was mainly due to the reduction in the prices of fossil fuels.

Nonetheless, since 1997 government and non-government organisations have aimed at the optimisation of the efficiency and economic viability of wind turbines. The capacity of wind turbines grew from 500 kW in the early 1990s to 2500 kW by the end of 1990s (Herberta et al., 2007).

Among other forms of renewable energy, wind power has been the fastest growing as well as the most sustainable form. Many studies were dedicated to research the technology of wind energy conversion. During the 1990s, the global installed capacity of wind power doubled every three years (Ackermann and Soder, 2000). Over the past decade, the worldwide capacity of wind-generated electricity has been growing rapidly. Figure 2.1 from the World Wind Energy Association (WWEA) suggests that the global installed capacity of wind power along with its integration to electricity grids grew from 7.48 GW in 1997 to 121.18 GW in 2008, and is predicted to reach 190 GW by 2010 (WWEA, 2009). The size of a typical wind turbine reached 3500 kW in 2007 (Herberta et al., 2007).

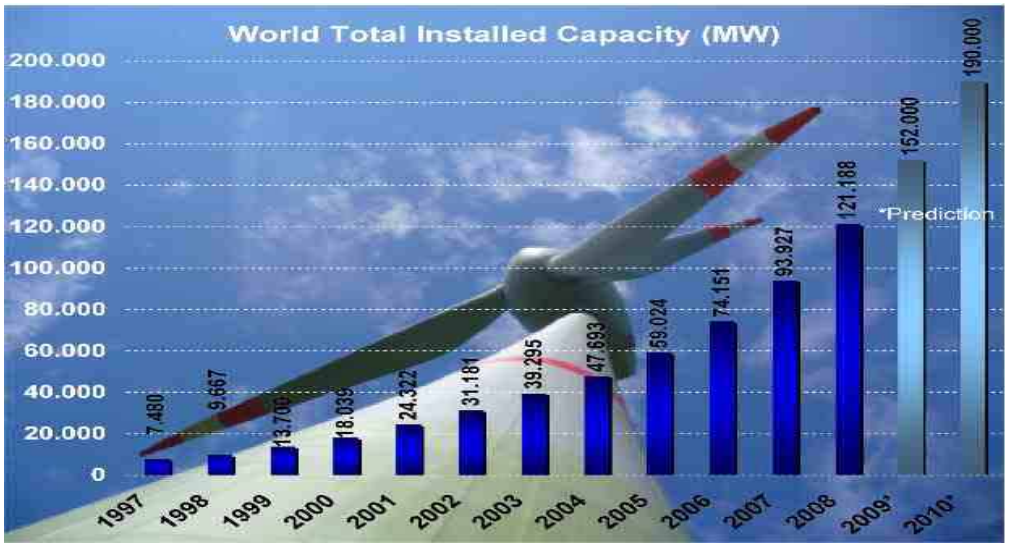

Figure 2.1: Total worldwide installed capacity of wind power (WWEA, 2009).

The improvement of wind energy industry is attributed to several factors including the awareness of climate change or global warming resulted from GHG emissions associated with the conventional power, the reduction in the costs of wind power, and the optimisation of the efficiency and reliability of wind turbines (AusAID, 2000). Today, wind turbines can be seen almost everywhere and there are many wind farms containing hundreds of thousands of small, medium, and large different wind turbines generating electricity around the world. One of these farms is the Tehachapi wind farm in the Tehachapi Mountains of California in the USA [Figure 2.2]. It is the second largest wind farm in the world as it has over 4600 wind turbines of different types and sizes, and supplies over 1.4 million MWhr of electricity per year (Chapo, 2007).

2.3 Advantages and Disadvantages of Wind Energy

Wind energy is an economical power source. The long-term costs of wind power is going down significantly (Jacobson and Masters, 2001, DOE, 2009). When all factors are taken into consideration in estimating the costs of wind power generation, wind farms can produce electricity at competitive costs to the costs of conventional electricity (Outhred, 2003). As stated by the USA Department of Energy (DOE), wind energy nowadays is

one of the cheapest renewable energy sources, and it can be generated at a cost of 0.04 to 0.06 USA cents/kWhr, depending on the wind resource and the finance of the project (DOE, 2009). In contrast, the costs of conventional electricity have been rising. Based on Energy Information Administration (EIA) Official Energy Statistics from the USA government, within a 1-year period from the first quarter of 2008 to the first quarter of 2009 the cost of conventional electricity of the residential sector increased by 8% from 10.4 up to 11.2 USA cents/kWhr, and an additional rise is predicted (EIA, 2009c).

Figure 2.2: The Tehachapi wind farm in the Tehachapi Mountains of California, the USA.

Moreover, wind energy industry can assist in decreasing the unemployment rate by creating many jobs. The WWEA has emphasised that within a 3-year period the number of jobs created by the global wind power industry increased almost twofold from 235000 in 2005 to 440000 in 2008 (WWEA, 2009).

Wind power is renewable. It is inexhaustible and sustainable. Unlike

conventional power sources, the wind will never stop blowing and there will be wind resources as long as the sun shines. On the other hand, fossil fuel reserves are finite, depletable, and cannot be renewed. The wind resource is abundant although it varies in time and space. It is believed that the wind energy existing on the earth accounts for about 2% of the solar energy obtained by the earth's atmosphere (Hubbert, 1971). It is estimated that the worldwide technical wind power is about 96 PWhr/year (Hoogwijka et al., 2004). A network of wind farms over some regions of Europe and Northern Africa could meet about 70% of the electricity needed in the entire European countries at a cost of less than 5 USA cents/kWhr (Czisch and Ernst, 2001).

Furthermore, wind power is regarded as one of the cleanest and most environmentally friendly energy sources. Wind farms produce neither much air pollution nor GHGs as modern wind turbines have been designed to be eco-friendly machines, unlike conventional power stations. Hence, utilising wind energy can minimise the GHGs that are being released in the atmosphere. The American Wind Energy Association (AWEA) has declared that on an annual basis a single 1MW wind turbine would reduce the CO2 emitted to the atmosphere by about 1800 tonnes (AWEA, 2005a). In the USA alone, the use of wind power in one year saved the environment from approximately 28 million tonnes of CO2 in the atmosphere (AWEA, 2005b). It is also estimated that by 2020 wind power alone would displace about 33% of the estimated CO2 emission growth that is caused by electricity production in the USA (AWEA, 2005b). According to Verve Energy, the 12-turbine Albany wind farm [Figure 2.4] in Australia reduces GHG emissions by around 77000 tonnes per year (Verve Energy, 2006).

Wind energy has only minor impacts on the environment. Every moving or rotating item, including wind turbines, creates sound, although the state-of-the-art wind turbines are designed to make very little noise in comparison to regular activities, such as road traffic and aircrafts. According to the British Wind Energy Association (BWEA), the sound of a

modern operating wind farm at a distance of about 300 m is perhaps the same as the noise from a running stream or the sound of tree leaves brought about by a gentile breeze at a distance of 50 to 100 m (BWEA, 2000). This could be equivalent to the sound level inside a normal house with a kitchen refrigerator or a modern air-conditioned room. Therefore, it can be seen that the noise emission generated by an ideal modern wind farm is very low and it would be negligible.

While it might be argued that wind turbines kill birds, their threat is small in comparison to the threat caused by common structures, such as electricity grids, transport accidents, buildings, pesticides, cats, communication towers. The AWEA has estimated that wind turbines cause one bird death in every 10000 bird deaths that are caused by human activities (AWEA, 2005a).

However, the most critical challenge facing wind power technology is that the wind resource varies according to the weather conditions. Unlike fossil-fuel power stations, the power outputs of wind turbines are not steady owing to regular temporal wind resource variations. The power outputs of wind turbines can be neither controlled nor accurately predicted as wind turbines can generate energy only when there are sufficient winds. The negative aspect is that wind does not blow at speeds suitable for wind power generation all the time, and over small time and spatial intervals, the wind could differ remarkably. The intermittency of the wind leads to fluctuations in the power outputs. This variability poses a critical problem for the utility operator systems since it may result in electrical overload or electrical deficiency in electricity networks, unless batteries are used to restore the power.

The problem of wind variations cannot be eliminated, yet, with recent developments in wind power meteorology, their effects can be reduced. Nonetheless, an accurate assessment of wind power resources needs to be done prior to the construction of any wind farm. Such an assessment

should identify areas with consistent and sufficient wind resources, and the economical viability of wind energy exploitation.

2.4 Wind Turbines

A wind turbine is a machine designed to capture the kinetic energy from the wind. It extracts some of the energy available in the wind and converts it into mechanical power, and in turn into electrical power.

Although the configuration of wind turbines varies according to their types and designs, the main components have the same functions. As illustrated in Figure 3.2, the basic components of a typical wind turbine include: a rotor consisting of a number of aerodynamic shaped blades transferring the kinetic energy in the wind into rotational shaft energy, a generator which converts mechanical energy into electrical power, a gearbox matching the speed of the rotor to that of the generator, a nacelle which protects the other parts of the wind turbine from damage, a tail vane system which maintains the turbine pointed to the wind direction, a high-speed shaft, a low-speed shaft, and a tower on which the generator is situated (Patel, 1999, AWEA, 2002, Gipe, 2004, Layton, 2008).

The mechanism of the operation of the rotor blades is similar to the wings of an airplane. The airfoil shape of the blade is a critical factor for determining the amount of energy captured by the turbine (Patel, 1999). When the wind blows towards the blade, some particles of the air move across the upper surface of the blade whereas the other particles pass beneath it. On account of the aerodynamic curved design of the blades, the air passes more rapidly over the upper and longer side of the airfoil shaped blade than below the lower side (Burton et al., 2001). According to the well-known theory of Bernoulli, this difference creates a low-pressure area above the blade, which in turn results in differential pressure between the upper and the lower surface of the blade. The pressure contrast produces a pressure gradient force, whose components are the lift force acting

perpendicular to the airflow, and the drag force acting parallel to the direction of the airflow (Mathew, 2006). As a result, the rotor blades linked to a thrust shaft turn an electronic generator in the turbine causing it to rotate. Then, the turbine starts to produce electrical power.

Wind turbines come in two main different types: horizontal-axis and vertical-axis wind turbines, both of which come in a variety of sizes and shapes (Logan and Kaplan, 2008). Figure 2.3 shows the configuration of selected horizontal-axis and vertical-axis wind turbines (Layton, 2008).

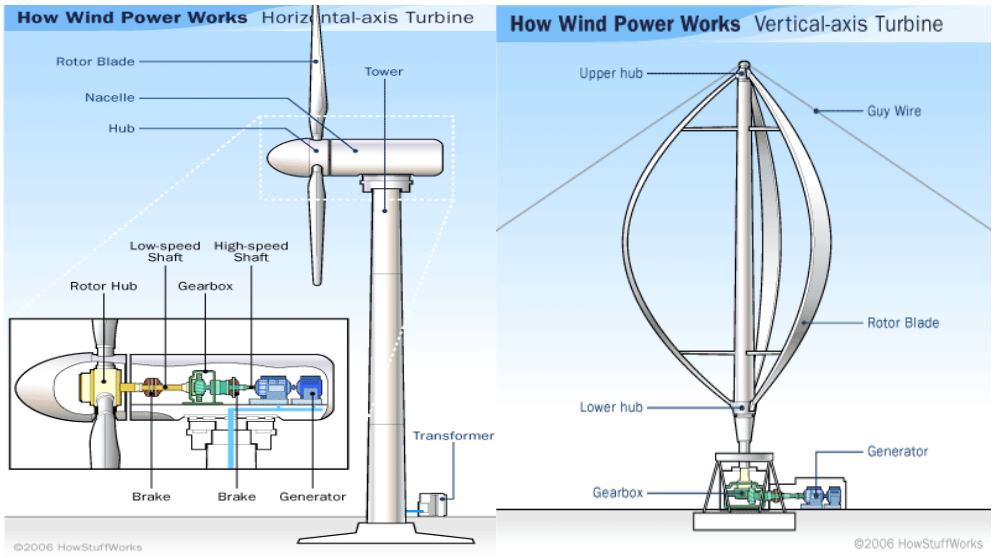

Figure 2.3: Simple horizontal-axis and vertical-axis wind turbines (Layton, 2008).

Horizontal-axis wind turbines need to face the wind for optimal efficiency. The tail vane and the servomotor in this kind of wind turbines keep them pointed in the direction of the wind. Horizontal-axis wind turbines can be subcategorized into upwind and downward turbines. Upwind horizontal-axis wind turbines are designed so that the rotor faces the wind. This design requires a yaw system by which the turbine is maintained oriented into the wind, and its blades need to be rigid and built at a distance from the tower. The use of upwind turbines helps to avoid the wind shade behind the tower even though there will be some shade in front of the tower. Most modern wind turbines used around the world are the three-

bladed upwind horizontal-axis turbines like those operating in the Albany wind farm in Australia, illustrated in Figure 2.4.

Figure 2.4: The Albany wind farm in Western Australia, Australia. Its turbines have a rated capacity of 1.8 MW with 65-m tower and three 35-m long blades (Verve Energy, 2006).

In contrast, downwind horizontal-axis wind turbines are installed so that their rotors facing the side away from the wind. In this design, there may not need for a yaw mechanism reducing the cost of the turbine, and the rotor blades are designed to be flexible. The rotor being flexible helps to lessen both the weight of the turbine and the load put on the tower, because they bend when wind speed is excessively high. Nevertheless, the power outputs of downwind turbines may fluctuate due to the wind shade behind the tower. According to the Danish Wind Industry Association (DWIA), when the wind starts blowing the air moves away from the tower and thus every time the rotor passes the tower the power generated by the turbine drops (DWIA, 2003).

Unlike horizontal-axis wind turbines, vertical-axis turbines have the rotor spinning on a vertical axis instead of horizontal axis. They are installed

perpendicular to the ground and always face the wind.

Vertical-axis wind turbines have the advantage that they do not require extra costs for the tower and yaw system as the gearbox and generator can be positioned on the ground, and also they do not need to be turned against the wind. Even so, the wind near the ground is usually slower and turbulent, especially on the lower part of the vertical rotor. Therefore, they have less efficiency of energy extraction.

2.5 The Physics of Wind Energy

In order to benefit from wind energy as a source of electricity, the first step needs to be taken is capturing this kinetic energy, and then converting it to a usable form. The energy in the wind can be described as the flux of kinetic energy passing through the cross swept area of rotor blades of a wind turbine. When the wind propels the blades of a wind turbine , these blades extract some of the energy contained in the wind, and then transform it into rotational energy and in turn into either mechanical or electrical power (Gasch and Twele, 2002, Mathew, 2006).

Theoretically, the kinetic energy (E) available in a moving air that has mass flow rate m and flows at velocity V over a given time can be expressed as follow (Burton et al., 2001, Gipe, 2004):

$$E = \frac{1}{2}.m.V^2 \tag{2.1}$$

According to the continuity equation governing atmospheric processes, the mass of the upstream wind should be equal to the mass of the downstream wind. When an air parcel passes through the swept area of the rotor blades, the rate of mass flow can be given by:

$$m = \rho . A .V \tag{2.2}$$

Substitute equation 2.2 into 2.1

$$P_{wind} = \frac{1}{2}.\rho.A.V^3 \tag{2.3}$$

However, the cross-sectional rotor swept area A can be expressed as

$$A = \pi.r^2 \tag{2.4}$$

Hence

$$P_{wind} = \frac{1}{2}.\pi.\rho.r^2.V^3 \tag{2.5}$$

Here: P_{wind} is the available wind power [W], r represents the radius of rotor blade swept area [m], ρ is the air density [kg/m^3], and V is wind speed [m/s] at the hub height.

In some cases, the existing wind energy is expressed based on its density per a unit area. The power density refers to the available power per one square metre of swept area. It does not depend on the efficiency of the design of the turbine but it is only a function of wind speed and air density. The power density can be given by:

$$WPD = \frac{1}{2}.\rho.V^3 \tag{2.6}$$

Where, WPD stands for the wind power density [W/m^2].

2.6 Maximum Energy Extracted from the Wind

When the wind passes through the swept area of the rotor blades, the turbine extracts some energy from this moving air, whose speed decreases owing to its energy loss. However, the kinetic energy in the wind cannot be extracted completely by wind turbines. If this occurred, the air parcel would stop moving at the swept rotor area, and then there would be no

space remaining for the next airflow.

As mentioned earlier in Section 2.2, the first finding by Betz in 1926, which is based on the principle of conservation of momentum and energy, indicates that an ideal wind turbine can only capture up to 59.3% of the energy contained in the wind passing through the rotor blades (Betz, 1966, Patel, 1999, Gasch and Twele, 2002). This suggests that the greatest amount of power captured by an optimal wind turbine can be achieved whenever the downstream wind speed is equal to one-third the speed value of the upstream wind. Thus, the theoretical maximum energy extracted from the wind by any design of wind turbine can be calculated by this formula (Patel, 1999, Gasch and Twele, 2002):

$$P_{wind} = \frac{1}{2}.C.\rho.\pi.r^2.V^3 \qquad (2.7)$$

Wherein C is the coefficient whose maximum value is 0.593. This shows that even if an efficient wind turbine operated all the time and extracted the entire possible energy, it yet could utilise only up to 59.3% of this energy. Still, usual modern wind turbines can achieve only up to 50% of the energy in the wind.

2.7 Parameters Affecting Wind Energy

Note that the Equation 2.7 indicates that the amount of the possible power available the wind varies according to wind speed, air density, and the size of the rotor blades. The power production of wind turbines is proportional to the cube of wind speed, and therefore the possible energy converted to electricity is strongly dependent on wind speed. Although the power outputs of any wind turbine vary with the size of the rotor diameter, wind speed is the most important parameter that determines the amount of power extracted by the turbine. Clearly, if wind speed at a site of a turbine is doubled, the power output of the turbine increases by a factor of eight. Moderate errors in wind speed can result in a huge difference in the power

output.

Nonetheless, the size of the rotor blades could also make a substantial difference for the energy extracted from the wind. When doubling the rotor diameter, the energy extracted from the wind increases fourfold. In fact, the area swept by the blades matters more than the power capacity of the generator. This is simply because the generator does not capture the energy from the wind the blades do that.

Wind velocity and hence wind power varies noticeably with height. Wind velocity is greater at upper altitudes due to the reduced drag. The wind in the boundary layer of the atmosphere is retarded by the frictional force generated due to the ground roughness, and the viscosity of the air. The ground roughness is mostly introduced by means of terrain attributes, such as the topography, vegetation cover, and synthetic obstacles. All these slow down the wind, and the rougher the earth's surface, the more the wind will be slowed down. Wind velocity close to the ground is too small and it increases with height above the ground.

The wind is also influenced by other meteorological fields. The power outputs of wind turbines are influenced directly or indirectly by other weather variables. Such an impact could come from the air density, temperature, atmospheric pressure, or relative humidity. These parameters influence the wind conditions at wind farms.

Wind power varies according to the air density. The more dense and heavy the air passing through the rotor blades, the more the power can be extracted from this moving air. That is why the actual air density should be included in the calculation when estimating the wind power since it provides more accurate indication about the wind power recourse.

If atmospheric pressure data are available, the air density can then be estimated using the atmospheric equation of the state (Holton, 1992, Patel, 1999):

$$\rho = \frac{P}{(1 + 0.61w)R.T} \tag{2.8}$$

Where: P stands for air pressure, w is the mixing ratio, and R is the general gas constant for dry air [287 J $kg^{-1}K^{-1}$].

The above formula suggests that unlike wind speed the air density goes down slightly with the height above the ground. This decrease, according to Equation 2.7, will lead to diminish the amount of energy contained in a moving air.

Both the temperature and pressure of the air passing through the blades can indirectly influence the magnitude of power available at the turbine's site. As illustrated in Equation 2.7, air temperature affects air density, which directly influences the amount of available power.

Variations in atmospheric pressure lead to the development of winds. Under the same conditions of temperature and moisture, high-pressure areas tend to be denser and the air will have more power per unit volume than low-pressure areas.

Relative humidity has a minor effect on the wind energy. When water vapour in an air mass increases, the air density will decrease and accordingly the energy in this air will go down.

It can be clearly seen that wind power is mainly dependent on the availability of the wind resource although air density and the length of the blade play roles as well.

Therefore, a precise selection of appropriate windy sites for constructing a wind farm plays a key role in the success and in the power productivity of the farm. An accurate evaluation of the wind resource is essential for examining the prospective of wind energy generation, the reliability of electrical systems, and the economical viability of any wind farm.

2.8 Vertical Wind Shear

The vertical wind shear depicts the change of wind velocity between two different heights. It is dependent on the stability of the atmosphere, the configuration of atmospheric layers, and the vertical advection of heat (Garratt, 2004). In wind energy applications, wind shear is normally calculated using the 1/7th power law. If wind speed is not measured at the hub height of a turbine, this law is used to extrapolate the wind speed to any required height. The 1/7th power law can be expressed as (Gasch and Twele, 2002, Gipe, 2004):

$$V(z) = V(z_{ref}) \left(\frac{z}{z_{ref}} \right)^{\alpha} \qquad (2.9)$$

Wherein, V (z) is the wind speed at the height z, $V(z_{ref})$ is the actual wind speed measured at a reference height z_{ref}, and α is the shear exponent.

The above formula assumes that the earth's surface is neither heated nor cooled. The exponent shear is typically assumed to be 1/7 (0.143), but it may vary depending on the stability of atmospheric layers, wind speed, roughness length, and the height interval. Hence, using one value for the shear exponent could result in large errors in wind speed and power, and that is why each location should have its own average shear exponent (Bailey, 1981). In a stable atmosphere the power law greatly depends on the stability and is slightly affected by surface roughness length, while the reverse is true in an unstable atmosphere (Irwin, 1978).

Wind shear is an important factor for wind power utilisation. Wind shear may advantage the use of wind power since increasing the hub height of wind turbines can allow them to capture more energy from the wind. Nonetheless, this is not always the case. Strong turbulent winds affect the installed turbines, as they may damage their blades by placing strong and turbulent forces on them. When wind speed varies remarkably across the

blades, high stress is put on the rotor blades resulting in the destruction of the blades and the generator.

Understanding the wind shear at a site properly requires a historic and high temporal and spatial resolution wind velocity measurements. Yet, one year of high-resolution hourly wind speed estimates, which are considered in this study, should provide a reasonable indication about the magnitudes of vertical wind shear.

Another useful contribution made by studying the wind shear at proposed locations is that it helps to determine and select the optimum hub height for the turbines. It is well known that wind speed increases with height above the surface, and so does the corresponding power. Yet, the extra costs added to install higher towers are sometimes not justified by the additional power obtained due to this extra height. In such a case, lower towers would be an optimum selection, because the success of a wind power project is explicitly a matter of cost.

2.9 Power Curve

The power curve of a wind turbine is a graph representing the relationship between the power generated by the turbine and wind speed. In other words, it denotes the quantity of power output from the wind turbine at a wide range of wind speed (DWIA, 2003). The power curve significantly differs according to the design and size of the wind turbine. Figure 2.5 demonstrates the power curve for a 2MW wind turbine.

Every wind turbine is designed to capture its maximum power, known as *rated power*, at a fixed wind speed. The wind speed at which the turbine generates its rated power is called *rated wind speed,* while the minimum speed at which the turbine commences operating and generating electricity is known as *cut-in wind speed*. Typically, the rated speed is in the range of 12-15 m/s whereas the cut-in wind speed range from 3 to 5 m/s, but they may differ depending upon the size and type of the wind turbine (Patel,

1999, Outhred, 2003). The *cut-out wind speed* refers to the speed at which the wind turbine stops operating and turns away from the prevailing wind direction. It is typically around 25 m/s depending on the wind turbine and the wind resource at the turbine's site (Outhred, 2003).

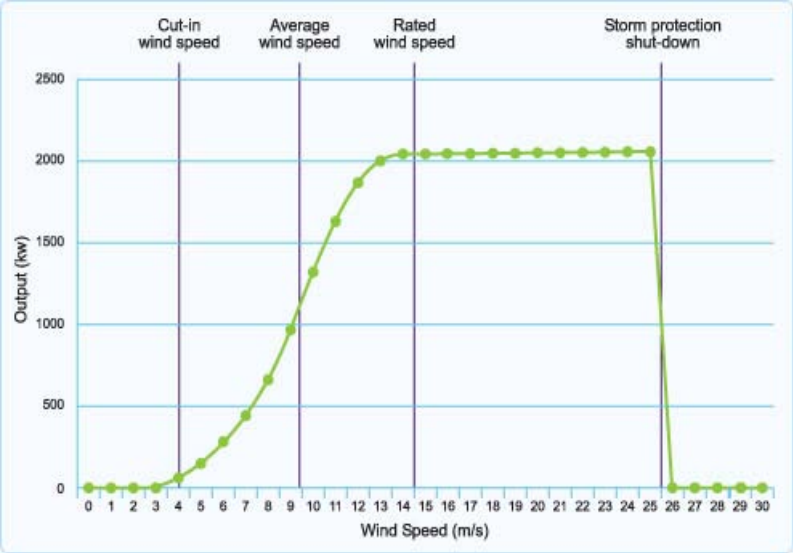

Figure 2.5: The power curve for a 2MW wind turbine (Partnership for Renewables, 2009).

Figure 2.5 indicates that below the cut-in wind speed there is not any power generated by the turbine. Once the wind starts blowing at the cut-in speed, the turbine operates and starts to produce power, whose amount increases as wind speed increases until the turbine achieves the maximum power output at the rated wind speed. Above the rated wind speed, the turbine continues to produce its rated power but at lower efficiency because some parts of the energy existing in the wind are spilled (Ackermann, 2005). When wind speed exceeds the cut-out speed value, the turbine ceases energy extraction and turns out of the prevailing wind direction. If the wind turbine did not shutdown under such extreme wind conditions, its generating system could experience severe damages. The turbine does not resume operation and power production instantly as soon as wind speed drops below the cut-out speed value, but it needs some time to re-operate again (Ackermann, 2005). That is why installing wind turbines in areas experiencing severe wind conditions should be avoided.

2.10 Wind Power Capacity Factor

The capacity factor of a wind turbine (CF) is defined as the ratio of the actual power output of the turbine over a specific time period (P_{act}) to the maximum power output if the wind turbine produced its rated power throughout this time period (P_{max}). It can be given by:

$$CF = \frac{P_{act}}{P_{\max}} \tag{2.10}$$

The capacity factor of a wind turbine or wind farm is often expressed in percentage. As an example, assume that there is a 500kW turbine that actually produces about 1.533 million kWhr/year. If this turbine operated for the entire year for 24 hours for 365 day, it would produce (500 kW) × (365 × 24 hours) = 4.38 million kWhr/year. In this case the turbine in that year would have 1.533/4.38 = 0.35 capacity factor. This does not mean that the turbine would operate for only 35% of the time, but rather it suggests that the turbine would produce 35% of its rated power.

Although the capacity factor varies according to the design of the turbine, it mostly depends on the wind characteristics of the turbine's site. The DWIA has pointed out that typical wind power capacity factors vary between about 25 and 30% (DWIA, 2003).

2.11 Summary

Wind power has served human beings for a very long time. It is the most promising, environmentally friendly, and developing form of renewable energy. Wind energy generation costs have been falling noticeably for the past two decades. The energy contained in the wind can be harnessed by wind turbines designed to extract some of this energy and convert it into usable forms of power. They can capture only a maximum of 59.3% of the energy available in the wind passing through the rotor blades. The amount of generated power depends mainly on the magnitude of wind velocity in

the region. Therefore, when assessing the wind power potential over Libya, the wind resource should be considered as a dominant factor in determining the feasibility of any wind energy project. The next chapter will look at the meteorology of wind energy.

Chapter 3

Wind Energy Meteorology

3.1 Introduction

The wind is simply air in motion. The wind is not only one of the main components of the weather systems, but it is also an important determinant of the climate condition of any region (Huang et al., 2008). It transports the energy, momentum, and moisture from place to place. The wind is also the crucial determinant for the success of wind power applications. It acts as fuels for the wind turbines, so without winds, wind turbines would not produce electricity. Hence, it is undeniable that when planning to install wind turbines, only sites with good wind resources should be considered. That is why wind power meteorology should be studied prior to the construction of any wind farm.

This chapter looks at the meteorology of wind power. It details information about the climate of wind and about the theoretical potential of wind energy exploitation in Libya. Section 3.2 elucidates the nature of the wind. Section 3.3 looks at global and regional wind resources. Subsection 3.3.1 describes the atmospheric general circulations, and Subsection 3.3.2 discusses local circulations. Atmospheric gravity waves are studied in

Subsection 3.3.3. The concept of wind resource assessment is interpreted in Section 3.4. Wind power status and potential in Libya are discussed in Section 3.5, and the problem over wind observations being insufficient is highlighted in Section 3.6. A very brief summery is provided in Section 3.7.

3.2 The Nature of the Wind

The wind is driven primarily due to an imbalance in the geographical distribution of the solar radiation incident on the surface. The variation in the insolation along with the surface albedo causes the heating and cooling of the ground to differ geographically. This generates pressure gradient forces and thus winds. Even so, there are other factors involved in the determination of the wind behavior.

Horizontal winds are controlled by four main forces including the pressure gradient force, the effect of the rotation of the earth (Coriolis force), the frictional force, and centripetal acceleration force. Yet, the major cause of air motion is the evolution of horizontal pressure gradients, and such gradients are maintained by means of Coriolis force (Barry and Chorley, 1998).

The wind is extremely variable as it varies from very small to very large temporal and spatial scales. The changes of wind over a scale of seconds to minutes are known as turbulence that is considered as one of the major challenges facing wind power generation. The wind is greatly affected by factors like the geographical location, the surface orientation, heterogeneous topography, artificial obstacles, and diurnal surface heating or cooling differences.

Areas along water-land interface are usually characterised by good wind resources while regions having similar surface orientations usually have less wind resources. Mountainous areas usually experience good wind energy resources as well.

Differential insolation generates airflows. The amount of solar radiation received at the ground depends on atmospheric features including the presentation of moisture and other gases, the cloud coverage, the latitude that affects the altitude of the sun, the surface characteristics such as wetness and vegetation cover, and the configuration of the terrain (Hartmann, 1994). The surface insolation is also influenced by the power transfer within the atmosphere, vertical shear of air temperature, and the sea and land (Barry and Chorley, 1998). Such factors cause incident solar radiation to vary geographically bringing about atmospheric temperature, and pressure gradients. Differential pressure creates a pressure gradient force causing air parcels to move from high-pressure zones toward low-pressure zones. The distance between these opposite pressure systems determines the wind scale while both the distance and the magnitude of the pressure gradient force affect the wind speed. Typically, large-scale temperature and pressure gradients result in the large-scale (global) circulation or global winds, whereas small-scale temperature and pressure differences give rise to regional circulations or local winds.

3.3 Global and Local Wind Resources

3.3.1 Atmospheric Large-scale Circulation

The large-scale circulation of the atmosphere is a global movement of air by which the energy is distributed on the surface of the earth. It contributes to the global wind resources, and is important factor in determining the climate. Even though the configuration of the global atmospheric circulation differs from one year to another as well as from season to season, its central pattern is almost permanent.

The general atmospheric circulation and weather systems are primarily the consequence of the imbalance of energy existing in the atmosphere. Energy fluxes are the cause of this circulation. The equilibrium of energy distribution governs the behavior of atmospheric processes as energy can

neither be created nor destroyed while it can be converted from one form to another. Great amounts of energy driving the atmosphere are obtained from the tropical ocean evaporation that transfers large quantities of latent heat to the atmosphere (Critchfield, 1983). Once the earth's atmosphere receives certain amounts of energy, this energy will never be destroyed but the wind transports it from one region to another in order to balance the energy in the atmosphere. However, some of this energy is lost due to the surface drag or converted to heat through turbulent dissipation.

Heating or cooling variations between the equatorial latitudes, tropics and the poles yield the global atmospheric circulation system. Yet, the Coriolis force partitions this circulation into three cells: Hadley cell, Ferrel cell, and Polar cell. A three-cell atmospheric circulation representation is shown in Figure 3.1. The three-cell large-scale atmospheric circulation is a general representation of the global wind conditions, but the actual wind pattern varies geographically and temporally because wind characteristics are complicated.

Hadley cells lay between the equator and about the latitudes of 30° in both hemispheres. Low latitudes receive more insolation than the subtropics. The surface equatorial air is heated and it becomes lighter than the air above it. As a result, it rises and cools due to the temperature lapse rate. The air rising creates clouds and lows within the surface layer and highs near the tropopause.

Due to the conservation of energy, mass, and momentum, the air aloft starts to move toward the subtropics. As the air continues to travel, it gains momentum but the Coriolis force deflects it westward until becomes almost westerly winds known as subtropical jet streams. As the upper air moves poleward it cools. At around 30°, some of the air subsides near the ground creating lows aloft, while the remaining air continues to flow poleward with an increased momentum and speed.

The equatorward pressure gradient force causes most of the surface air to

return to the equator replacing the ascending air, whereas the remaining air moves poleward within the lower layers. Consequently, semi-permanent subtropical highs are developed near the surface of the latitudes of 30°. These subtropical regions experience calm to variable horizontal winds, and hot dry climate. At these areas, the horizontal pressure gradient is small and there are usually downward movements of the air where Hadley and Ferrel cells meet. The Sahara Desert of Libya is affected by this climate.

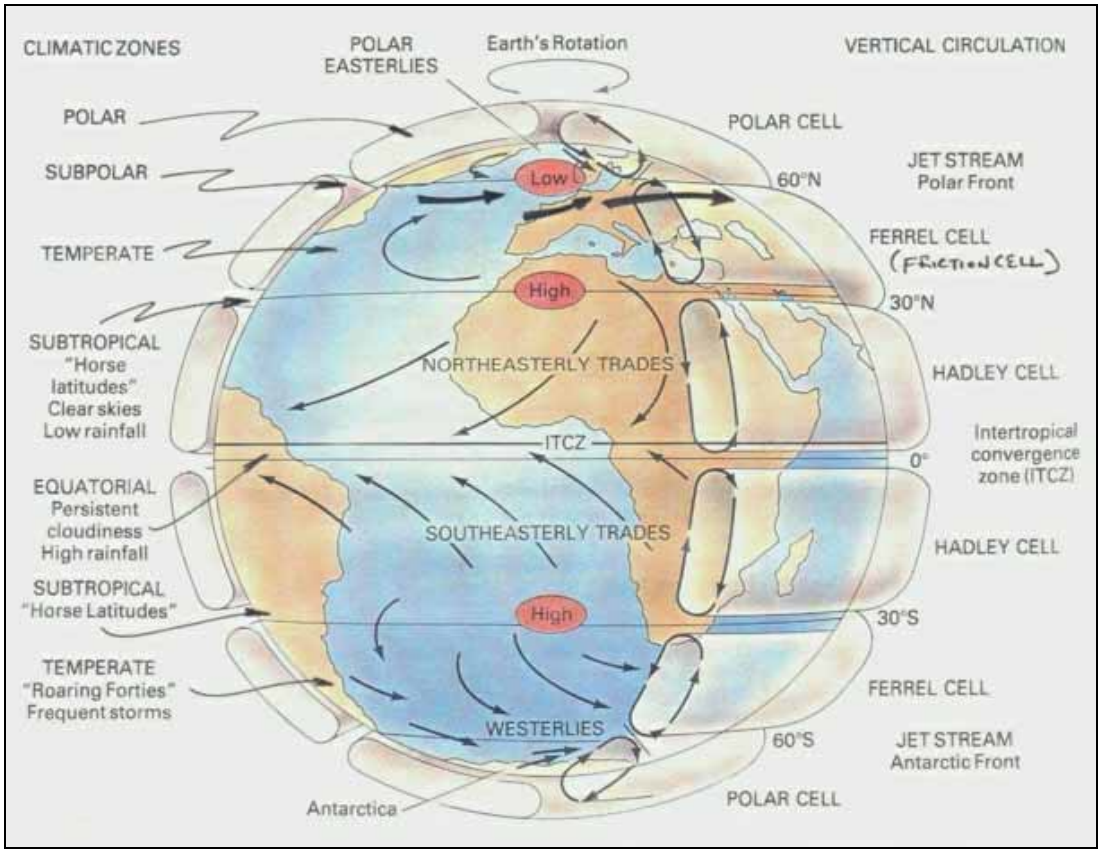

Figure 3.1: Global atmospheric circulation as depicted in the three-cell model (Miller, 2002).

However, the equatorward airflows do not move in a straight direction, because the Coriolis force diverts them westward and gradually they become almost easterlies. These surface prevailing winds blowing frequently from the subtropics toward the equator are known as the northeasterly trade winds in the northern hemisphere and southeasterly trade winds in the southern hemisphere. Since Libya is located in the

subtropics of the northern hemisphere, most of the country is generally characterised by northeasterly winds.

Northeasterly and southeasterly winds join at the converging belt near the equator creating the Inter Tropical Convergence Zone (ITCZ). The ITCZ is characterised with a calm cloudy weather and low-pressure systems. This is due to high surface heating, convection, and the condensation of the rising air. The extent of the ITCZ is variable since it moves north and south according to solar heating that varies with the time of the year.

Ferrel cell characterises the climate conditions of the area between the latitude of 30° and 60° in both hemispheres. As mentioned earlier in this section part of the surface diverging air at the subtropical latitudes moves poleward and due to the Coriolis force this air is deviated eastward. This movement brings about the prevailing westerly winds in the lower atmospheric layers. When this poleward air reaches about 60° latitude, it ascends, cools, and eventually creates low-altitude lows. This scenario generates clouds and precipitations over these regions. Yet, some of the rising air returns toward the equator aloft. The northern part of Libya is typically affected by this kind of cells, as it experiences westerly winds.

Regarding the Polar cell, it subsides over the poles to balance the radiative cooling and heating. Cold dense air parcels descend over the poles, creating low-altitude highs. These air parcels move along the surface to the mid-latitudes in lower troposphere creating polar easterlies. At around 60° north and south, the air has been warmed up allowing it to rise, creating surface lows. The polar front generates a pressure gradient force that gives rise to the mid-latitude strong jet stream.

3.3.2Local Circulations

Regional winds or local circulations are the result of either the local temperature gradient or the topographic configuration of the region. Annual and daily cycles of the surface heating and cooling result in a

variety of thermal regional winds. Some of the important local winds experienced in Libya include sea/land breezes, and mountain/valley breezes.

As far as wind energy applications are concerned especially for coastal regions like those of Libya, local winds are the most determinant factors for the feasibility of wind power conversion. Mesoscale winds occur regularly within the lower layers of the atmosphere within which wind turbines can be installed (Mathew, 2006). Mesoscale simulations investigating the wind power potential along the coastal plain of Western Australia have indicated that the estimated wind power of this region is mainly dependent on sea/land breeze circulations, and flows generated due to the terrain structure (Lyons and Bell, 1990).

3.3.2.1 Sea/Land Breezes

Sea/land breezes are moderate mesoscale convective flows that develop along the boundary between land and water. Differential cooling and heating between land and water bring about an air pressure gradient. The pressure gradient force causes the adjacent air to flow either landwards or seawards depending on where the temperature is higher.

Sea/land breezes play a major role in determining the meteorological condition of coastal regions (Simpson, 1994). Normally, sea breezes occur in summer as well as during daytime whereas land breezes are observed in winter in addition to during nighttime. Since Libya is located along the Mediterranean Sea, its coastal areas should experience good sea/land breezes. Hence, the behavior of local winds, in particular sea breezes, should be understood for wind energy applications in the country.

During daytime, as solar radiation strikes the earth's surface along land-sea boundaries, the surface of land is heated much quicker than that of the adjacent water. This is because water transfers and distributes heat between its layers either by conduction, or by upward and downward

movements of water currents. The air above the land surface starts to warm up due to heat distribution by the convective eddies and conduction.

Meanwhile, the air over water is still cooler than that over the land. As soon as there is a considerable temperature and pressure contrasts between the sea and the land, the air begins to flow landward owing to the inland-directed pressure gradient force. As the sun continues to shine, the pressure gradient force becomes more powerful driving the cooler and heaver air masses over the water. This scenario gives rise to an inshore breeze that replaces the rising air over the land.

When the surface air is heated, it becomes light, expands, and moves upward moving the pressure levels up, producing thermal low-altitude lows and high-pressure zones aloft (Simpson, 1994). The seaward-directed pressure gradient force aloft causes the rising air to stream back seawards. This creates heavy air masses over the water aloft that rapidly move downward to complete the circulation. This small-scale circulation is called a sea breeze circulation shown in Figure 3.2.

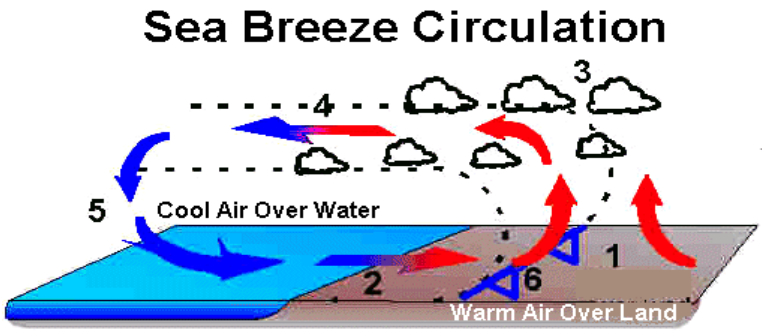

Figure 3.2: A simple model of sea breeze circulation (Heidorn, 1998).

As the sea breeze moves inland, the cooler sea air propagates inland creating a cold front characterised by a sudden wind shift, drop in air temperature, and increase in relative humidity. As the sea breeze front moves inland, thunderstorms may develop but the sky clears up after the passage of the front. Sea breezes continue to blow at normal speeds throughout the afternoon but by late evening, they subside given that the

amount and the flux of incoming solar radiation decrease.

Typically, when the sea breeze develops it blows perpendicular to the coastline but the Coriolis force deflects the wind gradually until it becomes parallel to the coastline. Nevertheless, this depends on the curvature of the coast structure and the latitudinal location affecting the Coriolis force. The frictional force also slows the breeze down.

When the sun begins to fall below the horizon, the air becomes calm for sometime because the difference between the air temperature above the land and the water is too small. In other words, there is no a strong pressure gradient force existing during this time period.

During nighttime, due to the outgoing longwave radiation the terrain and water along the sea-land interface cool gradually. Yet, the terrain cools faster than the water for the same reasons explained earlier in the sea breeze part. The air over the sea has higher temperature and lower pressure than that over the land. This scenario makes the circulation pattern of the sea breeze to reverse, generating what is known as a land breeze illustrated in Figure 3.3.

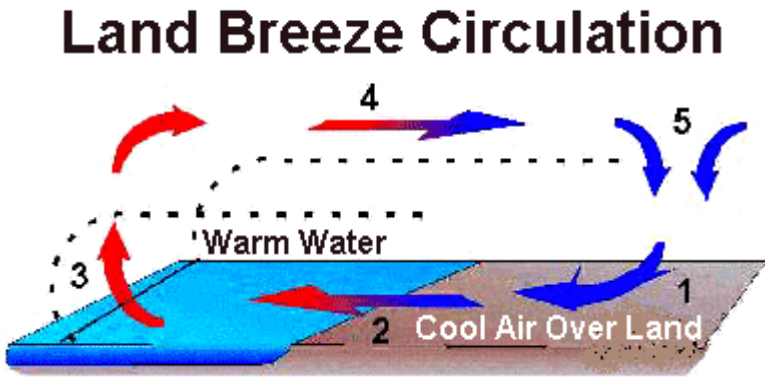

Figure 3.3: A simple model of land breeze circulation (Heidorn, 1998)

Seeing that the seaward pressure gradient force and the temperature gradient between land and water are both small at night compared to those during daytime, land breezes are often weaker than sea breezes. Land breezes reach their peaks during the early morning but they subside

shortly after sunrise (Critchfield, 1983).

During the development of sea/land breezes, the typical average land-water pressure difference between the land and sea is about 2 hPa (Barry and Chorley, 1998). The strength of sea/land breezes depends on the temperature difference between the land and water surfaces, the terrain roughness, the curvature configuration of the coastline, the moisture condition over the land, and the strength of large-scale winds along with synoptic flows (Simpson, 1994).

The horizontal extent of sea/land breezes ranges from a few to hundreds of kilometers. The typical inland penetration of sea breezes is about 1 km but it may penetrate up to 50 kilometres or more during the late evening (Critchfield, 1983, Barry and Chorley, 1998). Sea breezes blow at common speeds of 4 to 7 m/s although they can be greatly accelerated if there is a significant temperature inversion in the lower atmospheric layers, while land breezes are usually weaker blowing at speeds of around 2 m/s (Barry and Chorley, 1998). However, these values can vary depending on the location and other factors discussed previously.

3.3.2.2 Mountain/Valley breezes

Mountain/valley breezes are driven as a result of differential heating distribution along mountain-valley slopes. They develop on a daily basis through a procedure similar to that of sea/land breezebs but between mountains and valleys. On coastal mountainous regions, sea/land breezes combine with mountain/valley breezes, producing strong winds that penetrate deep inland. Green Mountain of Libya is located on the eastern coast and accordingly it is expected to experience this scenario with good wind power resources.

During cloudless nights, high terrains radiate longwave radiations faster than low ones. The upper slopes of mountains are cooled and consequently cooling the adjecent shallow atmospheric layer, making the air denser.

This generates pressesure and density gradiants. These gradiants along with the gravity force drive the dense air downslope to the valley floor. The downslope flow is called a mountain breeze [Figure 3.4].

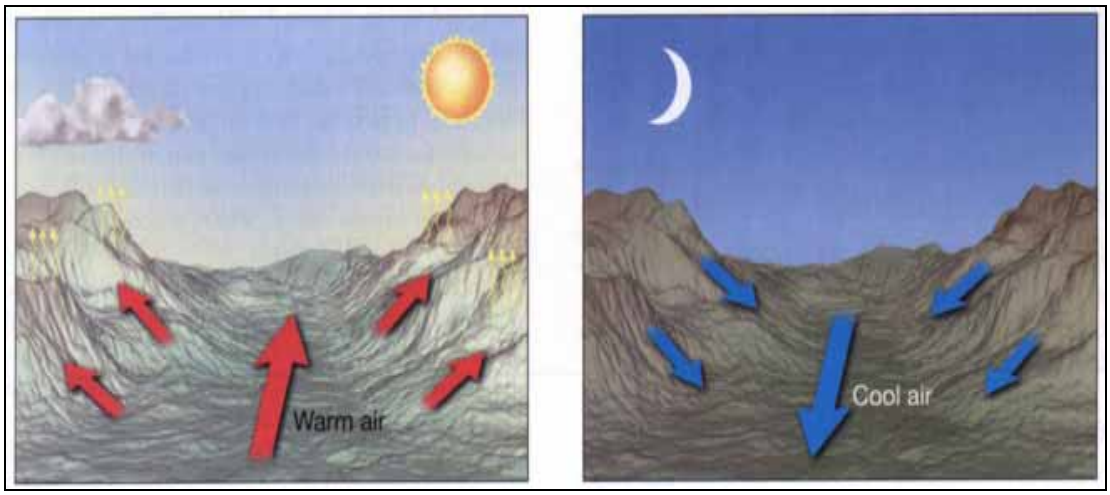

Figure 3.4: A simple model of mountain/valley breeze circulations (Miller, 2002).

Mountain flows create a temperature inversion. When mountain breezes are forced to flow through narrow channels in the topography, they may be accelarated and become faster (Critchfield, 1983). The velocity of mountain breezes peaks just before dawn when the durinal terrain cooling is at its maximum (Barry and Chorley, 1998).

During hot sunny days this senario is reversed. The heating of mountain slopes makes the neighbouring air warm and light, which in turn expands upward. This warm rising air at the top slope is replaced by the cooler air from the valley floor due to differential pressure and density. These gradiants give rise to an upslope flow called a valley breeze [Figure 3.4]. Valley breezes need a small pressure gradiant to facilitate their development, but they are often weak as they move against the gravity.

3.3.3Atmospheric Gravity Waves

An atmospheric gravity wave is an airwave moving through a stable atmospheric layer when this air experiences buoyancy oscillations. That is, gravity waves are convective air fluctuations resulting from the lifting force of buoyancy along with the restoring force of gravity (Nappo, 2002). They propagate both horizontally as well as vertically. Although atmospheric gravity waves may not be crucial for synoptic-scale atmospheric motions, they are extremely important for mesoscale weather forecasting (Holton, 1992).

Gravity waves are generated due to several different factors. One of these is the passage of wind across irregular terrain structures such as mountains and valleys. Others include thunderstorm updrafts, an interaction at the wind shear of the polar jet stream. When the air is constrained to move over an asymmetrical terrain, it is displaced upward and downward from its balance level. As it continues to flow over the heterogeneous topography, it experiences buoyancy fluctuations.

In atmospheric gravity waves, a parcel of air is forced to move upward in stable air. After rising up, it tends to subside again. The expanded air that is forced to rise in these waves is normally colder than its environment. The air momentum gained by falling causes the parcel to over-shoot its equilibrium level and to rise again, and the stability of the atmospheric layer forces this air parcel to sink back forming a full atmospheric gravity wave (Nappo, 2002). The spatial extent of atmospheric gravity waves varies between tens to hundreds of kilometres, and the temporal extent ranges from 5 minutes to 1 hour (Holton, 1992). As the terrain-generated gravity waves rise, their amplitudes may increase until ultimately they fragment similar to water waves at seashores (Nappo, 2002).

However, when the expanded air rises in unstable air, it continues to climb without creating any fluctuated wavy shape. If this rising air contains

enough water vapour, then the condensation occurs and clouds are formed.

Atmospheric gravity waves play an important role in determining the structure and dynamics of the atmosphere as well as the weather conditions of their regions, because they transport energy and momentum from the troposphere and lower stratosphere to the middle and upper atmosphere (Nappo and Chimonas, 1992, Holton, 1992, Nappo, 2002). They also result in air mixing and small-scale eddy transfers distributing heat, moisture, energy, and atmospheric gases.

In an atmospheric gravity wave, the upward moving region is the most favourable region for cloud development while the sinking region is characterised by clear skies (Nappo, 2002). This creates cloudy rows, between which cloudless rows are developed. The large spatial and temporal extents of gravity waves have significant implications for the atmosphere from the mesoscale to the global scale. This is one of the primary challenges to numerical weather predictions and simulations at all ranges.

3.4 Wind Resource Assessment

There are several steps needed to be taken when planning for a wind farm, but the most significant component of wind power applications is understanding and evaluating the wind resource of the region (Christiansen, 2006, AWEA, 2009). Wind resource assessment is the process by which the potential of wind power at a site/region is studied and determined. A good evaluation of wind resource magnitude and distribution is the most important factor for the success and the economic viability of wind power projects (Landberg et al., 2003b, Herberta et al., 2007, Lackner, 2008). Still, the wind turbulence, gust intensity, and the prevailing wind direction may also be required parameters for the estimation of wind power generation potential.

Monitoring the wind characteristics of the magnitude and the frequency

distribution of wind speed should be the first step taken by wind power planners. Such information helps to determine whether the selected site/region has a good potential of utilising wind power, and also helps to identify areas with sufficient wind power resources for additional site-specific investigations.

The most vital attribute of a site of wind turbine is wind speed. Wind speed should be examined at different heights to obtain good estimates for the feasibility of wind power generation at several proposed heights. With the widespread exploitation of wind power, the wind resource at different elevations is supposed to be evaluated using actual outputs of different sizes of wind turbines. This can assist in selecting the optimum hub height of any turbine. Estimating wind speed at different elevations can help in investigating the wind shear that may affect the components of wind turbines as well as the electricity stability.

As suggested by Equation 2.6, the power available in the wind varies with wind speed cubed. When planning to install wind turbines, wind speed at the hub height should be estimated as accurately as possible. An estimation error of 10% in wind speed will give rise to about 33% error in the possible wind power achieved by any wind turbine. If the actual wind speed at the hub height of a wind turbine was 9 m/s while the estimated value was 10 m/s, then the actual power density would be 729 W/m^2 whereas the estimated value of power density would be 1000 W/m^2. There would be an error of approximately 270 W/m^2. That is, for every 1 m^2 of the rotor swept area there would be a power overestimation of 270 W/m^2, which could result in large economic losses.

In order to regard a site as a good location for wind turbine installation, its wind speed should comply with the requirement of the proposed application. The AWEA has stated that for a location to be suitable for wind power generation, it must experience an annual mean wind speed in the range of 11-13 mph (≈ 4.9-5.8 m/s) or greater (AWEA, 2009).

Evaluating the feasibility of wind power generation at a site requires wind speed data. These data are initially used to estimate the power density using Equation 2.6. Nevertheless, the power estimated by means of this equation is independent of wind turbine characteristics, but it is only a function of wind speed and the density of atmospheric air. This theoretical power provides a good estimation of the available power over a region. However, it may overestimate the possible extracted energy by wind turbines seeing that wind turbines are designed to generate power only under a certain range of wind speed, and even under this range, they produce variable amounts of electricity. Using the actual power curve of the wind turbine to estimate wind power is more reliable because it does not overestimate the electrical power that can be generated by the turbine.

The prediction of wind velocity is complicated since wind is a stochastic meteorological variable. The characteristics of wind that bring about the concern associated with wind power conversion are the uncertainty and variability. The intermittency of wind is a major challenge facing the utilisation of wind power and the design of wind turbines. The intermittency of wind can also cause the power transferred to the electricity networks to differ considerably. This may damage the operator system of the turbine and result in electric load variations in the electricity systems. It is thus uneconomical to install a wind turbine at a site where wind speed and direction undergo incessant changes. The most favourable sites for wind turbine are those experiencing steady and reasonably high wind speeds.

The concern is that the intermittent nature of wind is heterogeneous and therefore cannot be predicted accurately. Despite that, wind has the capacity to supply great amounts of electricity but this necessitates a thorough wind resource evaluation.

3.5 Wind Energy Situation and Potential in Libya

Though wind energy in Libya was exploited to pump water during the mid-20th century, modern interests in wind power exploitation have only recently remerged in the country. The Libyan authorities have recognised the importance of seeking alternative sources of power as well as integrating wind power into electricity networks. The electricity decision makers in the country have realised that being dependent on oil and natural gases for power production is a heavy burden put on the economy of the country.

In 2000, the General Electric Company of Libya (GECOL) in collaboration with the Center for Solar Energy Studies (CSES) started to take some steps to study and develop small-scale wind power applications. They began to seek specialists in wind energy technology to evaluate the potential of harnessing the energy in the wind for generating electricity in Libya.

In 2001, a Danish-German group, consisting of the CUBE Engineering GmbH and other universities and institutes, formed an agreement with the GECOL to provide extensive knowledge and practical experience for Libyan engineers. The goal has been also to develop and supervise the construction of a small-scale wind power pilot and other wind farms. The general manager of the CUBE Engineering GmbH has stated that the proposal has been successfully implemented in both transferring technical training in the technology from Denmark and Germany to Libya, and also in preparing for several pilot projects (Chun, 2006).

Many sites were selected to be feasible to exploit wind power, yet one site was chosen to be suitable for a pilot with capacity of 25 MW and this location was in Darnah on the eastern coast of the country (Chun, 2006). However, the last stage of this project is continuing. Figure 3.5 shows a collage representation of the proposed wind farm in Libya.

Still, the wind resource of Libya is not well studied in terms of wind power purposes. There have been very few studies looked at wind power resources in the nation. Even these wind resource assessment studies have been limited to specific sites based on meteorological observations rather than the national resource.

Two studies of wind power evaluation have been implemented on Zuwarah, which is situated on the western coastline of Libya (El-Osta et al., 1995, El-Osta and Kalifa, 2003). Wind velocity measurements obtained from Zuwarah meteorological station have shown that the 10-m average wind speed is about 6.9 m/s and the predicted power density is roughly 399 W/m^2. Moreover, it is suggested that if wind turbines having capacities of 600 kW, 1000 kW, and 1500 kW were installed at this location, they would produce power at economical cost, especially the 600-kW turbine. It is also estimated that the use of wind power in this site would assist to reduce large amounts of GHG emissions.

Figure 3.5: A picture of the proposed wind farm in Libya (Chun, 2006).

In spite of that, the share of wind energy for electricity production in Libya has not begun yet. The wind power industry in the country remains in its infancy unlike other Mediterranean countries, which have taken considerable steps towards the exploitation of wind-generated electricity. A recent report from the WWEA indicates that by the end of 2008 the total

installed capacity of wind power in Italy ,Greece ,Egypt, Turkey , Morocco and Tunisia reached 3736, 989.7, 390, 333.4, 125.2, and 20 MW receptively, while Libya was not even among the list of the countries that are using wind power (WWEA, 2009).

Due to the lack of studies of wind resource evaluation in Libya, the next discussion will attempt to look at the wind resource of the Mediterranean region as it may slightly reflect the theoretical potential of wind power in Libya. Some other studies that have been carried out to investigate the global wind resource are presented below as well.

One of the global wind resource assessments has indicated that the worldwide technical wind power is nearly 96 PWhr/year being 6 times the global consumption of electricity of the year 2000 (Hoogwijka et al., 2004). Although wind power resources vary geographically, the technical potential of wind power generation in most parts of the world exceeds the electricity consumption of the region with the uppermost excess in East Africa. It is also found that approximately 7 PWhr/year of power could be extracted from the wind at a cost of 0.06 USA dollar per 1kWhr.

80-m wind observations from 8199 stations worldwide were extrapolated from 10-m wind speeds, and 1500-kW wind turbines were employed for calculating the estimated power (Archer and Jacobson, 2005). Nearly 13% of these stations throughout the globe experience annual average wind speeds higher than 6.9 m/s. This speed is in the range suitable for wind power production by most modern wind turbines. It is also estimated that the worldwide wind power potential of the year 2000 is about 72 TW, which would be enough to satisfy the whole world's energy need.

Cyprus experiences 10-m wind speeds greater than 5 m/s during 20-30% of the time (Pashardes and Christofides, 1995).

During most of the time 10-m winds of the northern and southern sectors of Morocco blow at approximately 6-10 m/s while the middle part of the

country has average wind speeds of about 4-6 m/s (Nfaoui et al., 1998).

The wind resource of Greece appears to be enough for small-scale wind energy utilisation, especially when it is coupled with solar energy systems (Vogiatzis et al., 2004).

Wind energy prospective in Turkey is found to be great. The average 10-m wind speed is about 7.3 m/s and the matching wind power density is roughly 222 W/m^2. (Karsli and Gecit, 2003). Theoretically, there is approximately 88000 MW of wind power existing over the Turkish region. Several coastal regions of the country, consisting of the eastern Mediterranean, have been identified to be very reliable for wind power development (Ozerdem and Turkeli, 2003, Hepbasli and Ozgener, 2004).

Wind energy resources along the coastline of the Egyptian Mediterranean coastline are encouraging, and several locations have been selected for wind farm construction (Shata and Hanitsch, 2006a). At 30-50 m above the ground, these places have power densities ranging from 180 to 330 W/m^2. The same authors have illustrated that the wind resource of a number of coastal meteorological stations located along the Red Sea in Egypt have annual average 10-m wind speeds of 7.3, 7.2, 6.4, and 5.5 m/s (Shata and Hanitsch, 2006b). During summer the average 10-m wind speed is about 6.9 m/s being suitable for large-scale wind turbines of 1000kW rated power or larger (Hanitsch and Shata, 2008).

Wind power resources along the Mediterranean coastline of Tunisia were studied, and it was concluded that at 30 m above the ground the average annual speed is 7.5 m/s and the power density is nearly 1900 kWhr/m^2/year (Amar et al., 2008). Other studies have shown that the northeastern mountainous coast of Tunisia has reasonable to good wind energy potentials, as the annual 10-m wind speed varies between 3.6 and 4.8 m/s and the annual power density is in the range of 537-893 kWhr/m^2/year (Elamouria and Amara, 2008).

The average long-term 10-m wind speed in Algeria ranges from 4.3 to 5.9 m/s (Himri et al., 2008). Wind farms of 30 1MW wind turbines were hypothetically employed to analyse and estimate the economical and technical feasibility of wind-generated electricity at some sites throughout the country. It is estimated that if the proposed wind farms at the selected locations were constructed, they would produce electricity of 98.832, 78.138, and 56.040 MWhr/year at a cost of 3.1-6.6 USA cents/kWhr.

It is stated that 50% of Sudan experiences average wind speeds of 4 m/s or higher being sufficient for water lifting (Omer, 2008). Yet, only the southern part of the country has mean wind speeds of 6 m/s suitable for electricity production.

Overall, it can be seen that most of the wind resource of Libya and the nearby countries seem to meet the requirement of large-scale wind turbines. Seeing that most studies have examined the wind characteristics at 10 m above the ground, the potential of wind power generation will be greater at higher altitudes. This is because wind speed and power density increase as the height increases. The wind resource encourages the development of wind power applications in the Mediterranean basin, though they differ from region to region. There exist good wind speeds that can meet large-scale electricity production, although some speed values may be suitable for water pumping or other applications. This gives confidences to examine and analyse the wind energy feasibility over Libya. Such an investigation requires wind data by which wind power resources can be evaluated.

3.6 Resource Assessment Data

It is well acknowledged that wind speed is the most important factor in determining the feasibility of wind energy utilisation. The data used in wind power evaluation is often derived from site-specific wind observations, the synoptic meteorological stations, or numerical

simulations. A precise wind resource assessment relies greatly on the quantity and quality of wind velocity data by which wind power decision-making analysis can be implemented (Coppin et al., 2003).

Evaluating the wind resource of a particular site/region requires a long historical collection of wind speed data and to a less extent the prevailing wind direction (Bailey et al., 1997). Other elective meteorological variables such as vertical wind shear, the atmospheric temperature, solar radiation, atmospheric pressure, and vertical temperature shear may also help in assessing the wind energy viability.

Modern wind turbines can be installed at different heights, depending on the size of the rotor blades and the wind condition. However, the challenge encountering this possibility is that wind data at meteorological stations are often collected at the height of 10m above the ground. It is uncommon when wind velocity is observed at more than one height, and even if multiple-height wind measurements are carried out they mostly take place in developed countries (Rehman and Al-Abbadi, 2005).

10-m wind velocity observations do not comply with the hub height of most of the state-of-the-art wind turbines, especially large-scale ones having large rotor blades. In such cases, wind speed is extrapolated to the hub heights of wind turbines. If the wind resource assessment is carried out based on weather station observations, several mathematical functions such as the power law [Equation 2.9] may be used to calculate wind seed at multiple elevations.

As far as wind power applications are concerned, a concentrated network of historical collections of wind velocity of 5 to 10 years should be used for understanding the wind resource at a site/region (Nfaoui et al., 1998, Landberg et al., 2003b). Practically, this appears to be unfeasible unless wind energy producers intend to start measuring the wind and collecting data at the selected sites. This process will take a long time and eventually the wind resource at proposed locations might or might not be suitable for

wind power generation.

Further, the other problem facing the assessment of wind power resources is that most wind observations were not collected for the objective of wind power generation because these observed data are usually available to reflect the average status of the wind. Libya occupies 1,759,540 km^2 of land, almost 90% of which is either desert or semi desert. In view of that, it is extremely difficult to distribute sufficient synoptic stations throughout the entire nation. The low horizontal resolution of wind observations is inadequate for assessing the national wind power resource of Libya. Meteorological parameters, including wind velocity, are normally measured at certain locations by weather stations. Therefore, even if long-term wind data exist they are only suitable for examining the wind energy viability at the areas nearby the synoptic stations. That is, it is only possible to perform site-specific investigations rather than monitoring a wide region like Libya.

The locations of meteorological stations collecting wind velocity data do not always represent the climate of the wind in the country. This is because weather stations are mostly found in inhabited areas where measuring the wind is easy unlike in mountainous or remote areas that may have better wind power resources. These remote regions are usually not covered by meteorological measurements.

In occupied areas, as mentioned earlier in Section 3.2, wind speed and direction are largely affected by buildings and other obstacles due to the frictional force. Rough obstructions cause the wind to change its velocity regularly over small temporal and spatial intervals, creating wind turbulences that do not suit wind turbines.

Furthermore, in the areas of weather stations, there are some difficulties in finding vacant lands for wind farms although it has recently become possible to install stand-alone wind turbines in various places even close to cities.

When bearing in mind the above discussion, it can be seen that although in the past wind power resources were evaluated and quantified based on meteorological observations, with the expansion and development of wind energy industry these measurements have become inadequate for providing detailed information about the wind characteristics at turbine's sites. Conventional meteorological observations have limited horizontal resolution and coverage, and thus they do not provide thorough depictions about the local condition of the topography and wind shear. Wind resource estimation requires a comprehensive description of the features of the terrain consisting of the surface roughness, vegetation cover, and other obstacles (Petersen et al., 1997). With the absence of wind measurements, one-year wind velocity data can give a reasonable indication of the potential for wind power generation with only 5 to 15% uncertainty about the long-term variability of wind speed (Frandsen and Christensen, 1992).

Due to the lack of wind observations in Libya, wind velocity data at different heights will be obtained from numerical simulations. Three-dimensional (3-D) real-data high-resolution nested numerical simulations will be used in this study to estimate the wind condition over the country using data of 2007.

3.7 Summary

This chapter has discussed the global and local wind resources, wind energy resource assessment and required data, and the theoretical wind power potential in Libya. The global wind resources appear to be abundant. Libya is located in the subtropics and therefore most parts of the country are affected by Hadley circulations while the northern part is influenced by Ferrel circulations. Since Libya stretches along the Mediterranean coastline, it is expected to experience diurnal cycles of sea/land breezes especially during summer. Some mountainous areas should see mountain/valley breezes. Coastal mountainous districts of Green Mountain should have a reasonable combination of sea breezes and mountain breezes

characterising these areas with good wind power resources.

Moreover, most global and regional studies carried out to investigate the wind energy potential in the countries located near Libya have indicated that the Mediterranean region has a great potential for wind power development, although this prospective varies geographically.

From what has been said, Libya appears theoretically to have good wind power resources. This encourages the assessment of the national wind resource of the country. The inadequacy of wind measurements will be overcome by the use of 3-D real-time high-resolution nested numerical simulations using the Non-hydrostatic Mesoscale Model dynamic core of the Weather Research and Forecasting system(WRF-NMM). The next chapter will look at Numerical Weather Forecasting models and at the WRF-NMM model.

Chapter 4

Numerical Weather Prediction and the Model Used in this Study

4.1 Introduction

The scarcity of spatial and temporal high-resolution wind velocity measurements in Libya can be overcome by numerical weather simulations. As highlighted in Chapter 3, wind energy resource evaluation requires historical wind velocity observations. Observed wind data are not adequate to study the national wind resource over a big arid region like Libya. This necessitates the use of Numerical Weather Prediction (NWP) method. The Non-hydrostatic Mesoscale Model dynamic core of the Weather Research and Forecasting system (WRF-NMM) will be used to perform three-dimensional (3-D) high-resolution real-time nested numerical weather experiments to estimate the wind condition over the country.

The aim of this chapter is to look at NWP and WRF-NMM. Section 4.2 gives information background about NWP. Subsection 4.2.1 provides an overview of NWP, and Subsection 4.2.2 discusses numerical weather

forecasting models and their ability to produce realistic data. The input data for such mathematical models are identified briefly in Subsection 4.2.2. Initial and boundary conditions are discussed in Subsection 4.2.3, and NWP model classification is explained in Subsection 4.2.4.

Section 4.3 describes WRF-NMM and discusses the model reliability. Subsection 4.3.1 provides an overview of the model, and Subsection 4.3.2 shows how the model supports multiple nesting. The vertical coordinate of WRF-NMM is identified and discussed in Subsection 4.3.3, and the governing equations are supplied in Subsection 4.3.4. Subsection 4.3.5 looks at the dynamics of the model, and the initial and boundary conditions of the used model are described briefly in Subsection 4.3.6. The physics parameterisations used by WRF-NMM in this study are discussed in Subsection 4.3.7, and Subsection 4.3.8 illustrates the model components. A very brief summary is given in Section 4.4.

4.2 NWP

4.2.1 Overview

NWP is the discipline of predicting the weather using complex mathematical atmospheric models that use a numerical time-stepping procedure to solve a set of nonlinear partial differential atmospheric equations. These equations govern and describe the special and temporal changes of atmospheric processes.

NWP is not a modern concept since it has attracted the attentions of human beings for nearly a century. The first NWP approach was implemented by the British meteorologist and mathematician Lewis Richardson in 1922, and this implementation of weather forecasts is presented in his well-known book “Weather Prediction by Numerical Processes” (Richardson, 1922). Richardson applied the method of finite differences to predict the next day’s weather condition, by solving a set of

nonlinear partial differential equations governing atmospheric flows based on mathematical calculations.

Richardson's scheme failed to produce realistic results for weather prediction, as there was an overestimation of atmospheric surface pressure. The predicted pressure had never been experienced, with an increase of 145 hPa within 6 hours. The prediction error was due to the inability of the smoothing techniques applied to filter out the waves in the atmosphere such as lee waves over mountains and clear-air turbulences, which eliminated unphysical surges in the pressure (Lynch, 2006). In spite of that, Richardson's notion has contributed to the numerical weather forecasting foundation, from which other meteorologists have started to expand and develop this prediction technique. NWP has gained a great importance by both individuals and meteorological institutes, and the basis of Richardson's method is still widely used in current NWP models.

4.2.2 NWP Models and their Capability

"An atmospheric computer model is a computerized mathematical representation of dynamical, physical, chemical, and radiative processes in the atmosphere"(Jacobson, 1999). NWP models are Computational Fluid Dynamics (CFD) models that estimate the future state of the atmosphere by means of solving coupled nonlinear partial differential equations, which govern the temporal and spatial changes of the behavior of atmospheric horizontal and vertical motions (Sorbjan, 1989, Krishnamurti and Bounoua, 1996).

Atmospheric flows are governed by three basic physical laws: the conversation of momentum, conservation of mass, and conservation of energy. In order to solve the temporal and spatial changes of atmospheric processes and properties numerically, these physics laws need to be expressed in mathematical relations. These relations solved by NWP models are a set of nonlinear partial differential equations that govern and

describe heat, mass, and momentum transfers in the atmosphere.

The coupled nonlinear partial differential equations used in numerical simulations and forecasts typically consist of four main equations: the equation of state, the equations of momentum, the continuity equation for air, water and mass substances, and the equation of thermodynamic energy (Haltiner and Williams, 1980, Krishnamurti and Bounoua, 1996). The meteorological parameters calculated in these equations include atmospheric pressure, temperature, air density, moisture, the vertical component of wind velocity, the horizontal components of wind velocity, and all functions of position and time (Haltiner and Williams, 1980, Petersen et al., 1997). The coupled nonlinear partial differential equations are very sophisticated and have no analytic solutions. Hence, complex numerical models are developed to provide approximate spatial and temporal solutions for these equations (Krishnamurti and Bounoua, 1996).

Numerical weather forecasts and simulations are becoming more accurate and reliable. With the growth of the computing technology, many NWP models have become available for the community use. Increasing the computational capability allows NWP models to provide more accurate forecasts and simulations, although the computational costs remain high because of the sophisticated physical parameterisations included in modern modeling systems. Running high-resolution weather forecasting models requires powerful computers since the 3-D derivatives in NWP model equations are complex and solved on vast computational grid points (Landberg et al., 2003a).

Numerical weather forecasting models are of need to overcome the present scarcity of wind velocity observations. Numerical simulations can provide a reliable and high-resolution description of the weather condition, including wind, at different elevations. The use of this method can contribute to good regional evaluations of wind power resources at different hub heights of wind turbines over a wide area.

Atmospheric flows are driven by several forces including pressure gradient force, surface frictional force, Coriolis force, and gravity. These forces can be generated on a wide range of spatial and temporal scales, and allow the scale of atmospheric motions to vary from about 1 mm to thousands of kilometers (Sashegyi and Madala, 1994). Conventional synoptic observations cannot provide detailed depictions of the fine-scale flows at sufficiently fine spatial and temporal resolutions.

Modern NWP models have adapted sophisticated microphysics parameterisation schemes that can depict fine-scale atmospheric processes affecting heat, moisture, and momentum transfers. They take into consideration the effects of terrain configuration, including topography, vegetation, land-use, roughness, soil properties, and other properties. These features have substantial effects on local weather characteristics, especially within the mixed boundary layer. 3-D weather simulations can provide detailed descriptions about atmospheric motions occurring over complex mountainous terrains (Maurizi et al., 1998). Limited-area high-resolution NWP models can deliver good wind estimates on the order of temporal range of 6 hours out to 6 days (McQueen and Watson, 2006).

High-resolution nested models have the ability to describe fine-scale atmospheric phenomena, and their results have gradually become competitive with synoptic observations. Non-hydrostatic weather forecasting models using nesting runs can supply good estimates of the wind conditions at local and simple synoptic scales, when their results are compared to wind measurements (Finardi et al., 1998). Many numerical studies of wind resource assessment of different regions have compared the estimated wind velocity with the measured winds, and the comparisons show a good agreement (Conte et al., 1998, Beaucage et al., 2007).

Yet, the representation and the solution accuracy of atmospheric processes in NWP models improve as the temporal and spatial resolutions of the model increase. A numerical study using different models to examine the

wind field over the western Mediterranean Sea has suggested that numerical meteorological models can give good estimates for the wind but the accuracy depends on the specification of the environmental situations in these models (Ardhuina et al., 2007). Increasing the resolution of numerical simulations along with the three-dimensionality representation of the topography can improve the model solution (Miglietta and Rotunned, 2009).

4.2.3 NWP Inputs

The input data of NWP models come from various sources consisting of observations from synoptic meteorological stations, satellite data, radar data, profiler observations, rawinsonde observations, aircraft observations, ships observations. However, the vast majority of NWP input data used by numerical models are from remote sources, such as satellites.

Data collected from such different sources at different times may contain errors. For that reason, these data should be quality-controlled, assimilated, and then used for numerical weather predictions as reanalysis meteorological data. Quality control attempts to check the data to identify apparent errors and unreliable meteorological observations in the inputs. It also designed to identify deviated and fine-scale observations, which cannot be solved by analysis schemes in the model (Sashegyi and Madala, 1994).

Data assimilation merges different-source datasets, removes obvious errors, and eliminates the gravity wave noise resulting from the instability between wind and mass in the initial variables. This makes the input data reliable for providing a good representation for the initial atmospheric conditions of NWP models. Data assimilation also provides time continuity in the data to be on a scale matching the scale solved by the model. The data are then used as inputs for the initialisation of numerical weather forecasting models.

4.2.4 Initial and Boundary Conditions

NWP models describe atmospheric motions by integrating a set of nonlinear partial differential equations forward in time in order to estimate how weather variables change in time and in space. These equations necessitate initial and boundary conditions as the meteorological fields formulating them experience temporal and spatial variations. The initial conditions bound the model in time while the boundary conditions bound the model in space.

The initial conditions refer to the preliminary values of the meteorological parameters throughout the model domain from which the atmosphere can evolve during the future time. At the initial time of any numerical simulation and before the integration starts, the model needs to identify the current circumstances of the atmosphere. Based on this information the model commences estimating the weather condition ahead to the desired forecast time over the simulation region.

The boundary conditions refer to the values of the meteorological variables along the boundaries of the model domain. There are two kinds of boundary conditions: vertical (top and bottom) boundary conditions and lateral boundary conditions. The vertical boundary conditions denote to the specifications used to identify the magnitudes of meteorological variables at the top and bottom of the model's atmosphere, whilst the lateral boundary conditions refer to the specifications used to determine the magnitude of meteorological variables at the horizontal boundaries of the simulation domain.

The boundary conditions are designed to set boundaries for the model during the forecast time. Their duty is to stop weather systems occurring near the edges of the simulation region from interfering in the model calculation, and so the forecasts are not contaminated. The boundary conditions provide information about the physical atmospheric activities,

such as outflows and inflows occurring along the boundaries of the simulation region. Weather systems like high-pressure and low-pressure systems may penetrate the simulation region from outside the boundaries at any time during the forecast calculation. In order for limited-area models to produce realistic forecasts or simulations, they need accurate information about the behavior of these weather systems.

There are several options of lateral boundary conditions, including specified, linear, fixed, time-varying, and symmetric boundary conditions. Simulation errors could exist as a result of erroneous boundary conditions, like when their resolution is too low in comparison to the fine resolution supported by mesoscale models being regularly used (Sashegyi and Madala, 1994).

While global models require initial conditions as well as vertical boundary conditions, they do not need lateral boundary conditions since they are run on the entire globe. Conversely, regional models do necessitate initial conditions as well as both lateral and vertical boundary conditions.

The initial conditions and the boundary conditions play key roles in determining the precision of the forecasts or simulation results (Sashegyi and Madala, 1994). Different initial and boundary conditions with an identical model set-up may produce quite different results. Even if the atmospheric model equations described all atmospheric motions accurately, the model solution would not reflect the actual weather condition unless the used initial and boundary conditions represented these motions correctly. Small errors in the initial conditions will enlarge during the forecasts and with time, they will contaminate the model forecasts.

4.2.5 NWP Model Classification

The technique that enables the model to provide the temporal solution of NWP model equations is known as time discretisation. In order to integrate these equations forward in time, NWP models use one of two techniques.

These techniques are either the spectral technique that was introduced by Silberman (1954), or the finite-difference technique that is based on grid points. However, most numerical models use the second technique. Based on these discretisation methods, NWP models are divided into two types: spectral models and grid-point models.

The spectral models attempt to predict the movement and variation of the amplitude of different wavelengths that compose the atmospheric geopotential height pattern. A spectral model truncates the simulation region into a number of waves that reflect atmospheric motions and this number represents the horizontal resolution of the model. The spectral method does not satisfy the representation of fields that have time-dependent lateral boundary conditions. That is why they are usually run on the entire globe rather than on a limited area to avoid the need for lateral boundary conditions.

Grid-point models integrate the nonlinear partial differential equations using the finite difference technique derived from Taylor series expansions and approximations. This expansion method is applied to these atmospheric equations in order to solve their partial derivatives, and the calculation of these equations is typically performed on 3-D computational grids.

A simulation domain is hypothetically divided by the model into a number of small grid boxes, each of which covers a small portion of the simulation region. The 3-D derivatives of the coupled atmospheric equations can then be discretised in space and in time, and approximated as differences between the model grid points on the domain. Based on the calculation of these equations, the model estimates each meteorological variable on each grid point, but physics parameterisation schemes predict sub-grid processes that cannot be directly solved by the model. Every grid point on the simulation region should represent the average condition of atmospheric motions occurring within the box around this point. The

results of the model calculation provide forecasts or estimates for the meteorological variables at each grid point in space every a specified time step. This scenario is applied at each layer in the atmosphere of the model.

Based on those criteria mentioned previously, numerical models can also be classified by another way into global (large-scale) and regional (limited-area) models. Global NWP models produce predictions for the entire planet. These models are usually sponsored by large government meteorological centres, owing to the high expense of their requirements and the enormous computational resources needed for running them.

Global NWP models are normally designed to produce short- and medium-range weather forecasts up to 15 days, with typical horizontal resolutions of 20-250 km. They are also used to provide initial conditions and boundary conditions for limited-area NWP models. There have been many operational global NWP models, such as the Global Forecast System (GFS) developed by the National Centres for Environmental Prediction (NCEP), the European Centre for Medium range Weather Forecasting (ECMWF) model developed by the European Centre for Medium-range Weather Forecasts (ECMWF), the Global Spectral Model (GSM) developed by the Japan Meteorological Agency (JMA), and the Global AnalysiS Prediction model (GASP) developed by the Australian Bureau of Meteorology.

With regard to regional NWP models, they are designed to produce weather forecasts and simulations for limited areas. The resolution of this kind of numerical models ranges from less than 1 to 30 km. The solution of limited-area models to describe and solve atmosphere activities is usually more accurate than that of global models. The additional accuracy of regional models over global models is due to a higher horizontal resolution used in these models, finer spatial and temporal resolutions of observations that provide the initial conditions for regional models, more sophisticated physics parameterisations that predict sub-grid atmospheric processes, and more detailed depiction and specification of terrain features. Limited-area

models typically obtain their initial conditions and lateral boundary conditions from forecasts and analysis of global models.

Over the last several years, regional meteorological models have experienced a significant improvement and enhanced reliability. Fine-scale atmospheric motions cannot be completely resolved neither by synoptic observations nor by global models, and therefore mesoscale limited-area NWP models are needed to provide an improved description for these small-scale atmospheric processors.

There have been many limited-area NWP models being run around the world such as the Weather Research and Forecasting (WRF-NMM) System, the Pennsylvania State University (PSU)/ the National Centre for Atmospheric Research (NCAR) numerical fifth-generation Mesoscale Model (MM5), and the High Resolution Limited Area Model (HIRLAM) developed cooperatively by several European meteorological institutes.

The WRF has been developed by a multi-institutional collaboration involving the NCAR Mesoscale and Microscale Meteorology (MMM) Division, the National Oceanic and Atmospheric Administration's (NOAA) NCEP, and Earth System Research Laboratory (ESRL), the Department of Defence's Air Force Weather Agency (AFWA) and Naval Research Laboratory (NRL), the Centre for Analysis and Prediction of Storms (CAPS) at the University of Oklahoma (OU), and the Federal Aviation Administration (FAA) (Skamarock et al., 2008). This modelling system consists of two dynamic solvers: the Advanced Research WRF (ARW) model and the WRF Non-hydrostatic Mesoscale Model (WRF-NMM). WRF-NMM will be employed to do 3-D real-data nested numerical simulations in this study, and the model will be described and discussed in more details in the following section.

4.3 WRF-NMM

4.3.1 Overview

The Numerical Weather Prediction model WRF-NMM (Janjic et al., 2001) will be used to perform about 365 3-D real-data nested weather simulations in this research. WRF-NMM is the abbreviation of the Non-hydrostatic Mesoscale Model dynamic core of the Weather Research and Forecasting system. The software of this model has been developed by NCEP, which is a part of National Weather Service (NWS) of NOAA. Some of the unreferenced description presented here has been cited and back-grounded from the WRF-NMM users webpage and its tutorials (WRF-NMM, 2009).

WRF-NMM is being frequently upgraded by NCEP/NOAA. It is run by this association for 4 times per day at 8 km grid spacing over a North American domain. The model is also used to produce forecasts for the Storm Prediction Center (SPC) on 4.5 km grid spacing for a domain covering the eastern USA.

WRF-NMM is a portable, grid-point, limited-area, three-dimensional, nested, and high-resolution atmospheric modeling system. It is a fully compressible non-hydrostatic model with a runtime hydrostatic option. The model can cover a wide range of applications across many scales ranging from few metres to thousands of kilometres. Such applications include 3-D real-time numerical simulations, meteorological forecasts, parameterisation research, and teaching purposes. The application of the current research is 3-D real-data nested numerical simulations, which will be performed to generate wind velocity data over Libya.

WRF-NMM has been selected for this research for its ability to solve mesoscale atmospheric flows at high temporal and spatial resolutions. The model has several advantages that incentivise users to adopt this system

as a reliable tool for simulating atmospheric motions over a limited region. Sophisticated physics parameterisation schemes are incorporated in WRF-NMM. Such schemes enable the model to represent fine-scale sub-grid atmospheric processes correctly. The model is efficient on extensive multiple computing platforms, so it can be run on serial processors, shared-memory or distributed-memory computers, depending on the availability of required computing resources and the desired usage of the number of processor.

4.3.2 Model Nesting

WRF-NMM has the ability to support multiple nesting procedures that allow the model to focus the calculations on a specific area with finer horizontal resolutions and smaller time steps. This technique can eliminate the need for implementing high-resolution simulations on a wide area, and it reduces the computer resources with a little or no accuracy penalty in the forecasts.

A fine domain can be configured anywhere inside the coarse domain, but it should be at least 5 computational grid points far from the boundaries of the coarse domain. Both the grid spacing and time step of the fine domain must be equivalent to one third those of the coarse domain, meaning that every third grid point on the fine domain coincides with a point on the coarse domain.

The coarse domain in WRF-NMM can handle more than one fine domain, which cannot have more than one parent domain. The model also supports telescoping nesting where the fine domain can have finer domain inside it.

4.3.3 Model Hybrid Vertical Coordinate

WRF-NMM uses (x,y,σ) coordinate system and the terrain representation in this model differs from most other previous numerical atmospheric models. The WRF-NMM equations are formulated using the hybrid

terrain-following mass-based pressure-sigma vertical coordinate (σ) [Figure 4.1], which was introduced by Arakawa and Lamb (1977).

This coordinate system provides very good representations for the features of the terrain of the simulation region. The vertical coordinate is divided so that the sigma coordinate is applied in the lower layers of the atmosphere, whereas the hydrostatic pressure coordinate is applied in the upper atmosphere (Janjic et al., 2001, Janjic, 2003). The model uses unequally distributed vertical levels, whose number along with the sigma-pressure interface value is runtime options. The model sigma-pressure vertical coordinate is defined in terms of hydrostatic pressure by the following relation:

$$\sigma = \frac{(\pi - \pi_t)}{\mu} \tag{4.1}$$

Here, π stands for the hydrostatic pressure, π_t represents the hydrostatic pressure at the top boundary of the atmosphere of the model, π_s refers to the hydrostatic pressure at the bottom boundary of the atmosphere of the model, and μ is the hydrostatic pressure difference between the surface and the top of the atmosphere of the model ($\mu = \pi_s - \pi_t$). Note that $\sigma = 1$ at the bottom of the model (surface) and decreases vertically until it becomes $\sigma = 0$ at the top boundary of the model.

The sigma-pressure coordinate system conforms to the topography. In this system, the vertical layers of the atmosphere are divided into two main regions based on their discretisation. The upper atmosphere is purely discretised by pressure while the bottom atmospheric layers are completely represented by sigma coordinate. This procedure allows the model to provide better representations for the topography. It is found that the topographic features have substantial effects on atmospheric motions as well as the solution of numerical models (Cavaleri and Bertotti, 2006, Miglietta and Rotunned, 2009).

Figure 4.1 shows that in the pressure-sigma hybrid coordinate unlike in pressure coordinate, sigma levels coincide with the terrain topography. Sigma levels are therefore sharply sloped over steep terrains and hence heterogeneous grounds are not intersected by them (Janjic et al., 2005). In other words, the vertical levels in pressure coordinate intersect the terrain whereas in sigma-pressure hybrid coordinate system, vertical sigma levels are parallel to the structure of the topography.

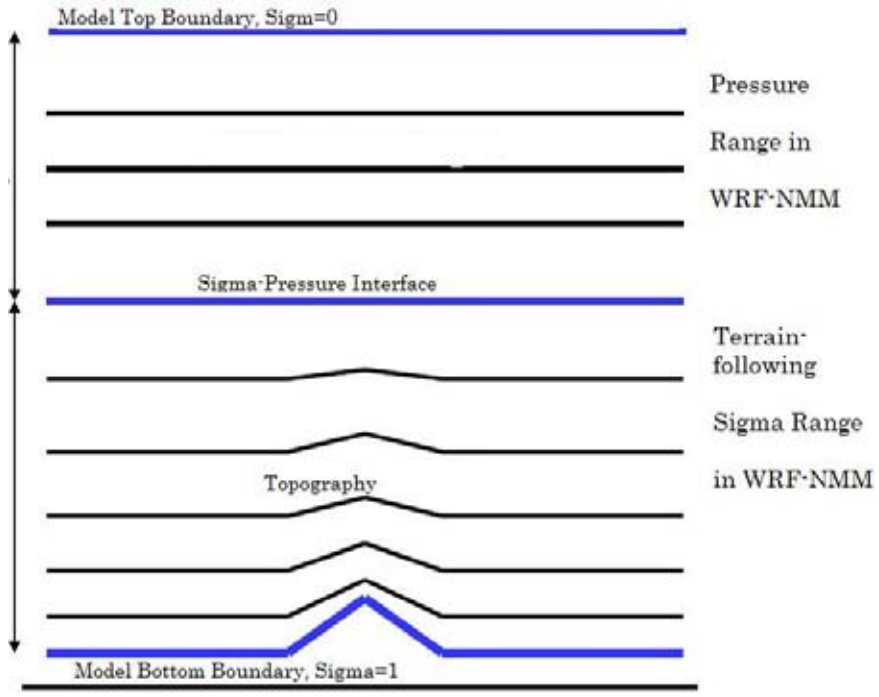

Figure 4.1: A schematic representation of vertical levels in hybrid sigma-pressure vertical coordinate.

The conservation of mass in hybrid coordinate system enhances the near-ground vertical resolution, and thus allows the model to provide reliable and accurate descriptions of atmospheric processes occurring within the mixed planetary boundary layer without computational penalties of using many fixed vertical levels (Janjic et al., 2001, Addis, 2005). The sigma-pressure hybrid coordinate uses uncomplicated boundary conditions, and the advection of heat and moisture properties are solved at constant and shallow atmospheric layers. This enables the model to depict fine-scale activities, such as heat and moisture fluxes, surface wind profile, and turbulent flows, taking place in the atmospheric boundary layer.

Because the wind field in numerical weather forecasting models is estimated based on the pressure gradient force, it is straightforward for the model to calculate the pressure gradient force in pressure coordinate system. On the contrary, in sigma coordinate the calculation of the wind may give rise to errors over a sharp topography, since the terrain slopes must be included in the model calculation (Mesinger and Black, 1992).

In spite of that, as the hydrostatic pressure coordinate is used in the upper layers of the atmosphere, the error resulting from sloping is limited to the lower half of atmospheric layers (Janjic et al., 2005). The sigma coordinate often introduces the largest errors at higher altitudes around the tropopause, and accordingly the most critical problems due to sigma sloping surface are eliminated (Janjic et al., 2005). Errors from the calculation of pressure gradient force in the stratosphere can be reduced by positioning the sigma-pressure interface in the stratosphere, and almost removed if the sigma-pressure interface is located just below the tropopause (Simmons and Burridge, 1981).

While the sigma hybrid vertical levels of the fine domain coincide with those of the coarse domain, the height and pressure levels of the fine domain differ from those of the coarse domain since they see different terrains owing to their resolutions (Janjic, 2003).

4.3.4 Governing Equations

Like any NWP model, WRF-NMM is based on a set of nonlinear partial differential equations that describe and approximate the hydrodynamics of atmospheric flows. The prognostic equations are configured with geophysical parameters suitable for the spheroid shape of the earth. These parameters oblige these equations to obey heat, momentum, and moisture conservation laws, which are applied to any existing parcel of air.

The governing equations discretised and solved by WRF-NMM comprise the equation of the conservation of momentum, the thermodynamic energy

equation, the mass continuity equation, the equation of state, and the hydrostatic equation. The model equations are similar to Euler equations described by Laprise (1992) but they are extended and improved by Janjic et al. (2001). The model equations (Janjic et al., 2001, Janjic and Pyle, 2009) include:

❖ The equation of conservation of motion (momentum equation):

$$\frac{\partial \mathbf{V}}{\partial t} = -\mathbf{V}.\nabla_\sigma \mathbf{V} - \dot{\sigma}\frac{\partial \mathbf{V}}{\partial \sigma} - (1-\varepsilon)\nabla_\sigma \Phi - \alpha \nabla_\sigma p + f\mathbf{k}\times\mathbf{V} \qquad (4.2)$$

❖ The conservation of heat (thermodynamic energy) equation:

$$\frac{\partial T}{\partial t} = -\mathbf{V}.\nabla_\sigma T - \dot{\sigma}\frac{\partial T}{\partial \sigma} + \frac{\alpha}{C_P}\left[\frac{\partial p}{\partial t} + \mathbf{V}.\nabla_\sigma p + \dot{\sigma}\frac{\partial p}{\partial \sigma}\right] \qquad (4.3)$$

❖ The mass continuity equation used in the hydrostatic models:

$$\frac{\partial \mu}{\partial t} + \nabla_\sigma.(\mu \mathbf{V}) + \frac{\partial(\mu \dot{\sigma})}{\partial \sigma} = 0 \qquad (4.4)$$

❖ The equation of vertical motion:

$$\frac{\partial p}{\partial \pi} = 1 + \varepsilon \qquad (4.5)$$

Equation 4.5 represents the relationship between the hydrostatic and the non-hydrostatic pressure.

❖ The hypsometric equation:

$$\frac{\partial \Phi}{\partial \sigma} = -\mu \frac{RT}{p} \qquad (4.6)$$

❖ The non-hydrostatic continuity equation:

$$w = \frac{1}{g}\frac{\partial \Phi}{\partial t} = \frac{1}{g}\left[\frac{\partial \Phi}{\partial t} + \mathbf{V}.\nabla_{\sigma}\Phi + \dot{\sigma}\frac{\partial \Phi}{\partial \sigma}\right] \tag{4.7}$$

Wherein:

$\alpha = \frac{RT}{p}$ (The equation of state),

and $\varepsilon = \frac{1}{g}\frac{dw}{dt}$

Where:

σ is sigma level, $\dot{\sigma}$ stands for the vertical velocity in sigma coordinates, Φ is the geopotential height, f is the Coriolis parameter, t represents the time, R is the gas constant for dry air, g is gravity, T stands for temperature, p represents the pressure, C_P is the specific heat at constant pressure, α represents specific volume, w stands for the time rate of the change of geopotential height following the motion of a fluid parcel, and ε is the ratio of the vertical acceleration and gravity.

4.3.5 Model Dynamics

WRF-NMM is based on a new technique. This technique is the relaxation of the hydrostatic dynamics in a hydrostatic model using hydrostatic pressure as the vertical coordinate allowing the model to include the non-hydrostatic motions that are already available in previous models (Janjic et al., 2001, Janjic, 2003).

Taking into consideration the separation of omega into two parts, the thermodynamic equation in the model is split into two parts: the hydrostatic contribution and non-hydrostatic contribution. One part is

solved when the none-hydrostatic module is turned on, while the other part of the equation is solved if the model is run on the hydrostatic mode.

The following shows how the thermodynamic equations in the model are split:

$$\frac{\partial \mathbf{V}}{\partial t} = -\mathbf{V}.\nabla_{\sigma} T - \dot{\sigma}\frac{\partial \mathbf{V}}{\partial \sigma} + \frac{\alpha}{C_P}\left[\omega_1 + \omega_2\right] \tag{4.8}$$

In the first part, the thermodynamic equation is reduced to the hydrostatic equation for vanishing ω :

$$\left(\frac{\partial T}{\partial t}\right)_1 = -\mathbf{V}.\nabla_{\sigma} T - \dot{\sigma}\frac{\partial T}{\partial \sigma} + \frac{1}{C_P}\alpha\,\omega_1 \tag{4.9}$$

Where:

$$\omega_1 = (1+\varepsilon)\frac{\partial \pi}{\partial t} - \mathbf{V}.\nabla_{\sigma} p + (1+\varepsilon)\dot{\sigma}\frac{\partial \pi}{\partial \sigma} \tag{4.10}$$

In the other part, the thermodynamic equation is for pure hydrostatic motions:

$$\left(\frac{\partial T}{\partial t}\right)_2 = \frac{1}{C_P}(\alpha\,\omega_2) \tag{4.11}$$

Where:

$$\omega_2 = \frac{\partial p}{\partial t} - (1+\varepsilon)\frac{\partial \pi}{\partial t} \tag{4.12}$$

The add-on none-hydrostatic dynamics improves the reliability of the model since it eliminates the need for linearisation, and also it directly considers the vertical motions without any approximation (Janjic et al., 2001). With the inclusion of non-hydrostatic dynamics, the advantageous characteristics contained in the hydrostatic framework are maintained

within the range of consistency of the hydrostatic approximation.

It is emphasised that the reliability of the hydrostatic approximation used in NWP models to represent atmospheric processes is diminishing, as the horizontal resolution is becoming finer (Janjic, 2003, Janjic et al., 2005). Moreover, running the model using the non-hydrostatic dynamics permits numerical model users to do simulations of small grid spacing without extensive computational efforts, although this may increase the computational costs of computer time and memory by 20% of those needed by the hydrostatic dynamics (Janjic et al., 2001, Janjic et al., 2005). Still, the extra costs should be accepted due to the widespread applications of the non-hydrostatic model even at medium spatial resolutions, and also no additional boundary conditions are required for real-data simulations (Janjic, 2003).

The incorporated non-hydrostatic module permits weather forecasters to perform straightforward comparisons between non-hydrostatic and hydrostatic results, since the new introduced non-hydrostatic component can be switched on or off depending upon the spatial resolution of the simulation.

Non-hydrostatic motions are often distinguished by numerical models at horizontal resolutions less than 10 km, and become important at grid spacing lower than 1 km. Non-hydrostatic numerical models tend to be effective and computationally stable at all resolutions although at a resolution of 8 km the influence of non-hydrostatic dynamics may be weak (Janjic et al., 2001). Yet, several comparisons between hydrostatic forecasts and non-hydrostatic forecasts have illustrated that there are considerable differences between these two dynamics even at a resolution of 8 km (Janjic, 2003).

All terms in WRF-NMM use the same time step. A number of first and second order quantities, including energy and entropy, is conserved (Janjic, 1984). The model uses the Adams-Bashforth scheme for non-split

horizontal advection of the basic dynamical variables and for Coriolis force, the forward-backward scheme for horizontally propagating fast waves, the implicit scheme for vertically propagating sound waves, explicit iterative for Turbulent Kinetic Energy (TKE) and water species called every second time step, and the Crank-Nicholson scheme (Crank and Nicolson, 1947) for vertical advection of heat (Janjic et al., 2003). The diffusion in WRF-NMM is split into a lateral diffusion and vertical diffusion.

The equations of WRF-NMM are solved on the Arakawa E-grid staggering introduced by Arakawa and Lamb (1977) and discussed by Janjic (1984). Arakawa E-grid uses the mass staggering points **(H)** and wind staggering points **(V),** as demonstrated in Figure 4.2. Terrestrial input datasets in the model are interpolated to every grid point using Arakawa E-grid. Conversely, meteorological parameters are interpolated differently since the wind components are interpolated to **V** staggering points, while other meteorological fields, such atmospheric temperature and pressure, are all interpolated to each **H** staggering points.

As shown in Figure 4.2, the diagonal distance **(D)** between either two neighboring wind points or two mass points represents the conventional spatial grid spacing of the model. The east-west distance **(dx)** and north-south distance **(dy)** between any mass point and the adjacent wind point are computed from **D** when configuring the domain and specifying the model spatial grid spacing.

The model utilises mass variables and wind variables to perform the prediction. The prognostic wind variables are **U** and **V** components of wind whilst predictive mass variables consist of the depth of hydrostatic pressure being the difference between the top pressure and the transforming pressure, non-hydrostatic pressure, total cloud water condensate ,sensible temperature, specific humidity, and TKE (Janjic and Pyle, 2009).

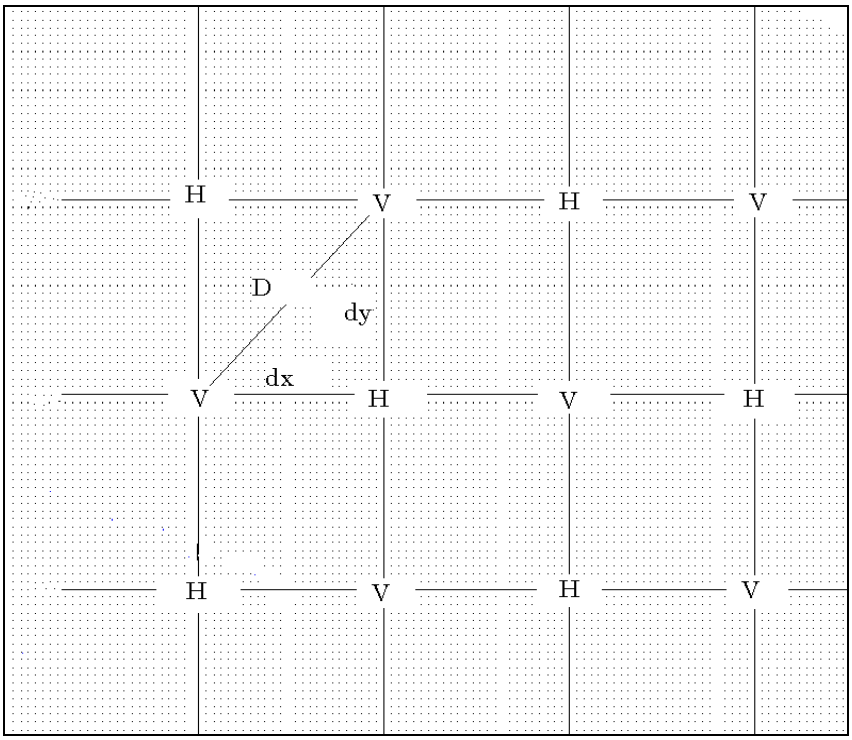

Figure 4.2: A diagram representation of Arakawa E-grid staggering.

4.3.6 Model Initial and Boundary Conditions

As discussed in Subsection 4.2.4, the initial conditions supply the model with information about the initial status of the atmosphere at time step = 0, whereas the boundary conditions provide the model with details about the meteorological systems happening near the boundaries of the model domain. WRF-NMM uses initial and lateral boundary conditions from forecasts and analyses of another global model.

Specified lateral boundary conditions known also as the relaxation boundary conditions will be used in this study's simulations. The specified lateral boundary conditions are designed mainly for real-data simulations. They are based on the understanding of atmospheric processors and accordingly the processor is forced to comply with specific conditions (Skamarock et al., 2008). East, west, north, and south boundaries, all will use specified boundary conditions in this research.

In nested model runs, the fine domain normally attains the required information such as the boundary conditions and initial conditions from the coarse domain. WRF-NMM supports one-way and two-way stationary nesting depending on the configuration of the model, but in this study two-way nesting will be used. In one-way nesting strategy, the coarse domain provides the solutions to the fine domain but the fine domain does not re-feed any information to the coarse domain. In contrast, in two-way nesting procedure the fine domain obtains information from the coarse domain and at the same time re-feeds the solutions to the coarse domain.

The boundary conditions of the fine domain are updated at each time step of the coarse domain, and the forecasts of the outmost rows and columns of the fine domain are constrained to be the same as those of the coarse domain. The forecasts of third rows and columns of the nested domain are not exactly identical to those of the coarse domain but their prediction calculations are performed internally within the fine domain. The solutions of the second rows and columns are a combination of the solutions of the first and the third rows and columns (WRF-NMM, 2009).

The model top boundary ($\sigma = 0$) conditions can be expressed as (Janjic and Pyle, 2009):

$$\dot{\sigma} \equiv \frac{\partial \sigma}{\partial t} = 0,$$

$$p - \pi = 0$$

Yet, the model surface boundary ($\sigma = 1$) conditions can be expressed as:

$$\dot{\sigma} \equiv \frac{\partial \sigma}{\partial t} = 0,$$

$$\frac{\partial (p - \pi)}{\partial \sigma} = 0$$

4.3.7 Model Physical Parameterisations

Physical parameterisations are introduced in NWP models so as to describe and solve the effects of important sub-grid atmospheric processes that cannot be solved directly by the model (Uliasz, 1994). These parameterisations simulate the sub-grid fine-scale atmospheric activities based on other variables, which can be estimated directly by the model. As an example, cloud and solar radiation parameterisations included in WRF-NMM are designed to enable the model to predict the effects of clouds and solar radiation using other weather fields, because the model cannot directly estimate the effects of cloud and radiation (Uliasz, 1994).

Sophisticated physics parameterisations are incorporated in the framework of WRF-NMM and these parameterisations can be compiled in many ways. They comprise microphysics, surface layer physics, land/water-surface layer physics, cumulus convection, longwave radiation physics, shortwave radiation physics, and planetary boundary layer turbulence physics.

Each one of these physics parameterisations supports several schemes. However, only the schemes that will be used in this study's simulations are discussed here.

- Microphysics parameterisation will use the Ferrier scheme (Ferrier et al., 2002). This scheme is simple and efficient and includes prognostic mixed-phase processes. It explicitly predicts the advection of total water condensation, the cloud water, and the ice-mixing ratio. During the advection of properties, this scheme assumes that the fractions of water and ice are fixed within the computational range. The mixing ratio of clouds attempts to diagnose liquid and solid precipitations, which are presumed to fall to the surface in a particular time step. However, this scheme has been recently improved so that the ice saturation is assumed when the temperature is colder than -30ºC rather than -10ºC.

- The cumulus convection in this study's simulations will be parameterised with the Betts-Miller-Janjic (BMJ) scheme. This scheme is derived from the Betts-Miller convective adjustment scheme, which was based on the instantaneous relaxation solutions of humidity and temperature parameters towards semi-equilibrium thermodynamic structures (Betts, 1986, Betts and Miller, 1986). Several important improvements have been introduced to the BMJ scheme. The atmospheric parameters that define the moisture and relaxation time in the deep convection are variables and dependent on "the cloud efficiency". The cloud efficiency modifies the Betts-Miller saturated profile so the post-convective profile can be unsaturated, and it can provide an extra freedom range in establishing the profiles of heat and moisture (Janjic, 1990, Janjic, 1994, Janjic, 2000). The cloud efficiency is a function of the entropy change and precipitation over the time step, and the average cloud temperature. Shallow cumulus convective adjustment is a crucial part of the parameterisation, and in the shallow convection profile the moisture is defined from the requirement that the entropy change is small and nonnegative (Janjic, 1994, Janjic, 2000).

- Longwave radiation will be parameterised with the Rapid Radiative Transfer Model (RRTM) scheme (Mlawer et al., 1997). The basis of this scheme is derived from the line-by-line transfer model. The RRTM scheme is an accurate spectral-band k-distribution scheme that calculates the longwave atmospheric radiative clear-sky fluxes and heating/cooling rates. Pre-set tables are used in order to provide effective solutions for longwave fluxes resulting from water vapour, CO2, trace gazes, ozone, and cloud optical thickness. The calculation of the effects of longwave processes is carried out by splitting the longwave region into multiple-band ranges based on the homogeneousness of contributing microphysics classes and radiative transfer properties. The RRTM scheme uses linear interpolation to determine all physical quantities. This feature enables the model to adopt micro-layering

procedures.

- Shortwave radiation will be solved by means of the Dudhai scheme (Dudhia, 1989). The downward integration of shortwave radiation and flux in this scheme is performed based on the effect of solar zenith angle, which reduces the downward component of solar radiation and increases the travelling distance of bands. The scheme integration also takes into account the affects of clear-sky scattering, water vapour absorption, cloud albedo, and cloud absorption. Bilinear interpolation is done on cloud scattering or albedo and absorption using lookup tables for clouds (Stephens, 1978). If the Dudhai scheme is used in high-resolution numerical simulations, the effects of sloping and shadowing may be described and considered in the model solution.

- Surface layer processes will be described by the Monin-Obukhov Similarity scheme. The foundation of this scheme is the similarity theory (Monin and Obukhov, 1954) and was modified and improved by Janjic (1996b) and Janjic (2002). Surface layer schemes deal with the advection of heat and the fluxes of momentum and moisture from the model surface to the boundary layer top. The surface heat, moisture, and momentum fluxes in this scheme are estimated using a series of iterations. The Monin-Obukhov Similarity scheme does the parameterisation of viscous sub-layers over both the terrain and water. Over terrains, the effects of the viscous sub-layer are considered through variable roughness heights for temperature and humidity (Zilitinkevich, 1995). Yet, over water surfaces, an explicit parameterisation is implemented on these viscous sub-layers (Janjic, 1994). In order to eliminate singularities caused by the instability of the surface layer and vanishing wind, the corrections made by Beljaars (1994) are taken into account. Note that this scheme should be used and run along with the Mellor-Yamada-Janjic (MYJ) Planetary Boundary Layer (PBL) scheme.

- The land/water surface processes will be parameterised with the Noah Land Surface Model (Noah-LSM). The scheme represents the land/water-atmosphere interactions by means of four soil temperature and moisture layers. It predicts land surface parameters, including soil temperature and soil moisture in these four layers, skin temperature, frozen temperature, soil draining, evapotranspiration, fractional snow cover, and canopy moisture. The Noah-LSM also supplies the PBL with heat and moisture fluxes. The spatial distributions of vegetation and soil categories determine the vegetation and soil features such as minimum stomatous friction and soil thermal conductivity (Chen and Dudhia, 2001a). The thermal and hydraulic conductivities are sensitive to soil moisture variations and this sensitivity affects the process of the advection of water soil. The ratio of energy fluxes from one medium to another by latent and sensible heats is correctly captured because the scheme provides consistent solutions of the latent and sensible heat fluxes for the PBL scheme (Chen and Dudhia, 2001b). Several used high-resolution parameters that characterise the land surface state enhance the diagnosis of the characteristics of land, vegetation, and water, and in turn solve mesoscale land surface forcing processes (Chen and Dudhia, 2001a). This is crucial for the PBL progress, mesoscale atmospheric flows, and cloud development (Avissar and Pielke, 1989, Chen and Avissar, 1994).

- The PBL processes will be predicted by the MYJ scheme. The MYJ scheme is based on a non-singular implementation of the Mellor-Yamada Level 2.5 turbulence closure model (Mellor and Yamada, 1982). It is an one-dimensional prognostic scheme that simulates the structure of the TKE advection in the PBL and in the free atmosphere (Janjic, 1990 , Janjic, 1996a, Janjic, 2002). The upper limit of the representation of atmospheric turbulent structures is proportional to the TKE, the shear, and the bouncy of the dominant flow. In the unstable range, the functional form of the upper limit is derived from

the requirement that the TKE production being non-singular in the case of growing turbulences. On the other hand, in the case of stable range the upper limit is derived from the requirement that the ratio of the variance of the vertical velocity deviation and TKE cannot be smaller than that of the corresponding to the regime of vanishing turbulences. The production/dissipation differential equation of TKE is integrated and solved by the iterative method (Janjic, 1996a, Janjic, 2002).

4.3.8 Model Components

Figure 4.3 illustrates the schematic diagram of the data flow in WRF-NMM modeling system (WRF-NMM, 2009). WRF-NMM mainly comprises three major sequential components: the WRF Pre-processing System (WPS), WRF-NMM dynamic solver, and WRF Post-Processor (WPP). The WRF-NMM dynamic solver in conjunction with the other components performs the numerical simulation.

WPS is configured to embrace three successive programs, which are *geogrid, ungrib,* and *metgrid.* The combined function of these programs is to set up the input data for the initialisation program.

The dynamic solver of the model is the fundamental component of the modeling system because it encompasses two important programs. These programs include the data initialisation program, which produces initial conditions and boundary conditions for the model, and the numerical integration program, which does the forecast or simulation calculation.

4.4 Summary

This chapter has discussed the discipline of numerical weather forecasting, and WRF-NMM. NWP is not a new science even though in recent years it has developed significantly to include sophisticated physics parameterisation schemes. Based on the method of discretisation of the model equations, NWP models are divided into spectral models and grid-

point models. Yet, the scale and the resolution of NWP simulations categorise numerical forecasting models into large-scale models and mesoscale regional models. One of the well-known regional mesoscale numerical models is WRF-NMM of NCEP. WRF-NMM is non-hydrostatic with a runtime option being hydrostatic, and it uses the hybrid sigma-pressure vertical coordinate. The model solves a set of compressible partial differential equations, and supports an enormous package of physics parameterisation schemes. WRF-NMM also supports multiple one- and two-way nesting that allows forecasters to do very high-resolution simulations. It has three main components that perform a weather simulation or forecast. WRF-NMM will be used to simulate the wind conditions over Libya. The detailed methodology followed in this study will be presented and explained in the following chapter.

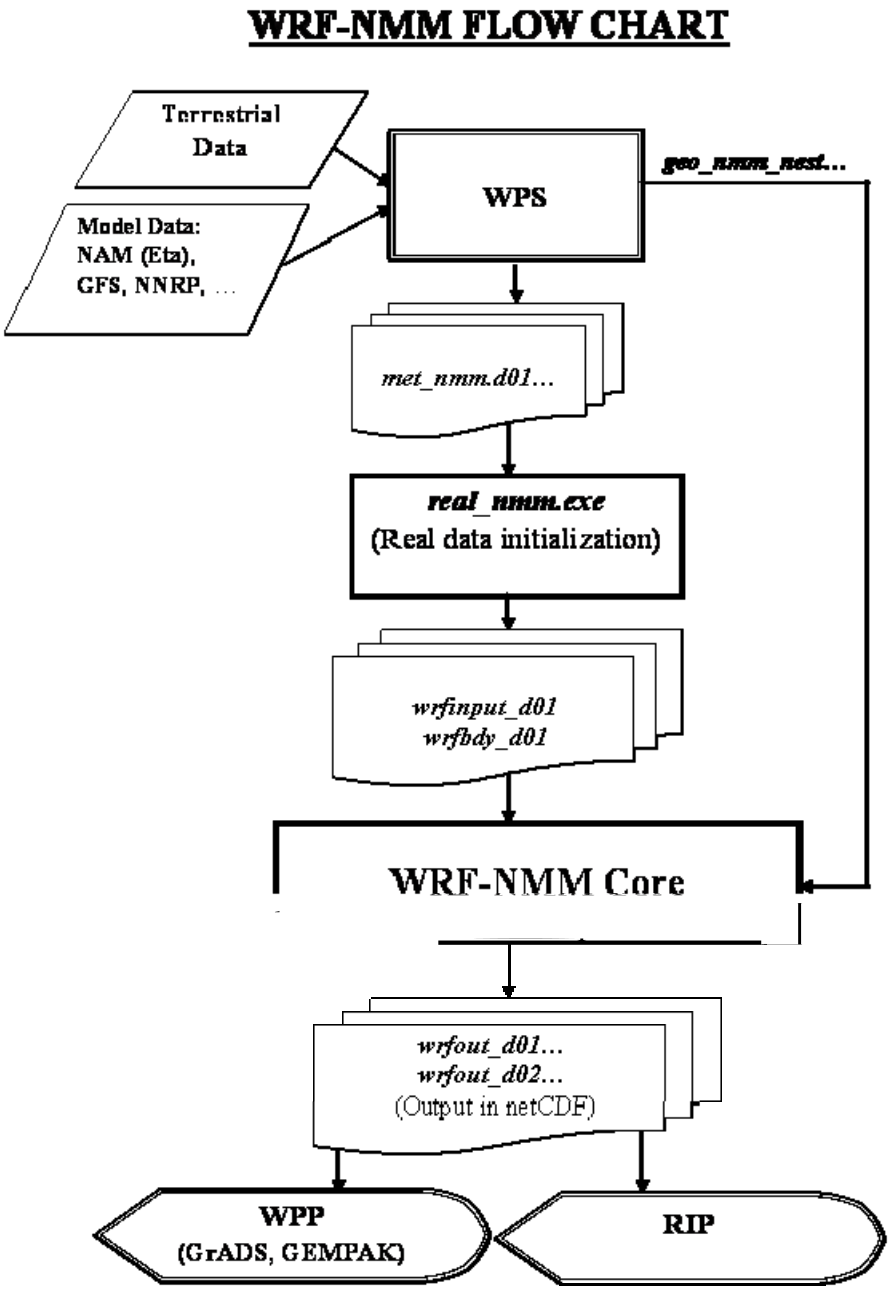

Figure 4.3: A schematic chart of the data flow in WRF-NMM.

Chapter 5

Methodology

5.1 Introduction

The regional wind resource evaluation for wind power applications requires high temporal and spatial resolution wind velocity data. Libya has inadequate wind velocity measurements that cannot satisfy the assessment of wind energy potential throughout the country. In this study, the scarcity of wind observations was overcome by using 3-D real-data high-resolution nested numerical weather simulations that generated hourly wind velocity data throughout Libya and the surrounding regions. The Non-hydrostatic Mesoscale Model of the Weather Research and Forecasting system (WRF-NMM) was employed to do these simulations.

This chapter details the methods employed in this study. Section 5.2 gives very brief information about the used resources, and Section 5.3 shows the configuration of the model domains. The model input data are identified in Section 5.4, and Section 5.5 explains the model testing. The model set up is summarised in Section 5.6, while Section 5.7 illustrates the model runs and data flow in the model. Section 5.8 discusses the preparation of the model outputs for wind power investigation. Lastly, Section 5.9 provides a

discussion about estimating the possible power available over the country based on the simulation results.

5.2 Used Resources

All simulations were carried out using version 3.0 of WRF-NMM. The software was obtained from the WRF-NMM website (WRF-NMM, 2009). The model was configured to support parallel runs on multiprocessors for real-time data case using multiple nesting simulations. After compiling the model using PGI compiler, the WPS and WPP were also obtained from the WRF-NMM website, both of which were compiled using the same compiler used to compile the model.

All model runs were executed on the Linux operating system using a cluster of machines, which is one of the computation resources of the UNSW School of Mathematics & Statistics computing centre. This cluster is called Matrix whose Hardware comprises one head node and about 23 other computing nodes, each of which has 4 cores and 4GB of RAM. It contains extensive numerical libraries, a queuing system, and several compilers that are needed to compile and run numerical models as well as to schedule job submissions. A huge data storage space was needed in this research to store the inputs and the outputs of the model. Data storage of about 3 TB was required.

5.3 Model Domain Localisation

After compiling the model, a few test runs on the default region were performed using the test-case data provided by the WRF community. The purpose of doing this was to ensure that the source code had been compiled correctly with the selected compilation options, and all required libraries had communicated together properly.

When it was demonstrated that the test runs had produced realistic results, the WRF Domain Wizard graphical user interface was used to

configure, define, and localise the model on Libya and the surrounding regions. The model was localised on two domains being the parent (coarse) domain and one fixed nested (fine) domain inside the coarse one. The fine domain had higher temporal and horizontal resolutions, and it was focused on Libya in order to predict mesoscale atmospheric processes affecting the wind condition over the nation more accurately. Both model domains were formulated in rotated Latitude/Longitude coordinate system, which is the only map projection supported by WRF-NMM.

The coarse domain covered a wide area including the entire Libyan territory and the nearby regions whereas the fine domain was fixed and located on the country totally inside the coarse domain. The coarse domain covered the area between the longitudes of 0.825° W and 32.887° E, and the latitudes of 14.98° N to 44.62° N centered at 31° N and 16° E, while the fine domain was bounded by the longitudes of 7.581° E to 26.325° E and the latitudes of 21.716° N to 37.524° N [Figure 5.1].

The numerical grid representing the coarse domain had about 345×313 computational grid points distributed over an area of 3586 km EW × 3223 km NS, and that representing the high-resolution domain had about 569×495 grid points distributed over area of 1943 km EW × 1758 km NS.

5.4 Input Data

Both domains ingested same datasets although the resolution was different. As any limited-area NWP model, WRF-NMM requires initial conditions, and lateral and vertical boundary conditions data. WRF-NMM necessitates two types of input data: static surface geographical datasets and time-dependent meteorological data covering the simulation region. The input data were obtained from the model website and stored in gridded binary (GRIB) format, and they needed a storage space of about 500 GB during the model runtime (WRF-NMM, 2009).

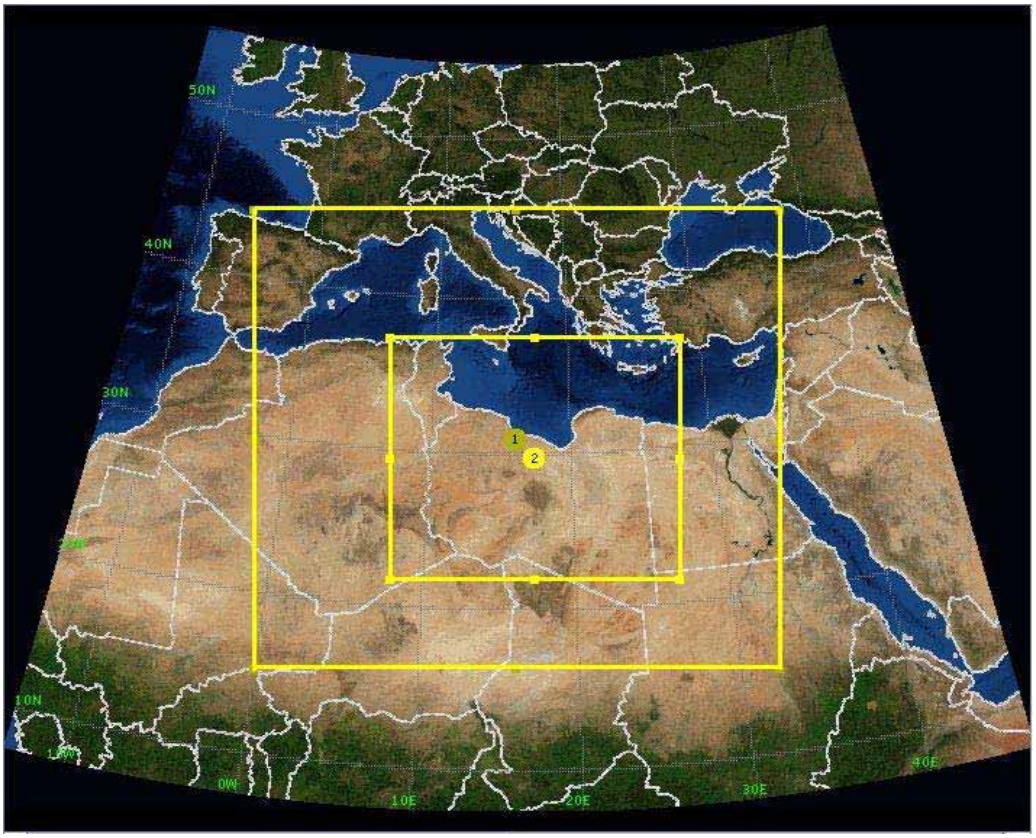

Figure 5.1: The model domains used in the simulations.

The static terrestrial geographical data utilised by the model consisted of soil categories, land use categories, terrain height, annual mean deep soil temperature, monthly vegetation fraction, monthly albedo, maximum snow albedo, and slope category. The terrestrial geographical data seen by the model over the coarse domain had a resolution of 2 minutes, which varies from about 3.5 to 4 km depending on the latitudinal location, whereas those seen by the model over the fine domain had a resolution of 30 seconds being equivalent to about 900 m.

Meteorological data that provided the initial conditions and boundary conditions for the model came from the lower-resolution spectral Global Forecast System (GFS). The input GFS data had a horizontal resolution of 0.5° latitude by 0.5° longitude equivalent to about 55 km. These datasets were for the whole year of 2007 and contained mainly atmospheric pressure, air temperature, geopotential height, specific humidity, and wind velocity.

The numerical experiments implemented in this research were 3-D real-data simulations, and they were not forecasts. That is why it is of importance to note that the used three-hourly GFS data were composed of 6-hourly analysis data at four main synoptic hours of 0000, 0600, 1200 and 1800 Coordinated Universal Time (UTC), and 6-hourly forecast data at 0300, 0900, 1500 and 2100 UTC. The GFS analysis data were mostly made up of meteorological observations, whereas the forecast data came from the GFS prediction based on these analysis data.

The initial conditions of all model simulations came totally from the GFS analysis data (1800 UTC), while the boundary conditions used a combination of both analysis and forecast GFS data. It could have been possible to use only 6-hourly analysis data but for more reliability, forecast data were considered to assist analysis data. That is, the use of 6-hourly forecast data in conjunction with the analysis data was a better solution along the model boundaries than using 6-hourly analysis data only.

The used observed real data (analysis data) along with forecast data were used for each run and each model simulation used 14 GFS data files. The 1st data file (1800 UTC) was from analysis data, 2nd file (2100 UTC) came from forecast data, 3rd data file (0000 UTC) was from analysis data, and so on until the 14th file (1200 UTC) that came from analysis data. This procedure was crucial for the simulation accuracy because it constrained the model to stay in the right track during the computation of its equations. Even if there existed errors in GFS forecast data, 6-hourly real analysis data would prevent the model from the deviation during its calculation. There was a 3-hour difference between each two successive input analysis data and forecast data, so if the model attempted to depart slightly from the actual meteorological condition of the atmosphere, it would not continue to depart as the next real analysis data would force it to return to the correct path.

5.5 Model Testing

Before the series model runs of actual simulations, several test runs were conducted throughout August on the actual domains rather than on the default test-case domain. This was done in order to

- Locate the boundaries of the model domains on the regions where there is no steep topography although it was not possible to avoid this problem completely because there is a series of mountains (the Tebisti Mountains) on the southern boundary. These mountains caused the fine domain to be cut at the southeastern boundary of the country.

- Compare different simulation results with different model boundaries in an attempt to determine as accurately as possible the most favorable locations for the boundaries. These simulations were done also to select the appropriate physical parameterisation schemes that could generate realistic results without isolations. As a start point, the model was tested using the default parameterisation schemes, yet there were obvious isolations in the simulation results. Thus, several simulations with different set of physics schemes were carried out to as accurately as possible select the most suitable schemes. The set of parameterisation schemes selected to predict sub-grid processes in the simulations of this research are summarised in Table 5.1, and detailed discussions about these schemes are provided in Chapter 4.

- Determine the optimal initialisation time for the model simulations, and eventually the considered initialisation time of the integration was 1800 UTC.

- Examine the integration time of the simulations and it was selected to be 42 hours. At the beginning, the model was tested to do the integration for 48 hours but it was just a waste of CPUs to run further.

5.6 Model Set up

Once the model was properly tested and checked, it was configured with the favorable configuration for the simulations. The atmospheric model had 38 vertical sigma levels, and the pressure level in which the model hybrid coordinate transfer from sigma coordinate to pressure coordinate (sigma-pressure interface) was set to 420 hPa in order to include high terrains within sigma coordinate. The bottom boundary of the model atmosphere is by default at the earth's surface, but its top boundary was located at the pressure level of 50 hPa.

The horizontal resolution was about 15 km x 15 km for the coarse domain, and 5 km x 5 km for the fine domain. The vertical resolution varied according to the atmospheric depth because it is represented by the mass-based hybrid sigma-pressure coordinate following the topography. The model performed the calculation on each computational grid point every 30 seconds on the coarse domain and every 10 seconds on the fine domain. For each run, the model integration was simultaneously performed on both the coarse domain and the fine one. The spatial and temporal resolutions along with the model configuration did not differ in any of the simulations. The set up options of the model simulation runs are summarised in Table 5.1.

Table 5.1: Model set up options for the simulations.

MODEL SETUP/FEATURES	OPTION
WRF dynamic solver	WRF Non-hydrostatic Mesoscale Model (WRF-NMM)
Number of model domains	Two domains including the coarse domain and the fixed fine domain
Application	Three-dimensional real-time simulation
Number of runs	365
Feed back	Two-way nesting
Model centre (latitude, longitude)	31° N, 16° E for the parent domain
Model grid dimension	345×313 for the coarse domain 569×495 for the fine domain

Table 5.1(continued): Model set up options for the simulations.

MODEL SETUP/FEATURES	OPTION
Map projection	Rotated Latitude-Longitude for both domains
Model horizontal grid spacing (model horizontal resolution)	About 15 km for the coarse domain About 5 km for the fine domain
Initialization time Integration time	1800 UTC 42 hours
Model vertical levels	38 sigma levels for both domains 1.000, 0.994, 0.983, 0.968, 0.950, 0.930, 0.908, 0.882, 0.853, 0.821,0.788, 0.752, 0.715, 0.677, 0.637, 0.597, 0.557, 0.517, 0.477,0.438, 0.401, 0.365, 0.332, 0.302, 0.274, 0.248, 0.224, 0.201, 0.179, 0.158, 0.138, 0.118, 0.098, 078, 0.058, 0.038, 0.018, 0.000
Integration time-step (Model temporal resolution)	30 seconds for the coarse domain and 10 seconds for the fine domain
Top model pressure	50 hPa for both domains
Sigma-Pressure interface	420 hPa for both domains
Model dynamics mode	Non-hydrostatic module
Lateral boundary condition option	Specified for the coarse domain
Run platform	Parallel on a distributed memory using 2 processors
Microphysics parameterisation	Ferrier (new Eta) microphysics scheme for both domains
Surface layer physics	Eta similarity based on Monin-Obukhov for both domains
Land/water-surface layer physics	Noah Land Surface Model (Noah-LSM)for both domains
Cumulus parameterisation physics	Betts-Miller- Janjic (BMJ) scheme for the coarser domain and no cumulus for the fine domain
Long wave Radiation physics	Rapid Radiative Transfer Model (RRTM scheme) for both domains
Short wave radiation physics	Dudhia scheme for both domains
Planetary Boundary Layer (PBL) physics	Mellor-Yamada-Janjic (MYJ) scheme for both domains

Table 5.1(continued): Model set up options for the simulations.

MODEL SETUP/FEATURES	OPTION
The number of soil layers in the land soil model	4 under-ground layers
Shortwave radiation time step	30 minutes for both domains
Longwave radiation time step	30 minutes for both domains
PBL/ Turbulence and microphysics time step	3 minutes for both domains

5.7 Model Runs and Data Flow

Once the processes of the localisation of the model domains and the setup of the model were completed, 365 successive 3-D real-time high-resolution nested simulations were carried out for the year of 2007 using different initial conditions and boundary conditions. All simulation runs done in this study were executed on two parallel computer processers. Each simulation took about 28 hours of runtime to finish, although it might have taken more or less depending on the load of the cluster.

Each model run was integrated for a total of 42 hours with an overlap of 18 hours between every two subsequent simulations. The initialisation time for all simulations was 1800 UTC on each day of 2007. The model runs were 24 hours apart. In other words, the first run was initialised on 01 January 2007 at 1800 UTC and its integration ended on 03 January 2007 at 1200 UTC. The next simulation run was initialised on 02 January 2007 at 1800 UTC, and it ended on 04 January 2007 at 1200 UTC. The same scenario applies on the remaining simulations until the end of 365th run on 01 February 2008 at 1200 UTC. The diagram shown in Figure 5.2 how the model was run based on the first runs.

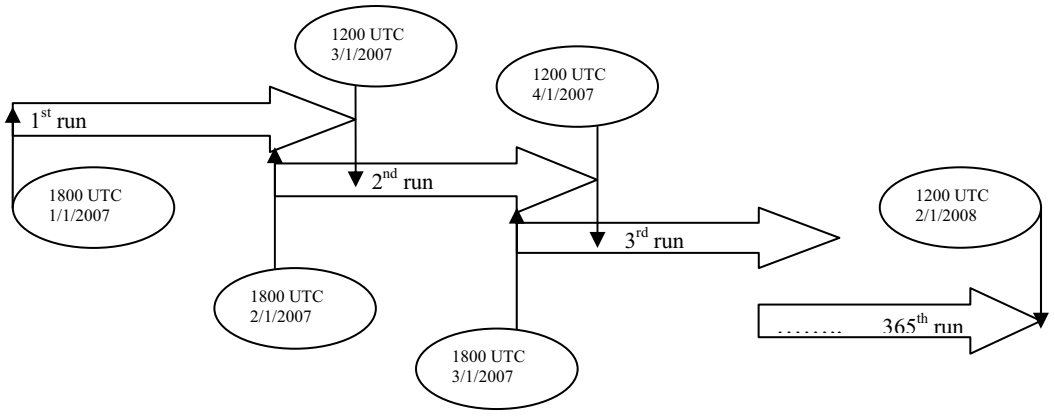

Figure 5.2: A schematic representation of model runs.

Each simulation went through three main stages that were the preprocessing and initialisation, integration, and post-processing. Chapter 4 provides the model components and a schematic diagram of the data flow in WRF-NMM.

The ***geogrid*** program was run first in order to define the simulation domains, define the map projection of the rotated latitude/longitude projection, interpolate static terrestrial data to every grid point of the model domains.

Then, the ***ungrib*** program was executed to extract the time-varying meteorological input data defined by the GFS variable table, and decode the input GFS data from their initial GRIB format to a simple format called the intermediate format that can be interpreted by the model.

After that, the ***metgrid*** program was run to do the horizontal interpolation on the meteorological fields extracted by ***ungrib*** to the grid points of both model domains defined by ***geogrid***. It also corrected the horizontal and the vertical components of wind to the direction of x-axis and y-axis respectively on the model grids, because the model assumes the wind components to be relative to the simulation domain.

After the data preprocessing, the real-data initialisation program was executed to carry out several essential tasks. These tasks consisted of

reading the name-list of WRF-NMM, allocating space to both simulation domains, initialising the remaining variables, attaining and reading the input data generated by WPS, preparing soil fields for its usage in the model, interpolating the meteorological variables vertically, checking to confirm the agreement between soil categories, land use, land mask, soil temperature, and sea surface temperature, and eventually producing the initial conditions and the lateral boundary conditions for the model.

After the initialisation, the integration program was run using the initial and boundary conditions produced from the initialistion. The numerical integration program performed the most important and the longest stage in the simulation since it carried out the integration and the calculation of model equations and produced forecasts for each domain.

The 365 simulation runs generated 15695 hourly output files for the coarse domain and as much for the fine domain throughout the year of 2007, and each of which represented the simulation result for one hour at each grid point. Every simulation had 42 data files including for ach domain.

The WPP was then executed to interpolate the WRF-NMM simulation outputs from their native grids to atmospheric pressure and height levels.

Each simulation generated 25 GB of data for many meteorological variables, about 10 TB of data for all simulations. The model postprocessor was configured to post-process only the weather parameters that were required in this study. These meteorological fields included topography, 2-m temperature, surface temperature, surface pressure, 2-m pressure, mean sea level pressure, surface specific humidity, 2-m specific humidity, 10-m specific humidity, and 10-m U and V wind components at sigma levels, surface solar radiation, atmospheric pressure and the geopotential heights of sigma levels, midday surface albedo, roughness length, and friction velocity for both domains at each model grid point.

5.8 Model Output Preparation

Note that all the data computations discussed afterward were done on each model grid point using FORTRAN programming language. Every simulation results was joined together to formulate one 42-hour file for the coarse domain and another 42-hour file for the fine domain for each run. Thus, the 15695 hourly history data files became only 365 files for each domain but the overlapping forecast hours did not dealt with yet.

To create time continuity in the output data, all these data were joined together in one file for every field for the entire year without any overlapping data or time gap. The first 12-hour forecasts from every run, excluding those of the first run, were excluded from the consideration. The last 7-hour forecasts from each run joined with the forecasts between hour 12 and hour 18 from the next run. This combination was done on each grid point by computing the weighted average for each forecast hour data with the corresponding data from the following run.

The outcomes of the combinations were one 8779-hour file for each field for each domain throughout the year. The model produced the wind velocity at each grid point at the geopotential heights. In order to obtain wind data at heights above the ground rather than above mean sea level, the topography over the model domains was subtracted from one of the geopotential heights at each model grid point. The wind velocity data became distributed in the atmosphere at variable heights of sigma levels above the ground but not at fixed heights.

The cubic spline method was used to perform the vertical interpolation from wind velocity at variable heights of sigma levels to several selected fixed heights. A cubic interpolation was done between each subsequent vertical grid point at variable heights to produce the wind velocity at six selected fixed heights of 25, 50, 75, 100, 125, and 150 m above the ground, in addition to the 10-m wind velocity generated initially by the model.

5.9 Estimating the Potential Power

To estimate the prospective produced power, two procedures were followed. The first one was the theoretical method estimating the hypothetical power density based on Equation 2.6, which indicates that the power density is only dependent on wind speed and air density. The hourly power density at each one of the seven considered heights at each grid point was estimated based on the hourly wind speed and hourly air density. Since hourly 2-m air temperature, pressure, and specific humidity data were available, the actual 2-m hourly air density at each grid point was calculated over the high-resolution domain, using Equation 2.8 presented in Chapter 2.

The estimation of the theoretical power using the kinetic energy formula [Equation 2.6] should be the initial stage in the assessment of wind power exploitation. Calculating the hypothetical energy available in the wind is a good indication of how much power exists over the country. Nevertheless, this technique may overestimate the feasible wind power that can actually be obtained by wind turbines. This is simply due to two reasons. The first one is that as discussed in Chapter 2 the maximum energy extracted from the wind is about 59.3%, but it varies from one turbine design to another. The second reason is that wind turbines generate power only at a certain range of wind speed, and out of this range, their outputs are zero. Even within this speed range, the power outputs of wind turbines do not increase as wind speed increases throughout the entire production course. As shown in Figure 5.2, if wind speed at any grid point increased from 17 m/s to 24 m/s, the power output from a 500kW turbine would not differ. Yet, by using the cubic kinetic energy equation [Equation 2.6], the power output would increase by almost a factor of three.

For the previously mentioned reasons, there was a demand for the use of the second technique, which was based on the actual power outputs of 10 existing commercial wind turbines. The considered wind turbines included B7-7.5kW, FL13-30kW, V29-225kW, V39-500kW, G58-850kW, FL54-

1000kW, G80-1500kW, G80-2000kW, N80-2500kW, and V112-3000kW [Table 5.2]. The estimated hourly wind speed at each point grid of the numerical model at the seven heights on the high-resolution domain were converted to the corresponding power using the power outputs (power curves) of the aforementioned wind turbines of different sizes and designs. This procedure can provide accurate estimates for the possible wind power over Libya. Using this method can offer good power estimates close to the power outputs of the used turbines if they were really installed at each point grid (every 5 km) at each considered height.

All used power curves, excluding the power curve of the V112-3000kW, were obtained from the website of the Idaho National Laboratory (INL, 2009). The power curve of the V112-3000kW was sourced from the Vestas website (Vestas, 2008). The power curves of the ten turbines are shown in Figures 5.3, 5.4, 5.5, and 5.6. If the power curves are incomprehensible, the reader is referred to Chapter 2. Additional information about the characteristics of the 10 used turbines is presented in Table 5.2.

Some of the considered turbines had a power curve having a power value for each corresponding 0.1 mile per hour (mph) interval wind speed from the data source, whereas others had a power value for every matching 2.2 mph. Therefore, the power curves were interpolated cubically in order to produce a power value for the same interval of wind speed. Then, the hourly wind velocity at each grid point at every candidate height was converted to mph to match the wind speed unit considered in the power curves. After that, wind speed was converted to power using the power curves of the considered turbines. Not all heights suited all the used turbines since their sizes differ, and accordingly it was taken into consideration that the size of the diameter of the turbine should comply with the height, at which the turbine installed theoretically.

The power curves of the mentioned turbines were initially formed based on the standard air density being 1.225 kg/m^3, and this meant that the actual

air density was not considered in the power outputs. Hence, the estimated hourly power at each grid point was divided by the standard air density and multiplied by the corresponding actual 2-m air density. Although the air density at 2 m differs from that at other heights, at least the effect of the terrain elevation on air density was taken into account. This should reflect as accurately as possible the actual energy available in the air.

The amounts of wind power produced by a turbine depend heavily on the speed of the wind. Wind direction can also provide additional understanding of the wind resource and of the prevailing wind at the sites of the turbines. Yet, at this initial stage of wind power assessment, wind direction can be overlooked, especially when taking into account that the bulk of modern wind turbines are designed to track the wind. Wind direction data will not be discussed in this study of initial wind power evaluation.

The estimated wind speeds, power densities, and power outputs of the turbines were calculated on an hourly basis, and then averaged to attain prospective diurnal, monthly, and annual corresponding data. However, only the simulation results of the high-resolution domain will be considered in this study's discussion in order to keep the thesis limited. The results will be presented and discussed in the following chapter.

Table 5.2: Basic features of the ten considered turbines.

Turbine Name	Manufacturer	Rated Power [kW]	Rotor Diameter [m]	Swept Area [m²]	Cut-in wind speed [m/s]	Cut-out wind speed [m/s]
B7-7.5kW	Bergey	7.5	7	38.5	4	20
FL13-30kW	Fuhrlaender	30	13	133	3	23
V29-225kW	Vestas	225	29	660	4	25
V39-500kW	Vestas	500	39	1194	5	25
G52-850kW	Gamesa Eolica	850	58	2640	3	21
FL54-1000kW	Fuhrlaender	1000	54	2289	4	20
G80-1500kW	Gamesa Eolica	1500	80	5024	4	25
G80-2000kW	Gamesa Eolica	2000	80	5024	4	25
N80-2500kW	Nordex	2500	80	5024	4	25
V112-3000kW	Vestas	3000	112	9847	3	25

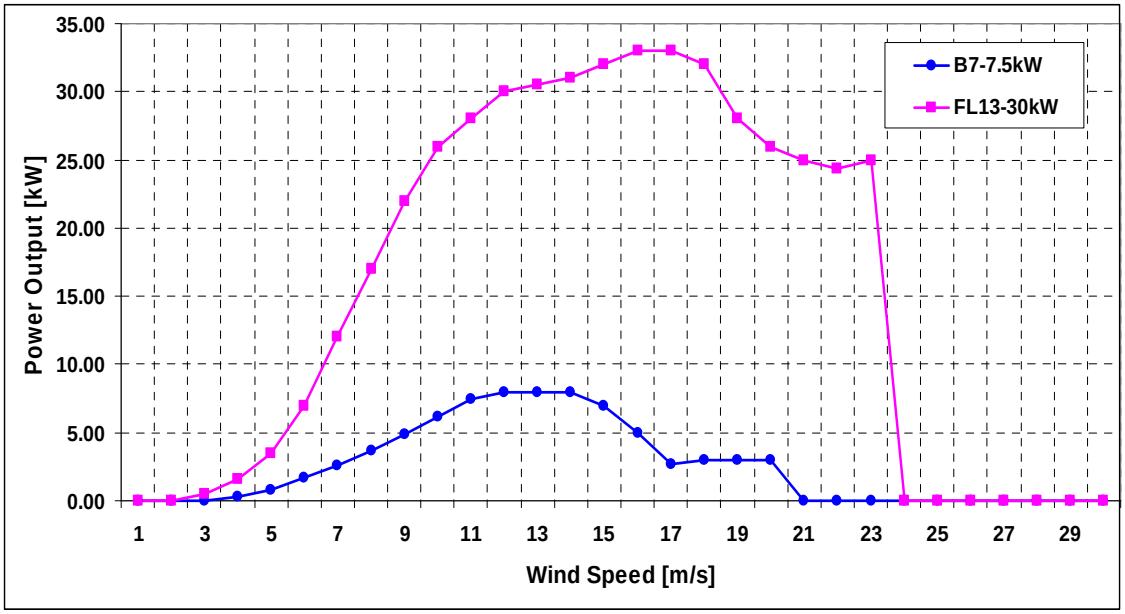

Figure 5.3: The power curves for B7-7.5kW and FL13-30kW turbines.

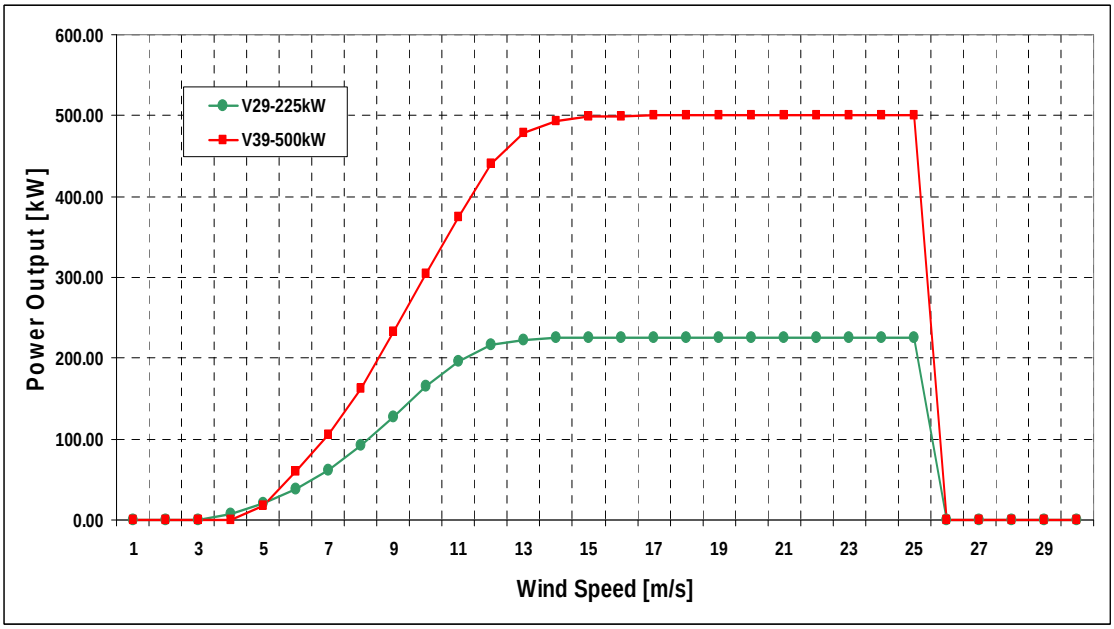

Figure 5.4: The power curves for V29-225kW and V39-500kW turbines.

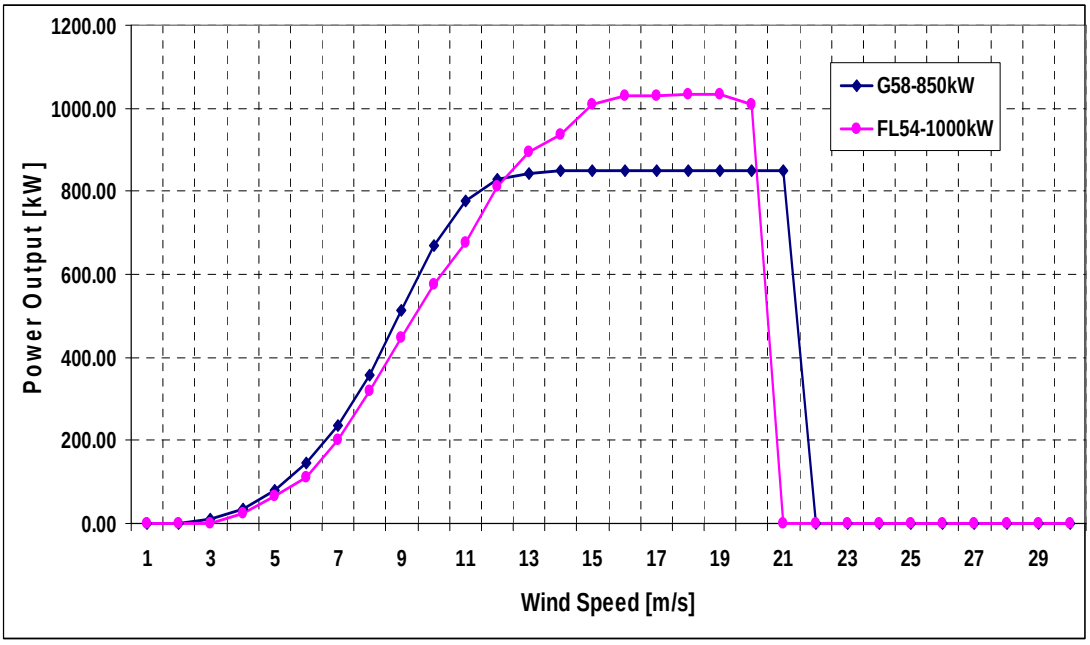

Figure 5.5: The power curves for G58-850kW and FL54-1000kW turbines.

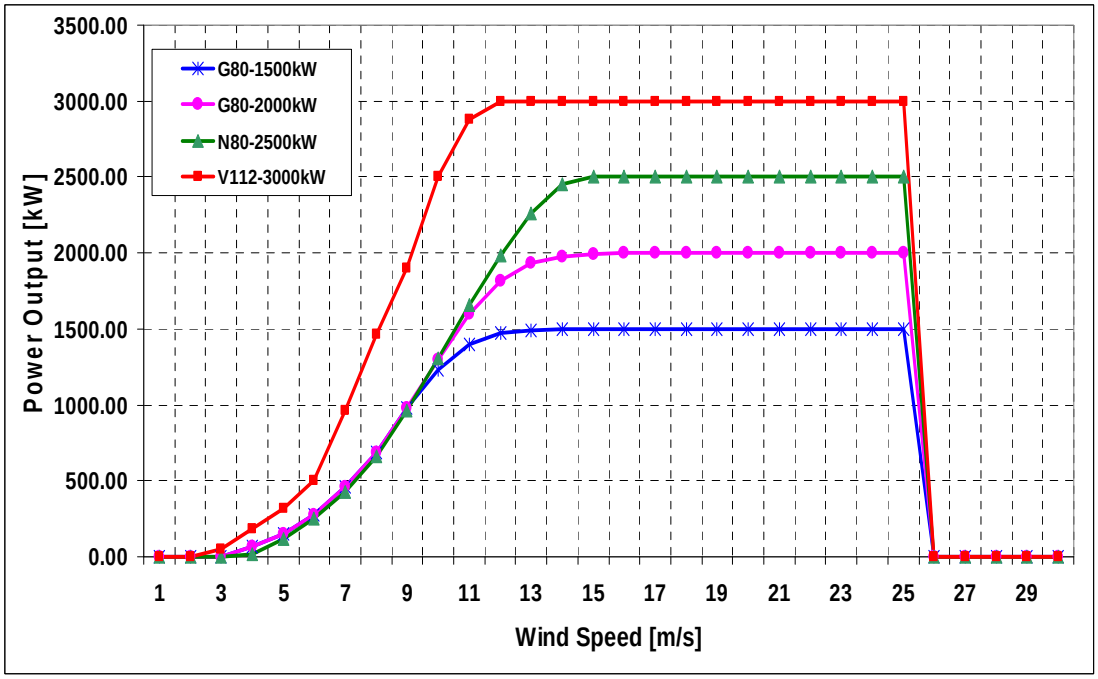

Figure 5.6: The power curves for G80-1500kW, G80-2000kW, N80-2500kW, and V112-3000kW turbines.

Chapter 6

Presentation and Discussion of Simulation Results

6.1 Introduction

Due to the lack of temporal and spatial high-resolution wind speed measurements in Libya, the wind conditions were modelled utilising the WRF-NMM of NCEP. As discussed in Chapter 5, a series of nested numerical simulation runs (365 runs) for 2007 was implemented to simulate the wind conditions over the country. Hourly wind speeds were predicted at every 5 km over the country at sigma levels of the model. A cubic spline interpolation was used to compute the hourly wind speed and power at 25, 50, 75, 100, 125, and 150 m above the ground, in addition to 10-m wind produced directly by the model, at each grid point of the model.

The estimated hourly wind speed data were used to calculate the hourly power density at 5 km spacing over the nation using Equation 2.6. As well, ten commercial wind turbines consisting of B7-7.5kW, FL13-30kW, V29-225kW, V39-500kW, G58-850kW, FL54-1000kW, G80-1500kW, G80-2000kW, N80-2500kW, and V112-3000kW were employed to estimate the wind power outputs. The estimated hourly wind speed, power density, and

power outputs of the turbines were then averaged on annual, monthly, and diurnal basis.

In this chapter, the results of the numerical simulations are presented and analysed. The simulation results of wind speed, the corresponding wind power density, and power output are analysed to examine and evaluate the wind resource over Libya for win power generation purposes. This chapter identifies areas with good wind power resources over the country.

Monitoring the wind characteristics over Libya should be the initial stage in order to determine whether good wind power resources exist. If so, the favourable regions rich in wind power resources will be highlighted. This will facilitate the estimates of the potential electrical power that can be obtained throughout prospective regions. The chapter also presents some on-site wind power assessments at several selected grid points. Note that the Libyan cities/towns/mountains used in the following discussion are shown in Figure 1.1 and Table 1.1.

The characteristics of the national wind resource are investigated in Section 6.2. Section 6.3 looks at the wind power resource attributes over the northeast region, including the annual pattern [Subsection 6.3.1], seasonal variations [Subsection 6.3.2], and diurnal variations [Subsection 6.3.3]. Section 6.4 examines the wind energy resource characteristics over the northwest region, including the annual pattern [Subsection 6.4.1], seasonal variations [Subsection 6.4.2], and diurnal variations [Subsection 6.4.3]. In Section 6.5, the wind power resource features over the southeast region, including the annual pattern [Subsection 6.5.1], seasonal variations [Subsection 6.5.2], and diurnal variations [Subsection 6.5.3] are discussed. Section 6.6 investigates the wind energy resource attributes over the southwest region, consisting of the annual pattern [Subsection 6.6.1], seasonal variations [Subsection 6.6.2], and diurnal variations [Subsection 6.6.3]. Regional estimated power outputs from several commercial wind turbines over the potential four regions are discussed in Section 6.7. On-

site wind power assessments, consisting of the frequency distribution, [Subsection 6.8.1], temporal variations [Subsection 6.8.2], and vertical wind resource shear [Subsection 6.8.3], at six selected locations using some existing turbines are presented in Section 6.8.

6.2 National Wind Energy Resources

Figure 6.1(a) illustrates the estimated annual mean wind speed at 10 m above the ground, and Figure 6.1(b) shows the corresponding power density throughout Libya. These figures suggest that the vast majority of inland districts have poor wind energy resources, as the prevalent annual 10-m wind speed varies between 3 and 4 m/s, and the matching wind power density ranges from 30 to 60 W/m^2. Along the coastal areas wind energy resources are higher as the average annual 10-m wind speed ranges from 4 to 5 m/s, and the power falls in the range of 60-120 W/m^2. The western coastline near the Libyan-Tunisian border, the eastern coastline over Green Mountain, Ghiryan, Yifrin, Dirj, southern Murzuk, Ghat, and Al Kufrah, are characterised by greater wind energy resources with an annual 10-m wind speed of 5-6 m/s and power density ranging from 120 and 180 W/m^2.

Figures 6.2(a) and 6.2(b) demonstrate the estimated annual mean wind speed and the matching power density at 25 m above the surface, in that order. They point out that over the predominant part of inland areas the average annual 25-m wind speed is between 3 and 5 m/s, and the power varies between 30 and 90 W/m^2. The eastern and the western parts of the coastline and the mountains located near the southern border of the country, specifically over Ghat and Murzuk, experience stronger winds blowing at speeds of 5-6 m/s, and the power available over these regions is in the range of 90 to nearly 240 W/m^2. Wind energy resources are greater at the northwestern corner of the country near Zuwarah, and also along the crescent-shaped region crossing Ghiryan, Yifrin, and Dirj, as the

annual 25-m wind speed is between 6 and 7 m/s and the power varies from about 150 to 240 W/m^2.

Figure 6.3(a) shows the estimated annual mean wind speed at 50 m above the surface, and Figure 6.3(b) demonstrates the matching wind power density. The first-mentioned figure suggests that the inland annual 50-m wind speed varies between 4 and 5 m/s. Along the Mediterranean coast, specifically over Green Mountain and along the curved region crossing Ghiryan, Yifrin, and Dirj, the 50-m wind blows at speeds of 5-7 m/s. The southern districts of the country have better potential of wind energy utilisation as the wind blows at about 6-8 m/s. Based on Figure 6.3(b), the wind power over the central part of Libya is poor, as it falls in the range of 50-100 W/m^2. Nonetheless, the coastline and the southern areas of Ghat, Murzuk, and Al Kufrah, all have more power being between 150 and 350 W/m^2.

Figures 6.4(a) and 6.4(b) illustrate the estimated annual mean wind speed and the matching power density at 75 m above the surface. Most of inland areas have 75-m wind blowing at speeds of 5-6 m/s, and the estimated power available over these districts is in the range of 100-200 W/m^2. However, the coastal regions suited between Misratah and the Tunisian boarder, Ghiryan, Yifrin, and Dirj, and the southern part of the country see good winds blowing at speeds between 6 and 8 m/s, with wind power of 200-400 W/m^2. Wind power characteristics at 75 m are even better over the Sahara Desert, namely over some zones of Ghat, Murzuk, and Al Kufrah, as the annual 75-m wind speed and the corresponding wind power reach around 9 m/s and 500 W/m^2.

Figure 6.5(a) shows the estimated annual mean wind speed at 100 m above the surface, and Figure 6.5(b) demonstrates the corresponding wind power density. The middle part of the country has 100-m wind speeds ranging from 5 to 7 m/s, and the estimated wind power varies between 150 and 300 W/m^2. Yet, the north western corner near the Tunisian edge, Ghiryan,

Yifrin, Dirj, and Green Mountain, all experience wind blowing at about 7-8 m/s, and have wind power ranging between 300 and 450 W/m^2. Some parts of the Sahara Desert have greater wind power resources as the annual 100-m wind speed and the matching energy fall in the range of 7-10 m/s, and 300-700 W/m^2.

Figure 6.6(a) demonstrates the estimated annual mean wind speed at 125 m above the surface, and Figure 6.6(b) illustrates the corresponding power density at the same elevation over the country. The annual 125-m wind speed is in the range of 6 to 8 m/s throughout most of the country, and the potential wind power is between 200 and 350 W/m^2. The astern and western coastal areas, Ghiryan, Yifrin, and Dirj are characterised by stronger winds. The annual 125-m wind speed ranges from 8 to 9 m/s, and the matching wind power is in the range of 350-500 W/m^2. The wind resource is even better in mountainous districts of Ghat, Murzuk, and Al Kufrah since the annual 125-m wind speed varies between 8 and 11 m/s, and the wind power ranges from 400 up to more than 750 W/m^2.

Figures 6.7(a) and 6.7(b) illustrate the estimated annual mean wind speed and the matching wind power density at 150 m above the ground, respectively. Throughout the majority of the country, the annual 150-m wind speed ranges from about 6 up to 8 m/s and the power varies between 250 and 400 W/m^2. Green Mountain has annual 150-m wind speeds of 8-9 m/s, and power varying between 400 and 550 W/m^2. The western coastline, Yafrin, and Ghiryan have wind blowing at speeds of 7-8 m/s, and the prospective wind power ranges between 400 and 600 W/m^2. The southern part of Libya, explicitly Ghat and Murzuk, has great wind resources bringing about abundant wind power. It experiences average annual 150-m wind speeds being between 8 and 11 m/s, with power ranging from 400 to more than 750 W/m^2.

Overall, when considering both the horizontal and vertical variations, wind energy resources throughout the country vary from poor to excellent.

Across all considered elevations, the average annual wind speed ranges from 3 to 11 m/s, and the estimated power varies between about 30 and more than 750 W/m^2. There exists a considerable variance in the wind speed and hence in the existing power. They differ significantly according to the height above the ground, and depending on how far from the coast. It is also noticed that wind power resources, especially over inland regions, follow the topographic features of the country. Wind speed and power density results at all elevations demonstrate that the wind energy prospective is greater over high-altitude terrains than over those having lower altitudes. However, some coastal areas near the northwestern corner of Libya have good wind power resources although their altitudes are low.

The areas characterised by low wind energy resources lie over the middle part of the country. This scenario is more evident below 75 m above the ground. The western part of the coastline around Zuwarah, the eastern coastal districts over Green Mountain, and high-altitude regions including Yifrin and Ghiryan, all experience very good wind power resources. Abundant wind energy resources are also observed over the high-altitude areas near the southern edge of Libya, namely over the Sahara Desert and around the Tibesti Mountains.

The initial power resource examination suggests that there is good wind energy potential suitable for wind power generation. The initial discussion shows that there is a good possibility of installing large-scale wind turbines with hub heights 50 m or higher at the eastern and western coastal districts, and over the Sahara Desert in the southern border of the country. Still, small-scale wind energy applications may be feasible even below 50 m height. If wind turbines are installed over these regions, they may produce sufficient wind power but the hub height of the turbine could make substantial differences.

The effects of the boundary layer including the surface drag on air movement are modest at heights of 100 m and above, because above 75 m

the wind speed gradient between over the land and water is small. Increasing the tower height of wind turbines from 75 m to 100m or higher would improve the power outputs of the turbines.

The reason for wind speed and wind power being higher at the coastal areas may be that these regions are exposed to sea/land breezes. Sea/land breezes develop along the water-terrain boundary, especially in areas having altitudes close to the sea level.

Mountain/valley flows may develop along the slope of these high terrains, in particular, over the mountains in the Sahara Desert during warm seasons. Green Mountain and the Tibesti Mountains may experience mountain/valley breezes. Some of these mountains extend up to about 1 km above sea level, and a few reaches more than 2 km elevation. The wind blows at high speeds over high-altitude terrains. In this case, airflows moving over mountainous regions are not affected by the drag resulting from the topography, even though mountainous districts are usually rougher than the surrounding areas. This is because the air has travelled, for a long period, in the upper layers far from the effect of ground roughness as well as the air bouncy within the atmospheric boundary layer. While the mountains below the travelling air may affect the movement of this air, this impact does not exist instantaneously, but rather it may appear after the air has passed the mountains. Coastal mountainous areas like Green Mountain may experience a combination of sea and mountain breezes.

While the annual average wind speed can give a general indication of how much wind power is available over the country, the wind resource characteristics vary temporally and spatially from one month to another throughout the year, and from one hour to another during the day. The diurnal and monthly patterns of wind power resources should be investigated since they provide additional indications about whether sufficient wind resources are stable during the entire year throughout the

day. The variability of wind power resources should be studied in order to determine the suitability of the resources for wind power generation over the identified favourable districts.

Hence, the coming discussion will only include the identified potential areas, which are initially found to be characterised by encouraging wind energy resources. To be able to examine and cover all the identified favorable areas for further assessment, the best four regions in terms of the wind resource will be considered in the following discussion. The four favourable regions that will be studied further include:

- The northeast region representing the eastern coastal districts over and near Green Mountain [Figure 6.8(a)]
- The northwest region representing the western coastal areas in addition to Ghiryan, Yifrin, and Dirj [Figure 6.8(b)]
- The southeast region representing part of Murzuk and Al Kufrah [Figure 6.8(c)], and
- The southwest region representing Ghat, and part of Murzuk [Figure 6.8(d)].

Due to the limitation of the size of this work, the wind resource assessment over these regions will be implemented only at 100 m above the ground representing other considered heights, except the last section. Hence, it should be kept in mind that from this point on, all sections will present and investigate wind energy resources at 100-m height only, excluding the last section in this chapter. The last section will present some results on other elevations as well.

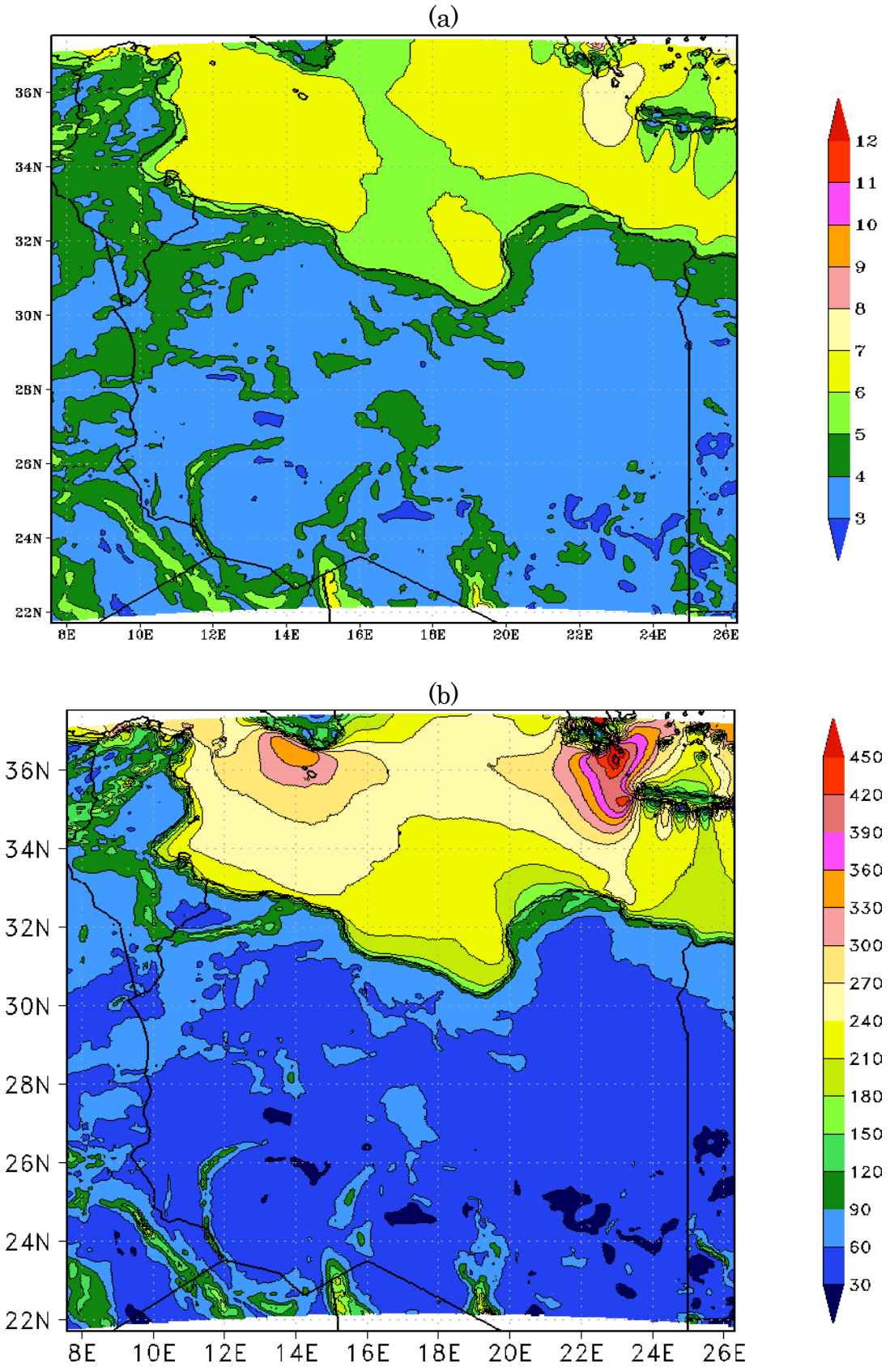

Figure 6.1: The estimated annual mean 10-m (a) wind speed [m/s] and (b) wind power density [W/m^2].

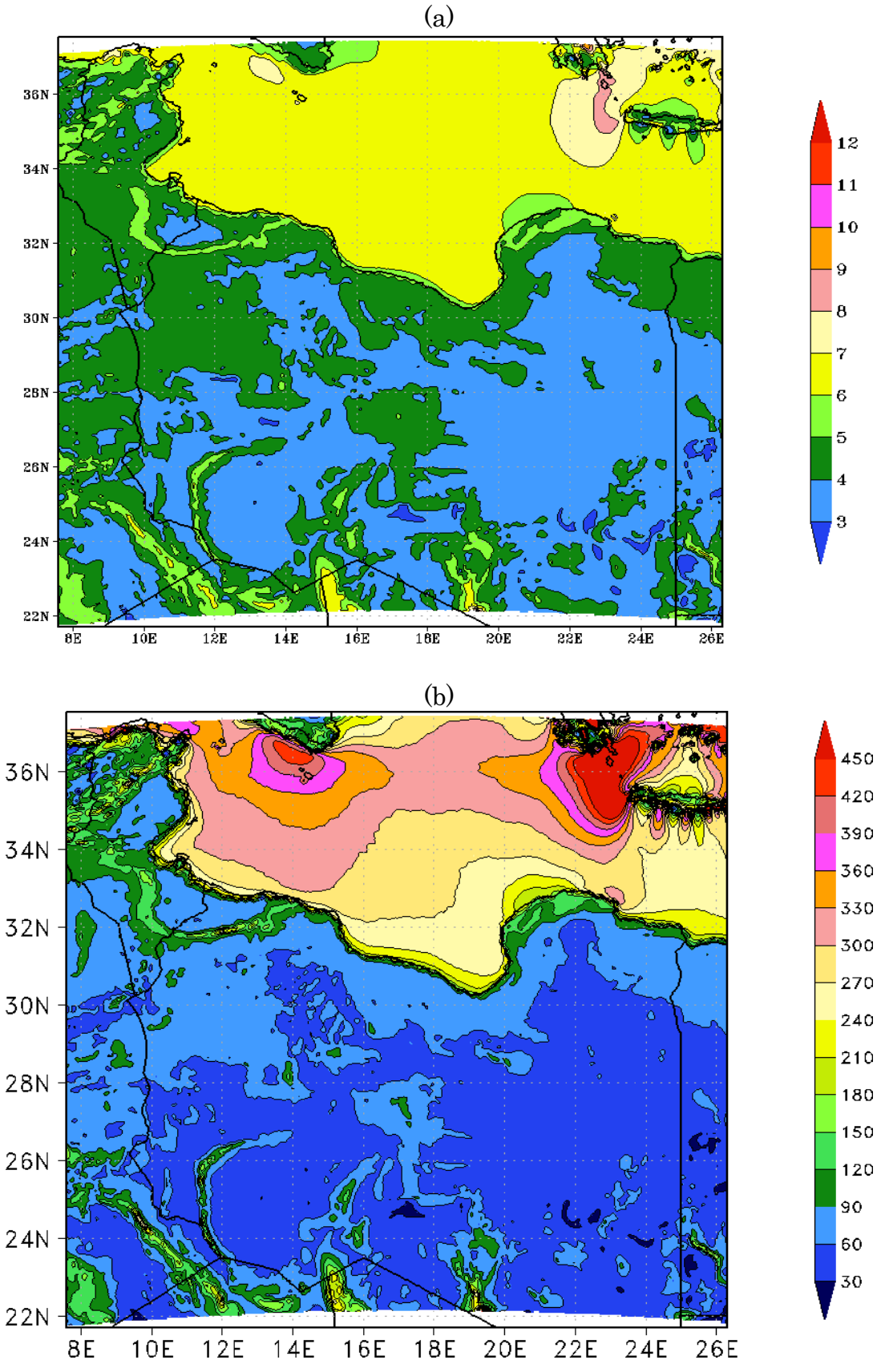

Figure 6.2: The estimated annual mean 25-m (a) wind speed [m/s] and (b) wind power density [W/m^2].

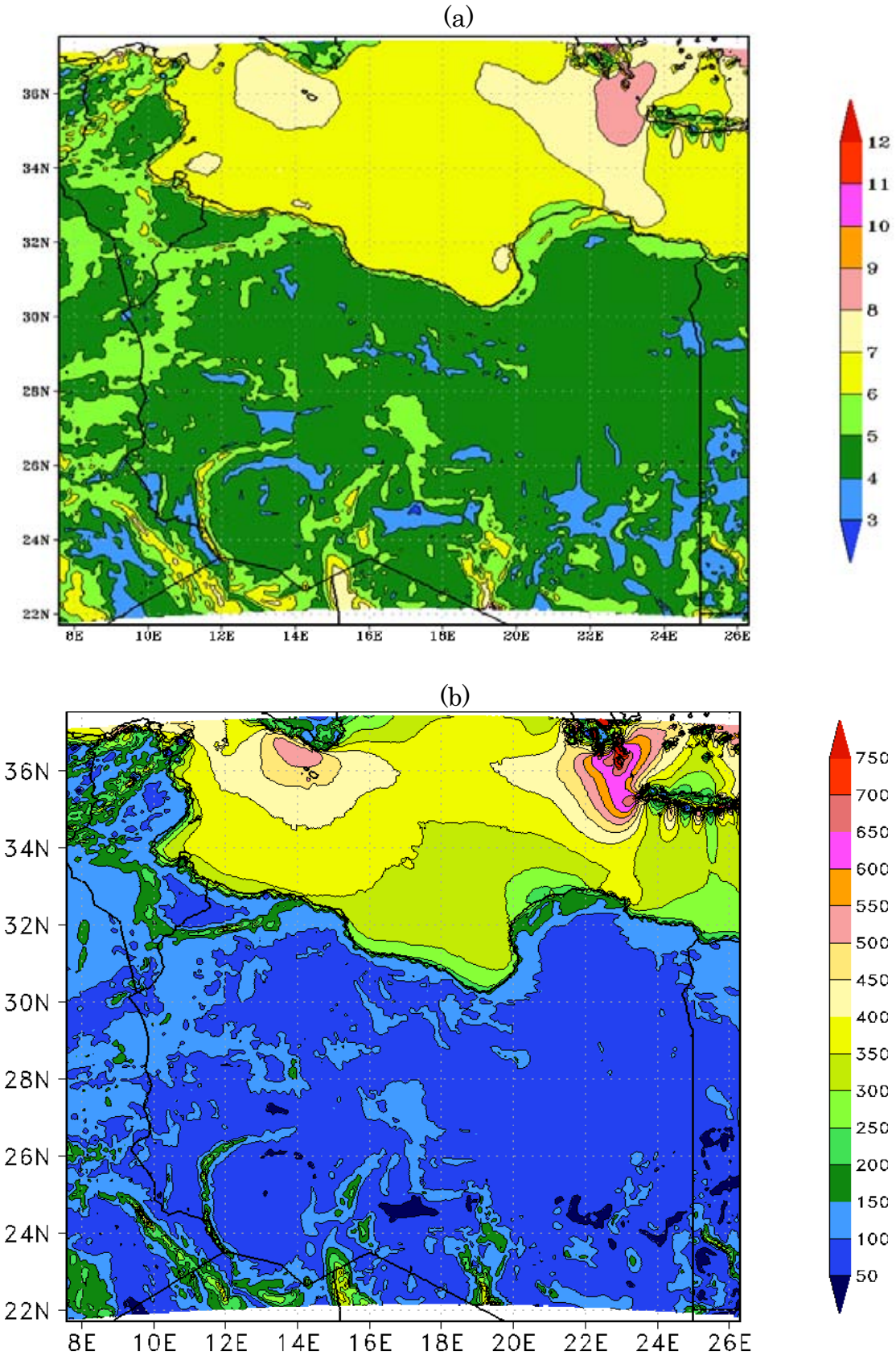

Figure 6.3: The estimated annual mean 50-m (a) wind speed [m/s] and (b) wind power density [W/m^2].

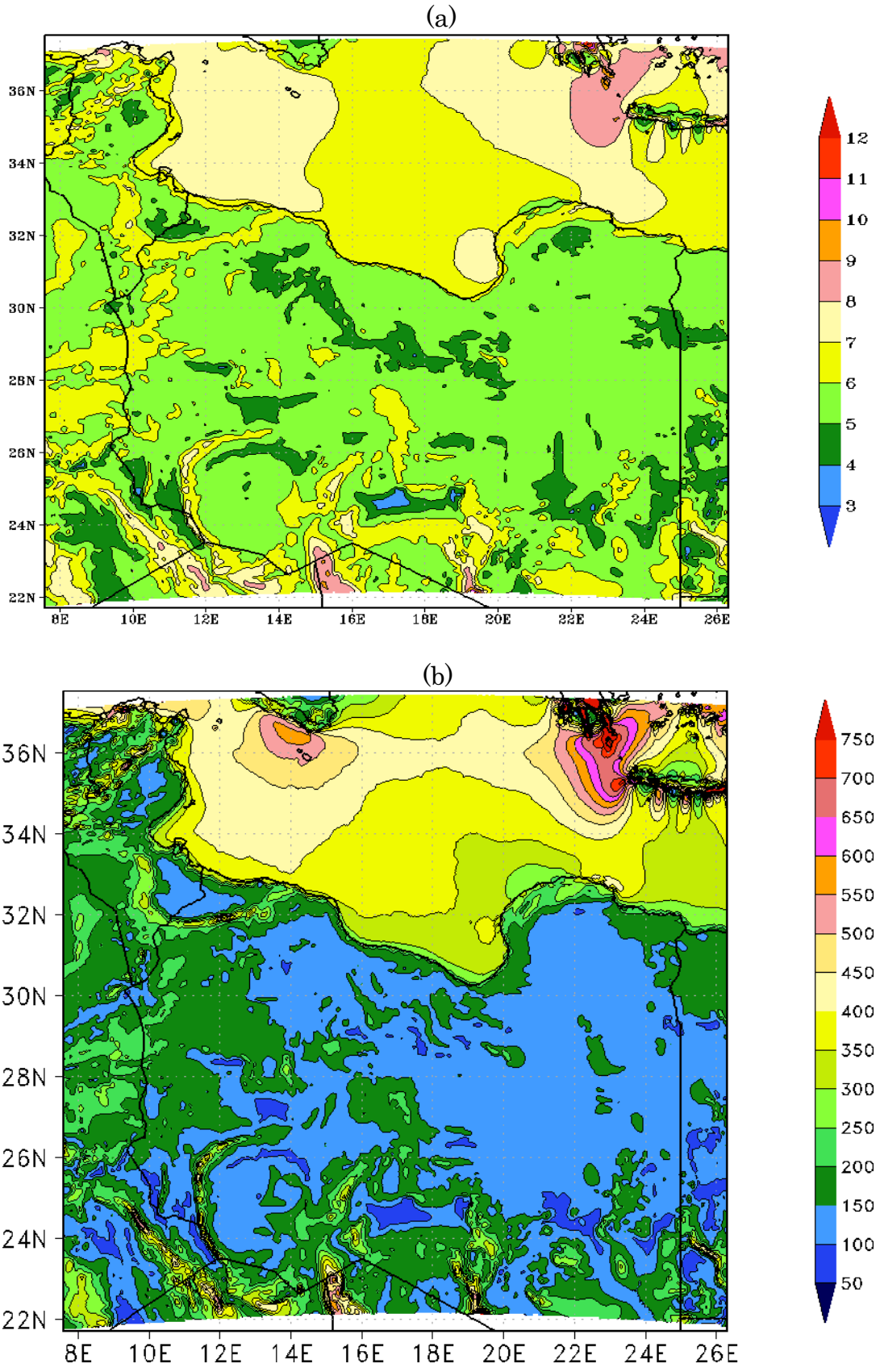

Figure 6.4: The estimated annual mean 75-m (a) wind speed [m/s] and (b) wind power density [W/m^2].

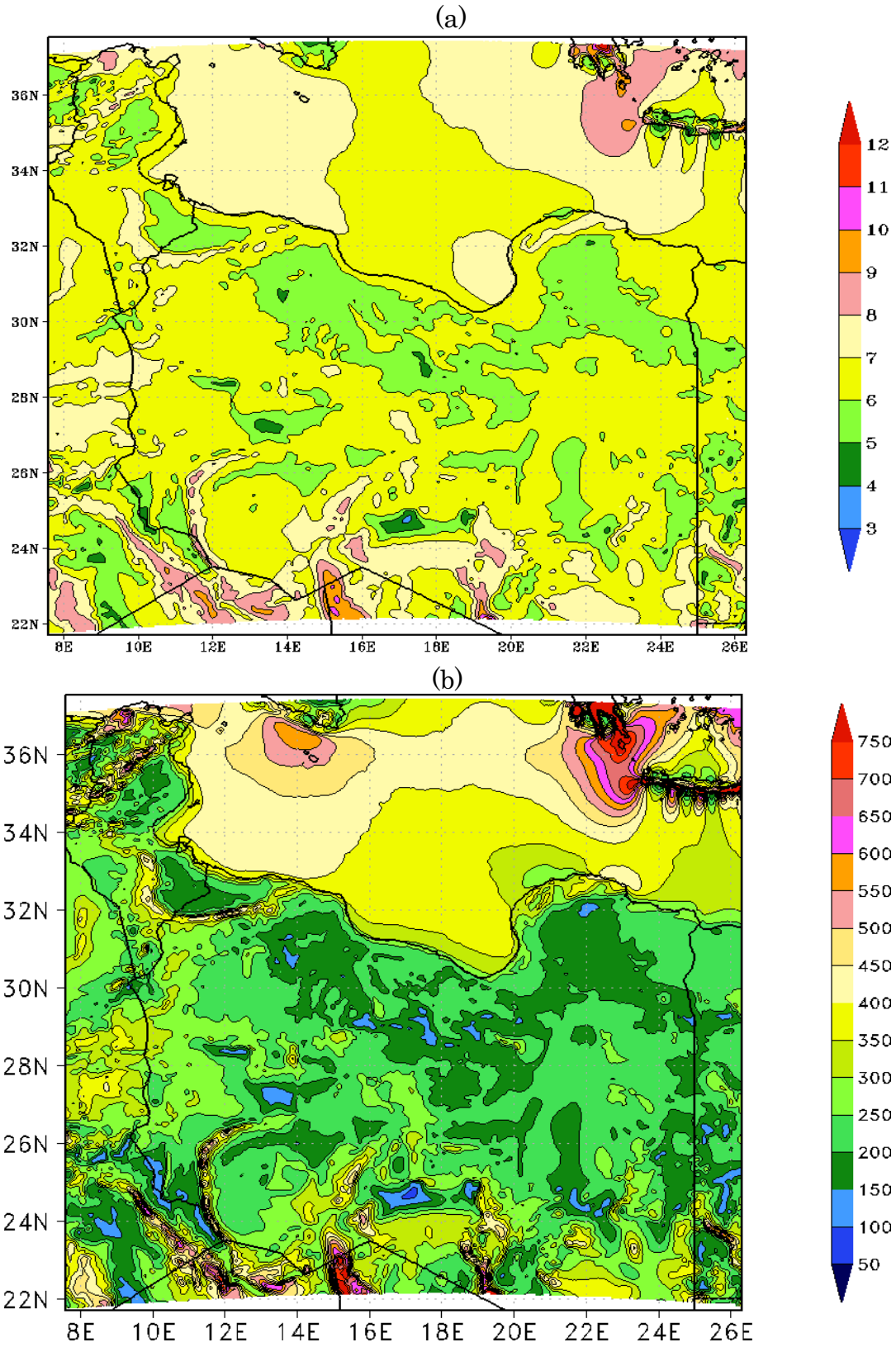

Figure 6.5: The estimated annual mean 100-m (a) wind speed [m/s] and (b) wind power density [W/m^2].

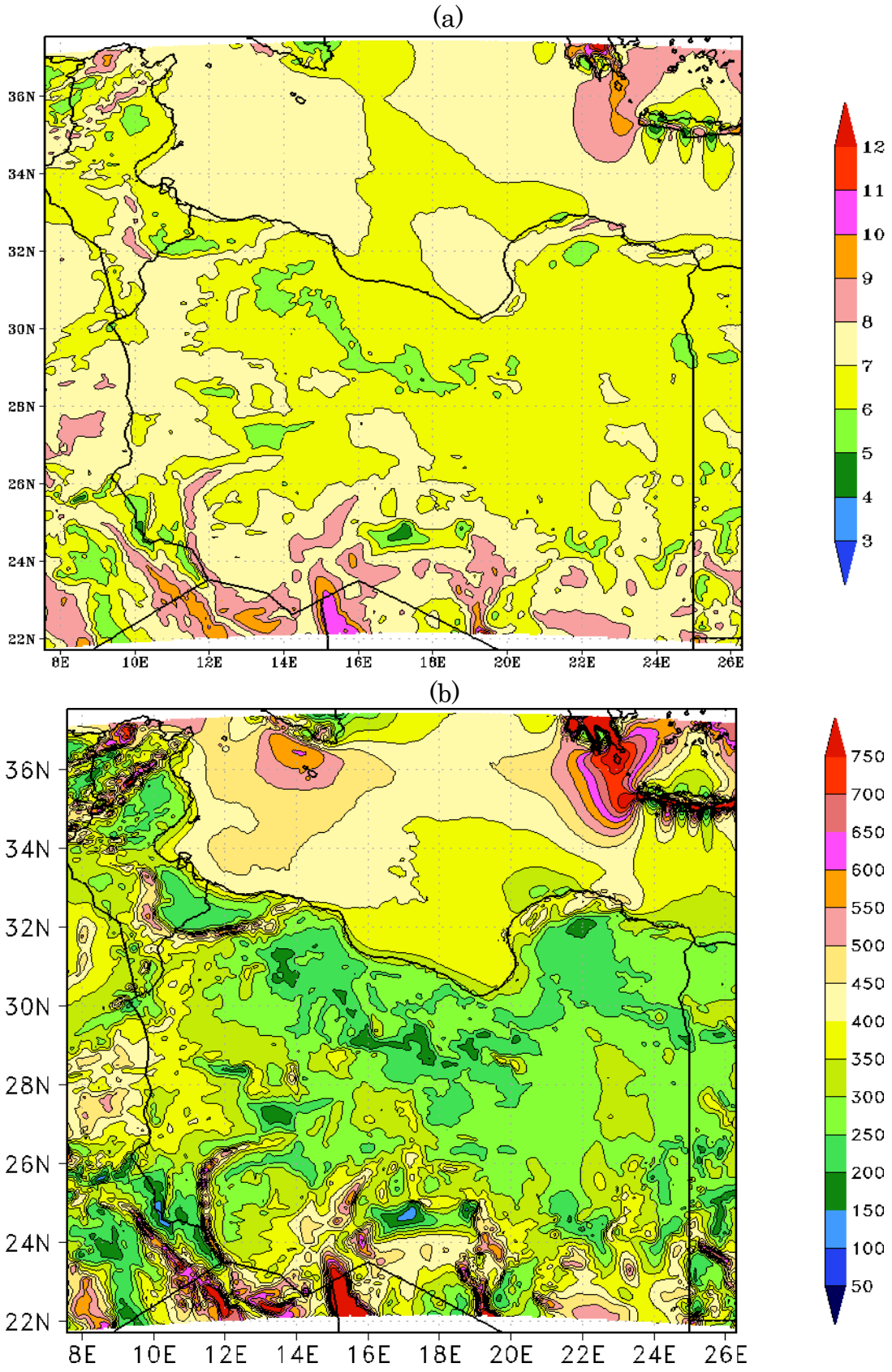

Figure 6.6: The estimated annual mean 125-m (a) wind speed [m/s] and (b) wind power density [W/m^2].

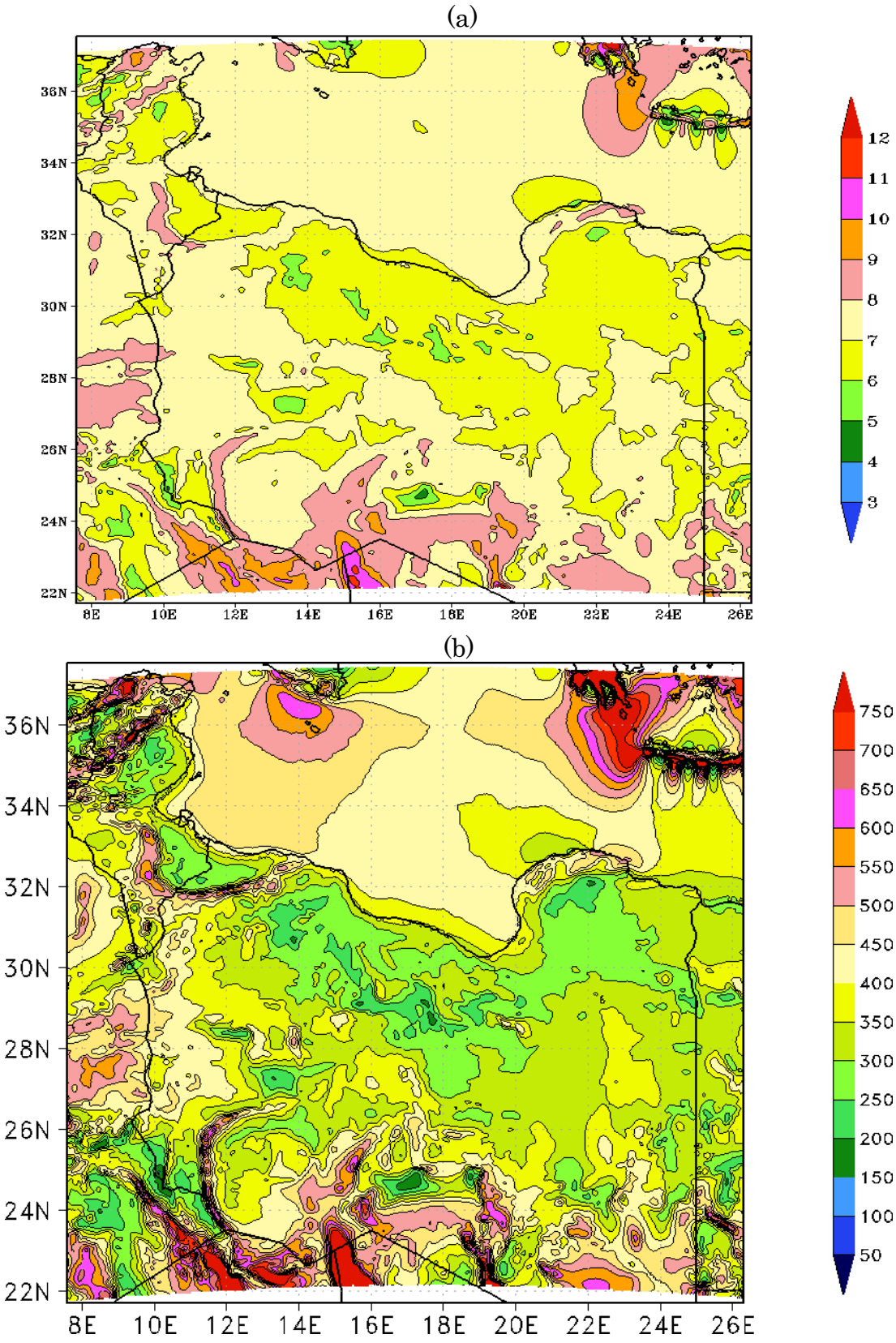

Figure 6.7: The estimated annual mean 150-m (a) wind speed [m/s] and (b) wind power density [W/m^2].

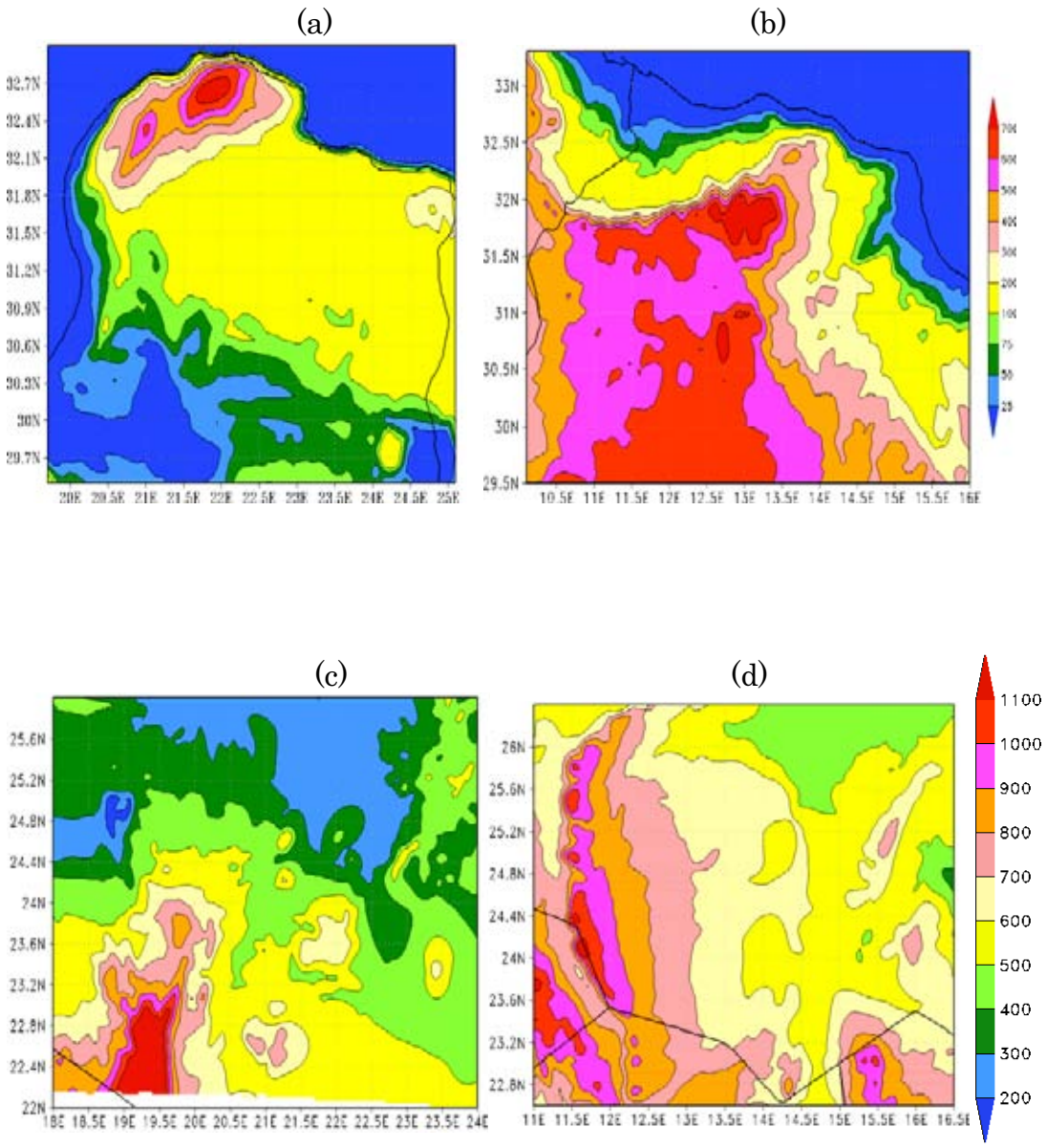

Figure 6.8: The identified potential regions with the topography [m] of (a) the northeast region, (b) the northwest region, (c) the southeast region, and (d) the southwest region.

6.3 Wind Energy Resources of Northeast Region

6.3.1 Annual Pattern

Figure 6.9(a) illustrates the estimated annual mean 100-m wind speed, and Figure 6.9(b) shows the corresponding power density for the northwest region. From these figures, the annual wind speed over the vast majority of this region ranges from about 5.5 to 8 m/s, and the estimated available power varies between 160 and 440 W/m^2.

Wind resource characteristics along the coastal zones are quite different from those over inland areas, owing to sea breeze penetration as well as the topographical features. Excluding the small zone north of Al Bayda, the coastal areas have very good wind energy resources. The wind over these districts blows at speeds greater than 6.5 m/s, and there is more than 240 W/m^2 of wind power. Darnah, Al Bayda, and the nearby areas have a great feasibility of wind energy generation, as the 100-m wind blows at speeds between 7.5 and 8 m/s, and they are characterised by good power ranging from 360 to 440 W/m^2.

Wind speed decreases gradually as airflows move further inland. This could be due to the effect of surface roughness in the atmospheric boundary layer, and also because of the inland pressure gradient being small. The inland wind speed is in the range of 5.5 to 6.5 m/s, and the power density varies between 120 and 240 W/m^2. The area southeast of Green Mountain has very poor wind energy resources, since it experiences wind blowing at speeds between 4.5 and 5.5 m/s and has power ranging between 120 and 200 W/m^2. Green Mountain extending up to more than 700 m above sea level [Figures 6.8(a)] acts as a barrier to sea breezes prevented from penetrating further inland.

6.3.2 Seasonal Variations

Figures 6.10(a), 6.10(b), and 6.10(l) demonstrate the estimated monthly mean 100-m wind speed over the northeast region for winter months of January, February, and December respectively. The matching wind power density for these months is shown in Figures 6.11(a), 6.11(b), and 6.11(l).

During winter, the coastal areas of Green Mountain and the nearby districts are characterised with excellent wind energy resources, especially in February [Figure 6.10(b) and Figure 6.11(b)]. February has wind speeds ranging from 7 to higher than 9 m/s, and its power density ranges from 280 up to greater than 600 W/m^2. December wind speeds and power over the coastal zones fall in the range of 6.5-8.5 m/s and 240-520 W/m^2 [Figure 6.10(l) and Figure 6.11(l)]. Among winter months, January [Figure 6.10(a) and Figure 6.11(a)] has the lowest wind energy resource, as the wind blows at speeds between 6 and 8 m/s, and the available power varies between 200 and 520 W/m^2.

Although most areas of the Mediterranean coastline, including Green Mountain, Darnah, Al Marj, and Benghazi experience very good wind energy resources, Al Bayda have the greatest resources throughout winter months. The monthly wind speed and the corresponding power over Al Bayda do not drop below 7.5 m/s and 440 W/m^2. In contrast, the wind energy resource of winter over inland districts varies between poor in January and good in February. Throughout winter months, the inland areas experience monthly wind speeds ranging from 5 to 6.5 m/s, with power in the range of 120-240 W/m^2.

Figures 6.10(c), 6.10(d), and 6.10(e) show the estimated monthly mean 100-m wind speed over the northeast region for spring months of March, April, and May, respectively. The matching wind power density for the same months is shown in Figures 6.11(c), 6.10(d), and 6.11(e), in that order.

The aforementioned figures show that spring is characterised with good wind power resources, especially along the coast. The coastline sees abundant wind resources as the monthly wind speed and power are in the range of 6-9 m/s and 200-600 W/m^2. Darnah, Al Bayda, and Green Mountain experience high and steady wind resources throughout the season, although the resource is greater in March. They have wind blowing at speeds of 6.5-9 m/s, and power ranging from 320 up to more than 600 W/m^2.

In March, the eastern coast around Tobruk has better wind energy resources than the western part of the coastline, namely over Ajdabiya [Figure 6.10(c) and Figure 6.11(c)]. This situation is reversed in April and May, since Ajdabiya has greater wind energy resources than Tobruk [Figures 6.10(d), 6.11(d), 6.10(e), and 6.11(e)]. This may be a good indication as if wind turbines were installed along the coastline they would produce electrical power cooperatively.

The zone north of Al Bayda has less wind resources decreasing gradually as the season passes. It has wind blowing at speeds of 6-6.5, 5-6, and less than 5 m/s in March, April, and May respectively. Wind speed over this district is significantly lower than over the neighbouring areas. This may be because after March, the terrain starts warm up faster than the water and so sea/land breeze circulations begin to develop. Once the surface air reaches this zone, it is blocked by Green Mountain preventing airflows from moving further inland. As a result, sea breeze circulations cannot be formulated over this zone.

Figures 6.10(f), 6.10(g), and 6.10(h) show the estimated monthly mean 100-m wind speed over the northeast region for summer months of June, July, and August. The corresponding power density for the same months is illustrated in Figures 6.11(f), 6.11(g), and 6.11(h).

According to the previously mentioned figures, the coastline is rich in wind energy resources throughout summer months, except the zone north of Al

Bayda that is discussed earlier in this section, and whose wind energy resources diminish as the weather gets hotter. Despite that, the inland territories are characterised with poor wind power resources.

The coastline has wind blowing at speeds ranging from 6 to stronger than 9 m/s, and the estimated available power varies from 160 to around 600 W/m^2. Darnah and Green Mountain experience the best wind power resources whose peak occurs in July [Figures 6.10(g) and 6.11(g)] as the monthly wind speed reaches 9 m/s, and the power is about 600 W/m^2. Ajdabiya's wind energy resources are reasonable during summer. Tobruk and Imsaad near the Libyan-Egyptian border have fluctuating monthly energy resources, since wind speed and power sometimes go down to 6 m/s and 160 W/m^2, particularly in June [Figures 6.10(f) and 6.11(f)], and August [Figures 6.10(h) and 6.11(h)].

Figures 6.10(i), 6.10(j), and 6.10(k) illustrate the estimated monthly mean 100-m wind speed over the northeast region for autumn months, namely September, October, and November. The corresponding wind power density for the same months is demonstrated in Figures 6.11(i), 6.10(j), and 6.11(k).

As shown in those figures, autumn has the lowest wind energy resource when it is compared to other seasons. In spite of that, the coastal regions experience reasonable wind resources, especially over Green Mountain, Darnah, Ajdabiya, and Al Bayda. The vast majority of coastal districts have wind blowing at speeds between 6 and 8.5 m/s and power ranging from about 160 up to more than 600 W/m^2. Among autumn months, September [Figures 6.10(i) and 6.11(i)] sees the lowest wind energy resource over Ajdabiya, while the wind blows at its minimum speed around Tobruk in October [Figures 6.10(j) and 6.11(j)]. However, the best wind resource for autumn is observed along coastal regions in November [Figures 6.10(k) and 6.11(k)].

6.3.3 Diurnal Variations

The diurnal cycles for all regions are averaged so that the wind condition presented at each mentioned hour represents the average condition of wind speed at this hour, the previous hour, and the next hour throughout the year. The time used to examine the temporal variation in wind power resources in Libya is the Coordinated Universal Time (UTC). The difference between UTC and the local solar time in Libya is 1 hour, but when considering the actual time used in the country there is a 2-hour difference.

Figures 6.12(a) to 6.12(h) show the annual mean diurnal cycle of the estimated 100-m wind speed at 0000, 0300, 0600, 0900, 1200, 1500, 1800, and 2100 UTC, respectively. The matching wind power density is illustrated in Figures 6.13(a) through 6.13(h). These figures suggest that the region obtains more wind energy resources at nighttime than during daytime, but the resource variability over the coastal districts is not as evident as over that over inland areas.

During the early morning at 0600 UTC [Figures 6.12(c) and 6.13(c)], the wind speed begins to fall noticeably, and continues to drop until the late morning after 0900 UTC [Figures 6.12(d) and 6.13(d)]. During this period, the wind blows at speeds between 5.5 and 8 m/s, and the power range from 160 to 520 W/m^2. The temperature difference between the water and the terrain during this time may be at its minimum, bringing about a relatively calm air near the ground. This prevents the air from completing sea/land breeze circulations.

During the early afternoon at 1200 UTC [Figures 6.12(e) and 6.13(e)], the wind regains its strength and its speed increases through the evening until it peaks at about 2100 UTC [Figures 6.12(h) and 6.13(h)]. The wind during this time blows at speeds of 6.5-9 m/s, and the power varies between 240

and 520 W/m^2. The coastline continues to experience strong winds until the midnight.

After 0000 UTC [Figures 6.12(a) and 6.13(a)], the wind remains strong over most parts of the region, especially on the coastline, until sunrise before 0600 UTC [Figures 6.12(c) and 6.13(c)]. During the second half of the night, the coastal nocturnal wind speed varies between 6.5 and 8.5 m/s, and the power ranges from 280 to 600 W/m^2.

The northeast region of Libya has a good potential of wind power exploitation, especially mountainous coastal areas. Green Mountain, Darnah, Ajdabiya, and Al Bayda receive good wind power resources throughout autumn, while Tobruk experiences varying wind energy resources.

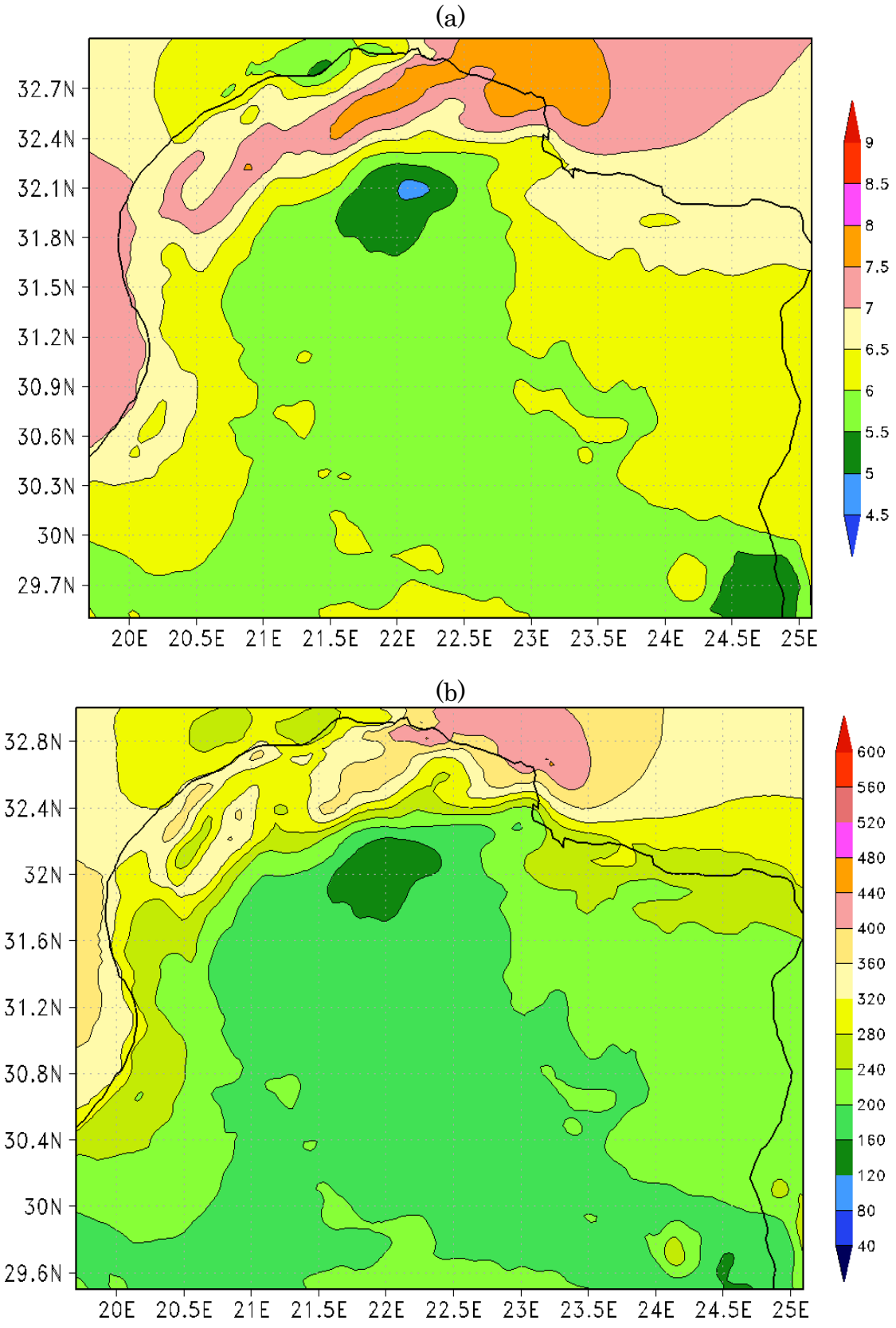

Figure 6.9: The estimated annual mean 100-m wind speed [m/s] and (b) the corresponding wind power density [W/m^2] for the northeast region.

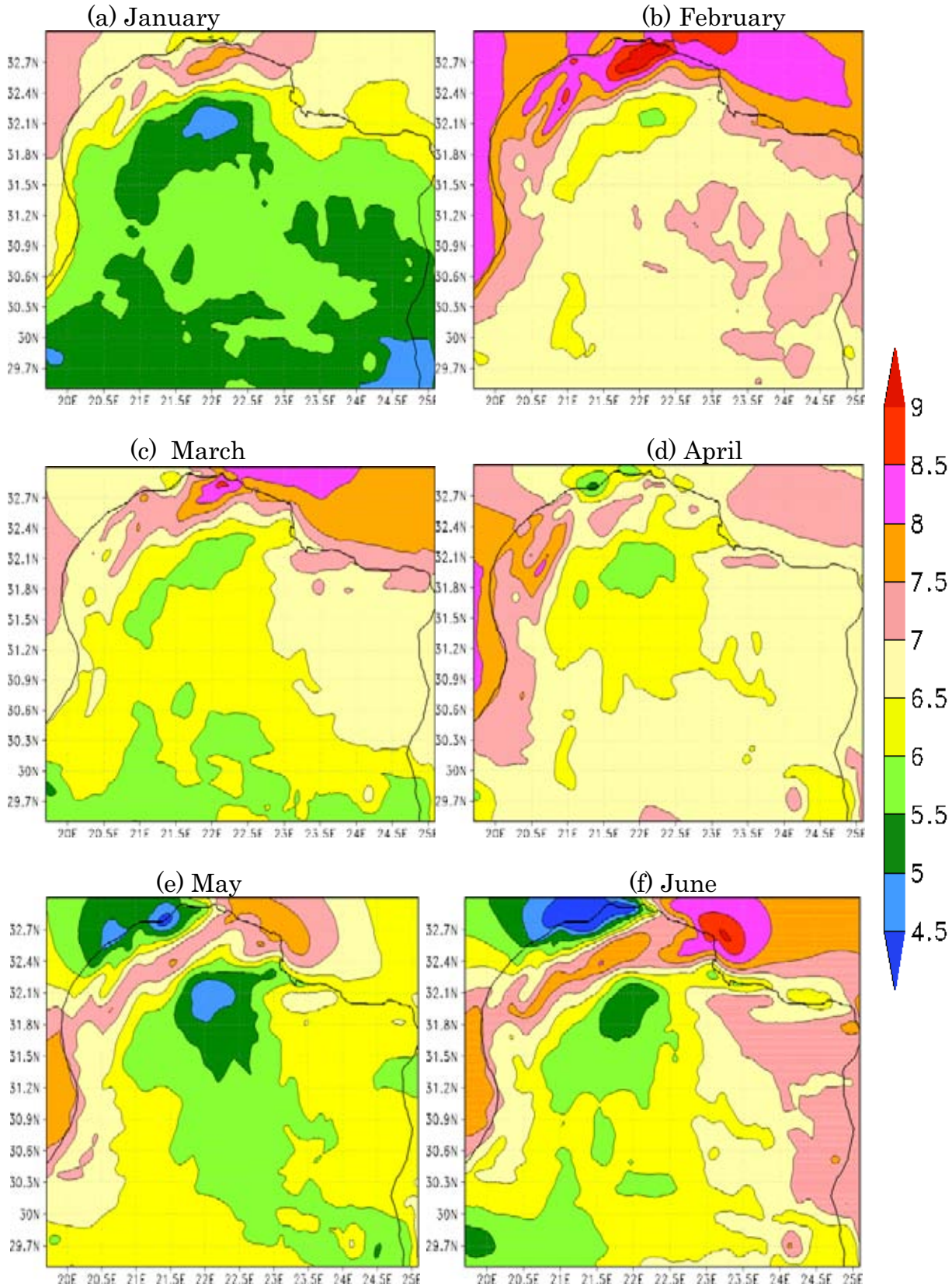

Figure 6.10: The estimated monthly mean 100-m wind speed [m/s] for the northeast region.

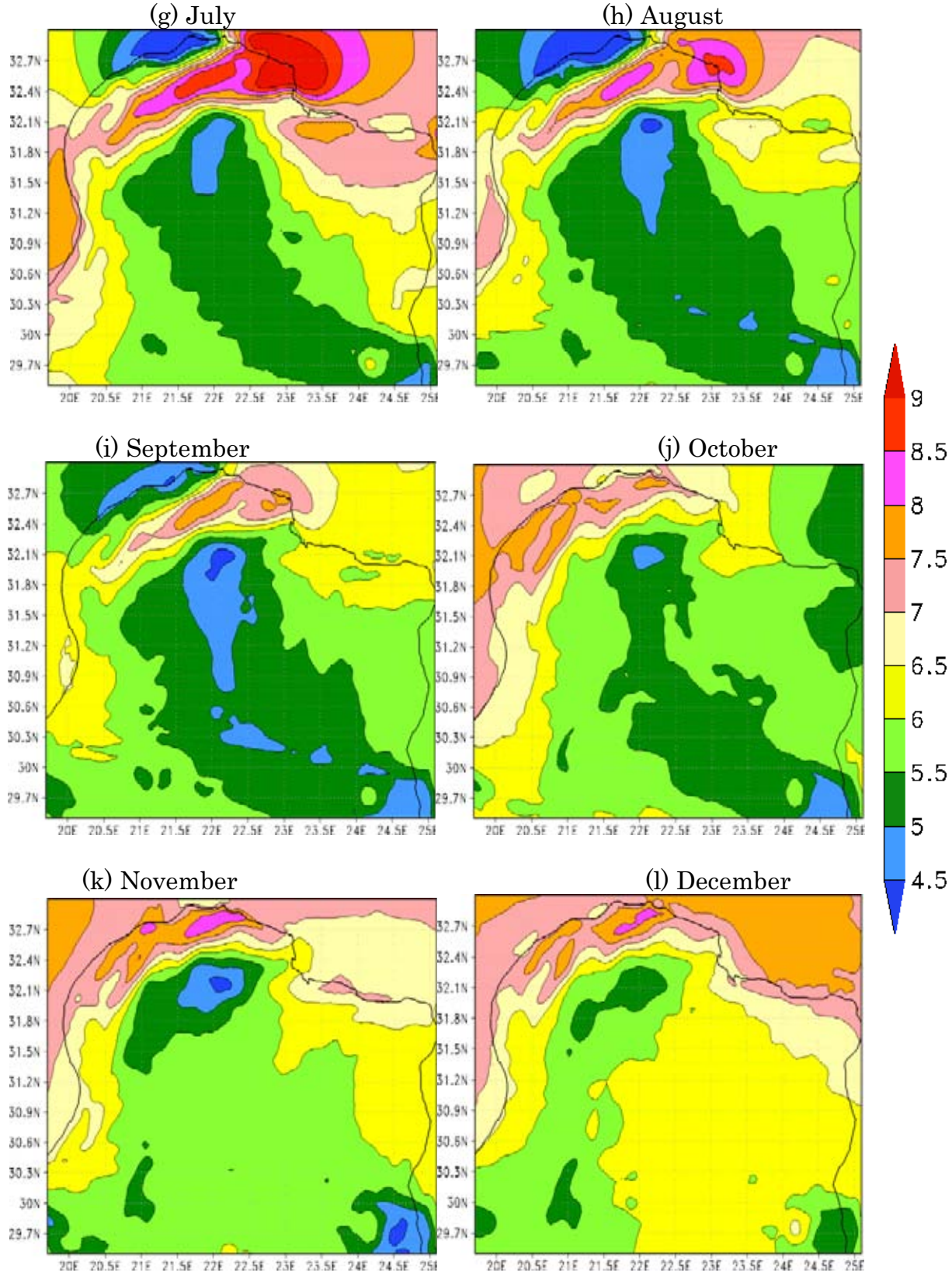

Figure 6.10 (continued): The estimated monthly mean 100-m wind speed [m/s] for the northeast region.

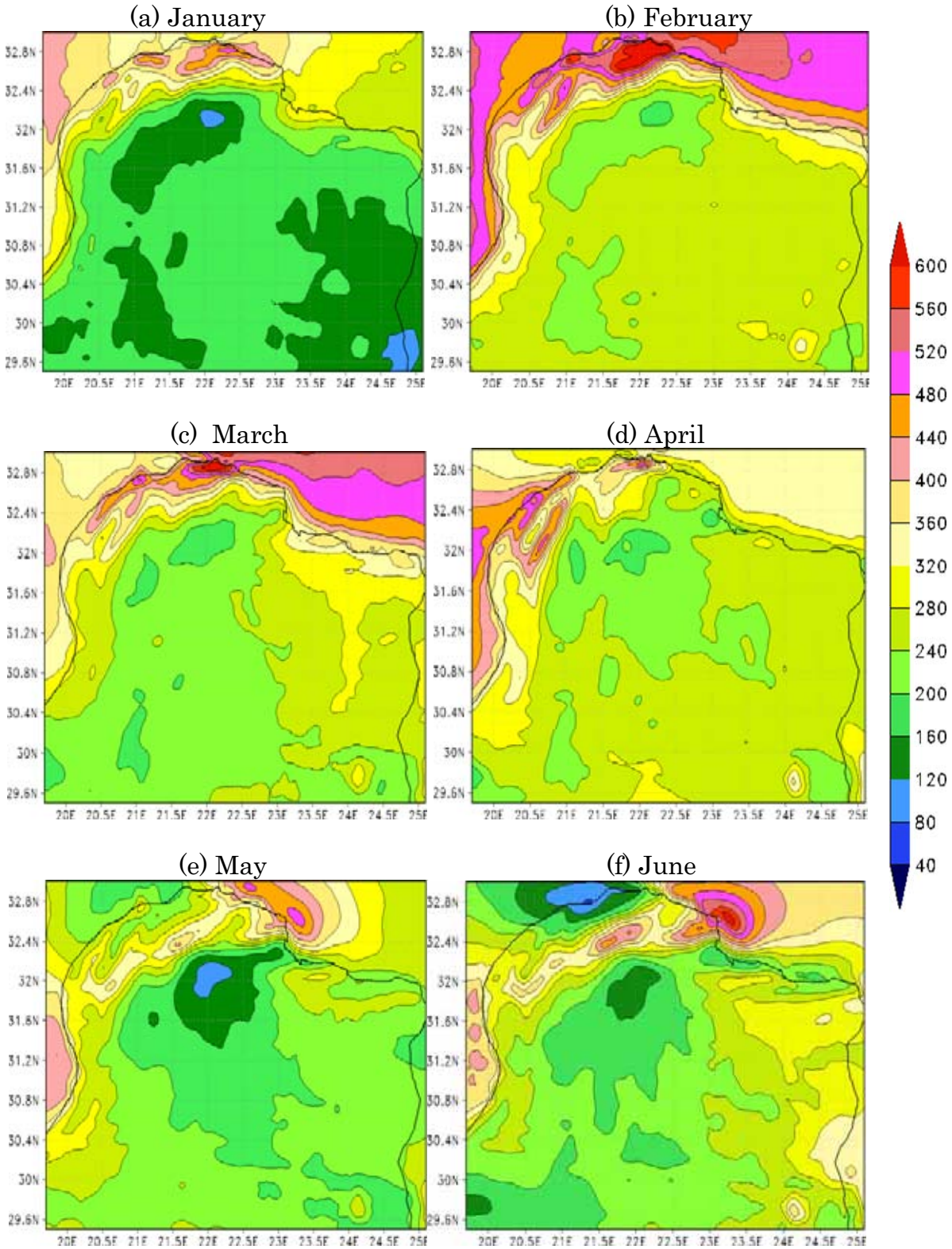

Figure 6.11: The estimated monthly mean 100-m wind power density [W/m^2] for the northeast region.

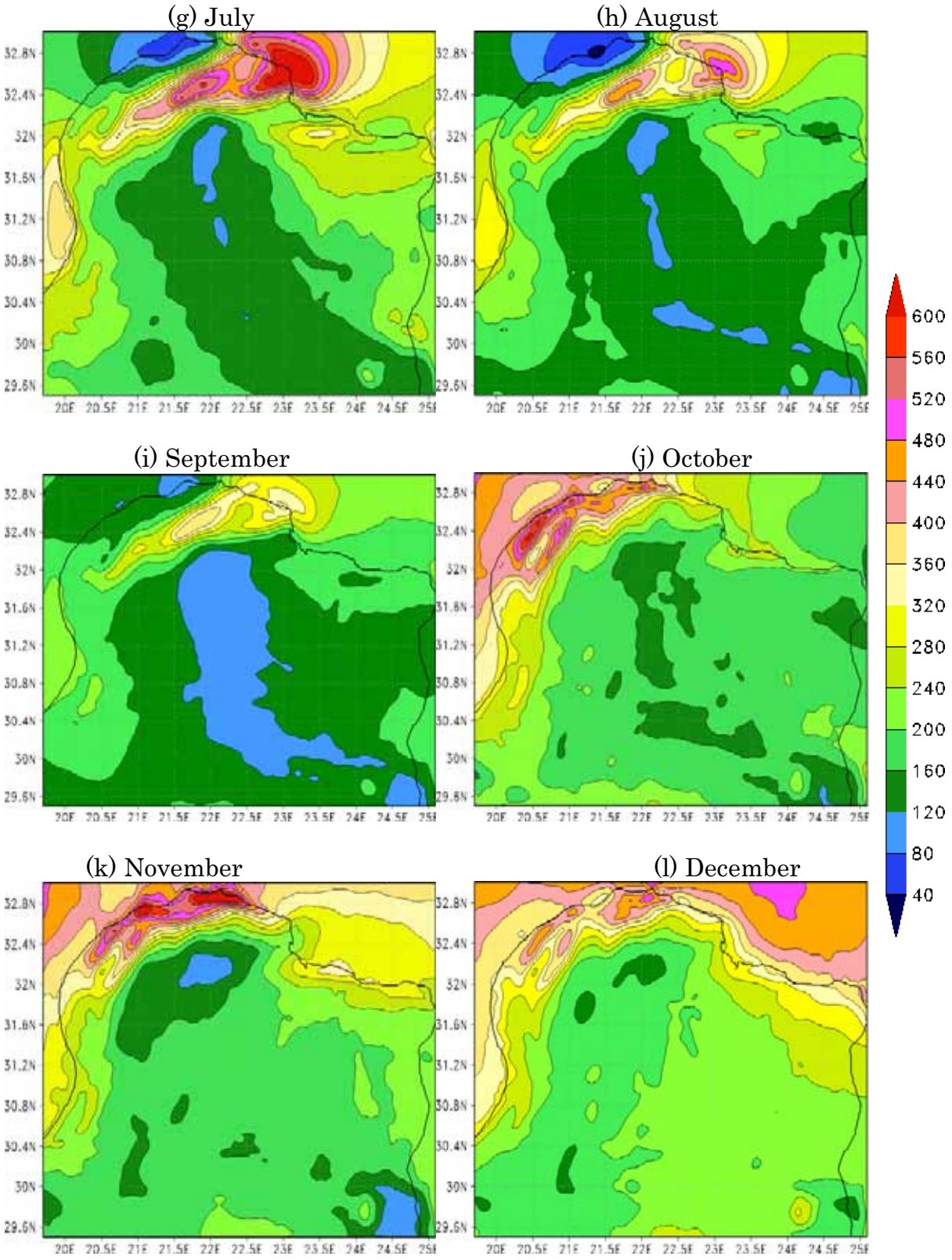

Figure 6.11 (continued): The estimated monthly mean 100-m wind power density [W/m^2] for the northeast region.

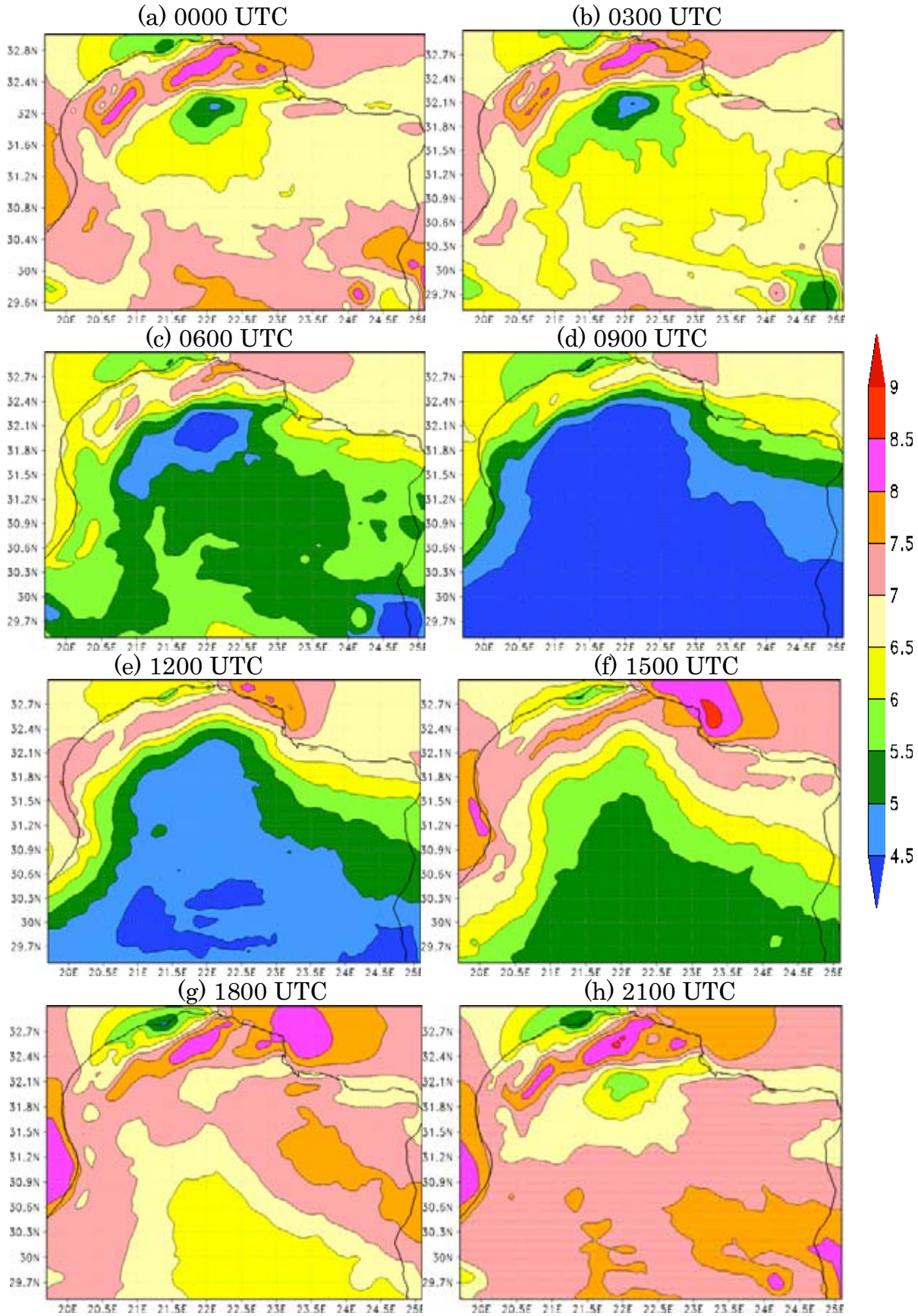

Figure 6.12: the estimated annual mean diurnal cycle of 100-m wind speed [m/s] for the northeast region.

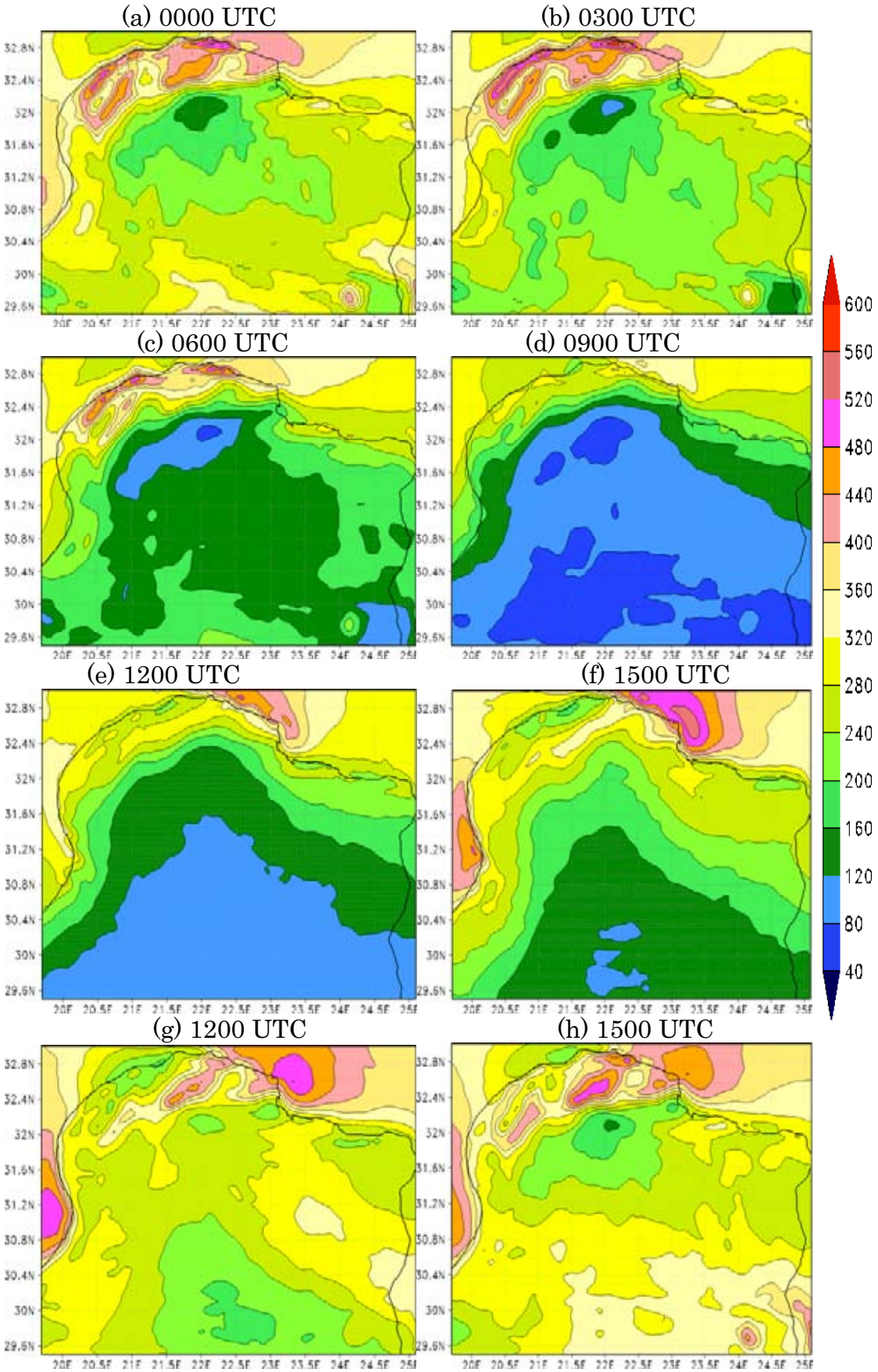

Figure 6.13: the estimated annual mean diurnal cycle of 100-m wind power [W/m^2] for the northeast region.

6.4 Wind Energy Resources of Northwest Region

6.4.1 Annual Pattern

The estimated annual mean 100-m wind speed for the northwest region is shown in Figure 6.14(a) and the matching wind power is demonstrated in Figure 6.14(b).

The figures show that more than half of this region is characterised by good wind energy resources. The coastline extending from the Libyan-Tunisian border eastward to Misratah has good wind blowing at speeds in the range of 6.5-7.5 m/s, and has power ranging from 320 up to 400 W/m^2. Among coastal areas, the location between Zuwarah and the Tunisian edge, and the zone bounded by Tripoli and Al Khums are the best from wind power point of view. They experience wind blowing at speeds between 7 and 7.5 m/s, and have power in the range of 360-400 W/m^2. The shore structure of these coastal areas enables them to receive stronger winds, as it is curved seaward, and exposed to sea/land breezes more than the surrounding zones. The altitudes of these districts are also close to mean sea level, meaning that sea breeze fronts are not blocked by the topography.

In addition to coastal regions, the crescent-shaped zone connecting Al Khums with Ghiryan and Jadu along to the Algerian border as well as Dirj, experiences more wind energy resources. It has wind blowing at speeds varying between 6.5 and 7.5 m/s, and the estimated power varies between 320 up to 520 W/m^2. These areas have high terrains extending up to around 800 m above sea level [Figure 6.8(b)].

On the contrary, the remaining areas of this region possess poor wind power resources with wind speeds ranging from 5 to 6 m/s, and power between 120 and 200 W/m^2. They do not seem to have a good potential for wind energy generation, and therefore they are out of the scope of the next discussions.

6.4.2 Seasonal Variations

Figures 6.15(a), 6.15(b), and 6.15(l) demonstrate the estimated monthly mean 100-m wind speed over the northwest region for winter months of January, February, and December, respectively. The corresponding power density for the same months is illustrated in Figures 6.16(a), 6.16(b), and 6.16(l).

As suggested by the figures, during winter the coastal zones have good wind power resources, particularly in February [Figures 6.15(b) and 6.16(b)]. The coastal wind speed falls in the range of 6-8.5 m/s, with about 240-600 W/m^2 of power.

The coastline situated between Tripoli and Misratah obtains more wind power resources than that extending from Tripoli westward to the Tunisian boarder. The mountainous districts around Ghiryan and Yifrin are also characterised by good wind power resources, since the wind blows at speeds ranging from 6.5 to 8.5 m/s, and the power ranges from 320 to 600 W/m^2. Of winter months, January experiences the lowest wind energy resource [Figures 6.15(a) and 6.16(a)].

Figures 615(c), 6.15(d), and 6.15(e) illustrate the estimated monthly mean 100-m wind speed for the northwest region for spring months of March, April, and May, respectively. The matching power density for the same months is demonstrated in Figures 6.16(c), 6.16(d), and 6.16(e).

These figures show that in spring the favourable areas consisting of the coastline, Yifrin, Ghiryan, and Dirj all experience great wind power resources, but the lowest energy resource occurs in May [Figures 6.15(e) and 6.16(e)]. These regions have monthly wind speeds in the range of 6-9 m/s, and power ranging from 320 up to more than 600 W/m^2.

As discussed earlier, the end of winter has great wind energy resources. Nevertheless, at the start of spring specifically in March [Figures 6.15(c)

and 6.16(c)] wind speed goes down slightly. After this month, wind speed increases to reach its maximum in April [Figures 6.15(d) and 6.16(d)], but it falls again in May. April enjoys the greatest wind energy resource of the year.

Figures 6.15(f), 6.15(g), and 6.15(h) show the estimated monthly mean 100-m wind speed over the northwest region for summer months of June, July, and August, respectively. The matching wind power density for the same months is shown in Figures 6.16(f), 6.16(g), and 6.16(h).

Summer wind energy resources vary from month to month. June [Figures 6.15(f) and 6.16(f)] experiences an apparent rise in the wind resource, but the resource diminishes in July [Figures 6.15(g) and 6.16(g)]. However, the wind resource re-increases gradually in August [Figures 6.15(h) and 6.16(h)], and continues to rise through the subsequent month.

In June, the favourable coastal and inland areas consisting of Zuwarah, Tripoli, Misratah, Ghiryan, Yifrin, Dirj, and the adjacent regions have monthly wind speeds in the range of 7-9 m/s, and power varying from 320 up to more than 600 W/m^2. In July and August, the wind over these districts blows at speeds of 5-8m/s, contributing to about 160-400W/m^2 of power.

The wind resource of Dirj and the surrounding regions varies between reasonable and good throughout summer months. The wind over these areas does not blow at monthly wind speeds lees than 6.5 m/s, while the power falls in the range of 280-600 W/m^2. This suggests that if wind turbines were installed over these regions, their power production would be stable during the time at which coastal wind turbines do not receive sufficient wind resources. They can complement each other so that electricity networks attain steady power during most of the time.

Figures 6.15(i), 6.15(j), and 6.15(k) show the estimated monthly mean 100-m wind speed over the northwest region for autumn months of September,

October, and November, respectively. The corresponding wind power density for the same months is demonstrated in Figures 6.16(i), 6.16(j), and 6.16(k).

The aforementioned figures point out that the monthly variability of wind energy resources over the favourable regions still exists even in autumn. Wind energy resources increase in September [Figures 6.15(i) and 6.16(i)] and October [Figures 6.15(j) and 6.16(j)], whereas they diminish in November [Figures 6.15(k) and 7.16(k)]. In October, the potential coastal and inland areas have monthly wind speeds varying between 6.5 and 8 m/s, and power in the range of 240-480 W/m^2.

The monthly variability in the wind resource of autumn may complement each other. September has good wind power resources along the western coastline near Zuwarah, and Dirj along with the nearby areas, while it sees less potential resources over the eastern coastal zone and Ghiryan. In contrast, November experiences greater wind energy potential over the eastern coastline than the western coastline as well as Dirj. October has good wind power resources over all the identified regions, except Dirj and the nearby districts. When installing some wind turbines over all these regions, the turbines can assist each other to generate steady and sufficient amounts of power continuously.

6.4.3 Diurnal Variations

Figures 6.17(a) through 6.17(h) demonstrate the estimated annual mean diurnal cycle of 100-m wind speed at 0000, 0300, 0600, 0900, 1200, 1500, 1800, and 2100 UTC, in that order. These figures illustrate that the favourable coastal and inner regions have larger amounts of wind power resources at nighttime than during daytime.

During sunrise at around 0600 UTC [Figures 6.17(c) and 6.18(c)], the wind speed begins to wane until midmorning between around 0900 UTC

[Figures 6.17(d) and 6.18(d)] and midday. During these hours, the wind blows at speeds of 5.5-8 m/s, and it contains about 120-480 W/m^2 of power.

After 1200 UTC [Figures 6.17(e) and 6.18(e)], the wind speed begins to increase gradually through the afternoon and evening until it reaches its maximum at night, specifically at about 2100 UTC [Figures 6.12(h) and 6.13(h)]. The wind speed and the matching power fall in the range of 6.5-9 m/s, and 240-560 W/m^2, respectively. The increase rate of coastal wind speeds is higher than that of inland wind speeds, especially in the afternoon at 1500 UTC [Figures 6.17(f) and 6.18(f)]. The coastline, Ghiryan, Yifrin, Dirj, and the neighbouring areas continue to obtain good wind power resources until midnight.

After 0000 UTC [Figures 6.17(a) and 6.18(a)] through to sunrise before 0600 UTC [Figures 6.17(c) and 6.18(c)], the wind resource is high over the coastline, Ghiryan, Yifrin, and Dirj. These regions have winds blowing at speeds between 6.5 and 9 m/s, and wind power varying from 280 to more than 600 W/m^2. During the second half of the night, the favourable inland zones obtain larger amounts of wind energy resources than those along the seashore.

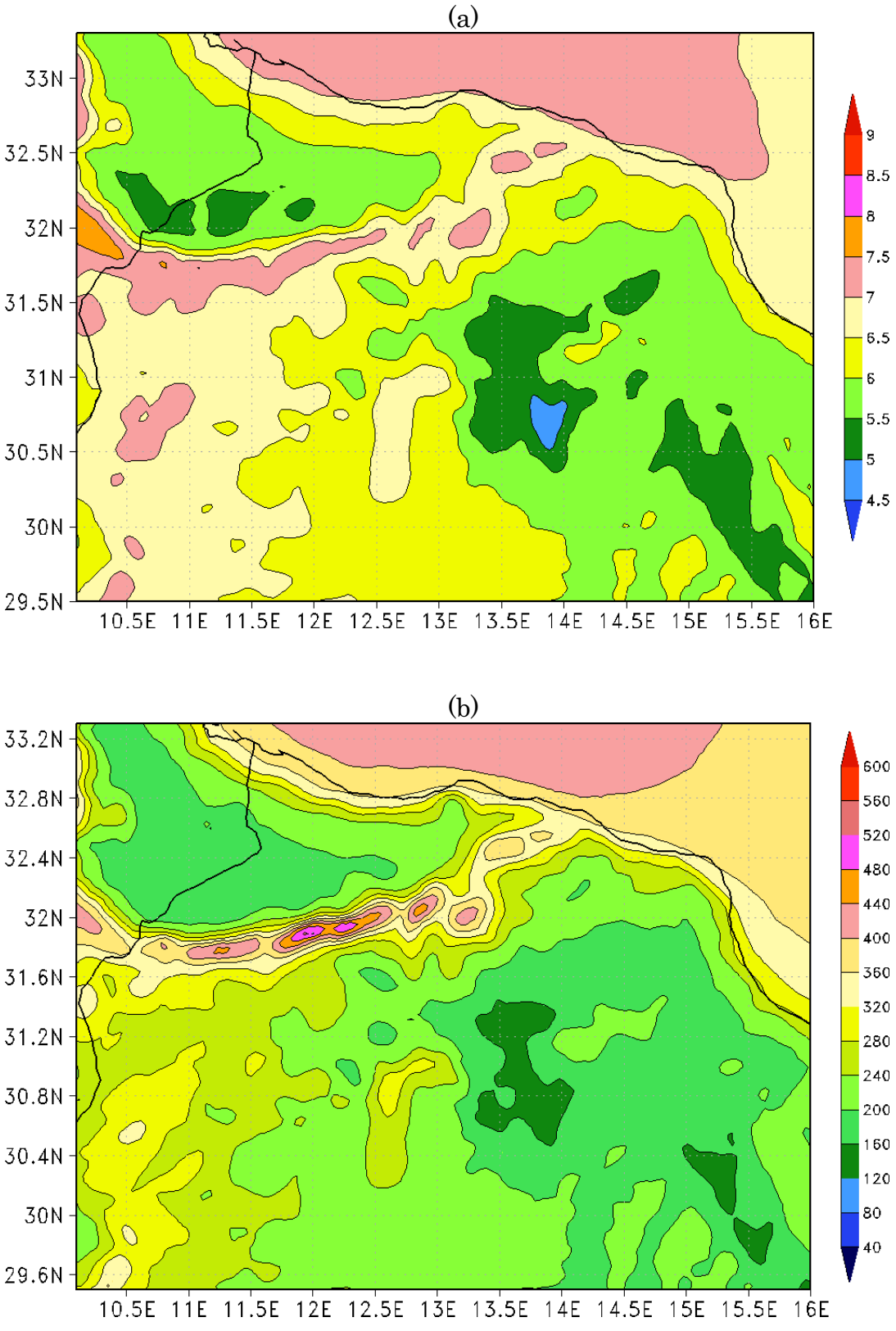

Figure 6.14: (a) The estimated annual mean 100-m wind speed [m/s] and (b) the corresponding wind power density [W/m^2] for the northwest region.

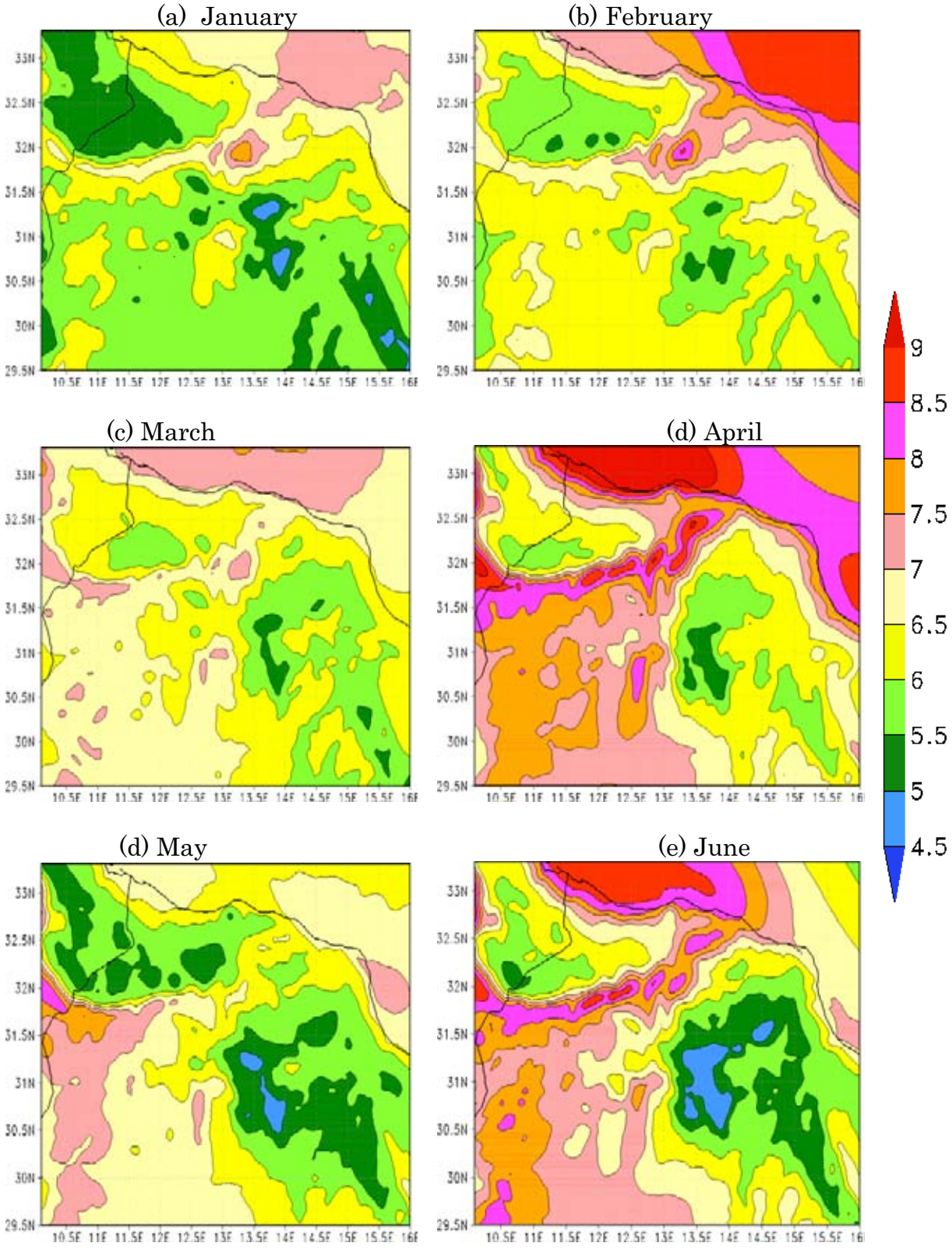

Figure 6.15: The estimated monthly mean 100-m wind speed [m/s] for the northwest region.

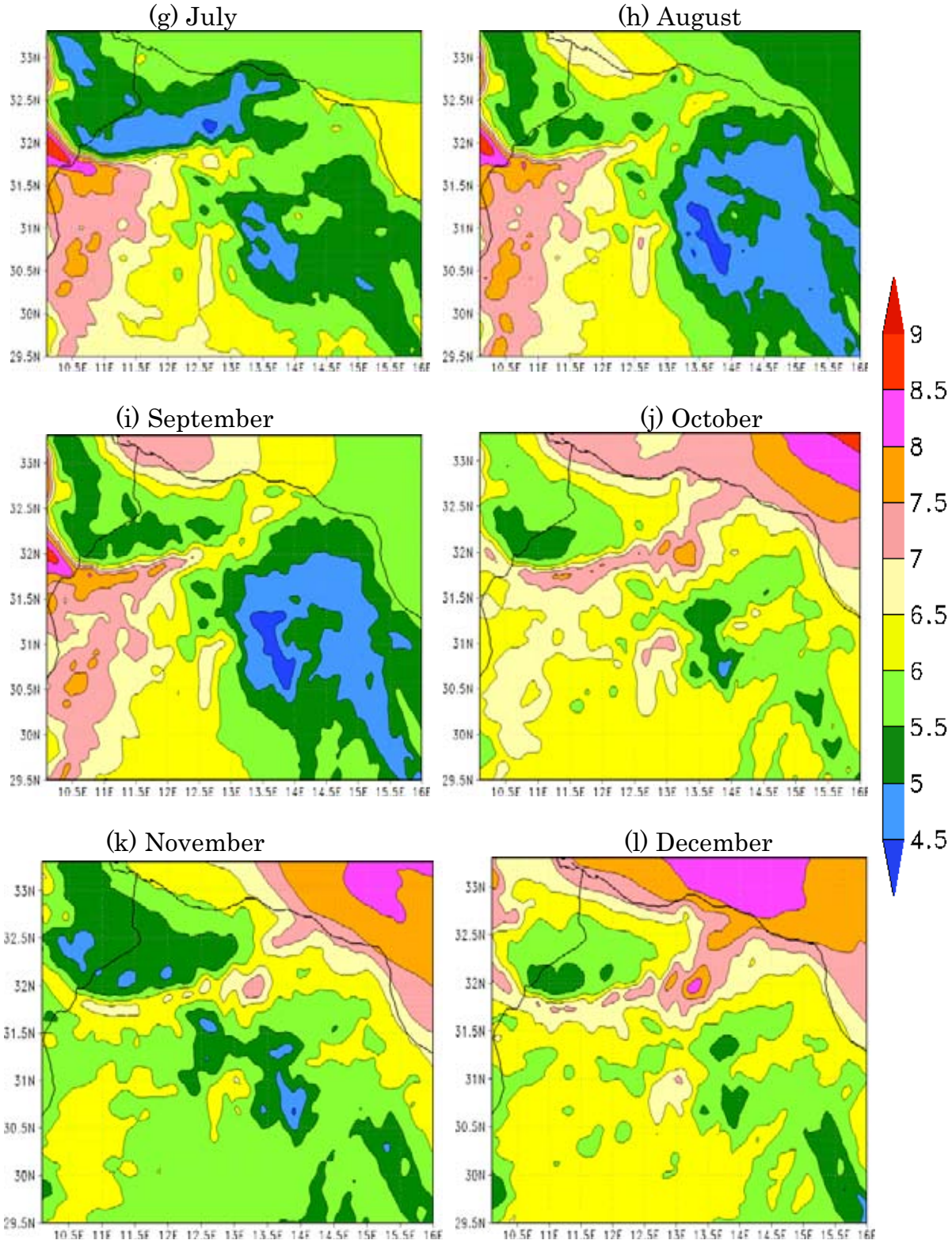

Figure 6.15 (continued): The estimated monthly mean 100-m wind speed [m/s] for the northwest region.

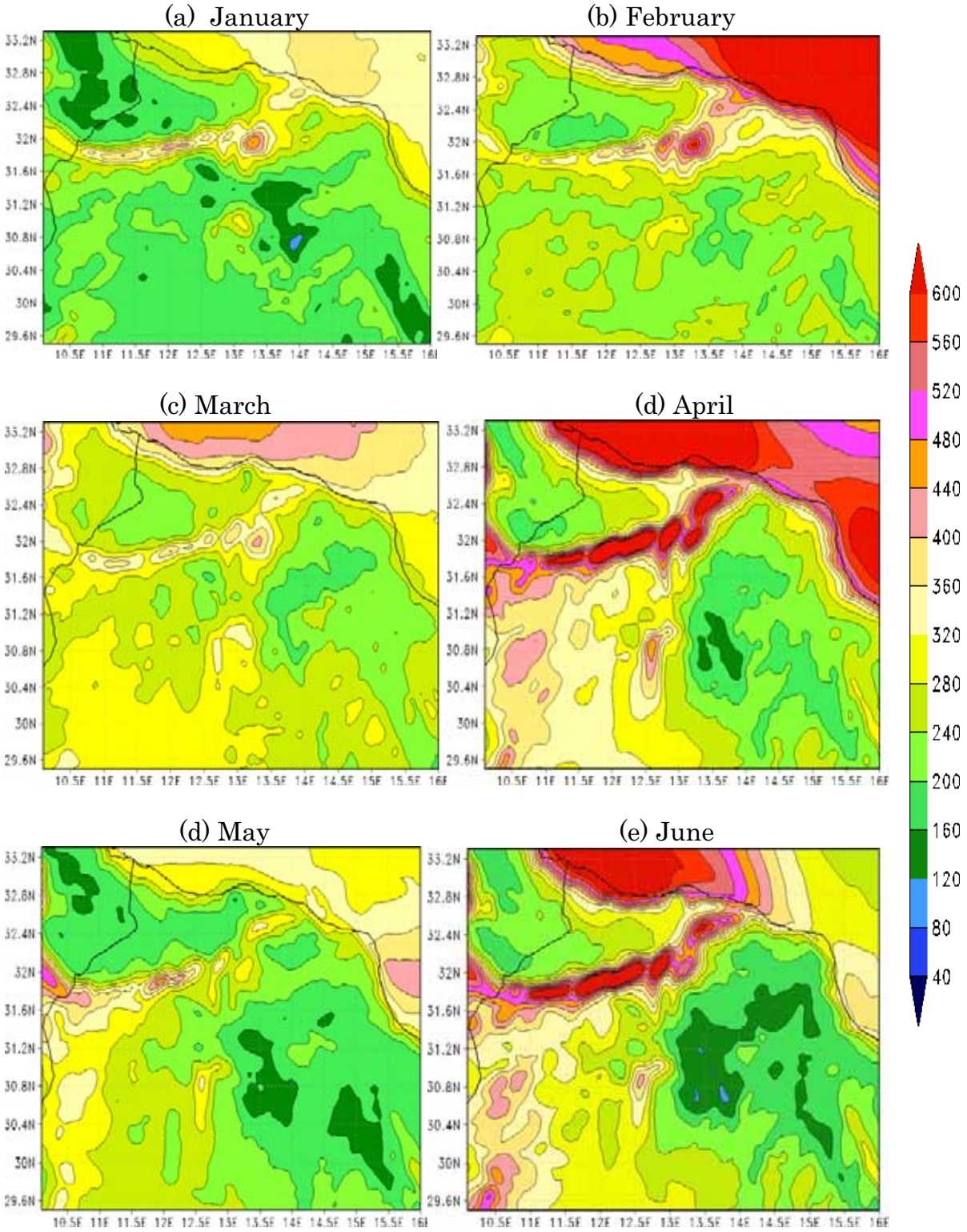

Figure 6.16: The estimated monthly mean 100-m wind power density [W/m^2] for the northwest region.

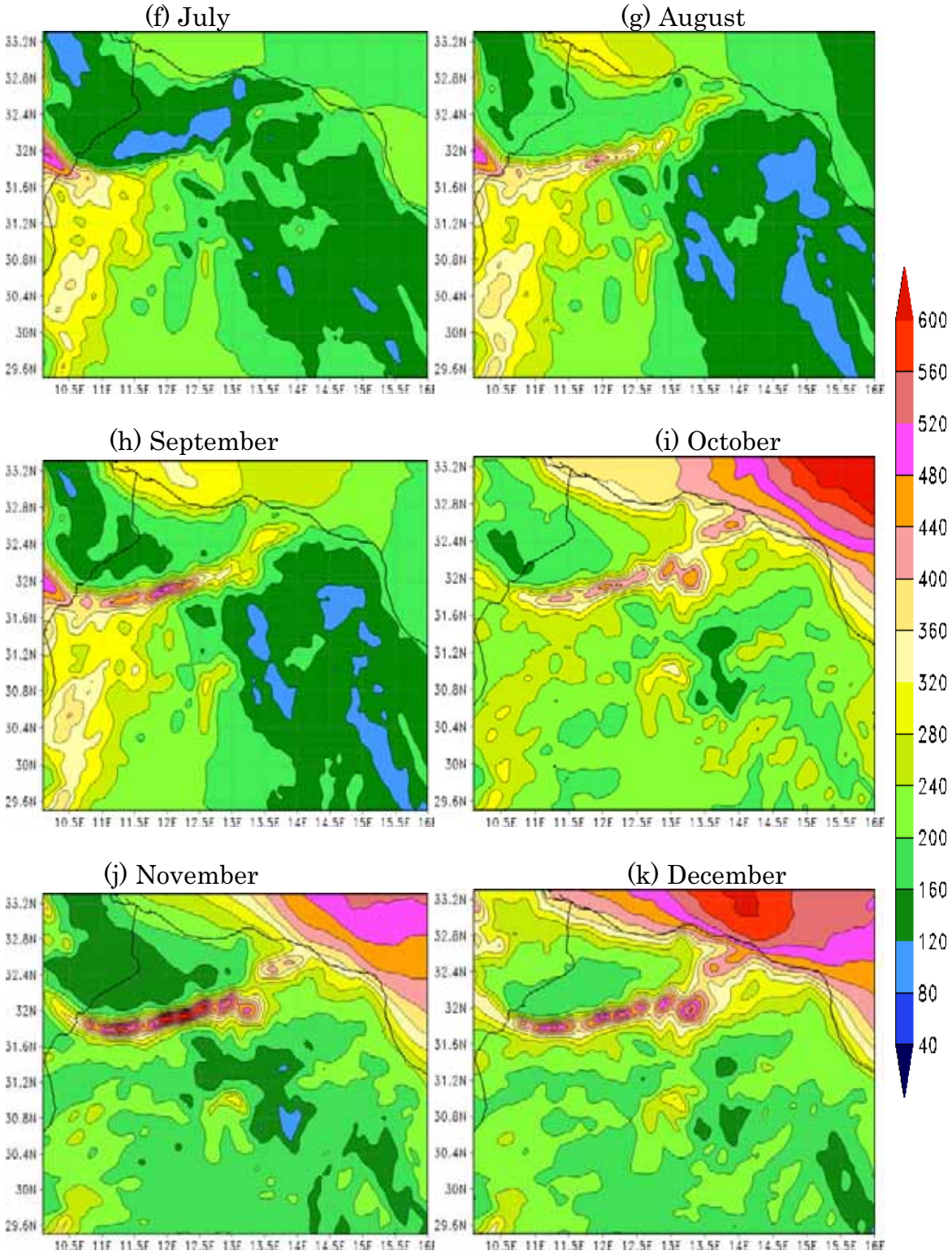

Figure 6.16 (continued): The estimated monthly mean 100-m wind power density [W/m^2] for the northwest region.

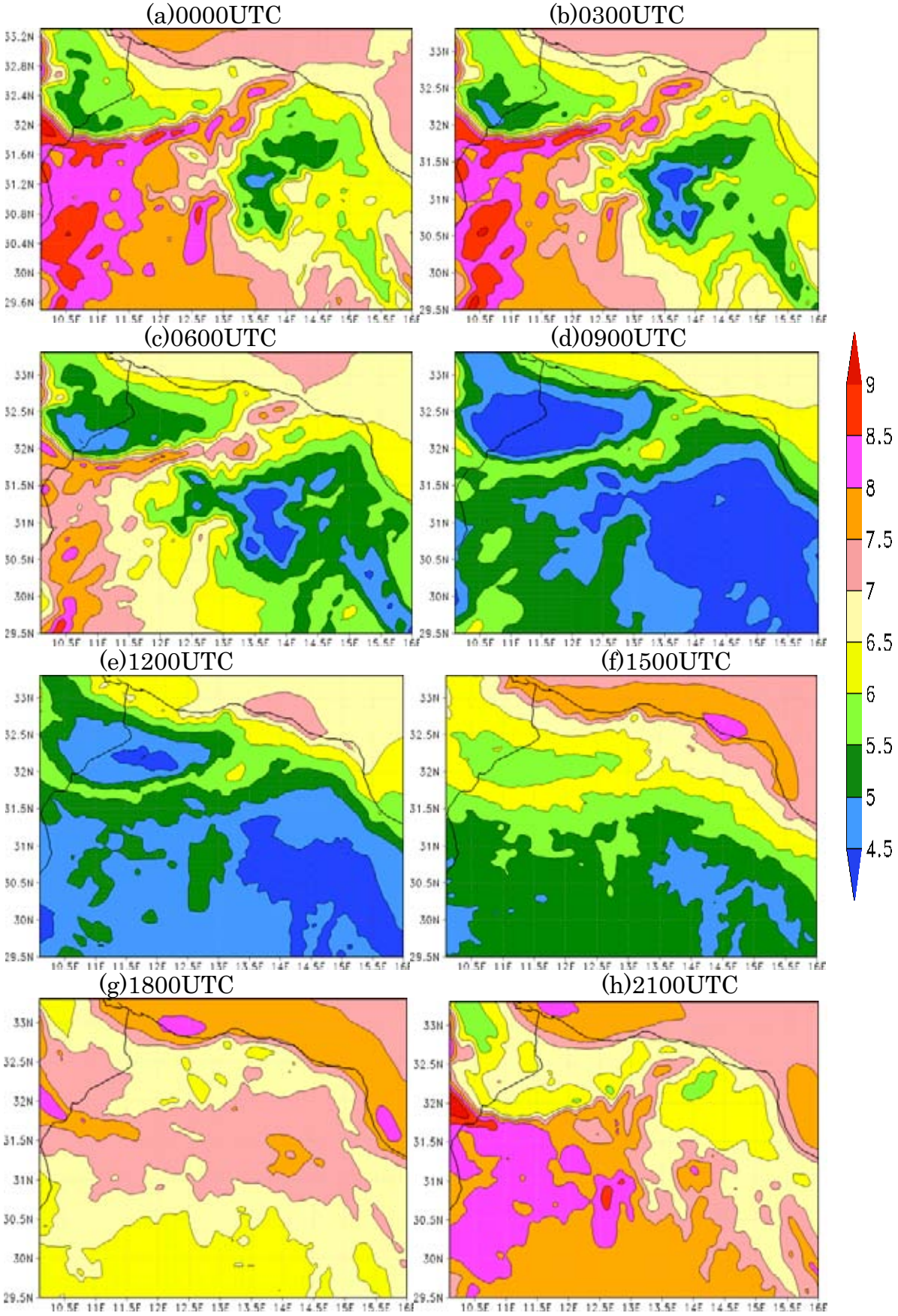

Figure 6.17: The estimated annual mean diurnal cycle of 100-m wind speed [m/s] for the northwest region.

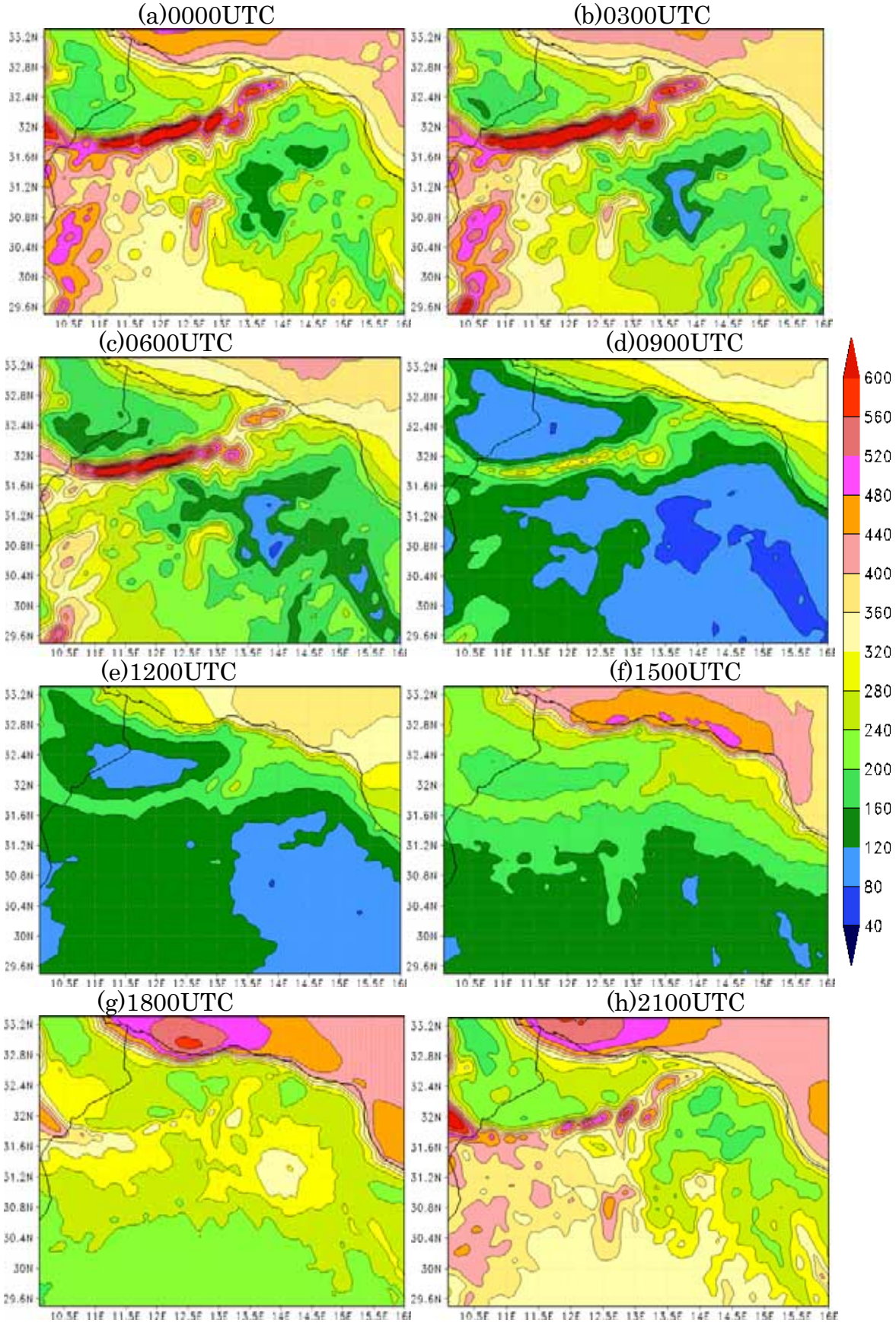

Figure 6.18: The estimated annual mean diurnal cycle of 100-m wind power density [W/m^2] for the northwest region.

6.5 Wind Energy Resources of Southeast Region

6.5.1 Annual Pattern

Figures 6.19(a) and 6.19(b) show the estimated annual mean 100-m wind speed and the corresponding wind power density of the southeast region, respectively. They suggest that the vast majority of the Sahara Desert of Libya has very good wind resources, especially on high-altitude terrains. Surprisingly, this region enjoys stronger winds than those zones along the Mediterranean coast.

More than half of the territory experiences annual wind speeds between 6.5 m/s and 11 m/s, and the corresponding power falls in the range of 250-750 W/m^2 [Figures 6.19(a) and 6.19(b)]. The favourable areas are those having elevations higher than 500 m above mean sea level [Figure 6.8(c)].

The northwest of Al Kufrah and the central part of the region receive low wind power resources accounting for the lowest resource in this region. These zones have wind blowing at speeds between 5.5 and 6.5 m/s and power of 150-250 W/m^2.

The Tibesti Volcanic Mountains, extending from Chad to short distances into the southern part of Libya, obtain the greatest amount of wind resource not only in this region but also throughout the country. Their rocky slope located in Libya is about 2000 m above sea level. The wind blows at high speeds reaching 11 m/s or more, and the matching power reaches 750 W/m^2. The north of the Tibesti Mountains is also characterised by strong winds. It may be affected by mountain-valley breezes generated along the northern slop of the mountains due to differential surface heating or cooling.

Based on the equation of atmospheric state the air density diminishes with height. Although the mountainous inland regions have higher wind speeds than coastal regions, they sometimes experience less wind power. That is

why it is advantageous for wind power applications to calculate the power using the actual condition of air density rather than the standard one. If the standard air density (1.225 kg/m^3) was used to estimate the power density, there would be an overestimation in the power available in regions like these mountains.

6.5.2 Seasonal Variations

Figures 6.20(a), 6.20(b), and 6.20(l) demonstrate the estimated monthly mean 100-m wind speed for the southeast region for winter months of January, February, and December, respectively. The matching wind power density for these months is shown in Figures 6.21(a), 6.21(b), and 6.21(l). Based on these figures, wind power resources for winter tend to fluctuate.

The wind resources over the Tibesti Mountains and the northern zone in December [Figures 6.20(l) and 6.21(l)] are great. The monthly wind speed at these areas varies between 7 and 9 m/s, and the resulting power ranges from 300 to more than 550 W/m^2. January [Figures 6.20(a) and 6.21(a)] experiences a decline in wind power resources, as the wind blows at speeds in the range of 6.5-9 m/s and the power falls in the range of 250-550 W/m^2. Wind speed increases in February [Figures 6.20(b) and 6.21(b)], and continues to rise during the following months.

Figures 6.20(c), 6.20(d), and 6.20(e) illustrate the estimated monthly mean 100-m wind speed over the southeast region for spring months of March, April, and May, in that order. Figures 6.21(c), 6.21(d), and 6.21(e) show the corresponding wind power density for the same months. As indicated by these figures, spring is characterised by increasing wind energy resources.

The Tibesti Mountains and the northern areas have monthly wind speeds varying between 7 and 10.5 m/s, and power between 350 and 750 W/m^2. Ever since the end of winter, wind speed has risen gradually and so March [Figures 6.20(c) and 6.21(c)] experiences higher wind resources than February. In April [Figures 6.20(d) and 6.21(d)] and May [Figures 6.20(e)

and 6.21(e)], the monthly wind speed over the favourable regions reaches 10 m/s, and the power is about 650 W/m^2.

Figures 6.20(f), 6.20(g), and 6.20(h) demonstrate the estimated monthly mean 100-m wind speed for the southeast region for summer months of June, July, and August, in that order. Figures 6.21(f), 6.21(g), and 6.21(h) show the matching wind power density for the same months. These figures point out that summer has very good energy resources. There is no marked differences in the temporal distribution of summer resources, since the monthly wind speed and the matching power density throughout June [Figures 6.20(f) and 6.21(f)], July [Figures 6.20(g) and 6.21(g)], and August [Figures 6.20(h) and 6.21(h)] are quite similar. The monthly wind speed over the potential zones falls in the range of 7-11 m/s, while the power varies between 350 and 750 W/m^2.

Figures 6.20(i), 6.20(j), and 6.20(k) illustrate the estimated monthly mean 100-m wind speed for the southeast region for autumn months of September, October, and November, respectively. The matching wind power density for these months is illustrated in Figures 6.21(i), 6.21(j), and 6.21(k). Although in autumn some regions obtain lees wind energy resources than other seasons, the favourable areas being the Tibesti Mountains and the northern zones persist to receive steady and good wind energy resources. These areas experience winds blowing at speeds of 7-11 m/s, and wind power ranging from 350 to 750 W/m^2. Among autumn months, November [Figures 6.20(k) and 6.21(k)] has the lowest wind energy resource.

6.5.3 Diurnal Variations

Figures 6.22(a) through 6.22(h) present the estimated annual mean diurnal cycle of 100-m wind speed at 0000, 0300, 0600, 0900, 1200, 1500, 1800, and 2100 UTC, in that order. The matching wind power density is shown in Figures 6.23(a) to 6.23(h). Similar to previous regions, the figures indicate

that nocturnal wind energy resources are higher than daytime ones, although this temporal resource variability over low-altitude districts is more distinguishable than over high-altitude ones.

During the early morning at about 0600 UTC [Figures 6.22(c) and 6.23(c)] wind speed begins to fall dramatically, and continues to wane until around 1200 UTC [Figures 6.22(e) and 6.23(e)]. Between 0900 UTC [Figures 6.22(d) and 6.23(d)] and 1200 UTC, most parts of the region see a significant decline in wind energy resources. Wind speed over the Tibesti Mountains and the surrounding areas varies between 5.5 and 9 m/s, and the corresponding power ranges from 150 to 650 W/m^2.

Wind power resources are also good over the northern areas of the Tibesti Mountains. Strong winds over these districts could be generated due to thermal mountain-valley circulations. Yet, during sunrise and morning hours, the temperature and pressure gradients are small and local thermal breezes are weak, and so upper air circulations cannot be formed. This might be the reason why wind speed drops significantly in the morning.

During the late afternoon at about 1500 UTC [Figures 6.22(e) and 6.23(e)], local flows may start to develop, and the wind regains its strength. Wind speed over the identified potential region increases in the evening. The wind peaks at night, namely at about 2100 UTC [Figures 6.22(h) and 6.23(h)]. At the commencement of the development of the air movement at 15000 UTC, wind speed varies between 5.5 and 9 m/s. Between this time and midnight, wind speed increases to 8-11 m/s, and the power ranges from 350 to more than 750 W/m^2.

After 0000 UTC [Figures 6.22(a) and 6.23(a)], the wind continues to blow at high wind speeds over most areas of the region but it slows down slightly through dawn at about 0600 UTC [Figures 6.22(c) and 6.23(c)]. During this time, wind speed over the favourable zones ranges from 7.5 to more than 11 m/s, and the power varies between 350 and more than 750 W/m^2.

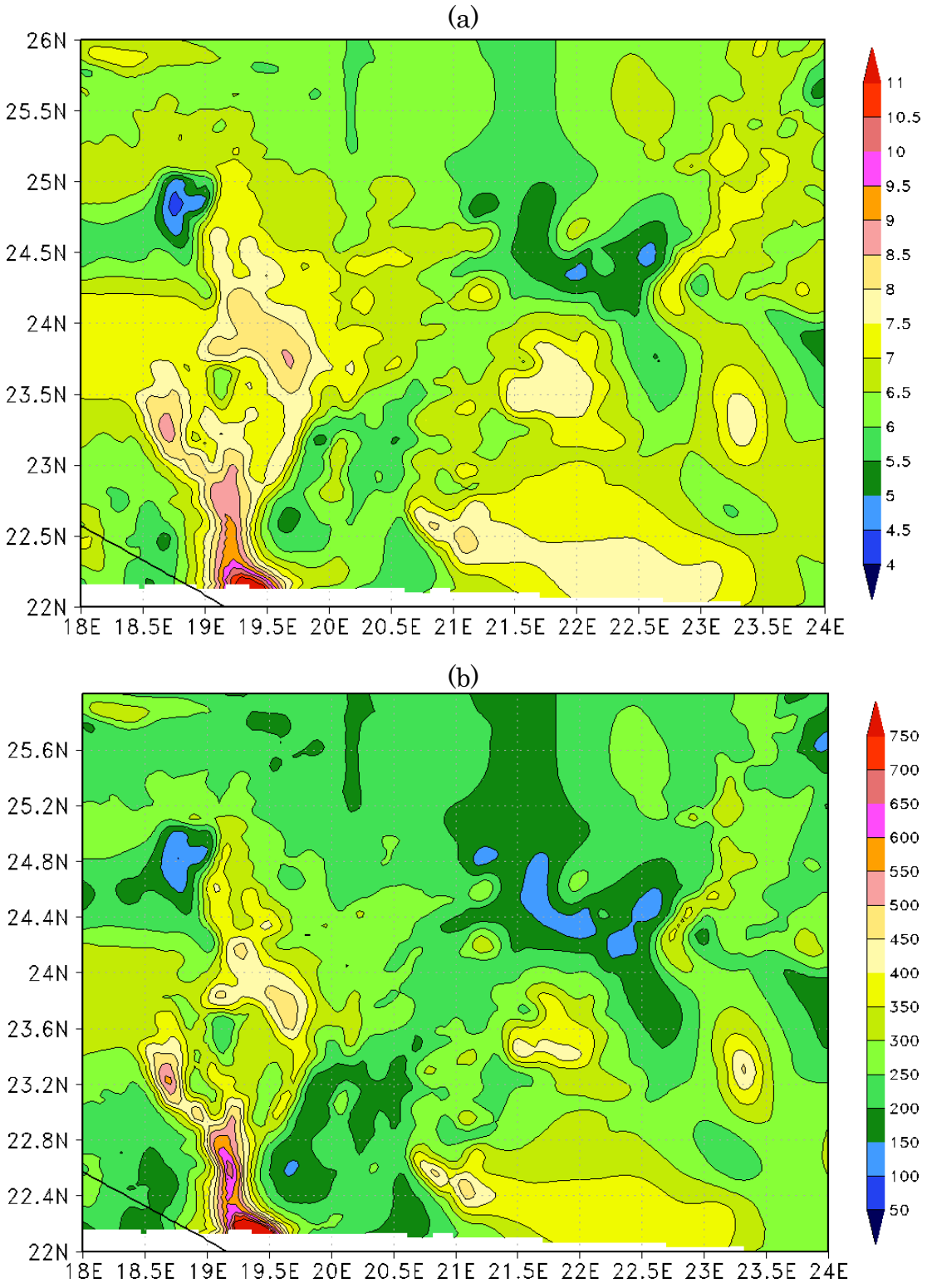

Figure 6.19: (a) The estimated annual mean 100-m wind speed [m/s] and (b) the corresponding wind power density [W/m^2] for the southeast region.

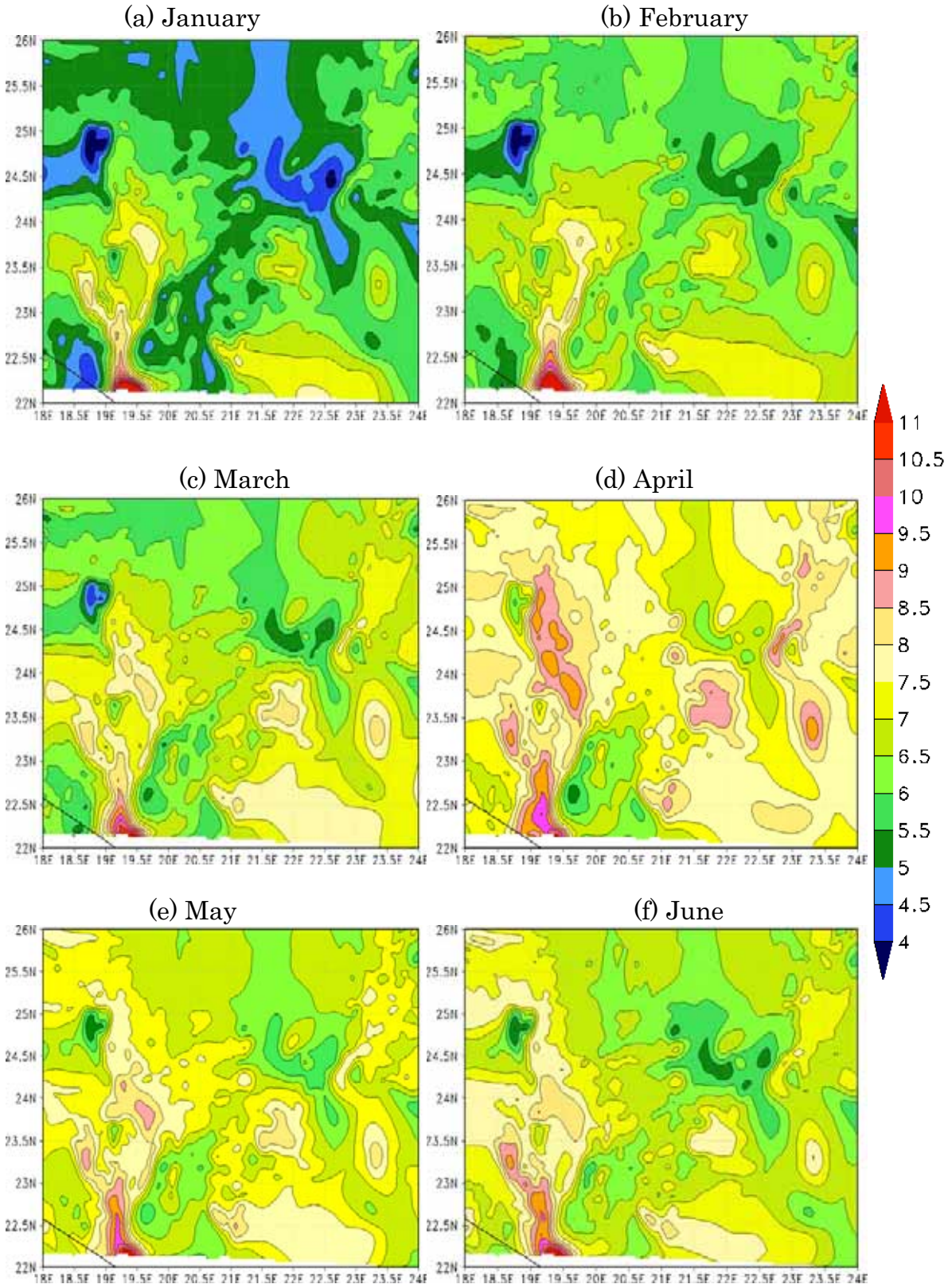

Figure 6.20: The estimated monthly mean 100-m wind speed [m/s] for the southeast region.

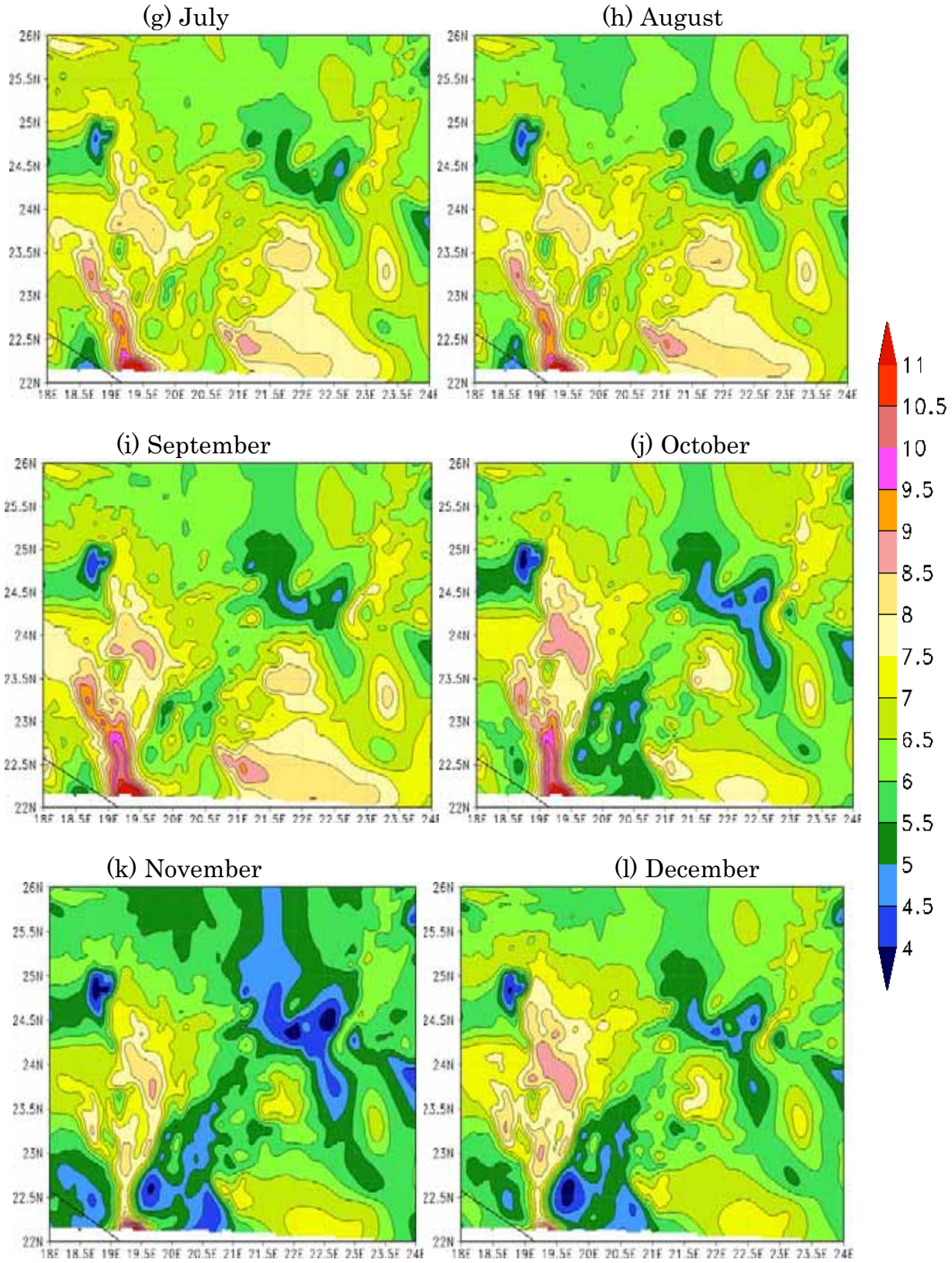

Figure 6.20 (continued): The estimated monthly mean 100-m wind speed [m/s] for the southeast region.

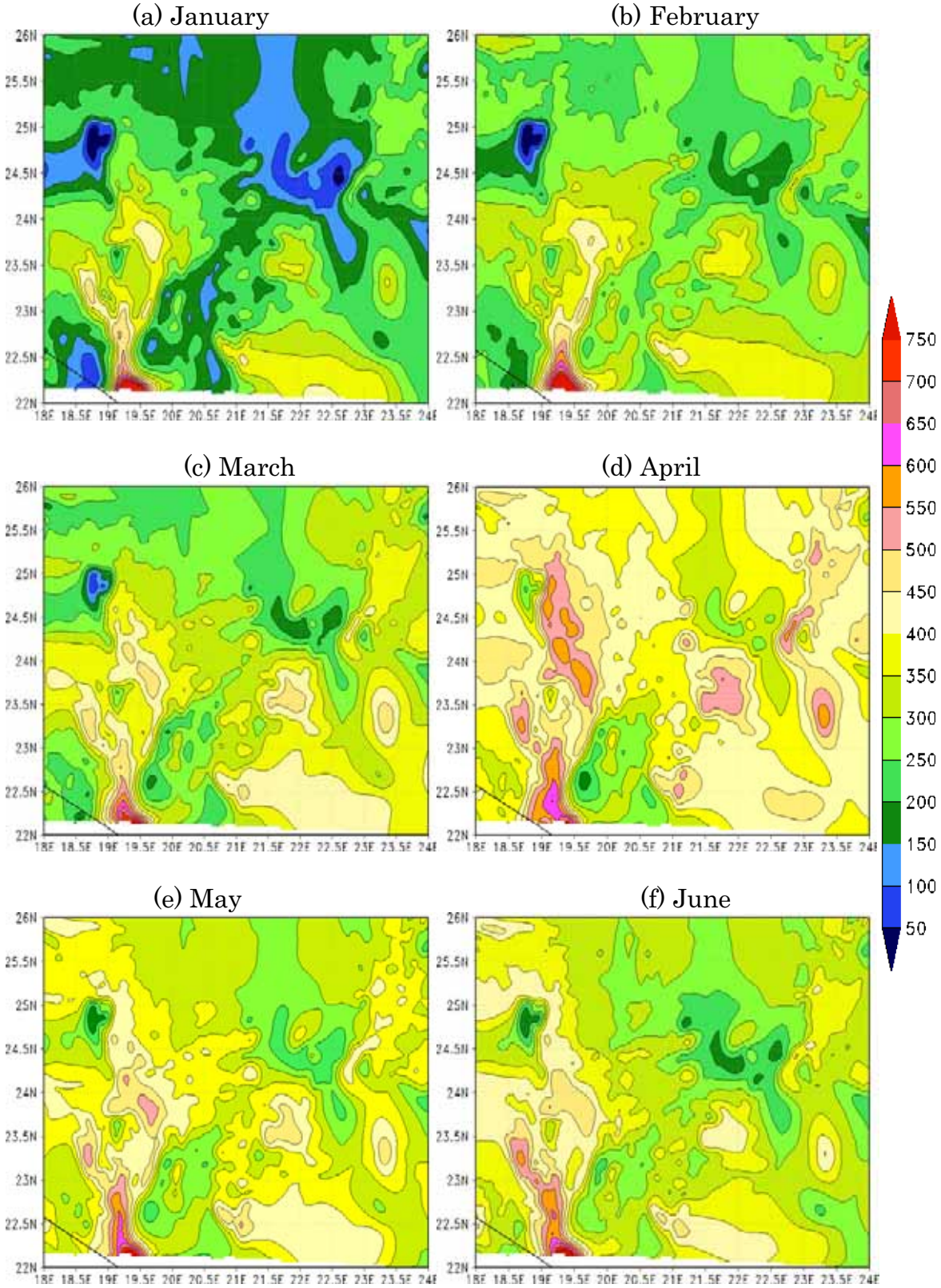

Figure 6.21: The estimated monthly mean 100-m wind power density [W/m^2] for the southeast region.

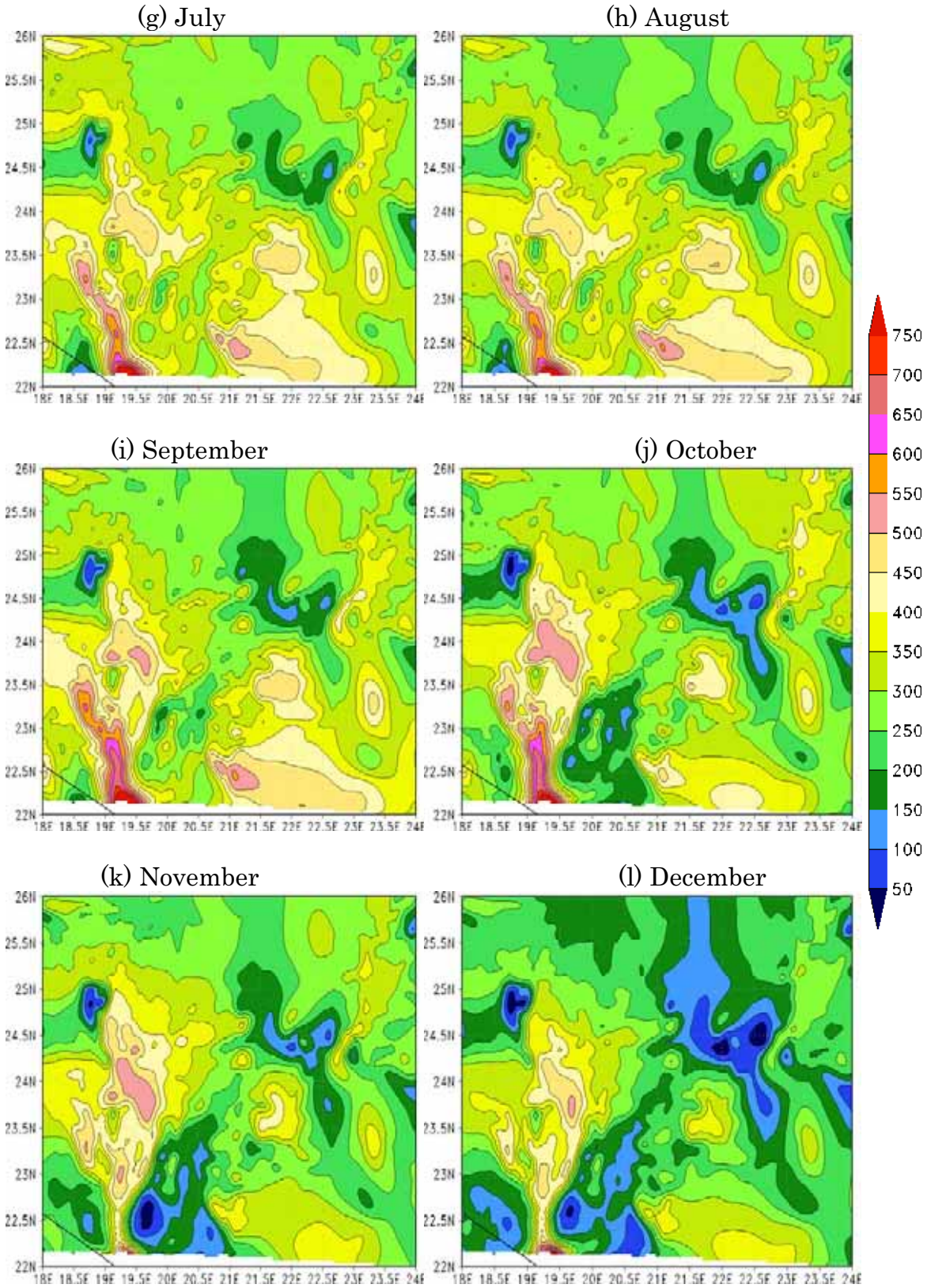

Figure 6.21 (continued): The estimated monthly mean 100-m wind power density [W/m^2] for the southeast region.

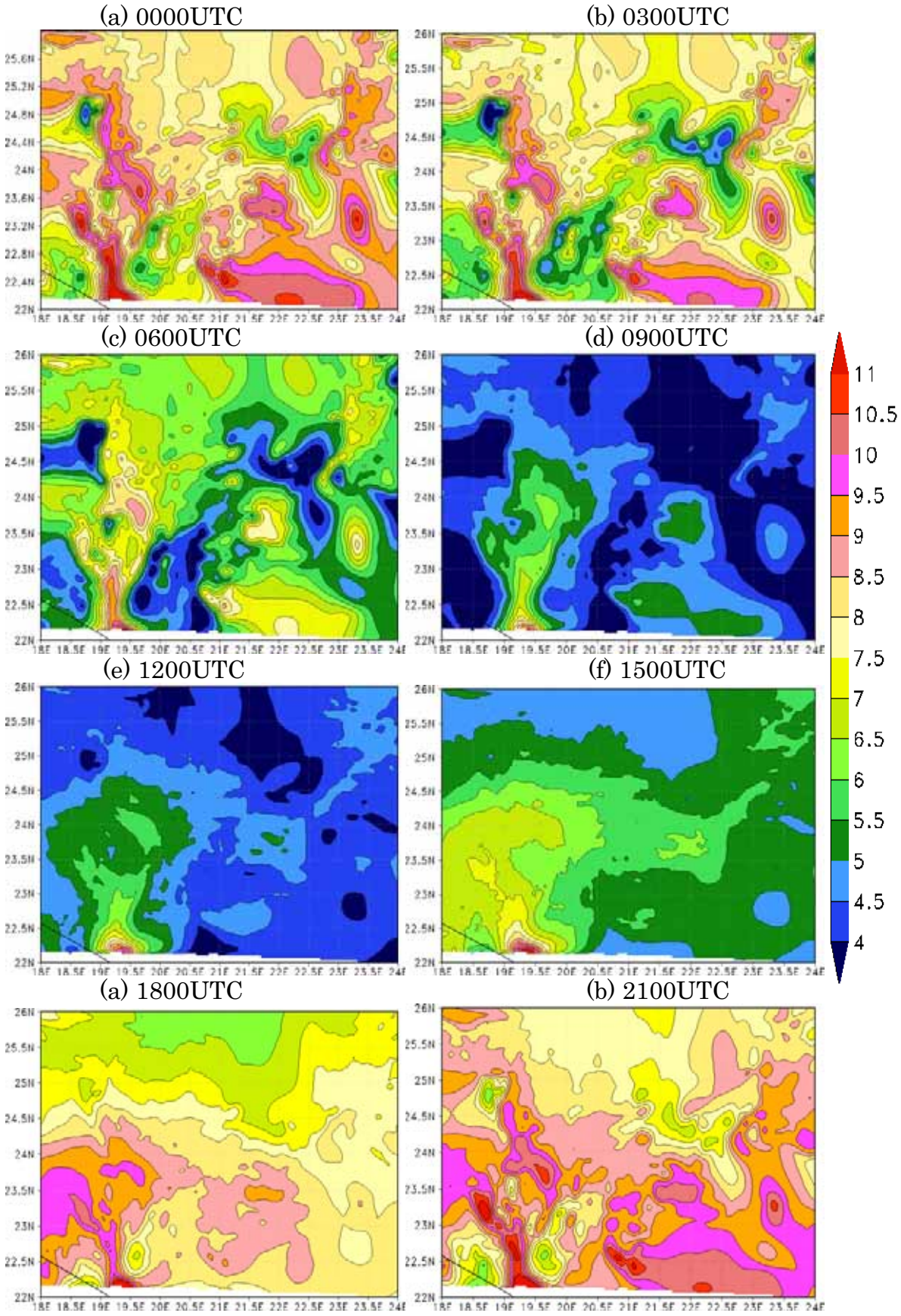

Figure 6.22: The estimated annual mean diurnal cycle of 100-m wind speed [m/s] for the southeast region.

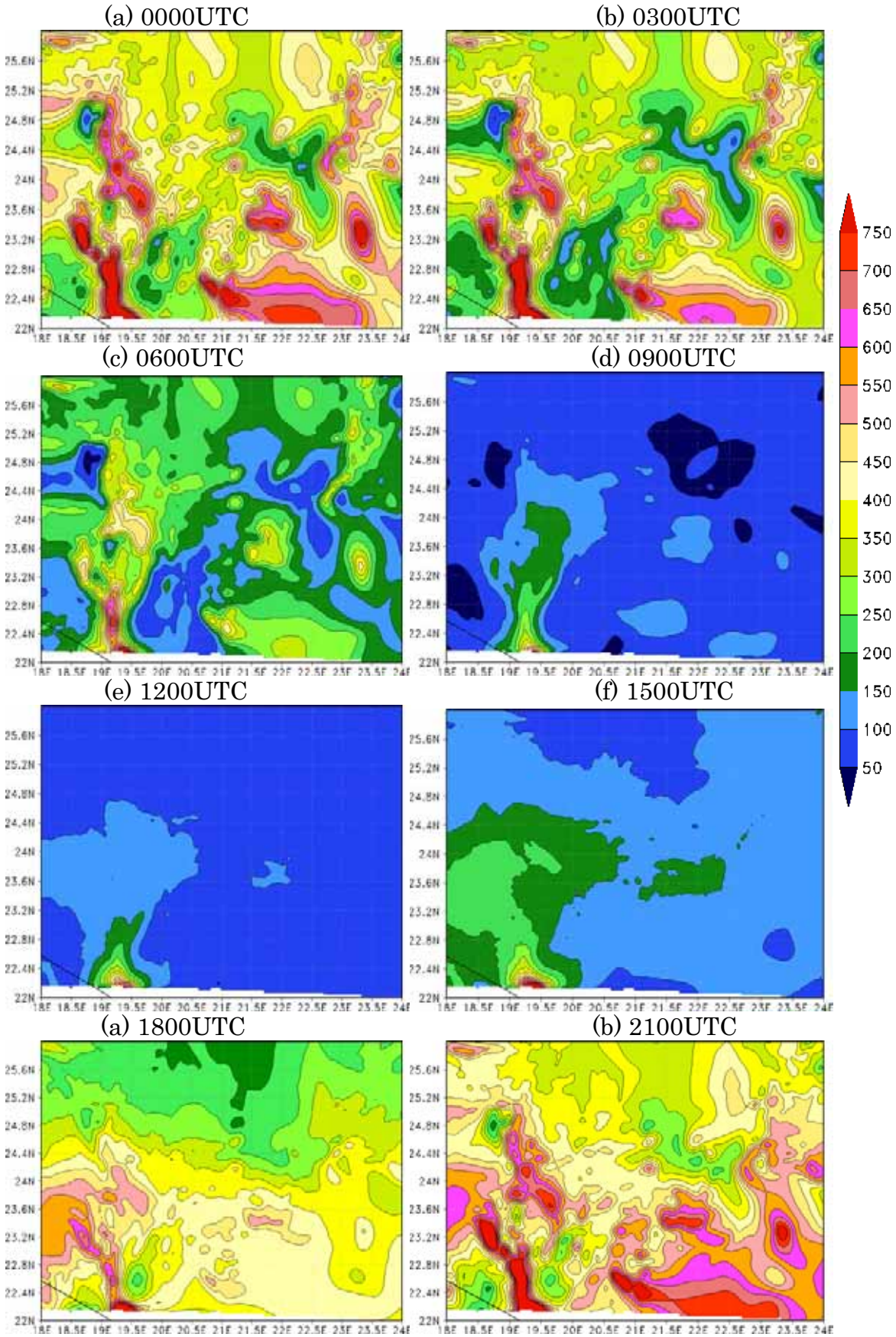

Figure 6.23: The estimated annual mean diurnal cycle of 100-m wind power density [W/m^2] for the southeast region.

6.6 Wind Energy Resources of Southwest Region

6.6.1 Annual Pattern

Figure 6.24(a) demonstrates the estimated annual mean 100-m wind speed and Figure 6.24(b) shows the corresponding wind power density of the southwest region. Like previously discussed regions, these figures suggest that the wind is stronger on hilly and mountainous areas, and it is weaker on low-altitude areas.

The bulk of this region experiences very good wind power resources since the annual wind speed is between 6.5 and 10 m/s, whereas wind power is between 250 and 750 W/m^2. The west of Al Malaki near the Chad boarder and the mountainous region extending from the junction point of Algeria, Niger, and Libya northwards to Awbari enjoy vey strong winds. These regions have high altitudes [Figure 6.8(d)]. Wind speed falls in the range of 7.5-10 m/s and the corresponding power density varies between 300 and 750 W/m^2. Al Wigh and Toummo also get reasonable wind resources. Winds blowing at speeds of 7-9 m/s are experienced over these areas, and the available power ranges from 300 to 550 W/m^2. The mentioned regions have good potentials for wind energy utilisation.

6.6.2 Seasonal Variations

Figures 6.25(a), 6.25(b), and 6.25(l) show the estimated monthly mean 100-m wind speed over the southwest region for winter months of January, February, and December, respectively. The matching wind power density for these months is illustrated in Figures 6.26(a), 6.26(b), and 6.26(l). These figures point out that winter has steady and good wind energy resources over the favourable districts. Winter has wind speeds varying between 6.5 and 10 m/s, and power of 300-750 W/m^2. January [Figures 6.25(a) and 6.26(a)] has slightly more wind resources than February [Figures 6.25(b) and 6.26(b)] and December [Figures 6.25(l) and 6.26(l)]. This scenario is opposite to what happens in the other discussed regions.

Figures 6.25(c), 6.25(d), and 6.25(e) show the estimated monthly mean 100-m wind speed over the southwest region for the spring months of March, April, and May in that order. The corresponding wind power density for these months is illustrated in Figures 6.26(c), 6.26(d), and 6.26(e). These figures indicate that the wind does not fluctuate much in spring. Spring is characterised by rising wind speeds. The favourable regions mentioned earlier continue to have increasing wind power resources, and the wind gets stronger as the season passes. The season has monthly wind speeds in the range of 7-10 m/s, and power of 300-700 W/m^2. The wind resource over this region does not vary temporally as much as over the other discussed regions.

Figures 6.25(f), 6.25(g), and 6.25(h) illustrate the estimated monthly mean 100-m wind speed for the southwest region for summer months of June, July, and August, respectively. The matching wind power density for these months is shown in Figures 6.26(f), 6.26(g), and 6.26(h). Resembling spring, summer has very high and stable wind power resources. The wind blows at speeds ranging from 7.5 to 10.5 m/s, and the available power falls in the range of 300-750 W/m^2. Al Malaki, Al Wigh, Tuommo, and the areas located between the intersection point of Niger, Chad, and Libya to Awbari, all are promising locations for wind power generation. As mentioned before, wind speeds concur with the topographic formation of the district.

Figures 6.25(i), 6.25(j), and 6.25(k) demonstrate the estimated monthly mean of 100-m wind speed for the southwest region for autumn months of September, October, and November, respectively. The corresponding wind power density for these months is presented in Figures 6.26(i), 6.26(j), and 6.26(k). According to these figures, wind power resources drop slightly in autumn. The wind for September [Figures 6.25(i) and 6.26(i)] blows at high wind speeds, but it slows down in October [Figures 6.25(j) and 6.26(j)] and November [Figures 6.25(k) and 6.26(k)]. Even so, overall wind resource characteristics for autumn are quite feasible for wind energy utilisation.

The monthly wind speed of the season varies between 6.5 and 10.5 m/s, and the power range from 200 to 750 W/m^2.

6.6.3 Diurnal Variations

Figures 6.27(a) to 6.28(h) illustrate the estimated annual mean diurnal cycle of 100m wind speed at 0000, 0300, 0600, 0900, 1200, 1500, 1800, and 2100 UTC, correspondingly. Figures 6.28(a) to 6.28(h) show the corresponding wind power density. As expected, the figures demonstrate that the district sees less wind energy resources during the day than at night.

When the sun rises at about 0600 UTC [Figures 6.27(c) and 6.28(c)], wind speed starts to drop, and continues to go down until around 1200 UTC [Figures 6.27(e) and 6.28(e)]. Noticeable falls in the wind resource occur during midmorning to the late afternoon, namely between 0900 UTC [Figures 6.27(d) and 6.28(d)], and 1500 UTC [Figures 6.27(e) and 6.28(e)]. Wind speed over the west of Al Malaki, Al Wigh, and Toummo, and the curved areas from the intersection point of Niger, Chad, and Libya to the southwest of Awbari ranges from 5 to 11 m/s, and the power varies between 100 and 700 W/m^2.

Most areas of this region have an elevation higher than 400 m, and some mountainous districts extend up to more than 1100 m above sea level [Figure 6.8(d)]. The topographic structure is heterogeneous. Hence, the wind over this region could be generated due to local thermal-driven mountain-valley circulations. These flows may develop later during the day, when the temperature and pressure gradients are high. It could be this is the reason for the wind being low during the morning and the afternoon.

During the early evening after 1500 UTC, local flows start to develop and the wind starts blowing at high speeds in the evening at 1800 UTC [Figures 6.27(g) and 6.28(g)]. However, wind speed peaks by 2100 UTC

[Figures 6.27(h) and 6.28(h)]. Between 1800 UTC and midnight the wind blows at speeds ranging from 7 to more than 11 m/s, with power varies between 300 to more than 750 W/m^2.

After 0000 UTC [Figures 6.27(a) and 6.28(a)] through the early morning, namely at 0600 UTC [Figures 6.27(c) and 6.28(c)], the wind remains strong over the potential areas. Wind speed over these regions ranges from 7.5 to more than 11 m/s, and the power ranges from 300 to more than 750 W/m^2.

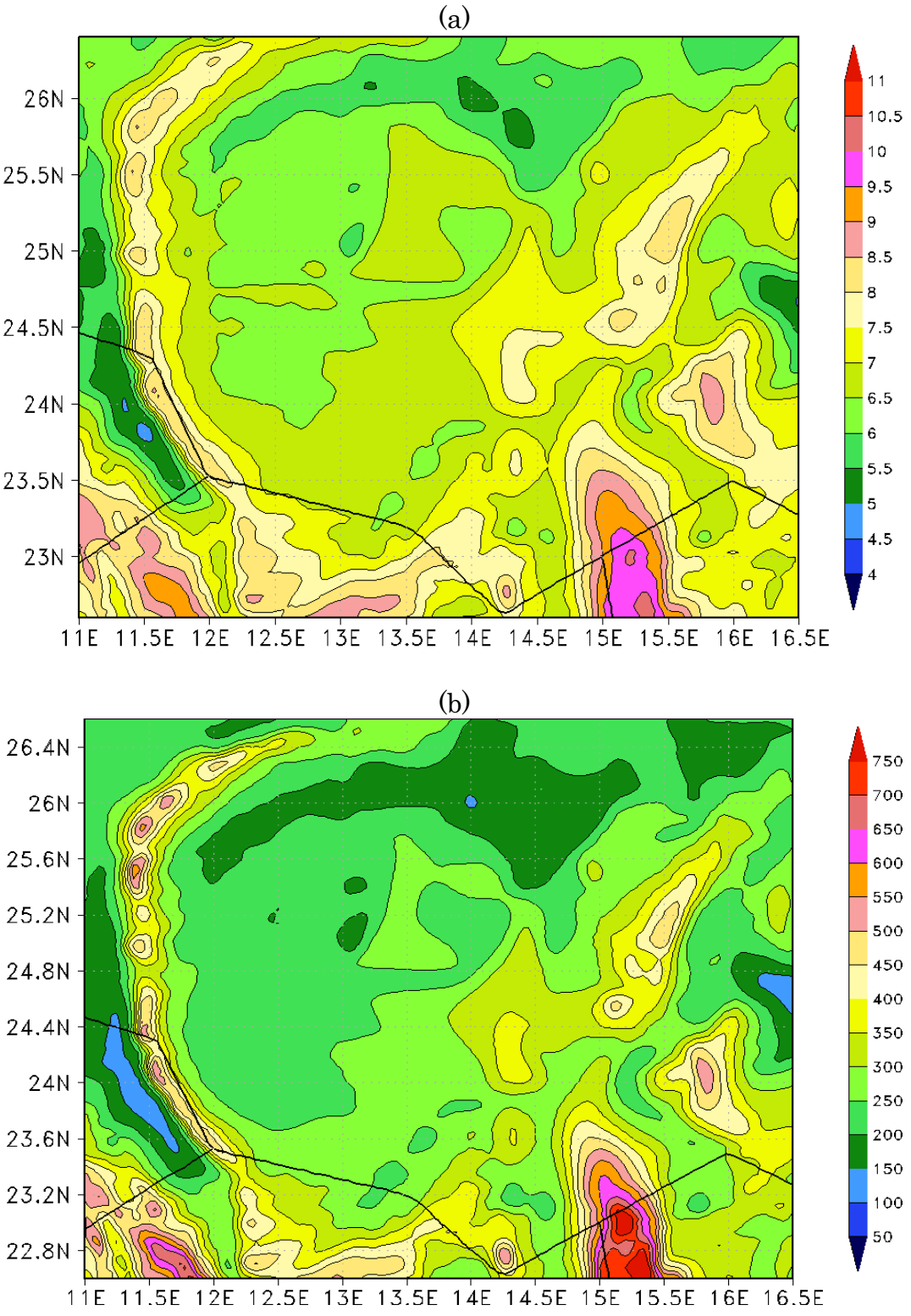

Figure 6.24: (a) The estimated annual average 100-m wind speed [m/s] and (b) the corresponding wind power density [W/m^2] for the southwest region.

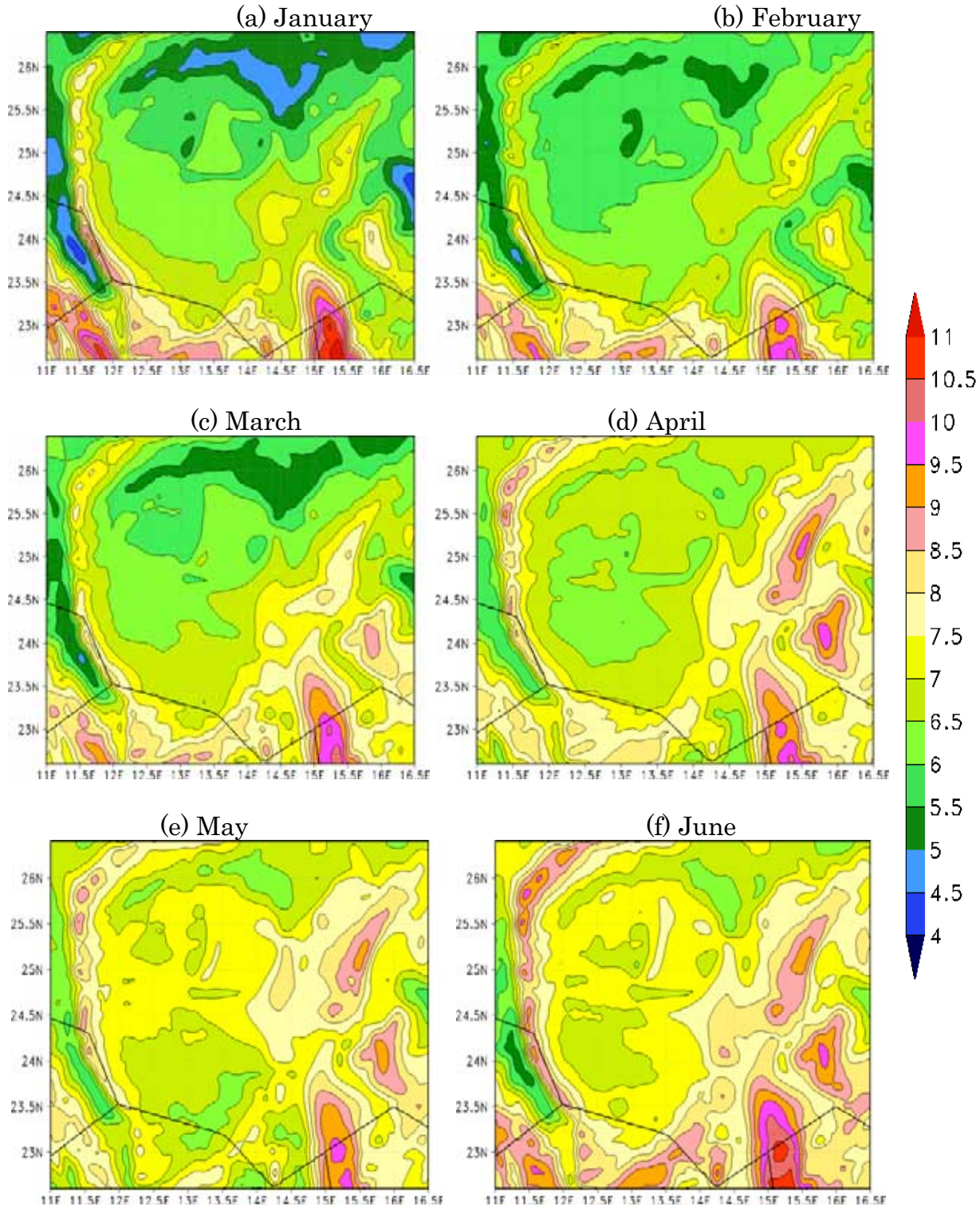

Figure 6.25: The estimated monthly mean hourly 100-m wind speed [m/s] for the southwest region.

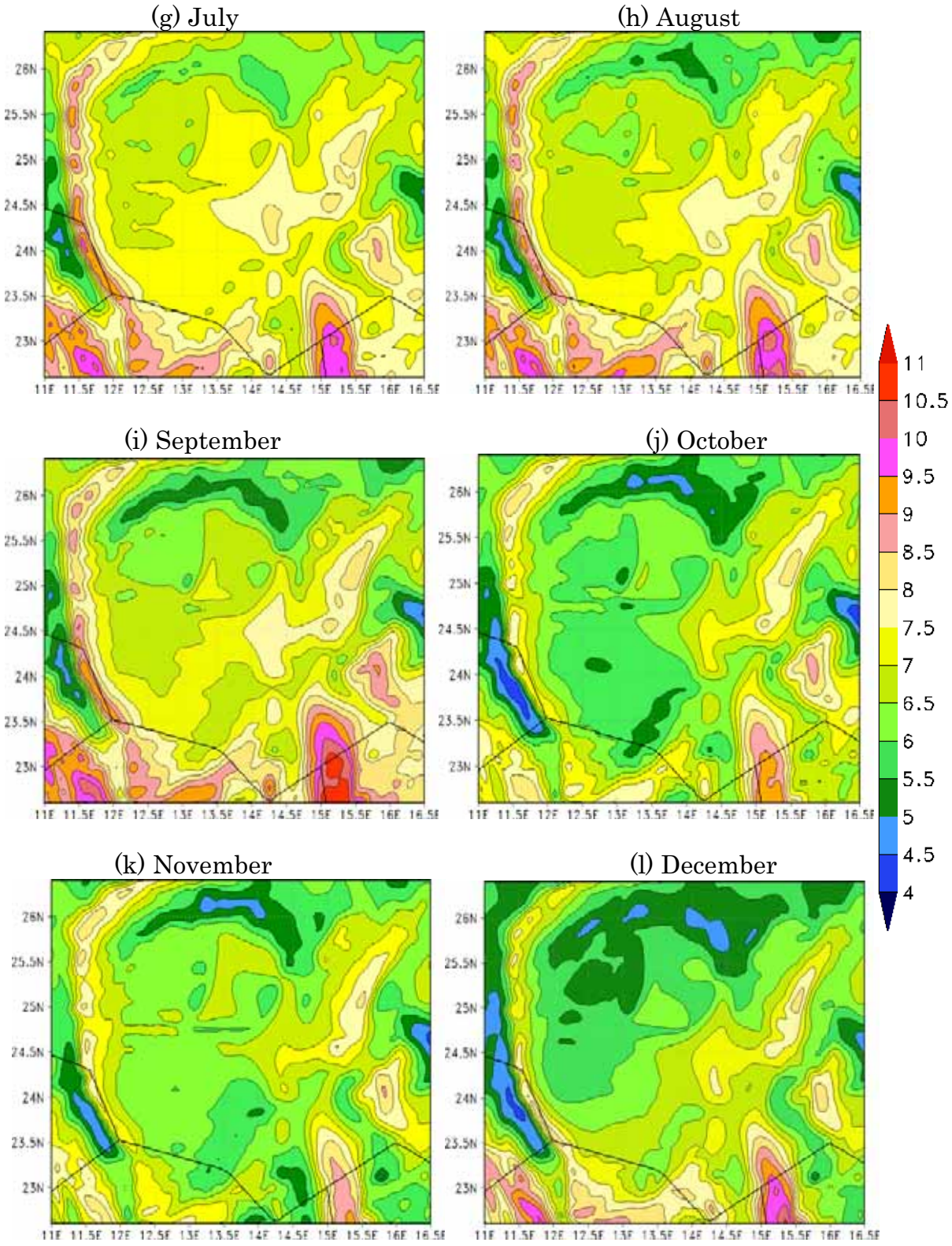

Figure 6.25 (continued): The estimated monthly mean 100-m wind speed [m/s] for the southwest region.

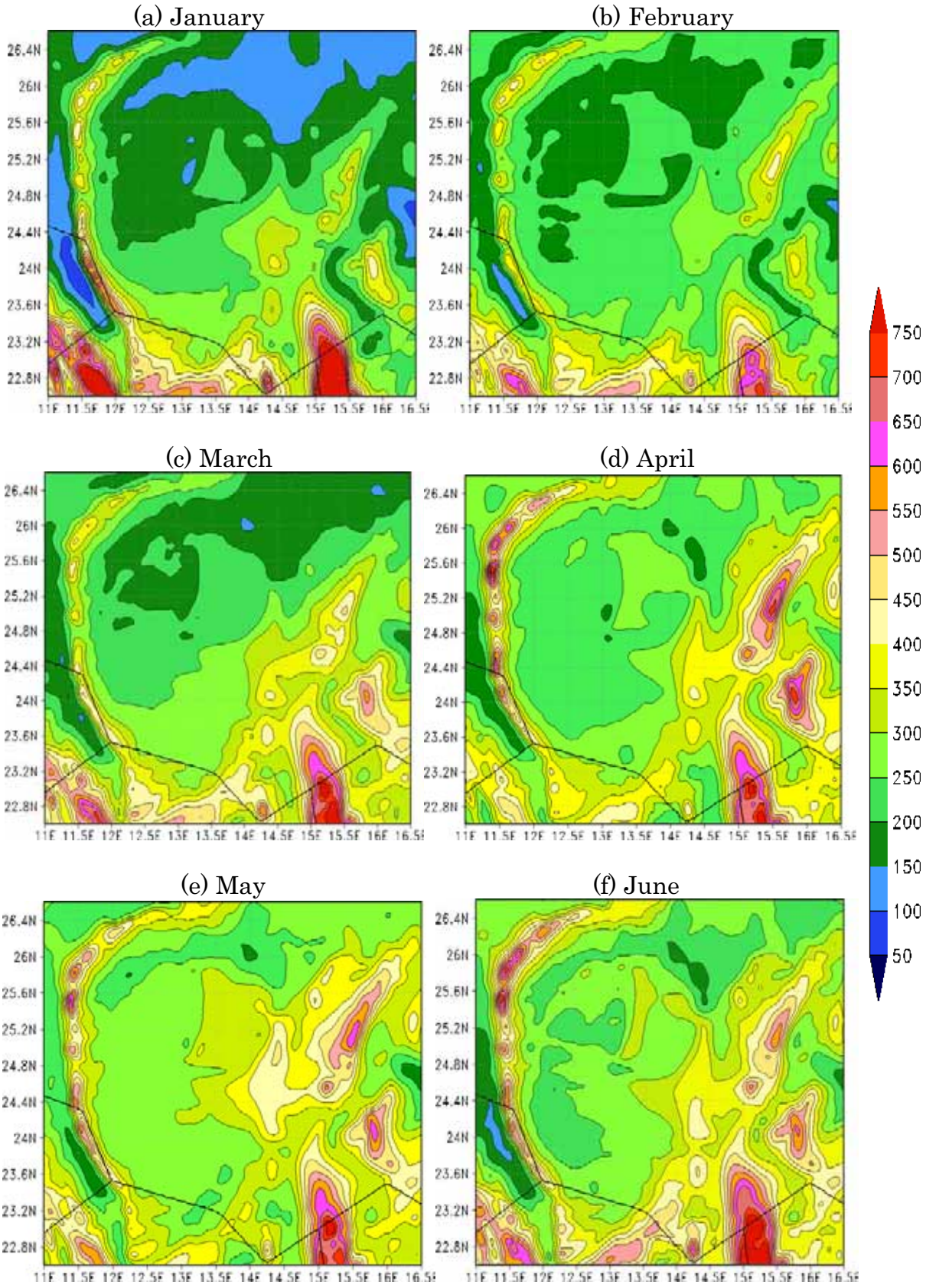

Figure 6.26: The estimated monthly mean 100-m wind power density [W/m^2] for the southwest region.

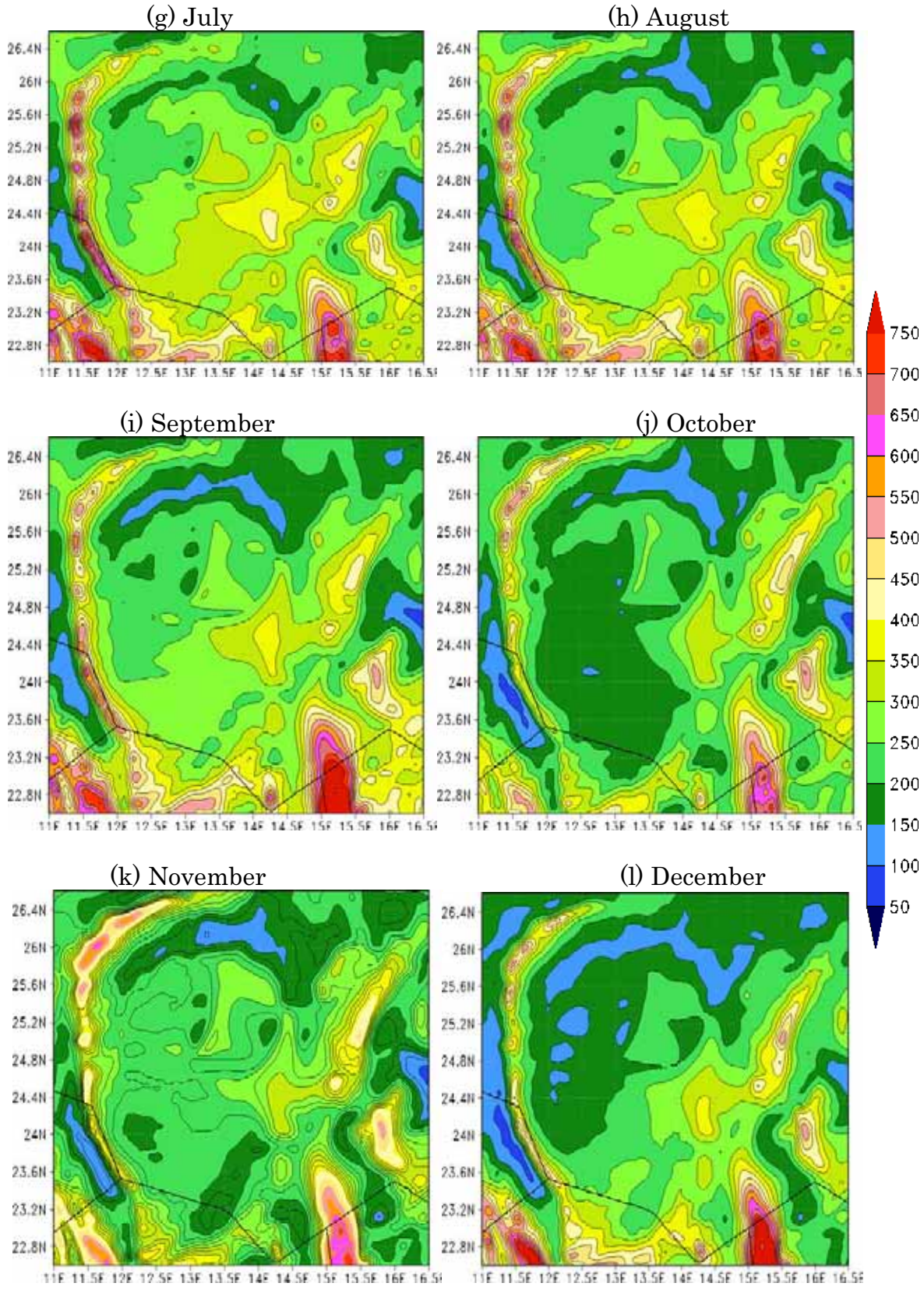

Figure 6.26 (continued): The monthly average of estimated hourly 100-m wind power density [W/m^2] for the southwest region.

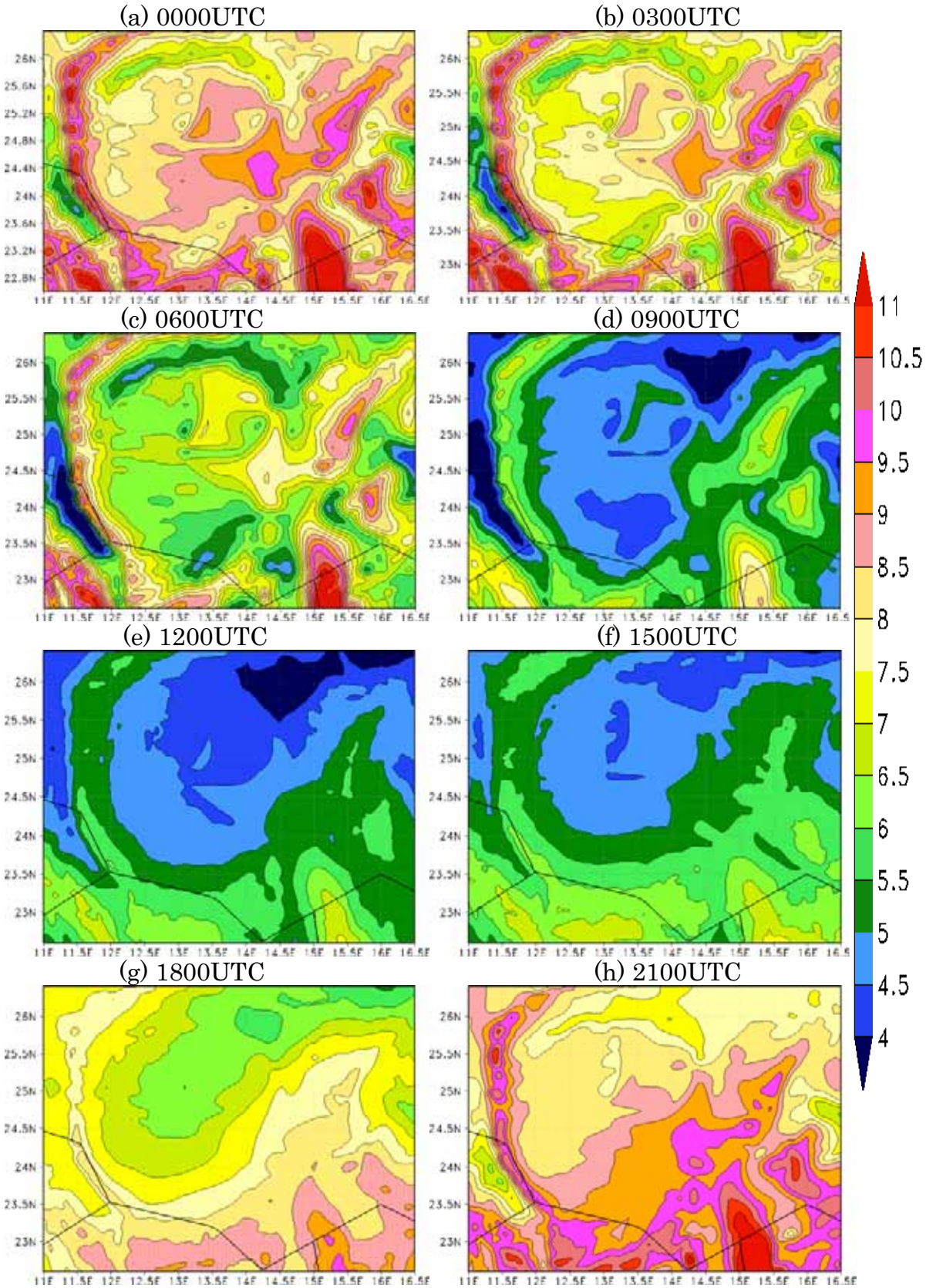

Figure 6.27: The estimated annual mean diurnal cycle of 100-m wind speed [m/s] for the southwest region.

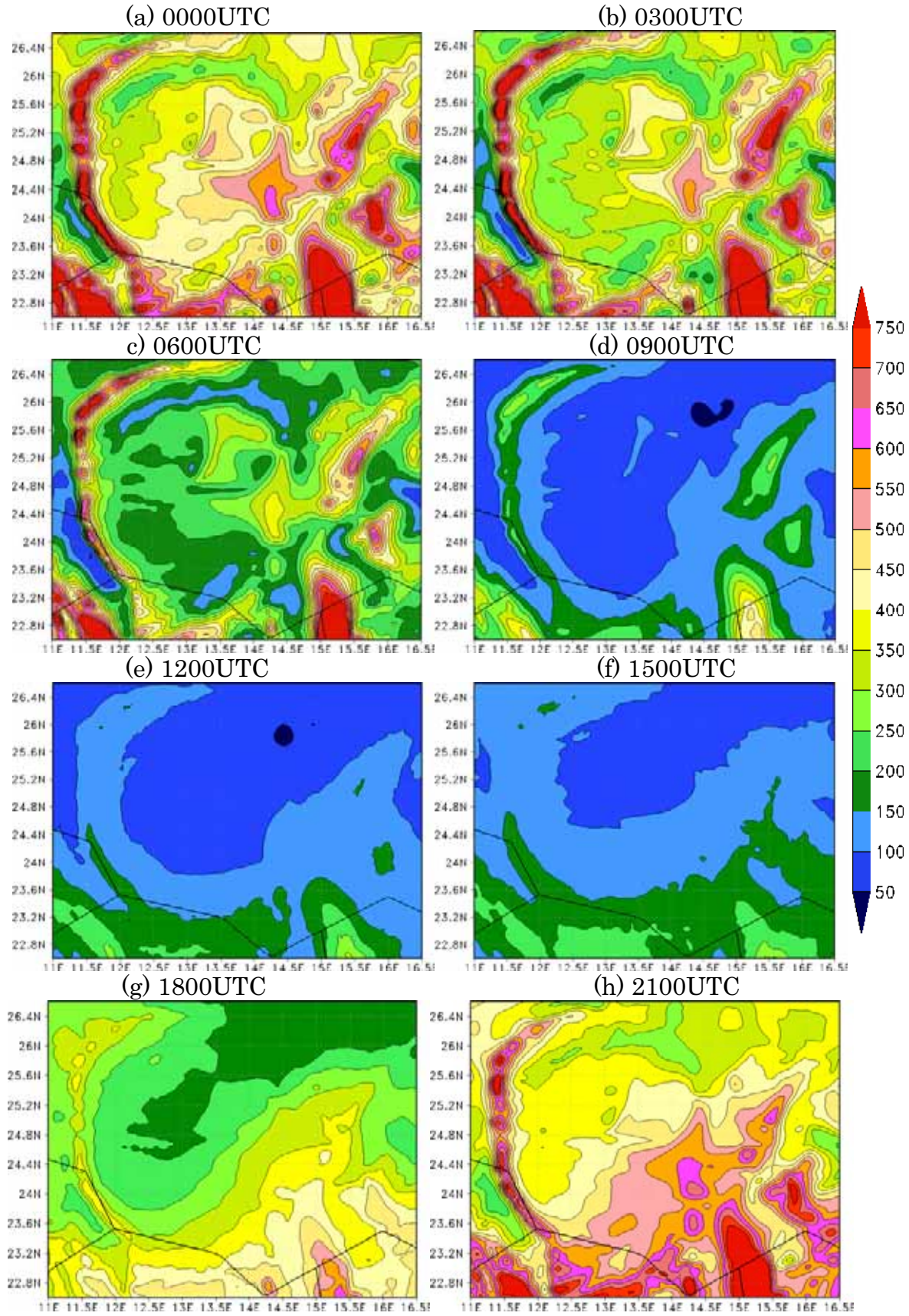

Figure 6.28: The estimated annual mean diurnal cycle of 100-m wind power density [W/m^2] for the southwest region.

6.7 Estimated Power Outputs of Wind Turbines

Out of ten turbines mentioned in Section 6.1 and discussed in Chapter 5, the potential annual 100-m power outputs of six turbines being G58-850kW, FL54-1000kW, G80-1500kW, G80-2000kW, N80-2500kW, and V112-3000kW are presented and discussed below. The rotor swept areas of these turbines are approximately 2640, 2290, 5024, 5024, 5024, 9847 m^2, respectively. If these turbines extracting power from the wind with their full capacities without stoppage throughout the entire year, they would yield the maximum power outputs, which are about 7.44, 8.76, 13.14, 17.52, 21.9, and 26.28 GWhr/year, in that order.

Figures 6.29(a) to 6.29(d) show the estimated annual power output of the G58-850kW installed at 100 m above the ground over the northwest, northeast, southwest, and southeast regions, in that order. A first glance to these figures suggests that this turbine has very good potential of producing economical electricity over the coastal regions as well as over the southern regions, although it would produce more electricity over the southern mountainous regions. If some turbines of this design were installed along the coastal areas in both the northeast and the southeast regions, each of which would generate electrical power between 2.25 and 3.5 GWhr/year [Figure 6.29(a) and 6.29(b)].

This type of turbines is more promising on areas consisting of Green Mountain, Darnah, Al Bayda along Ajdabiya, and the coastline situated between Misratah and the Tunisian boarder. Over these locations, the G58-850kW would output electricity between 2.5 and 3.25 GWhr/year. These amounts of electrical power account for about 34 to 43% of the maximum possible electrical power generated by this turbine. This implies that the rotor blades of the turbine would extract power in the range of 0.95 and 1.23 MWhr/m^2/year.

If the G58-850kW was installed over hilly and mountainous districts in the southern part of the country, it would yield good amounts of power,

especially over the potential regions [Figure 6.29(c) and 6.29(d)]. On the Tibesti Mountains in the southwest and southeast regions, Toummo, Awbari, and Al Wigh, this turbine would produce electricity varying between 2.5 and more than 3.75 GWhr/year. This indicates that the turbine would have capacity factors ranging from about 34 t6 50%. It also suggests that the rotor blades of this turbine would capture power between 0.95 and 1.42 MWhr/m^2/year.

Figures 6.30(a) to 6.30(d) show the estimated annual power output of the FL54-1000kW installed at 100 m above the ground over the northwest, northeast, southwest, and southeast regions, in that order. This turbine has a reasonable potential of producing satisfactory amounts of power over the favorable regions discussed in the previous sections. If some turbines of this design were distributed over the prospective areas consisting of Green Mountain, Darnah, Al Bayda along Ajdabiya, and the coastline located between Misratah and the Tunisian boarder, each of which would generate electricity between 2 and 3 GWhr/year [Figure 6.32(a) and 6.32(b)]. The turbine would yield power with capacity factors between about 23 and 34%. The turbine's rotor blades would attain power between 0.87 and 1.31 MWhr/m^2/year.

In the southern region of the country near the national boundaries, particularly on the mountainous districts, the FL54-1000kW would achieve more power [Figure 6.30(c) and 6.30(d)]. Over the favorable regions of the Tibesti Mountains and Al Wigh, this generator would supply electrical power between 2 and more than 3.75 GWhr/year. This suggests that the turbine would have capacity factors ranging from around 23 to 42%. The turbine's rotor blades would capture power ranging from 0.87 to 1.63 MWhr/m^2/year.

Figures 6.31(a) to 6.31(d) demonstrate the estimated annual power output of the G80-1500kW installed at 100 m above the ground over the northwest, northeast, southwest, and southeast regions, respectively.

These figures show that this turbine has a great possibility of producing very good amounts of electricity over the favorable regions identified previously in this chapter. A single turbine of this type installed along the northeast and the northwest coastal districts would produce power varying between 4 and 6 GWhr/year [Figure 6.31(a) and 6.31(b)].

The G80-1500kW is even more suitable for Green Mountain, Darnah, Al Bayda along Ajdabiya, and the coastline situated between Misratah and the Tunisian boarder. Installing this turbine over theses districts would supply power ranging from 4.5 to 6 GWhr/year. Theses quantities of electricity are equivalent to 34-45% of the maximum power output of this turbine. This also denotes the rotor blades of the turbine would extract power between 0.89 and 1.2 MWhr/m^2/year.

Over some parts of the Libyan Desert, the turbine can yield even more power [Figure 6.31(c) and 6.31(d)]. On the potential areas being the Tibesti Mountains in the southwest and southeast regions, and Al Wigh, this generator would yield electricity ranging from 4.5 and more than 7.5 GWhr/year, meaning that the turbine's swept area would attain power ranging from 0.89 to 1.5 MWhr/m^2/year. The turbine would generate power with capacity factors of around 34-57%.

Figures 6.32(a) to 6.32(d) illustrate the estimated annual power output of G80-2000kW installed at 100 m above the ground. As shown in these figures, this turbine does a reasonable job. If this generator was installed over the districts of Green Mountain, Darnah, Al Bayda along Ajdabiya, and the coastline situated between Misratah and the Tunisian boarder, it would generate between 4.5 and 6.5 GWhr/year of electricity [Figure 6.32(a) and 6.32(b)]. The turbine would produce electrical power with capacity factors in the range of 26-37%. The rotor blades of the turbine would capture power between 0.89 and 1.30 MWhr/ m^2/year.

The G80-2000kW would achieve more electricity over the southern part of the nation, more specifically in the south of Murzuk and Al Kufrah [Figure

6.32(c) and 6.32(d)]. Over the encouraging regions, including the Tibesti Mountains and Al Wigh, this generator would yield potential power varying between 5 and more than 8 GWhr/year. Its capacity factors would range from 28 to 45%, whereas the rotor's blades would extract power between nearly 1 and 1.6 MWhr/m^2/year.

Figures 6.33(a) to 6.33(d) show the estimated annual power output of the G80-2500kW installed at 100 m above the ground. Based on these figures, this generator can provide cost-effective power over the favorable regions. The figures suggest that if a wind farm of this turbine was constructed along the coastlines of both the northeast and the southwest regions, each turbine would produce power varying between 4 and 7 GWhr/year [Figure 6.33(a) and 6.33(b)]. The turbine does a better job on the favorable districts consisting of Green Mountain, Darnah, Al Bayda along Ajdabiya, and the coastline lying between Misratah and the Tunisian boarder. Over these locations, it would yield electricity ranging from 4.5 to 7 GWhr/year. This accounts for about 20 to 32% of the maximum annual power output of this turbine. The rotor blades of the turbine would extract wind power in the range of 0.89 and 1.4 MWhr/m^2/year.

The southern part of Libya near the Chad, Nigerian, and Algerian borders is the most suitable area for installing the G80-2500kW, as the turbine has more prospective power outputs [Figure 6.33(c) and 6.33(d)]. If the turbine was installed over the identified areas, which include the Tibesti Mountains in the southwest and southeast regions, and Al Wigh, it would yield power ranging from 4.5 to more than 8.5 GWhr/year. This indicates that the turbine would output electrical power with capacity factors varying between about 20 to 39%. This also implies that the turbine's rotor blades would capture power ranging from 0.89 to 1.7 MWhr/m^2/year.

Figures 6.34(a) to 6.34(d) demonstrate the estimated annual power output of the V112-3000kW installed at 100 m above the ground. The figures show that this turbine is very promising for producing economical wind power,

especially over the favorable identified districts. If some turbines of this design were installed along the coastal areas in both the northeast and the northwest, each of which would have power outputs varying between 8.5 and 12 GWhr/year [Figure 6.34(a) and 6.34(b)].

The generator shows a great potential of wind power generation over the districts of Green Mountain, Darnah, Al Bayda along Ajdabiya, and the coastline located between Misratah and the Tunisian boarder. Over these areas, it would output electrical power ranging from 9.5 to 12 GWhr/year. This means that the turbine would produce electricity with capacity factors in the range of 36-46%. Another implication is that the rotor blades of the turbine would extract wind power between 0.96 and 1.22 MWhr/m^2/year.

Over the southern part of the Sahara Desert, the V112-3000kW would generate much more electricity, and it would do a very good job over most parts [Figure 6.34(c) and 6.34(d)]. Over the encouraging potential districts consisting of the Tibesti Mountains in both regions, and Al Wigh, this turbine would have power output ranging from 9.5 to more than 13 GWhr/year. This is equivalent to about 36-49% of the maximum power output of the turbine. The turbine's rotor blades would capture power ranging from 0.96 to 1.32 MWhr/m^2/year.

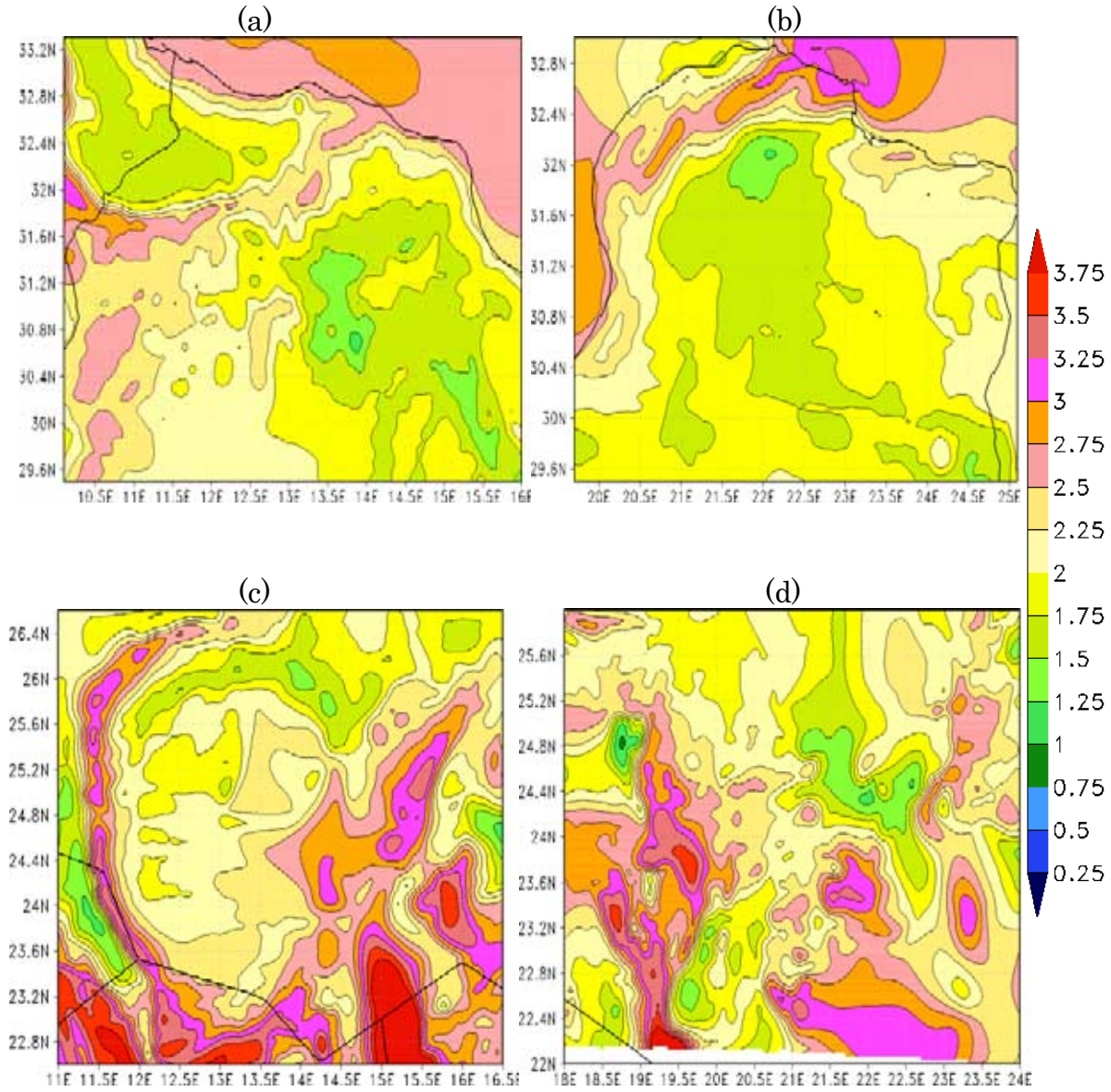

Figure 6.29: The estimated annual 100-m power output [GWhr/year] of the G58-850kW wind turbine over the (a) northwest, (b) northeast, (c) southwest, and (d) southeast regions.

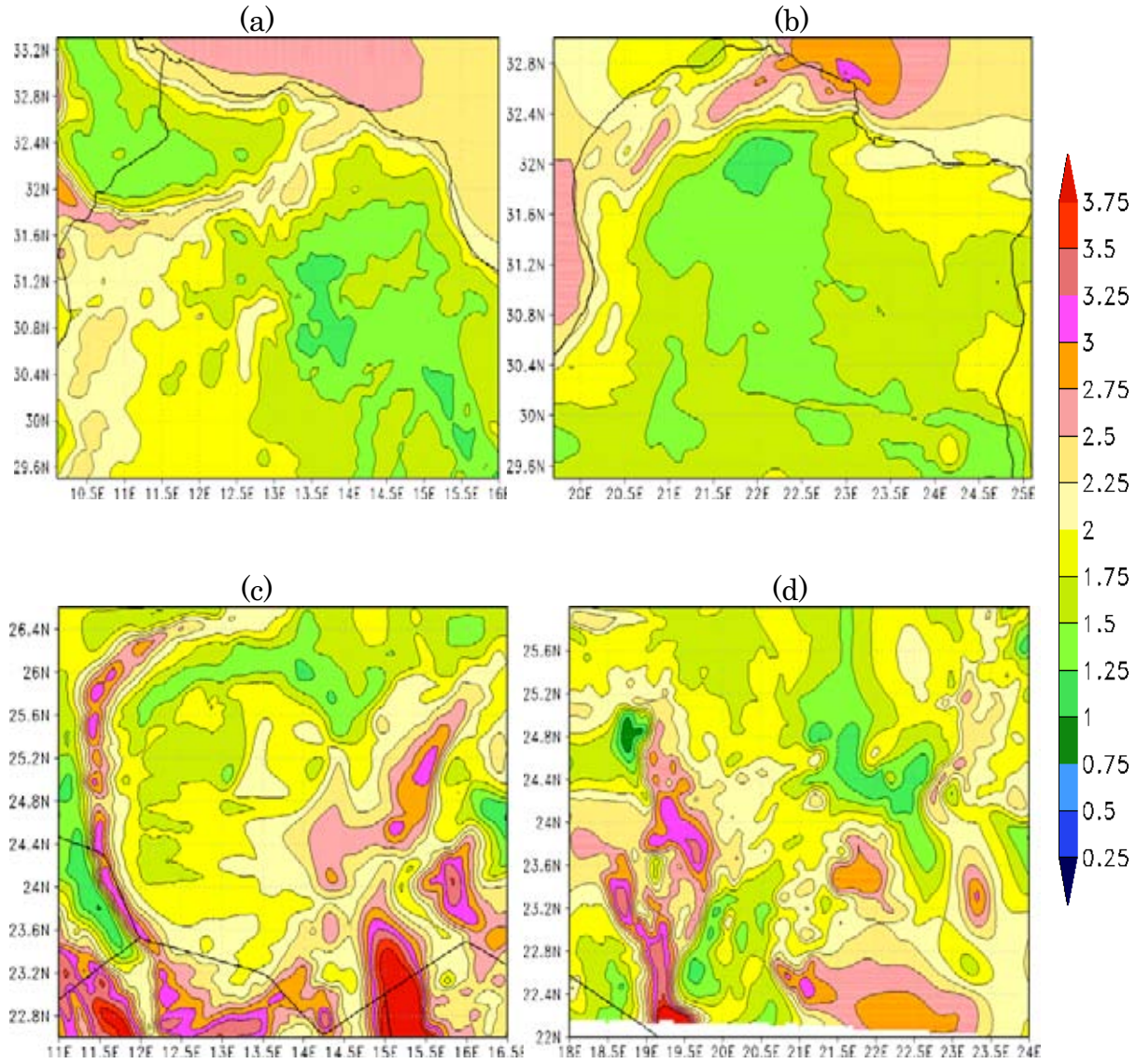

Figure 6.30: The estimated annual power output [GWhr/year] of the FL54-1000kW wind turbine over the (a) northwest, (b) northeast, (c) southwest, and (d) southeast regions.

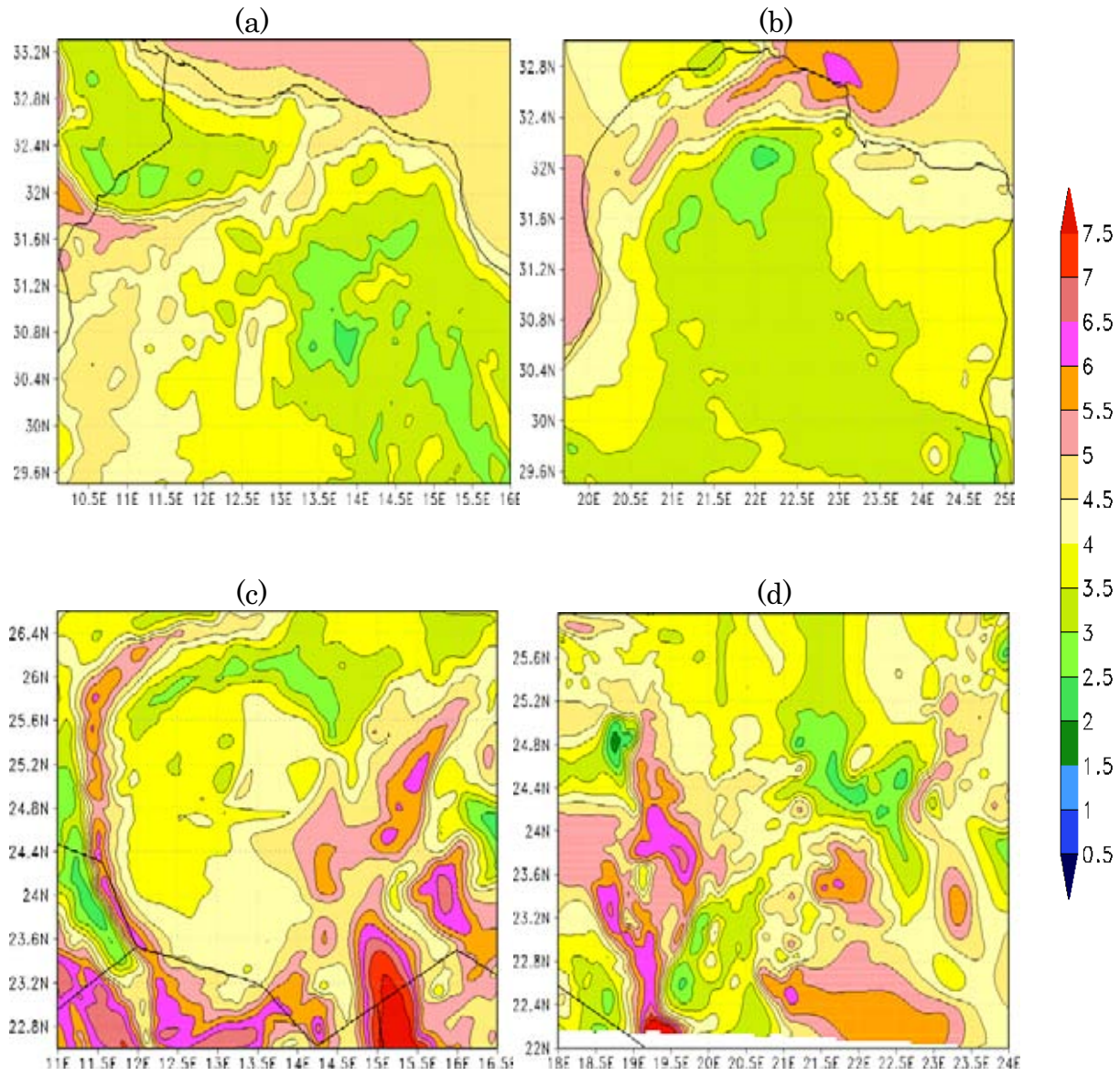

Figure 6.31: The estimated annual power output [GWhr/year] of the G80-1500kW wind turbine over the (a) northwest, (b) northeast, (c) southwest, and (d) southeast regions.

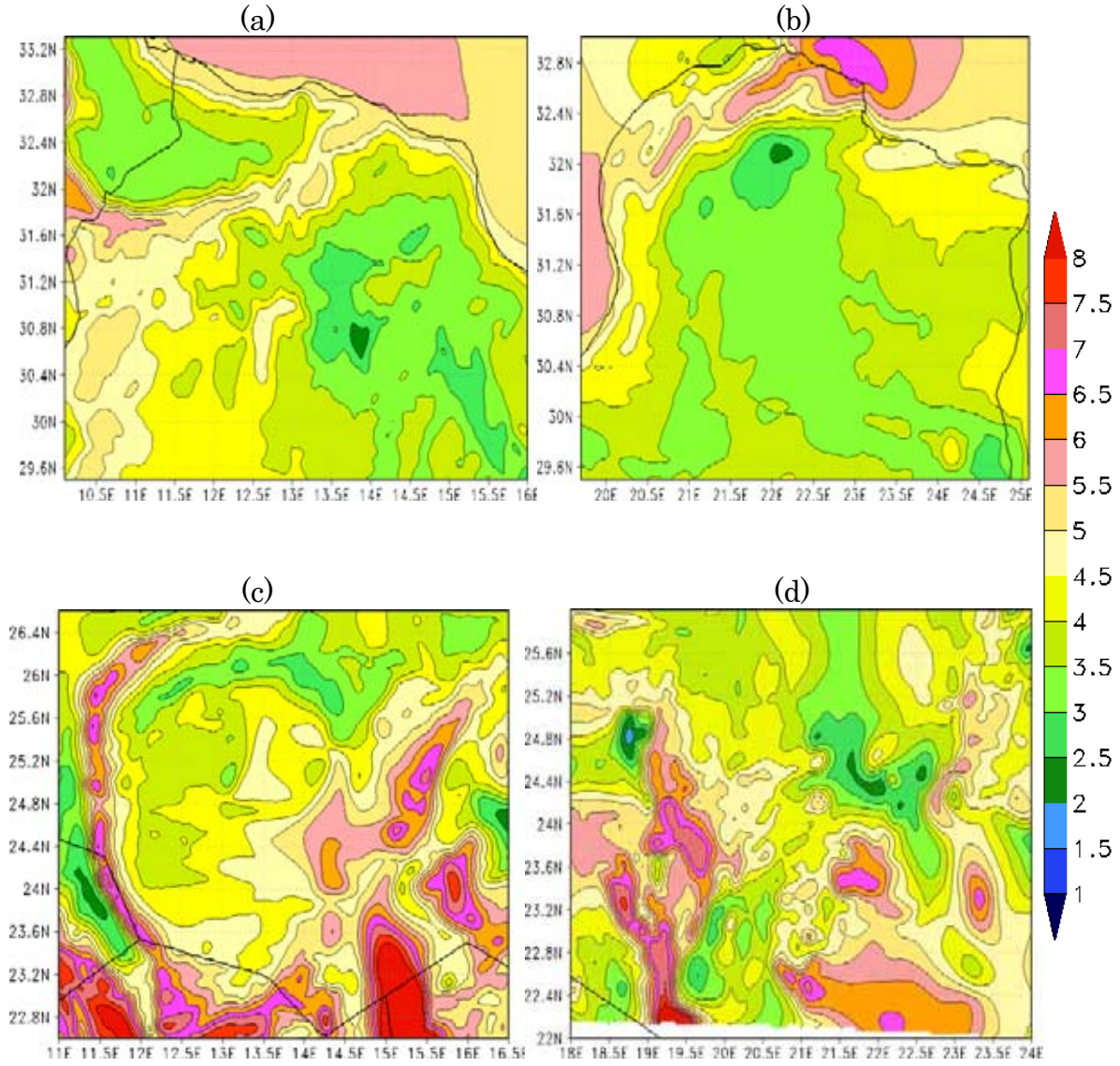

Figure 6.32: The estimated annual power output [GWhr/year] of the G80-2000kW wind turbine over the (a) northwest, (b) northeast, (c) southwest, and (d) southeast regions.

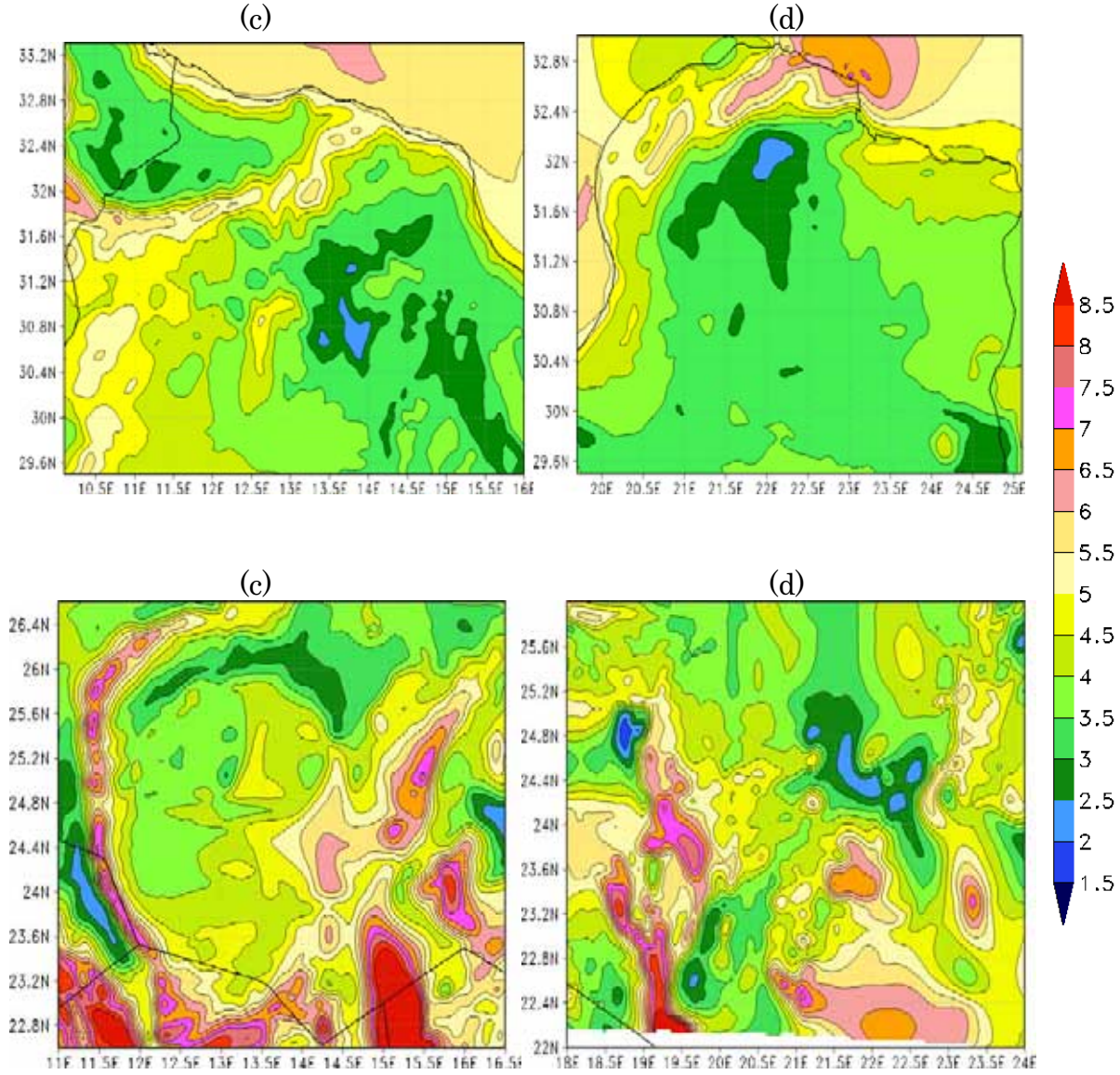

Figure 6.33: The estimated annual power output [GWhr/year] of the N80-2500kW wind turbine over the (a) northwest, (b) northeast, (c) southwest, and (d) southeast regions.

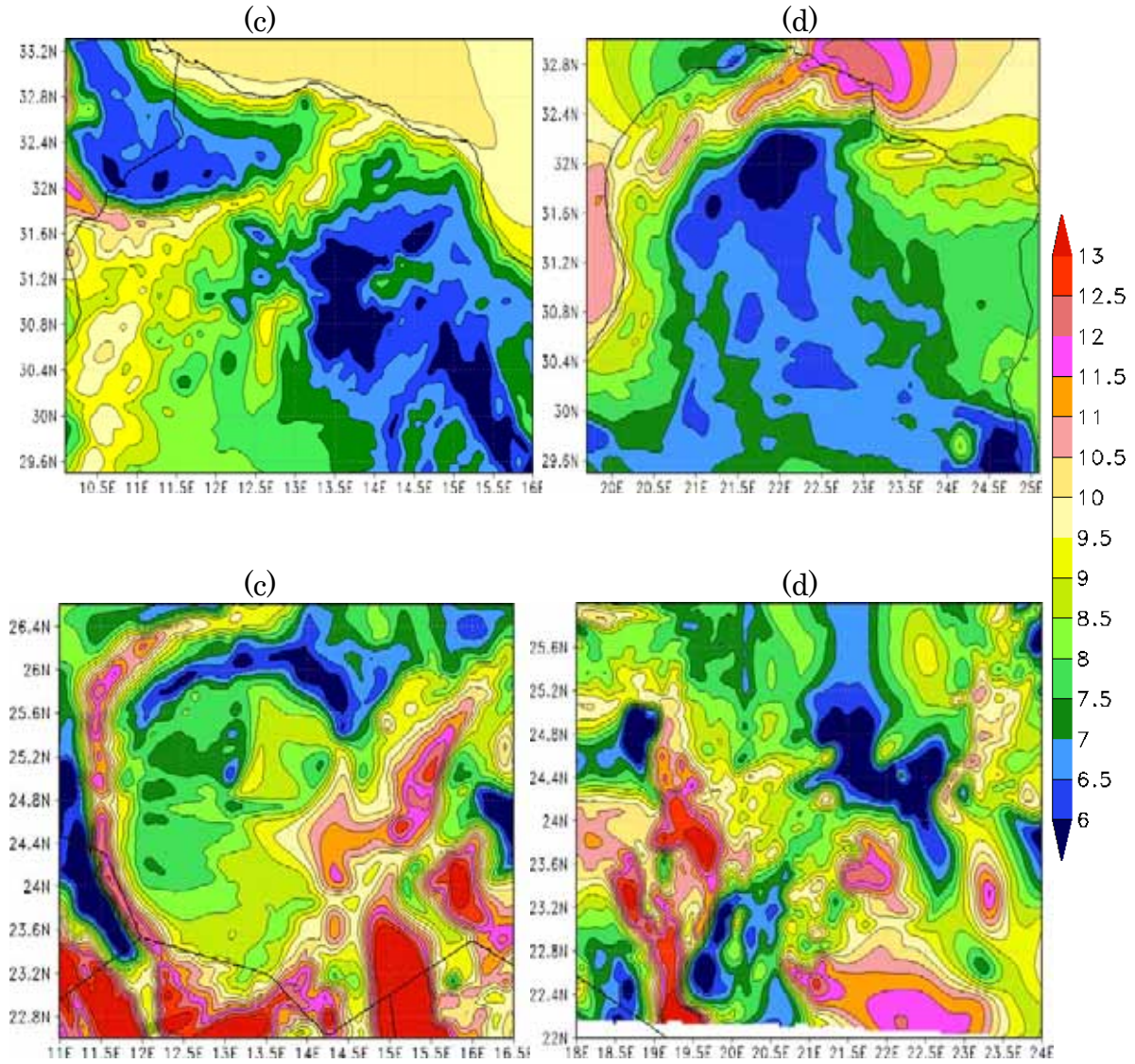

Figure 6.34: The estimated annual power output [GWhr/year] of the V112-3000kW wind turbine over the (a) northwest, (b) northeast, (c) southwest, and (d) southeast regions.

In view of the above discussion, it can be seen that the optimum turbines are the G58-850kW, G80-1500kW, and V112-3000kW. The other turbines also have reasonable potentials of producing wind-generated electricity, and their outputs over all regions vary between satisfactory to good. From wind power generation point of view, the G58-850kW, G80-1500kW, and V112-3000kW seems to produce very cost-effective electrical power per unit than the rest. This does not denote that the FL54-1000kW, G80-2000kW, and N80-2500kW are not high-quality machines, but rather it indicates that the wind resource of Libya does not match their requirements well. This is due to the difference in the cut-in wind speed, and suitability of the wind turbine to the existing wind resource.

As shown in Figure 5.5, the FL54-1000kW does not start extracting energy from the wind until wind speed reaches 4 m/s, while the G58-850kW begins generating power once the wind starts blowing at speed of 3 m/s. When the wind blows at speeds between 3 and less than 4 m/s, the FL54-1000kW produces no electrical power whereas the G58-850kW yields between around 9 and 25 kW. This range of wind speed occurs frequently, especially when considering that the prospective power outputs that have been obtained based on hourly wind speeds.

Even though the FL54-1000kW has more rated capacity than the G58-850kW, their power curves [Figure 5.5] illustrate that when the wind blows at speeds between 4 and 12 m/s, the G58-850kW produces more electricity. The wind resource of Libya mostly falls in this range. Yet, when wind speed is higher than 12 m/s the FL54-1000kW yields much more power, but the disadvantage is that these speed values are not common in Libya, as far as the previous discussions are concerned.

Similar scenarios can be seen in the power curves of the G80-1500kW, G80-2000kW, N80-2500kW, and V112-3000kW [Figure 5.6]. The G80-1500kW and G80-2000kW have the same cut-in wind speed, and below the speed of 9 m /s they have exactly the same amounts of power output. However, the

N80-2500kW has a higher cut-in wind speed and less power output when the wind blows at speeds below 8 m/s.

Among all mentioned turbines, the V112-3000kW is the most favorable turbine. It would yield large amounts of power even when wind speed is not high. This turbine starts extracting energy from the wind at low wind speed of 3 m/s, and the power output goes up as wind speed increases. For example, at the wind speed of 6 m/s, this turbine would produce more than double the power that is generated by the N80-2500kW [Figure 5.6].

Still, the distribution of wind speed has not been studied yet. The above discussions are based on the previous regional wind resource analysis. When investigating the frequency distribution of wind speed at several model grid points, it should become more apparent which turbines are more suitable for the Libya's 100-m winds. The next section will investigate the frequency distribution, the temporal variations, and the wind shear of wind energy resources at several selected grid points.

6.8 Wind Energy Resources at Selected Grid Points

To improve the understanding of wind power resources over the country, six model grid points (G1, G2, G3, G4, G5, and G6) have been selected over which site-specific wind energy assessments will be performed. Four of these locations are in the north of the country, while the remaining two are in the southern part. The purpose of doing this is that these sites should provide reasonable representations for the neighboring regions, since it is certainly not possible to study the wind resource at every grid point in the model. The positions of these six points are shown in Figure 6.35. Details about these selected locations, including the estimated annual power outputs from the considered turbines at these locations, are summarised in Table 6.1.

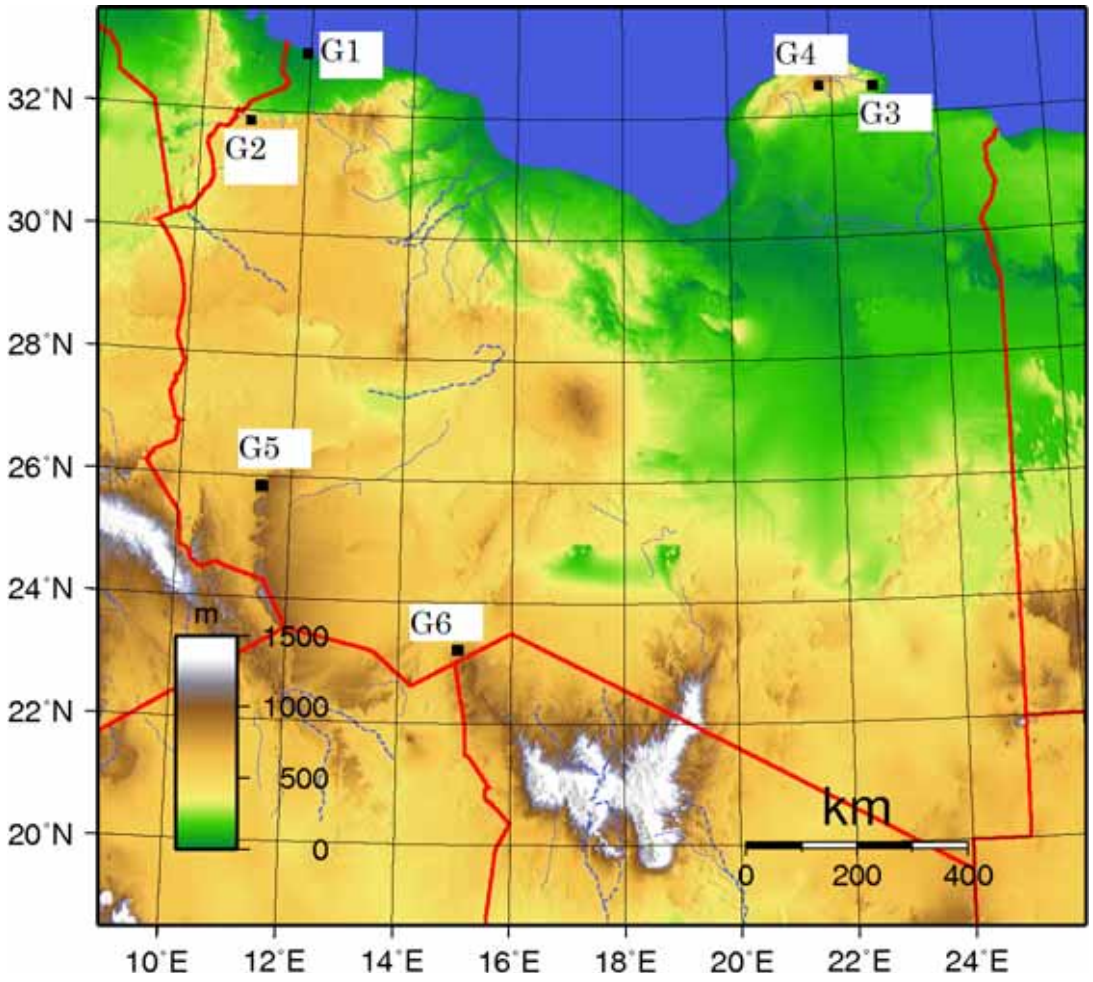

Figure 6.35: Selected sites (grid points) over Libya.

The objective of the forthcoming discussion is primarily not to examine the suitability of the turbines. Rather, it is dedicated to investigate the wind energy resources at specific sites, although general comparisons between the six considered turbines may take place every now and then.

A first impression can be taken from Table 6.1 is that all sites have good wind power potential. G6 has the greatest wind energy resource, while G1 appears to have the lowest. The table also suggests that the G58-850kW, G80-1500kW, and V112-3000kW would suit the wind resource of these sits more than the other turbines, even though all chosen turbines would do good jobs. This confirms what have been discussed in the previous section, but there will be more discussions about the wind resource and the suitability of wind turbines.

Table 6.1: Information about the selected model grid points.

	G1	G2	G3	G4	G5	G6
Latitude [Degree]	32.9°N	31.7°N	32.6°N	32.6° N	25.8° N	23.2° N
Longitude [Degree]	11.9°E	10.8°E	22.8°E	21.8° E	11.5° E	15.1° E
Elevation in the model [m]	7	567	302	780	1023	760
Annual Wind Speed [m/s]	7.1	7.5	7.6	7.7	8.4	9.5
G58-850kW output [MWhr/year]	2646	2881	3100	2997	3304	4194
FL54-1000kW output [MWhr/year]	2440	2604	2769	2705	3126	4062
G80-1500kW output [MWhr/year]	4892	5319	5736	5538	6027	7592
G80-2000kW output [MWh/year]	5412	5829	6230	6055	6904	8943
N80-2500kW output [MWhr/year]	5602	5973	6319	6198	7381	9790
V112-3000kW output [MWhr/year]	9944	10823	11683	11262	12243	15401

Data of the year 2005 from the World Resources Institutes indicate that the average electricity consumption per capita in Libya is about 3.34 MWhr. This means that if a single turbine of V112-3000kW operated at G1, it would provide annual electricity for about 2977 persons and for about 4611 persons if the turbine was installed at G6. The estimated outputs of the turbines mentioned in Table 6.1 as well as wind speed at the selected sites will be employed to study the frequency distribution, the temporal variation, and the vertical shear of wind speed and the corresponding wind power.

6.8.1 Frequency Distribution

The frequency distribution refers to the number of times at which an observation occurs in the data. Table 6.2 presents the frequency distribution of grouped hourly wind speeds, at the six candidate sites. It represents the numbers of occurrences of grouped hourly wind speeds. Figure 6.36 shows the matching cumulative frequency distribution of the predicted hourly wind speeds. It demonstrates the percentage of the number of the occurrence of each value of wind speed to the total number (8779) of estimated hourly wind speeds. Note that the tables and graphs illustrate the same information, but in two different ways.

It can be seen from Figure 6.36 and Table 6.2 that the wind speed probability distribution at all locations indicates that winds suitable for wind power generation are well presented in the total range of wind speeds. High wind speeds occur less at G1 than at other locations, while they are very frequent at G5 and G6. G5 and G6 have excellent potentials of wind power generation. The other three sites have frequent high speeds but not as frequently as those of G5 and G6.

Table 6.2 indicates that the wind at G1 can blows at speeds higher than 20 m/s but not often, since this speed occurs at 8 times out of 8779 estimated hours. However, wind speed never reaches 25 m/s being the cut-out wind speed of most modern turbines. This is a good sign for electricity grids, because operating turbines would not be forced to shut down.

The wind is, to a certain extent, strong during the majority of the time. The wind at G1 blows at hourly speeds of 7 m/s or higher during 50% of the time. Hourly wind speeds of 7 m/s or greater are dominant at G6, as they occur during 6550 hours out of 8779 simulated hours (over 74% of the time) [Figure 6.36 and Table 6.2].

The same scenario is experienced at G2, G3, G4, and G5 since they have frequent strong winds. These sites have hourly wind speeds of 7 m/s or

higher during about 60% of the estimated speeds [Figure 6.36 and Table 6.2]. Indeed, these locations look promising for developing wind power projects. This proposes that most state-of-the-art wind turbines would generate electrical power during the predominant time period.

Tables 6.3 to 6.8 summarise the number of occurrence of each grouped power output. Figures 6.37 to 6.42 illustrate the cumulative frequency distribution of the estimated hourly wind power output generated by the G58-850kW, FL54-1000kW, G80-1500kW G80-2000kW, N80-2500kW, and V112-3000kW, at the six chosen locations. These charts display the frequency of each value of power generated by each turbine.

The class of every occurred power output interval for the same turbines installed at the same sites is also shown in the above-said tables. It may be argued that hourly power outputs should not be classified as they represent short time intervals. This is a valid argument but this classification of the hourly power outputs of wind turbines is designed specifically for the purpose of this study as a convenient way of representing the potential electricity produced by these turbines. It should be kept in mind that when classifying the power output of a turbine, it is somewhat taken in consideration the size of its blades as well as its rated power.

A first glance to Figures 6.37 to 6.42 indicate that the graph lines representing the cumulative frequencies of the turbine outputs seem to follow quite similar trends in all graphs. In other words, the lines of the frequency distribution of electricity outputs at G1 lay in the top, while that of electricity outputs at G6 appears in the bottom and G5's line is located above G6's line. The other grid points' frequency distribution lines lay between G1's and G5's lines. The instantaneous indication from this would be that the lower the line, the higher the median of the data, and therefore the better wind power distribution will have.

At all candidate sites, every one of the considered turbines would do a good job during most of the hours of the year. The generators produce sufficient amounts of power falling in high classes at all sites. Over most of the time of the year, they would generate power of class 3 or higher at the six locations, and other than that, the power outputs of class 7 occur frequently. Even so, the estimated power outputs vary from one location to another.

As summerised in Tables 6.3 to 6.8, more than 50% of the estimated hourly power outputs at the six sites fall in class 3 or greater. When installing the wind turbines at G1, they would have good amounts of electricity, although their power output classes are lower than at the other locations. G5 and G6 show the greatest potentials of producing cost-efficient electrical power, especially when using the G58-850kW, G80-1500kW, and V112-3000kW. At these locations, most of the hours of the year would experience electricity outputs of class 7. The distribution of the predicted hourly power outputs at the remaining locations is in the middle range between the outputs of G1 and G6.

At G1, the G58-850kW, G80-1500kW, and V112-3000kW would deliver electrical power belonging to class 3 or greater over about 50, 55, and 52% of the time, respectively. G2, G3, and G4 show a similar distribution of power outputs during most of the time. If these turbines were sited at G2, G3, or G4, they would provide the electricity networks with power classified 3 or higher during 57-65% of the hours of the year. Yet, electricity grids would attain power of class 3 or greater throughout nearly 63%, 65%, and 65% of the time, if the previously mentioned turbines were installed at G5. G6 is a great site for wind power generation. At this site, the estimated hourly power outputs of the G58-850kW, G80-1500kW, and V112-3000kW fall in class 3 or higher in around 75% of the total number of the outputs. Out of 8779 estimated hourly power outputs, about 6576, 6721, and 6635 occurrences of theses power outputs fall in the range of class 3 or greater

[Figure 6.37 and Table 6.3], [Figure 6.39 and Table 6.5], and [Figure 6.42 and Table 6.8].

The FL54-1000kW, G80-2000kW, and N80-2500kW have less efficiency of wind power generation compared to the other three generators. Nevertheless, their estimated power outputs are reasonable, as most of them are in middle classes. The FL54-1000kW would deliver more than 300 kW (class 3 or higher) of electricity over about 47, 54, 58, 58, 60, and 73% of the time, at G1, G2, G3, G4, G5 and G6, respectively. The G80-2000kW power outputs of higher than 600 kW (class 3 or higher) would occur during around 45, 50, 55, 55, 57, and 70% of the year. The estimated hourly power outputs of the N80-2500kW are in class 3 or higher in 37, 44, 46, 46, 52, and 65% of the 8779 estimated outputs [Figure 6.38 and Table 6.4], [Figure 6.40 and Table 6.6], and [Figure 6.41 and Table 6.7].

In terms of the probability distribution on the daily basis, the estimated hourly power outputs of the G80-1500kW of each day are summed to produce the daily power at the six locations. The cumulative distribution of the daily power generated by this turbine at the six considered locations is illustrated in Figure 6.43.

This figure expresses that if this turbines operated at G1 having the poorest wind power resources, it would produce 10 MWhr/day or more of electricity during nearly 60% of the year days (about 219 days), and 20 MWhr/day or more on about 80 days. At G2, G3, and G4, the G80-1500kW would yield 10 MWhr/day or higher during around 70% of the year days. During 23, 33, and 30% of the time the turbine would supply electricity grids with 20 MWhr/day or more, respectively.

Furthermore, the cumulative distribution of the estimated daily power produced by the G80-1500kW at G5 and G6 provides a great encouragement to wind power producers. At these locations, there would be about 10 MWhr/day or more of generated power during 85 and 95% of the year days. From a single turbine, the Libyan electricity networks would get

power being about 20 MWhr/day or more during 33 and 39% of the time [Figure 6.43]. There would be an economical power, less burnt fossil fuels, and hence less GHG emissions.

The considered sites have wind power resources ranging from good to excellent, but G1 has the lowest wind power resources. The best ones are G5 and G6. In general, all sites have great potentials of generating electricity from their wind resources.

Regarding the turbines, the G58-850kW, G80-1500kW, and V112-3000kW yield very good amounts of electricity at the selected sites. The other turbines show good potentials as well, but less than those three turbines said lately. The lowest power outputs are those of the N80-2500kW due to its power curve trend.

Table 6.2: The frequency distribution of grouped estimated hourly 100-m wind speeds [m/s] at the selected sites.

Hourly Wind Speed [m/s]	G1	G2	G3	G4	G5	G6	Total
<3	930	763	596	623	666	386	**3964**
3-<5	1632	1369	1202	1071	1158	746	**7178**
5-<7	2071	1808	1878	1878	1483	1097	**10215**
7-<9	1852	1887	2185	2300	1580	1439	**11243**
9-<12	1483	2282	2466	2185	2361	2537	**13314**
12-<15	584	618	408	643	1303	2431	**5987**
15-<20	219	52	43	79	228	143	**764**
≥20	8	0	1	0	0	0	**9**
Total	**8779**	**8779**	**8779**	**8779**	**8779**	**8779**	**52674**

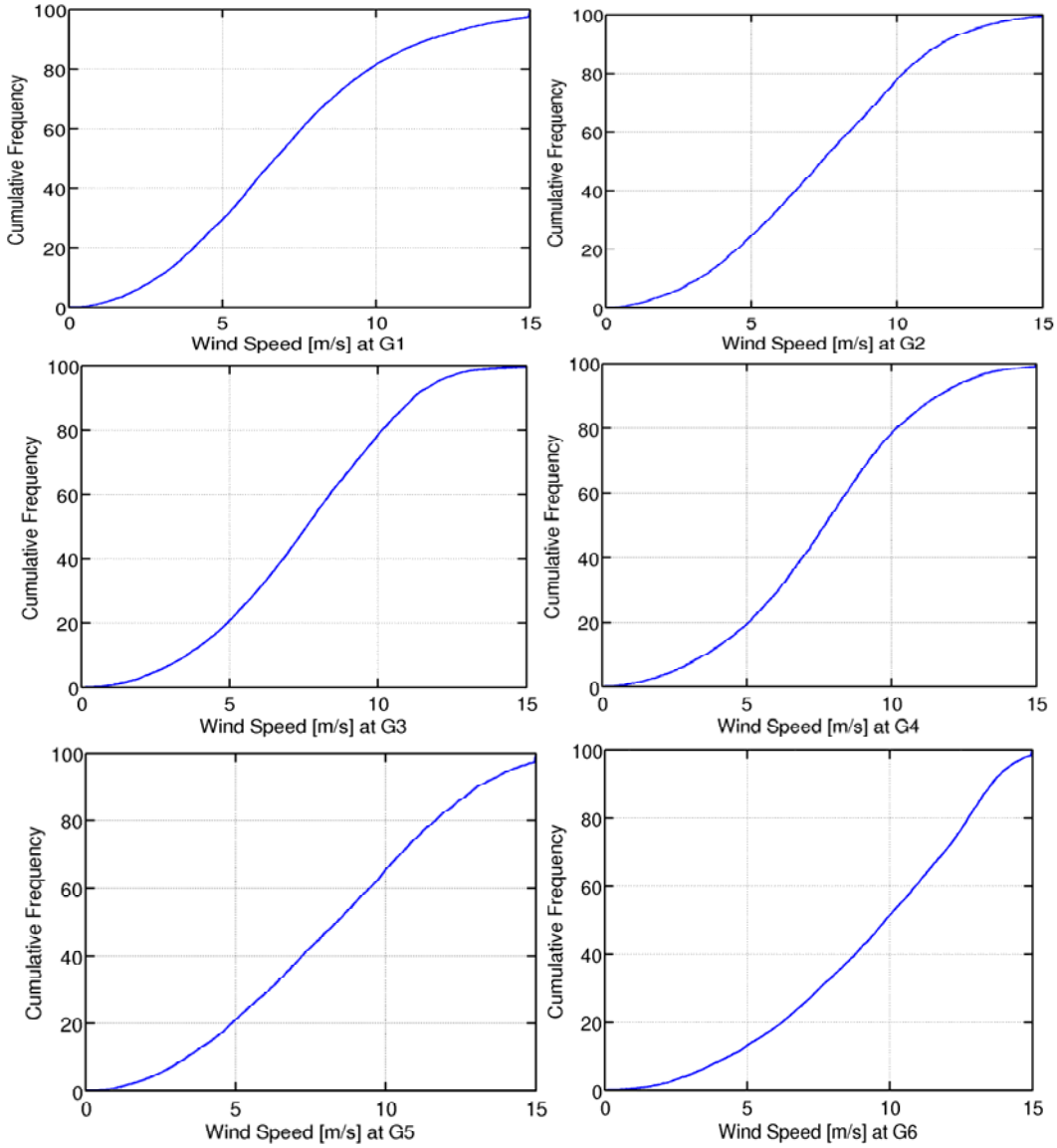

Figure 6.36: The cumulative frequency distribution [%] of estimated hourly wind speed [m/s] at the selected sites.

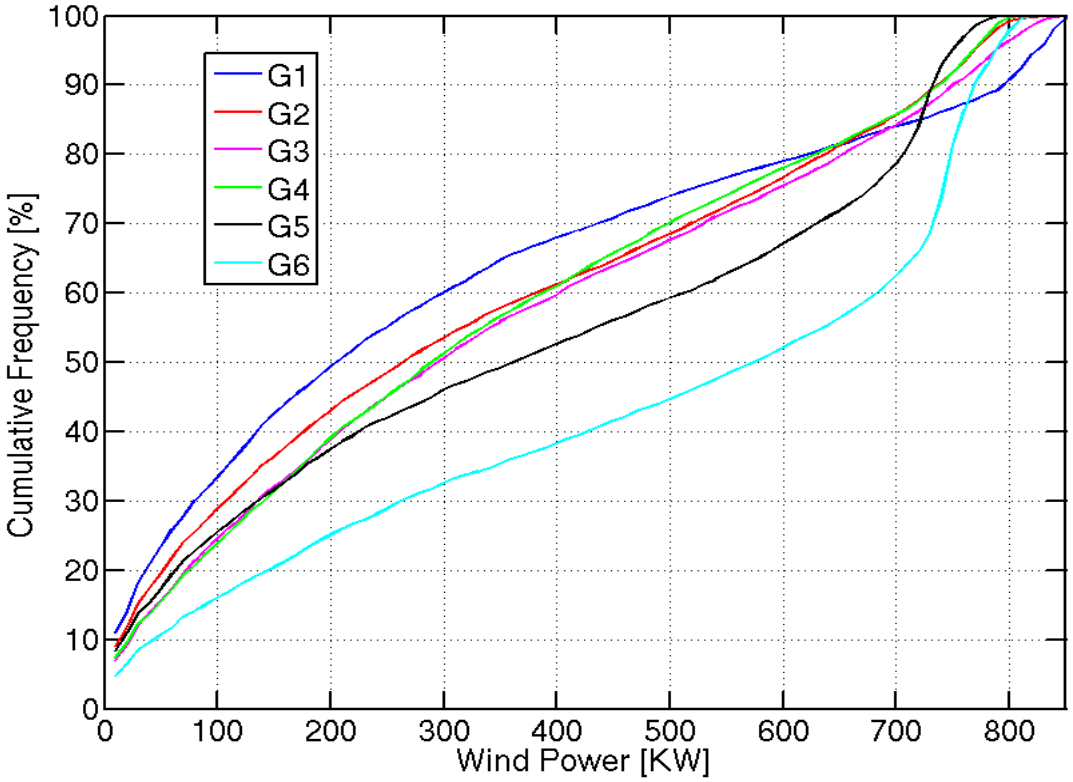

Figure 6.37: The cumulative frequency distribution [%] of estimated hourly power outputs [kW] of the G58-850kW turbine at the selected sites.

Table 6.3: The frequency distribution of grouped estimated hourly 100-m wind power [kW] generated by the G58-850kW turbine at the selected sites.

Hourly Power Output [kW]	Matching Capacity Factor [%]	Class	G1	G2	G3	G4	G5	G6	Total
<100	<11.7	1	2932	2528	2158	2089	2238	1404	**13349**
100-<200	11.7-<23.5	2	1395	1238	1254	1343	1053	799	**7082**
200-<300	23.5-<35.3	3	948	922	1034	1071	754	658	**5387**
300-<400	35.3-<47	4	694	684	806	852	571	509	**4116**
400-<500	47-<58.8	5	528	641	702	808	589	554	**3822**
500-<600	58.8-<70.6	6	438	720	675	685	685	649	**3852**
≥600	≥70.6	7	1844	2046	2150	1931	2889	4206	**15066**
Total			**8779**	**8779**	**8779**	**8779**	**8779**	**8779**	**52674**

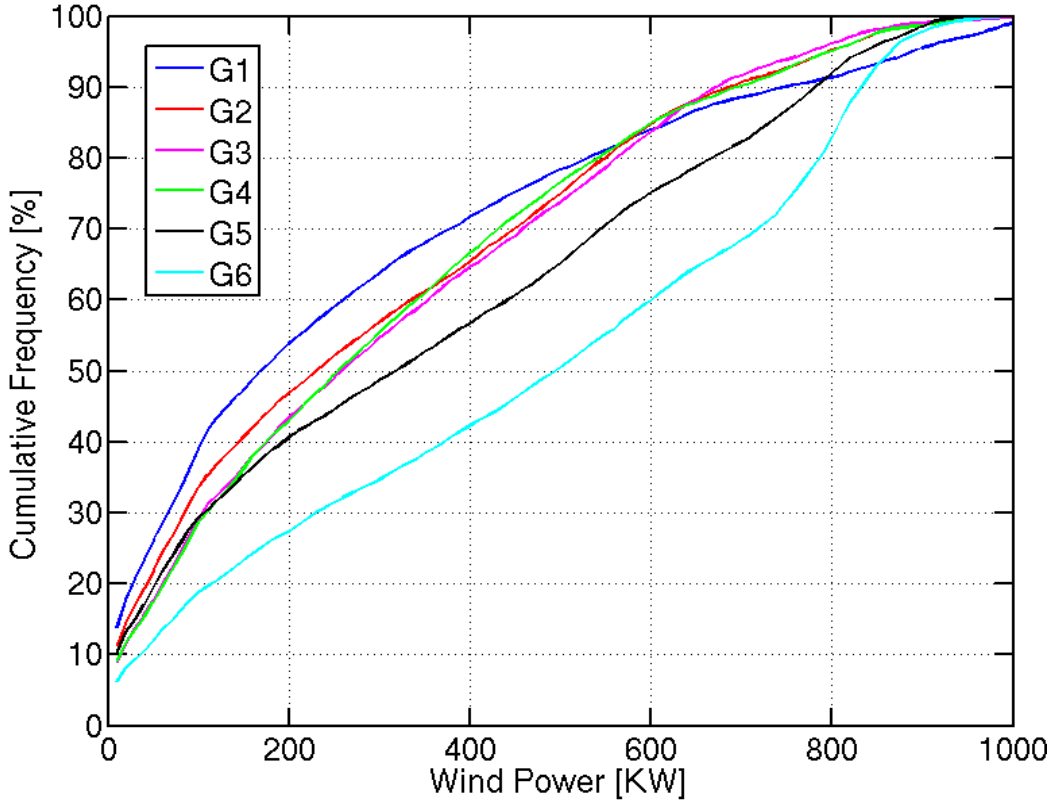

Figure 6.38: The cumulative frequency distribution [%] of estimated hourly power outputs [kW] of the FL52-1000kW turbine at the selected sites.

Table 6.4: The frequency distribution of grouped estimated hourly power outputs [kW] of the FL52-1000kW turbine at the selected sites.

Hourly Power Outputs [kW]	Matching Capacity Factor [%]	Class	G1	G2	G3	G4	G5	G6	Total
<100	<10	1	3412	2949	2554	2519	2563	1648	**15645**
100-<200	10-<20	2	1288	1158	1264	1255	1000	744	**6709**
200-<300	20-<30	3	876	886	983	1088	702	638	**5173**
300-<400	30-<40	4	693	747	869	992	711	667	**4679**
400-<500	40-<50	5	588	843	808	869	747	728	**4583**
500-<600	50-<60	6	500	852	870	728	869	834	**4653**
≥600	≥60	7	1422	1344	1431	1325	2187	3520	**11229**
Total			**8779**	**8779**	**8779**	**8779**	**8779**	**8779**	**52674**

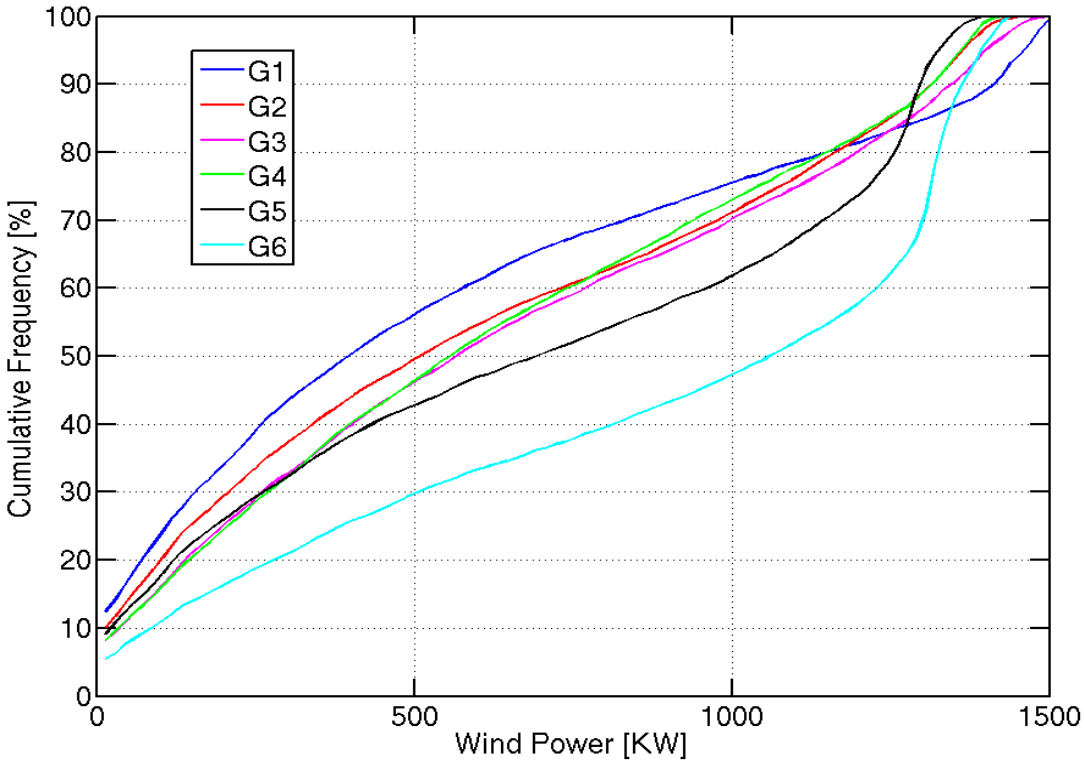

Figure 6.39: The cumulative frequency distribution [%] of estimated hourly power outputs [kW] of the G80-1500kW turbine at the selected sites.

Table 6.5: The frequency distribution of grouped estimated hourly power outputs [kW] of the G80-1500kW turbine at the selected sites.

Hourly Power Output [kW]	Matching Capacity Factor[%]	Class	G1	G2	G3	G4	G5	G6	Total
<150	<10	1	2596	2221	1852	1792	1970	1227	**11658**
150-<350	10-<23.3	2	1517	1342	1316	1382	1136	831	**7524**
350-<550	23.3-<37	3	1044	1027	1136	1186	827	721	**5941**
550-<750	36.7-<50	4	762	743	882	940	640	543	**4510**
750-<950	50-<63.3	5	567	709	754	894	670	636	**4230**
950-<1150	63.3-<76.7	6	536	913	849	823	938	845	**4904**
≥1150	≥76.7	7	1757	1824	1990	1762	2598	3976	**13907**
Total			**8779**	**8779**	**8779**	**8779**	**8779**	**8779**	**52674**

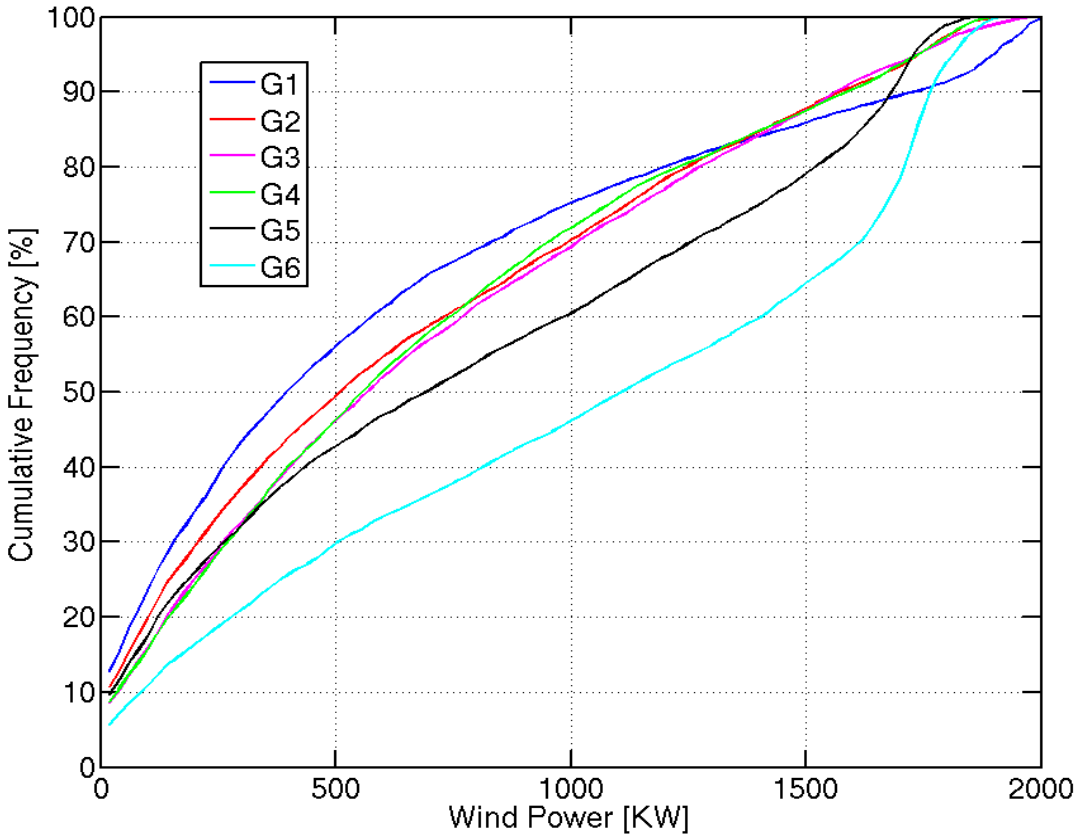

Figure 6.40: the cumulative frequency distribution [%] of estimated hourly power outputs [kW] of the G80-2000kW turbine at the selected sites.

Table 6.6: the frequency distribution of grouped estimated hourly power outputs [kW] of the G80-2000kW turbine at the selected sites.

Hourly Power Output [kW]	Matching Capacity Factor [%]	Class	G1	G2	G3	G4	G5	G6	Total
<250	<12.5	1	3414	2943	2549	2511	2567	1645	**15629**
250-<500	12.5-<25	2	1505	1393	1502	1551	1187	976	**8114**
500-<750	25-<37.5	3	999	995	1134	1236	816	701	**5881**
750-<1000	37.5-<50	4	683	837	896	1006	736	729	**4887**
1000-<1250	50-<62.5	5	527	863	856	769	815	754	**4584**
1250-<1500	62.5-<75	6	415	676	746	605	825	862	**4129**
≥1500	≥75	7	1236	1072	1096	1100	1833	3112	**9449**
Total			**8779**	**8779**	**8779**	**8779**	**8779**	**8779**	**52674**

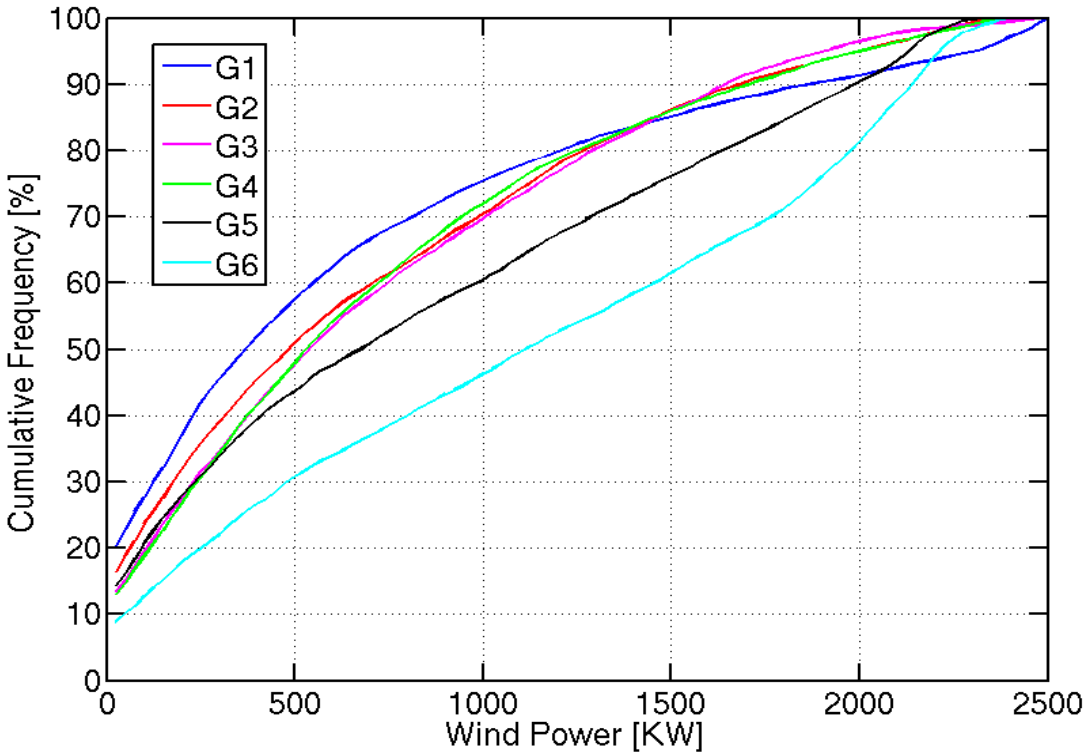

Figure 6.41: The cumulative frequency distribution [%] of estimated hourly power outputs [kW] of the N80-2500kW turbine at the selected sites.

Table 6.7: The frequency distribution of grouped estimated hourly power outputs [kW] of the N80-2500kW turbine at the selected sites.

Hourly Power Output [kW]	Matching Capacity Factor [%]	Power Class	G1	G2	G3	G4	G5	G6	Total
<300	<12	1	3996	3431	3043	3015	2974	1937	**18396**
300-<600	12-<24	2	1485	1467	1641	1736	1201	1049	**8579**
600-<900	24-<36	3	901	976	1119	1226	893	815	**5930**
900-<1200	36-<48	4	633	976	940	940	844	824	**5157**
1200-<1500	48-<60	5	455	715	804	633	772	777	**4156**
1500-<1800	60-<72	6	372	505	639	495	733	852	**3596**
≥1800	≥72	7	935	705	589	729	1358	2524	**6840**
Total			**8779**	**8779**	**8779**	**8779**	**8779**	**8779**	**52674**

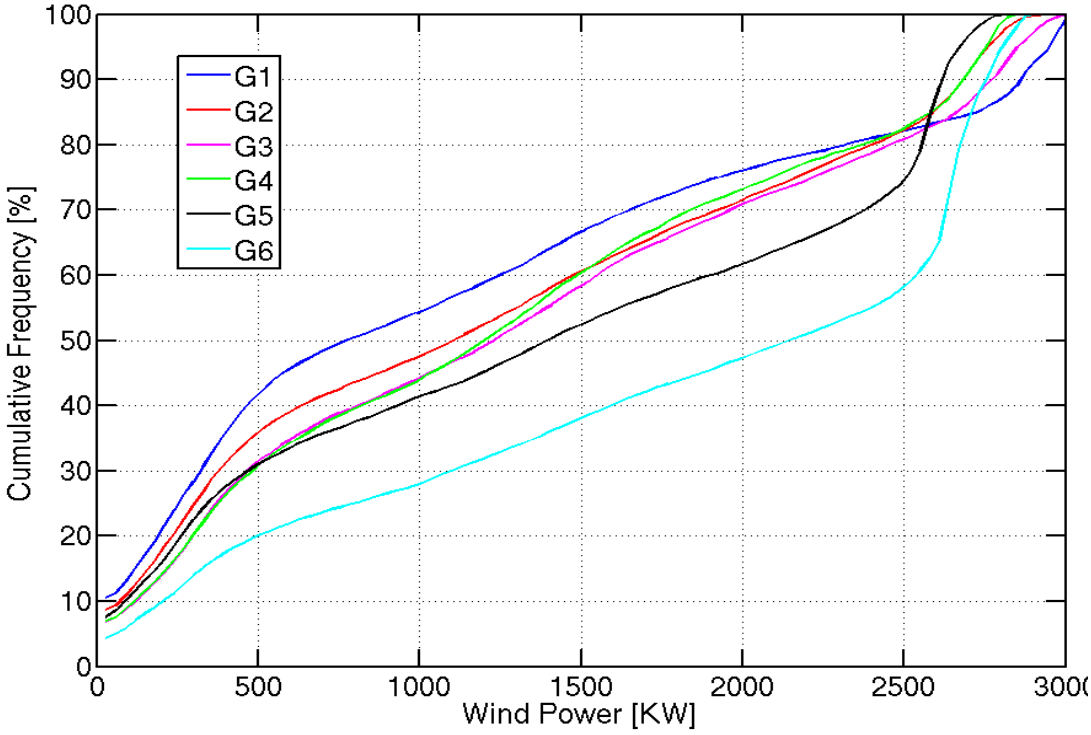

Figure 6.42: the cumulative frequency distribution [%] of estimated hourly power outputs [kW] of the V112-3000kW turbine at the selected sites.

Table 6.8: the frequency distribution of grouped estimated hourly power outputs [kW] of the V112-3000kW turbine at the selected sites.

Hourly Power Output [kW]	Matching Capacity factor [%]	Class	G1	G2	G3	G4	G5	G6	Total
<400	<13.3	1	3136	2739	2336	2298	2419	1536	**14464**
400-<750	13.3-<25	2	1211	990	1076	1074	789	605	**5745**
750-<1100	25-<36.7	3	622	645	688	738	572	501	**3766**
1100-<1450	36.7-<48.3	4	757	836	893	1050	724	605	**4865**
1450-<1800	48.3-<60	5	670	719	837	895	621	598	**4340**
1800-<2150	60-<71.6	6	455	623	631	633	545	559	**3446**
≥2150	≥71.6	7	1926	2222	2313	2088	3104	4372	**16025**
Total			**8779**	**8779**	**8779**	**8779**	**8779**	**8779**	**52674**

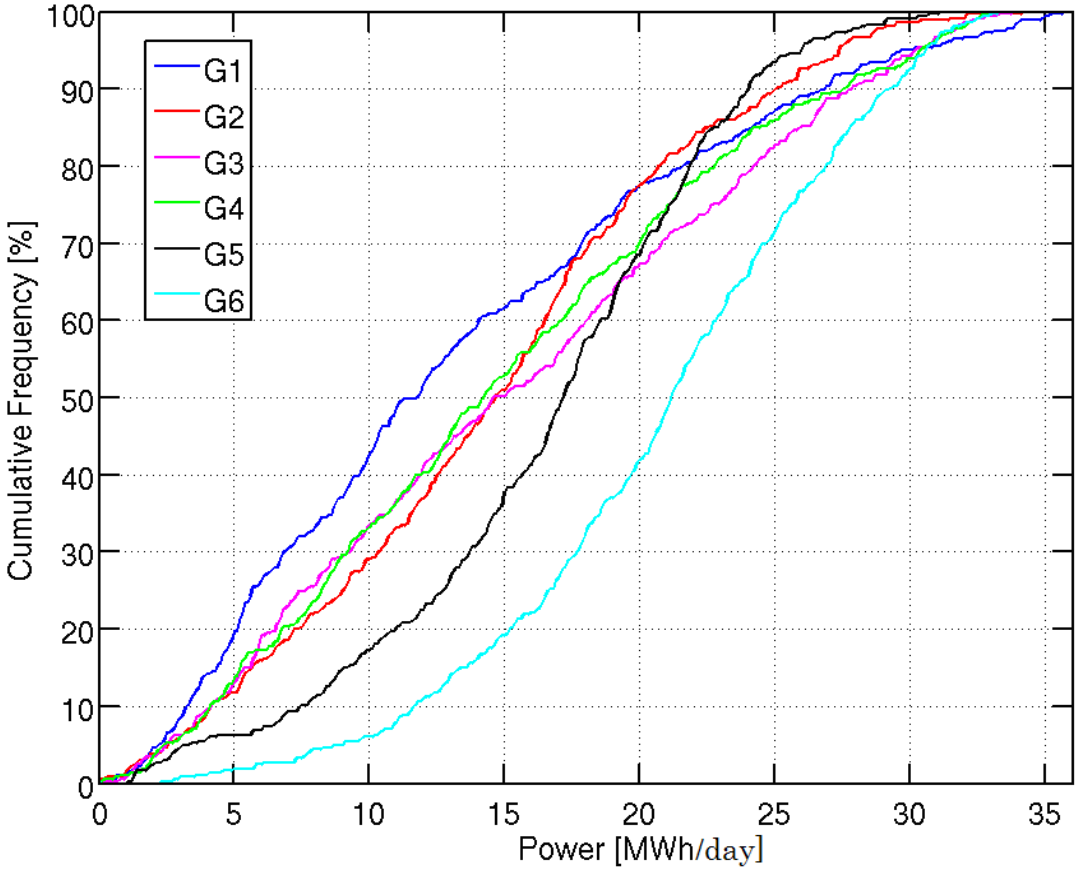

Figure 6.43: The cumulative frequency distribution [%] of daily power outputs [MWhr/day] of the G80-1500kW turbine at the selected sites.

6.8.2 Temporal Variations

The temporal variation of the estimated power outputs has been examined based on all considered turbines. However, the power outputs generated by these turbines have shown quite similar results in terms of the time variability of the power outputs. In view of this, the temporal variation is studied further based on the estimated power outputs of the G80-1500kW only. The temporal variations of wind speed and power output are presented and discussed below.

Regarding the variation of wind power resources from month to month, the monthly variations of wind speed and power output of the G80-1500kW installed at six selected locations are shown in Figures 6.44(a) and 6.44(b), in that order. These figures indicate that throughout all months most locations experience good wind speeds within the range required by most modern turbines. Once again, G1 has the lowest power resource, while G6 possesses the highest resource. At each one of the considered locations, the monthly average wind speed is 7 m/s or higher, and the estimated average power produced by the G80-1500kW is 500 kW or more in most months. Confirming the regional assessment, during summer the inland locations (G2, G5, and G6) have higher wind power resources than the coastal areas.

Figures 6.44(a) and 6.44(b) demonstrate that all months receive wind speeds suitable for wind power generation and the G80-1500kW would provide to electricity systems great amounts of power, especially at G5 and G6. When considering all sites as a group, summer months (June, July, and August) experience the highest wind energy resource and the turbine performs well in this season. The climate of Libya in summer is very hot, and hence more electricity is consumed during the daytime and nighttime as well.

Figures 6.45(a) to 6.45(f) illustrate the daily wind speed variation at the six applicant locations. Figures 6.46(a) to 6.46(f) show the daily wind power

output of the G80-1500kW. The daily average wind speed is computed by taking the mean of the estimated hourly data of each day in the year, while the daily power output is computed by summing the hourly power output of the turbine of the day.

As mentioned several times previously, the graphs of the daily pattern of wind speed and power output indicate that of the six locations, G1 has the lowest potential of wind power utilisation, whereas G6 has the greatest. Overall, the daily mean of wind speed and power output of the G80-1500kW at most locations vary from reasonable to very good on most days of the year.

During summer days (between about day 150 to about 250), there is no much a day-to-day variability in the wind speed and the electricity outputs, especially when they are compared to other seasons' days. The reverse scenario is applied on winter power resources, as they vary observably from day to day. During the midyear, the trends of daily mean wind speed and power output tend to rise at all sites, excluding at G1 and G4 [Figures 6.45(a) and 6.45(d)], and [Figures 6.46(a) and 6.46(d)].

In addition, as said earlier the daily mean wind at G1 occasionally exceeds 15 m/s [Figures 6.46(a) and 6.46(a)]. These values are out of the predominant range of wind speed. Nevertheless, this would not negatively affect the electricity generated by the turbine, but rather it enhances its productivity since wind speed does not reach the cut-out speed value of the turbine.

Figures 6.47(a) to 6.47(f) show the mean diurnal cycles of seasonal and annual wind speeds for the selected locations. The mean diurnal cycles of the corresponding power outputs of the G80-1500kW installed at these sites are demonstrated in Figures 6.48(a) to 6.48(f). The seasonal mean diurnal cycles of wind and wind power data for each hour are averaged over the number of days in the season, while the annual mean diurnal cycles are averaged over 8779 estimated hourly data.

The coastal locations (G1, G3, and G4) have a quite similar pattern in terms of the diurnal variability of wind speed and wind power output [Figures 6.47(a), 6.47(c) and 6.47(d)], and [Figures 6.48(a), 6.48(c), and 6.48(d)]. The diurnal distributions of wind and wind power at these places are strongly correlated. They tend to fluctuate during the day more than at the inland locations. At these sites, winter sees fairly steady and good wind power resources throughout the hours of the day.

The estimated wind speed and power output at the inland locations (G2, G5, and G6) also follow the same pattern of decreasing wind speed and power during the daylight hours and increasing speed and power during nighttime. These locations experience dramatic diurnal changes in wind speed and electricity in all seasons [Figures 6.47(b), 6.47(e), and 6.47(f)] and [Figures 6.48(b), 6.48(e) and 6.48(f)].

Of all locations, G1 appears to be the inferior site in terms of wind speed and power output distributions over the day. At the other nominated sites, during most hours of the day the mean wind speed is 7 m/s or higher, and the corresponding power output generated by the G80-1500kW is about 300 kW or greater, for all seasons.

During the night, this generator would do a very good job, as its estimated power outputs are reasonably high. Yet, before sunrise at 0500 UTC, its productivity would begin to fall gradually until mid-morning (around 0900UTC) at the coastal locations, and until the afternoon (about 1300UTC) at the inland locations. After these times, the turbine would start to produce increasing amounts of electricity peaking at night.

The other apparent situation is that at all sites nocturnal wind speeds and power outputs are higher than daytime ones. Summer has the greatest amount of power during the most hours of the day at all locations, excluding at G1.

This situation is more evident when considering high nocturnal wind speeds and the electrical power outputs of the selected turbine. The peaks of wind speed and power outputs are seen in summer at all places.

This suggests that the electricity generation potential in the country is great, especially when using batteries to store the nocturnal wind power for daytime electricity consumptions. Summer is the season of high electricity demand in Libya, even during nighttime as the temperature in June, July, and August gets very high.

(a)

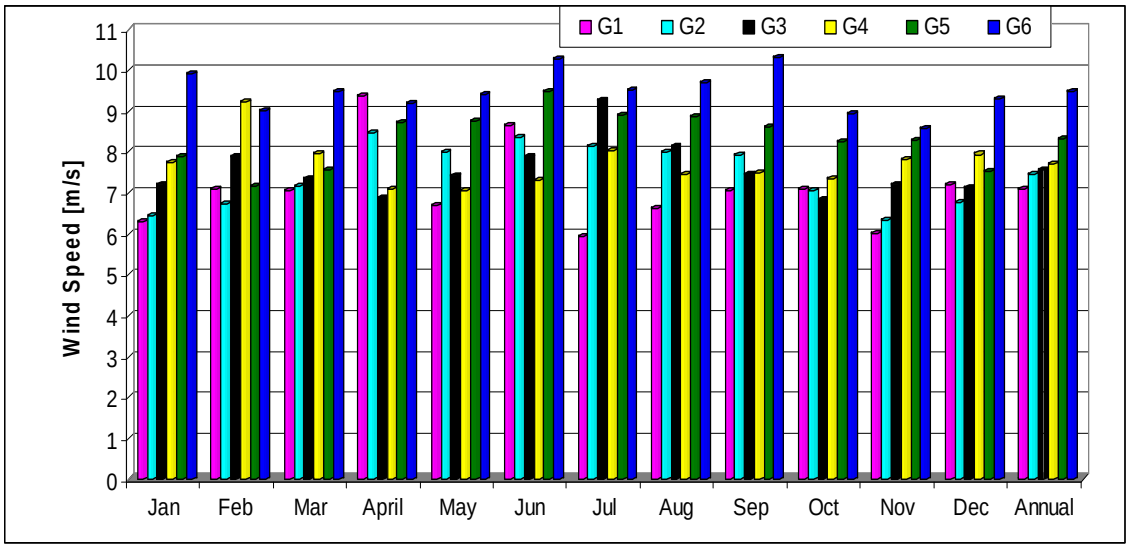

(b)

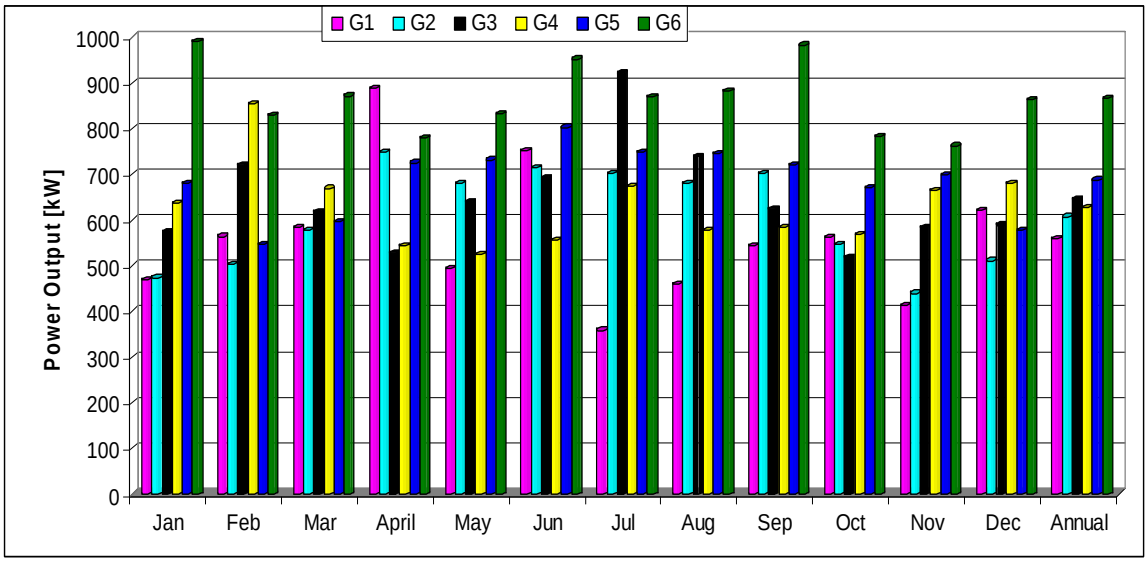

Figure 6.44: The estimated monthly mean (a) wind speed [m/s] and (b) power outputs [kW] of the G80-1500kW turbine at the selected sites.

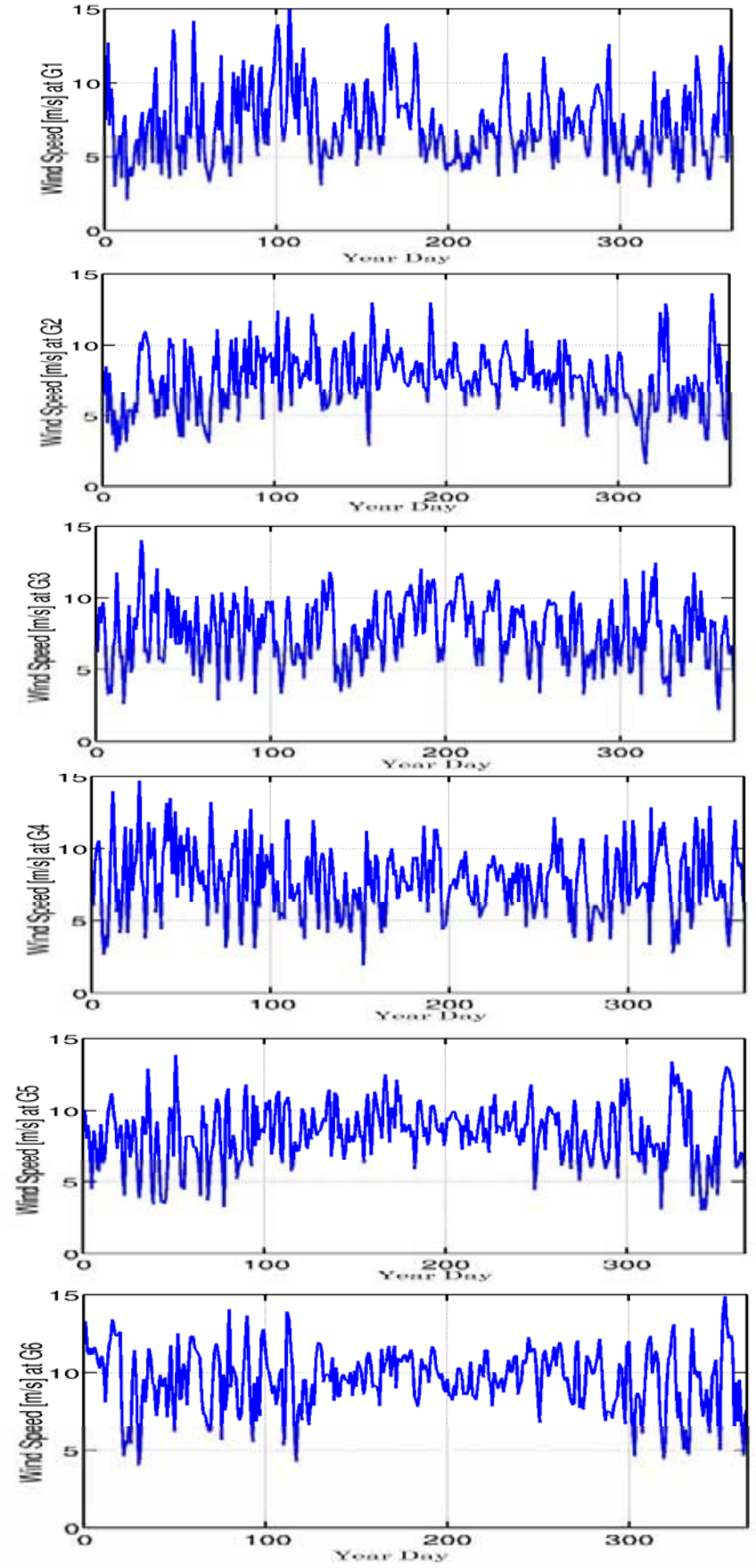

Figure 6.45: The estimated daily mean wind speed [m/s] at the selected sites.

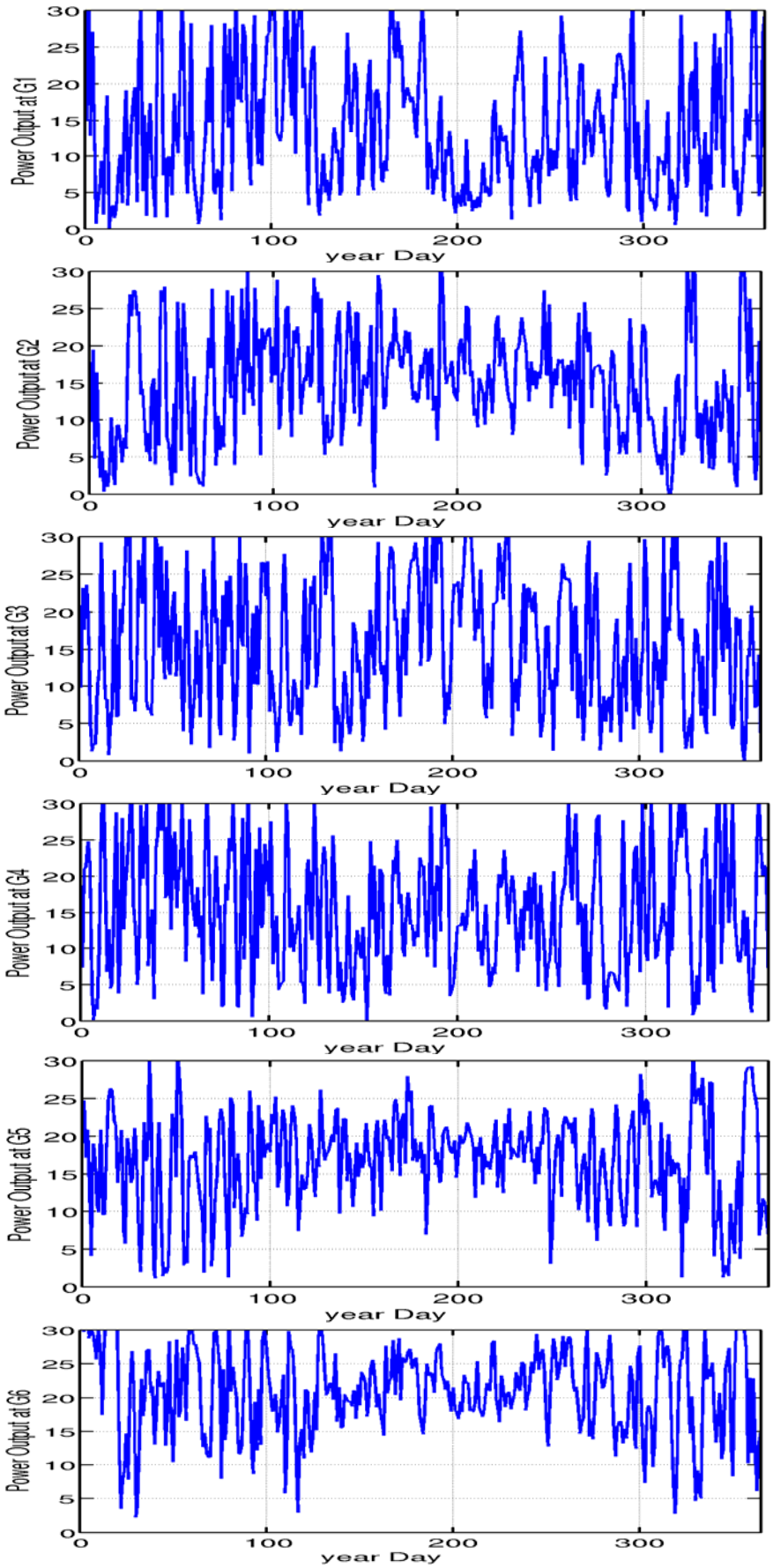

Figure 6.46: The estimated daily mean power outputs [MWhr/day] of the G80-1500kW turbine at the selected sites.

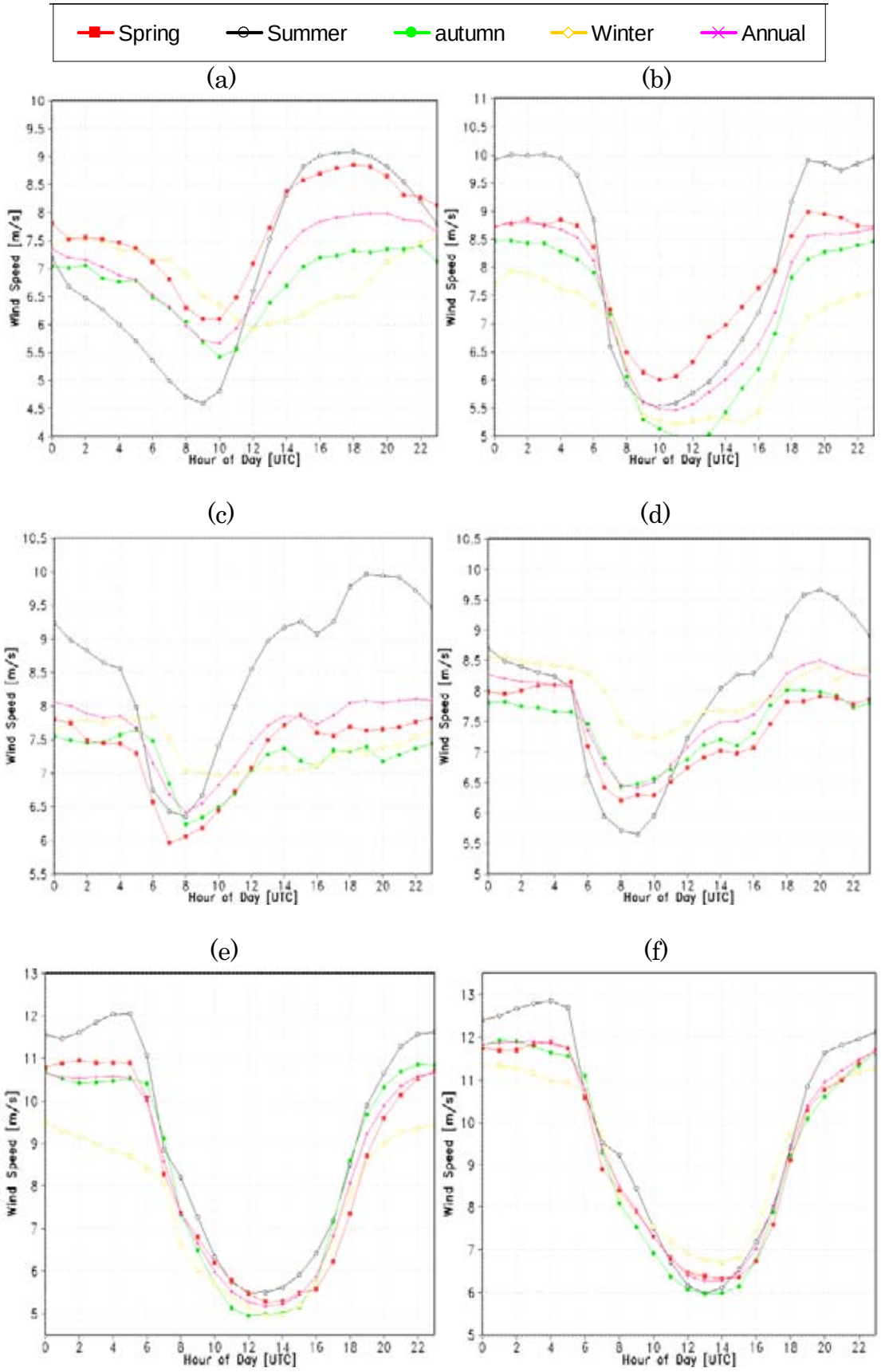

Figure 6.47: The estimated diurnal mean wind speeds [m/s] at the selected sites.

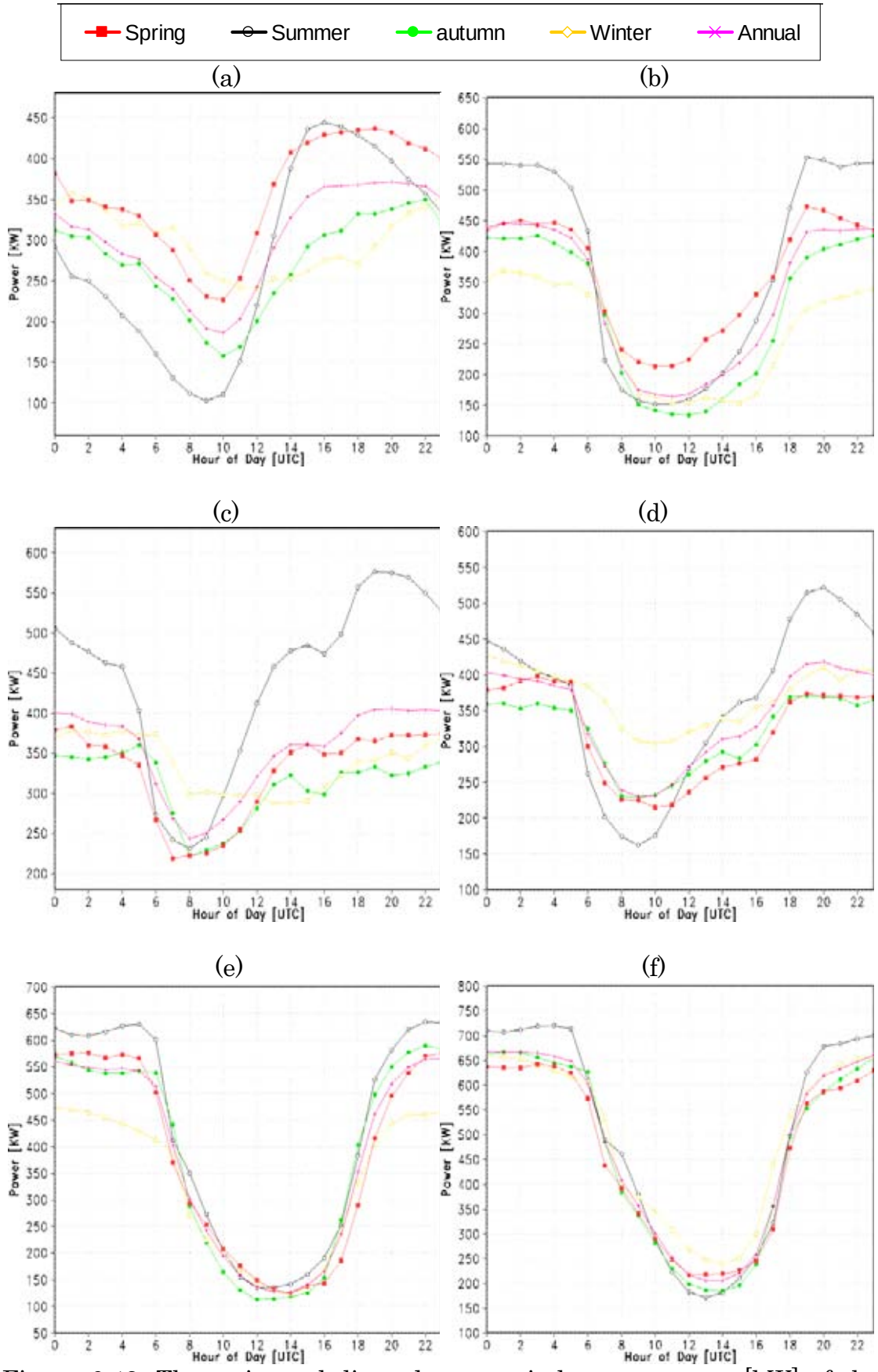

Figure 6.48: The estimated diurnal mean wind power output [kW] of the G80-1500kW turbine installed at the selected sites.

6.8.3 Vertical Variations

This section provides discussions about the vertical shear of on-site wind speed and the matching wind power generated by the G80-1500kW. The vertical wind shear stands for the change of wind velocity between two different atmospheric heights. As explained in Chapter 2, wind shear is one of the required parameters that need to be understood when installing wind turbines.

Figures 6.49 (a) to 6.49(f) demonstrate the estimated monthly mean wind speed at the six considered locations at 10, 25, 50, 75, 100, 125, and 100 m above the ground. The corresponding power produced by the G80-1500kW having a hub height of 75, 100, 125, and 100m at the mentioned sites is shown in Figures 6.50(a) to 6.50(f). The outputs of the turbine below 75 m have not been estimated because its rotor diameter's length is 80 m.

Prior to the wind shear discussion, it should be noted that the bulk of these figures indicates that all months have good wind and power outputs. The predicted monthly average of wind speeds and power outputs at all considered heights confirm that summer is the season of the greatest wind power potential.

Figures 6.49(a) to 6.49(f) suggest that the vertical wind shear does not vary significantly from month to month. This scenario is also applicable to the power outputs of the G80-1500kW [Figures 6.50(a) to 6.50(f)]. However, at G1, there is a small seasonal variability with the largest vertical wind gradient occurring in June.

Based on the wind profile at these six locations [Figures 6.49 (a) to 6.49(f)], the shear exponents for these sites can be estimated using the $1/7^{th}$ power law [Equation 2.9] presented in Chapter 2. Calculating the shear exponent for a site can assist to extrapolate wind speed to any elevation, with the provision of the wind speed at another height. This can be done using the same equation of wind power law.

Knowing the wind shear exponent facilitates the selection of the appropriate tower height for a turbine. The turbine can be installed theoretically at any elevation since wind speed can be estimated at any hub height. Estimating wind shear exponent provides reasonable representations for the wind profile over these sites although there may be diurnal and seasonal variability in the exponent. The shear exponent varies depending on the atmospheric stability and the roughness length of the region. Yet, estimating the annual shear exponent specifically for a site should predict vertical wind changes more accurately than the use of the value of 1/7 (0.143), which is commonly used to extrapolate wind speed to the hub height , especially at the height of 50 m.

Thus, the annual shear exponent for each atmospheric layer in the lowest 150 m, with a thickness of 25 m, has been calculated using Equation 2.9. The results of these estimates are summarised in Table 6.9. Table 6.9 indicates that for all locations, the first layer of 10-25m sees the minimum value of shear exponent among other layers. In this layer, wind shear exponent is in the range of 0.036-0.083.

Vertical wind shear at G1 does not appear to be significant. This site is located on a relatively flat coastal area. The effect of the surface friction resulted from the terrain is very low as this site is situated near the water over which the vertical wind speed gradient is at its minimum. As surface roughness increases, the same does the shear exponent. Other sites have higher wind shears as they are situated on mountains where the friction force generated by the surface drag is high.

At G1, the highest wind shear is seen when moving from 25 m up to 50 m. The annual wind speed in this atmospheric layer increases by around 0.4 m/s, and the annual shear exponent of the layer is around 0.097. Above 50 m, the vertical change in wind speed decreases until it peaks in the 75-100m layer where the annual shear exponent is approximately 0.084. When moving the turbine from 75 m up to 100 m, the wind speed at the

hub height increases by only 0.1 m/s and the turbine would produce about 20 kW of additional power. This means that the capacity factor of the production of the turbine would improve by 1.3% only. The increase of the tower height does not justify the increased electrical power output. Nevertheless, the decision is up to the economists. Above 100 m, the wind shear starts to rise, but at a very small rate. In the layer of 100-150, wind speed increases by about 0.25 m/s, and the annual shear exponent of this layer is about 0.087.

Wind shears at other sites (G2, G3, G4, G5, and G6) are entirely opposite to that at G1. Vertical wind speed changes are moderate and fall within the same value range. The wind shear is low in the first layer, and then increases gradually with height until it peaks in the layer of 75-100m. In the layers of 25-50 and 50-100m, the annual wind speed increases by about 0.6-1 m/s every thickness of 25 m. At all locations, excluding G1, the vertical wind shear exponents for these layers vary between 0.293 at G3 up to 0.384 at G6. Above this layer, the vertical shear goes down. By moving the tower of the turbine from 75 m to 100 m height, the turbine would produce about 100 kW of extra power. Between 100 and 125 m, wind speed continues to increase but at a lower rate in comparison to lower layers. The vertical wind gradients above this height vary between 0.2 and 0.5 m/s per 25 m in the layer of 100-125, and the vertical increase of estimated power outputs of the G80-1500kW ranges between 35 and 70 kW in this layer. The annual shear exponent in this layer is in the range of 0.216-0.293 at G2, G3, G4, G5, and G6. Above 125 m, the wind shear diminishes more, especially at G5. The wind speed and power output increase very slightly. The annual wind speed and estimated power output of the turbine rise by about 0.1-0.3 m/s and 3-25 kW per 25 m. The estimated annual shear exponent is between 0.074 and 0.193.

It may be not economical to move the hub height of the turbine above 100 m, especially above 125 m above the ground. However, as mentioned previously, this can be determined only by calculating and comparing the

The estimated values of the annual shear exponent summarised in Table 6.9 can be used to estimate wind speed at these sites at any desirable elevation suitable for the potential turbines. Table 6.9 shows that all considered sites, excluding G1, have an annual shear exponent above 0.143, especially at 50 m at which this value is commonly used to estimate the wind speed at higher elevations. This indicates that for G2, G3, G4, G5, and G6, the assumed shear exponent value of 0.143 is too conservative, as it underestimates the wind shear at these locations. As a result, it underestimates the increase in wind speed and potential power generated by the turbine. For G1, this value overestimates wind speed and potential power changes.

Assuming that wind speed is measured at 50 m (V(50)) and there is a turbine with a tower of 75 m installed at G6. If the standard value of the shear exponent (0.143) is used to extrapolate wind speed at the hub height of this turbine, as calculated below the wind speed at 75 m increases by 5% only over that of 50-m.

$$V(75) = V(50) * (75/50)^{0.143}$$

$$V(75) = 1.05 * V(50)$$

However, when using the estimated annual value of shear exponent (0.37) presented in Table 6.9, based on the calculation below the wind speed at 75 increases by about 16%.

$$V(75) = V(50) * (75/50)^{0.37}$$

$$V(75) = 1.16 * V(50)$$

There exists a substantial error, and this may lead to selecting an inappropriate elevation for the turbine. Thus, the values of the estimated annual shear exponent shown in Table 6.9 can assist to estimate the wind speed at any height at the six considered sites in future additional assessments if there are no sufficient wind speed measurements.

This chapter has investigated the potential of wind energy generation over Libya. It has presented discussions about the theoretical wind power resources over the country, and over four identified favourable regions. Several turbines have been used to estimate the power outputs at the four potential districts. Besides, six model grid points have been chosen for on-site detailed assessments. These discussions show that Libya has a good potential of wind power exploitation. The next chapter will present the conclusions and the recommendations of this research.

(a)

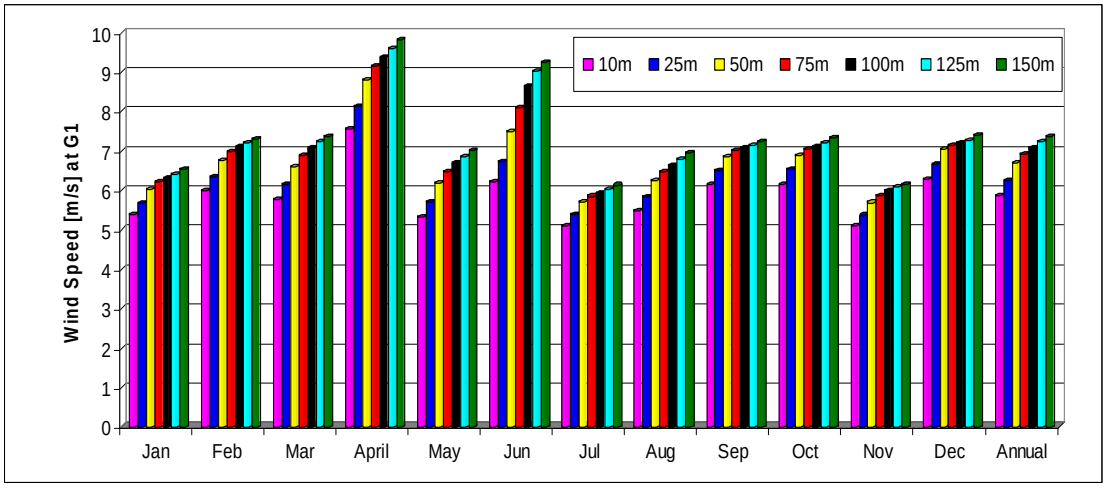

(b)

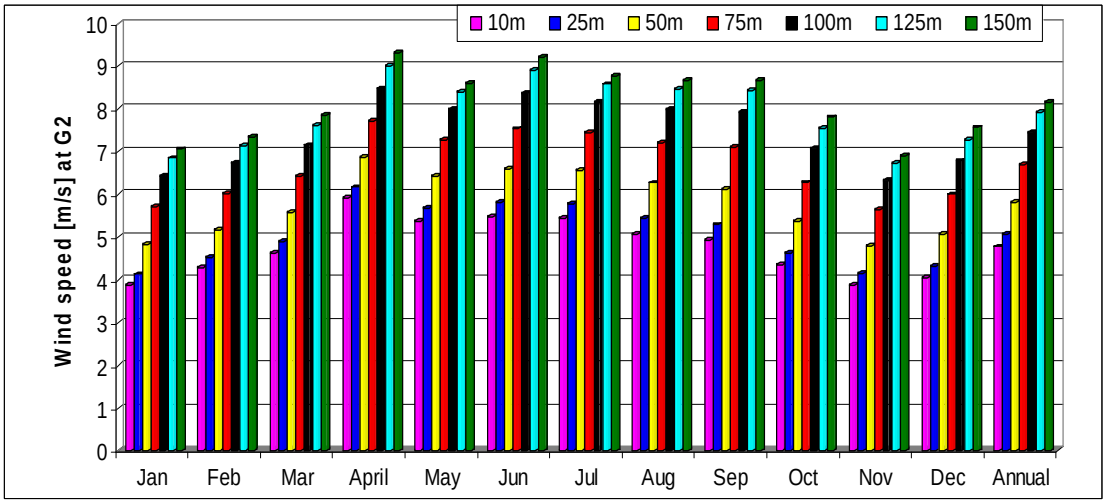

(c)

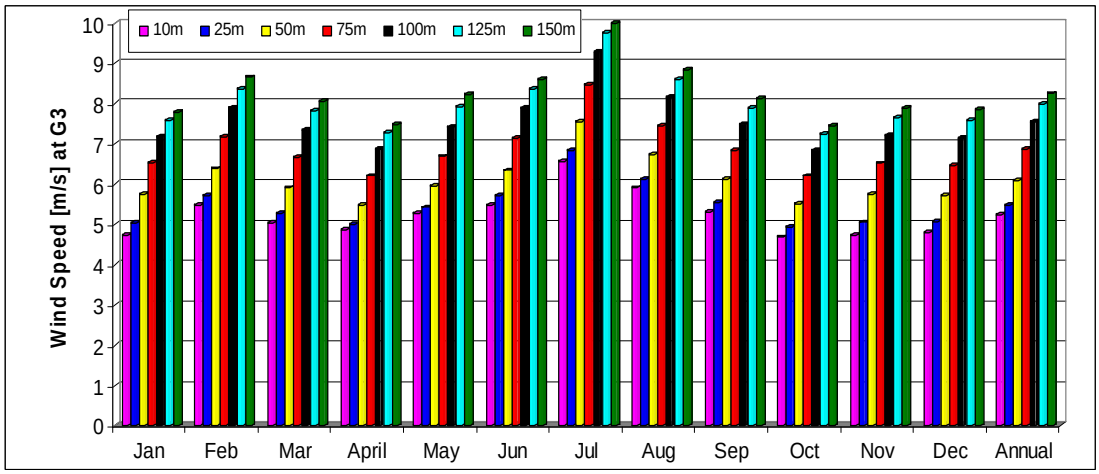

Figure 6.49: Vertical changes in monthly and annul wind speeds [m/s] at (a) G1, (b), G2, and (c) G3.

(d)

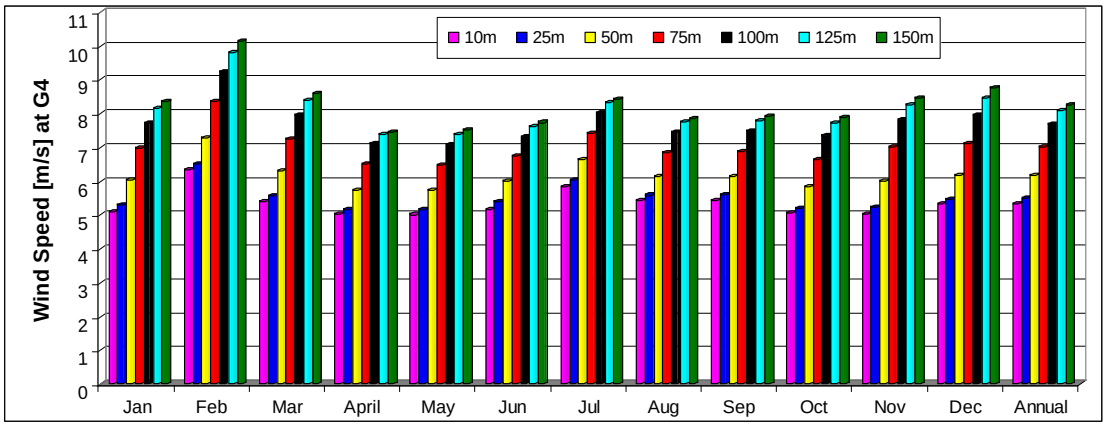

(e)

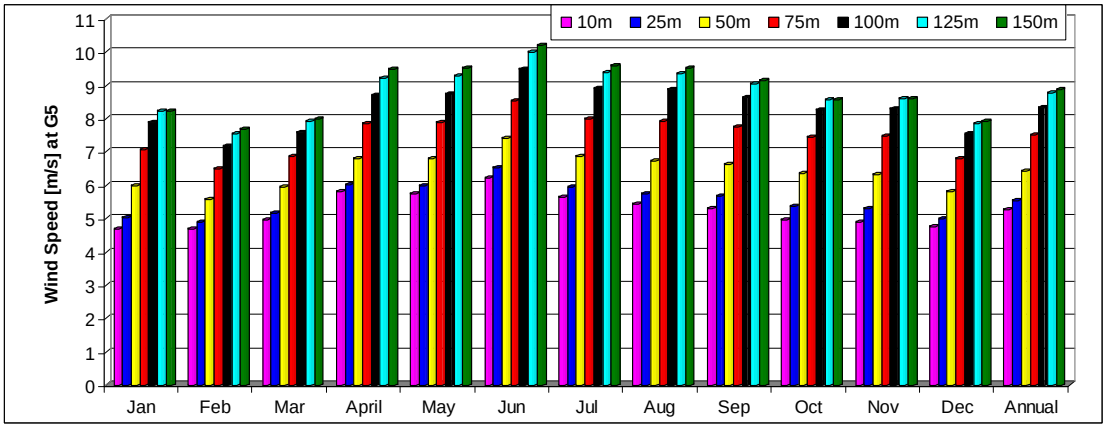

(f)

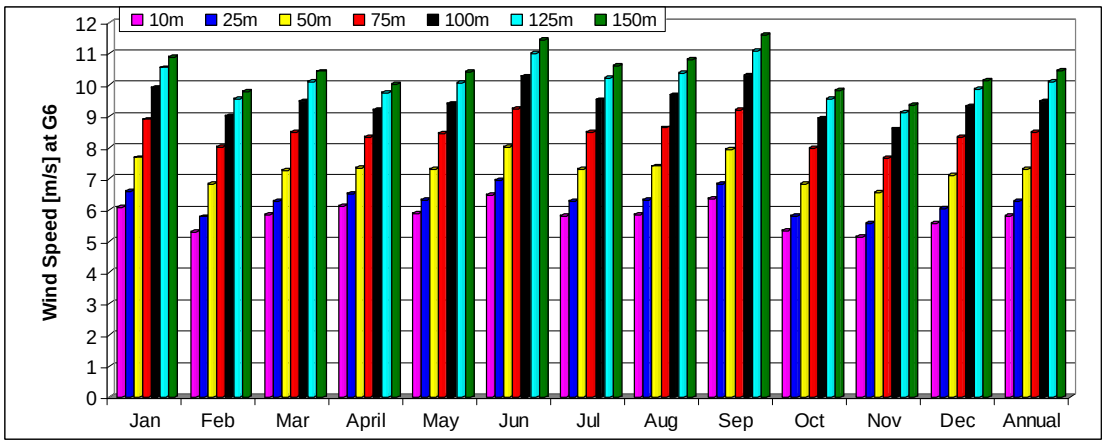

Figure 6.49 (continued): Vertical changes in monthly and annul wind speeds [m/s] at (d) G4, (e) G5 and (f) G6.

(a)

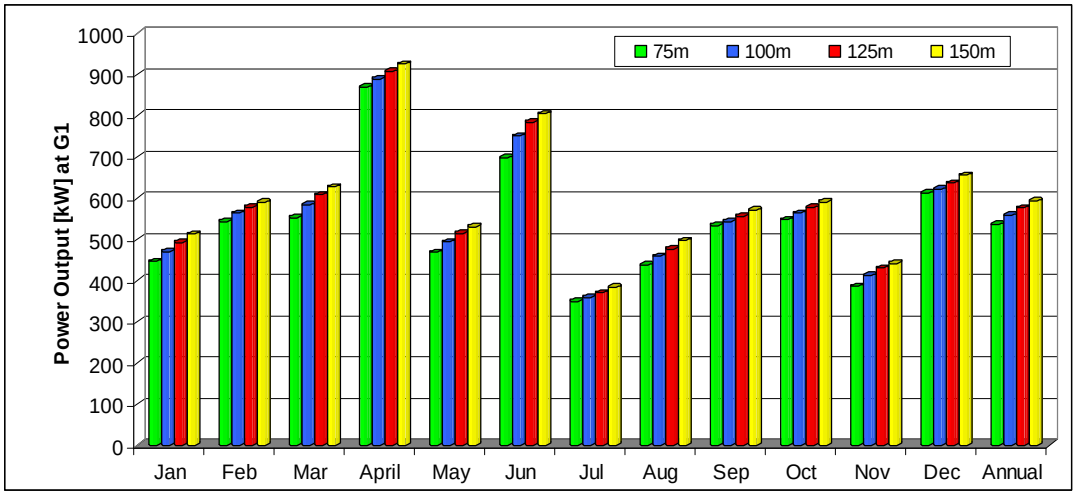

(b)

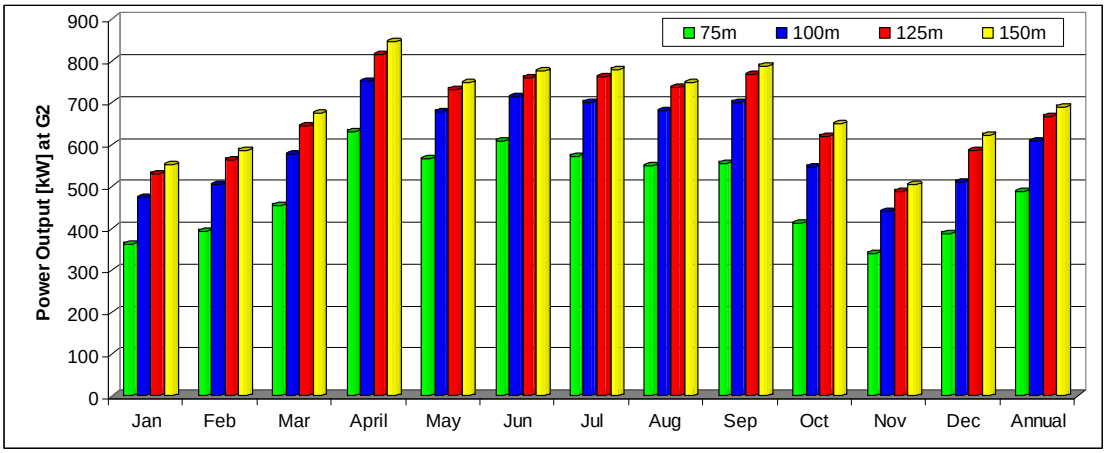

(c)

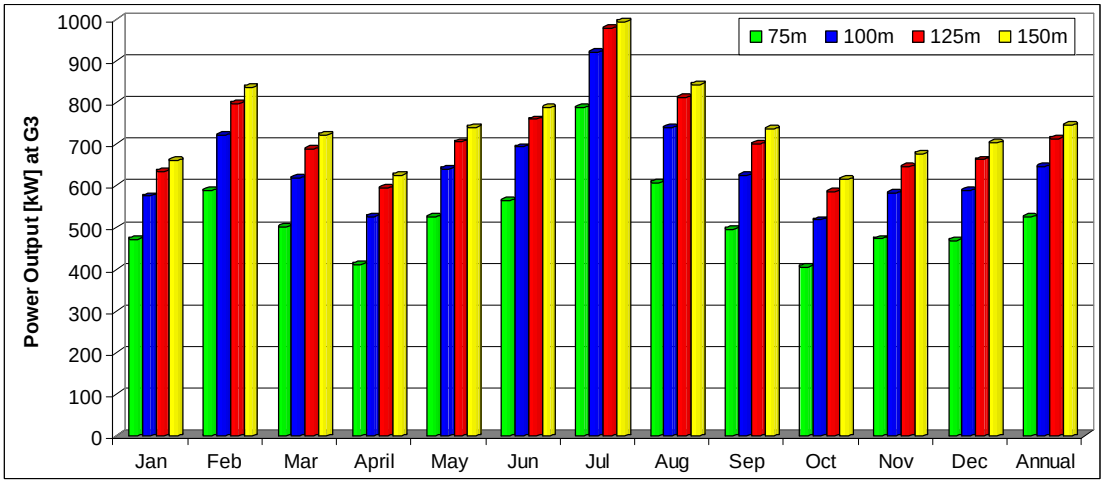

Figure 6.50: Vertical changes in monthly and annul power outputs [kW] of the G80-1500kW turbine installed at (a) G1, (b), G2, and (c) G3.

(d)

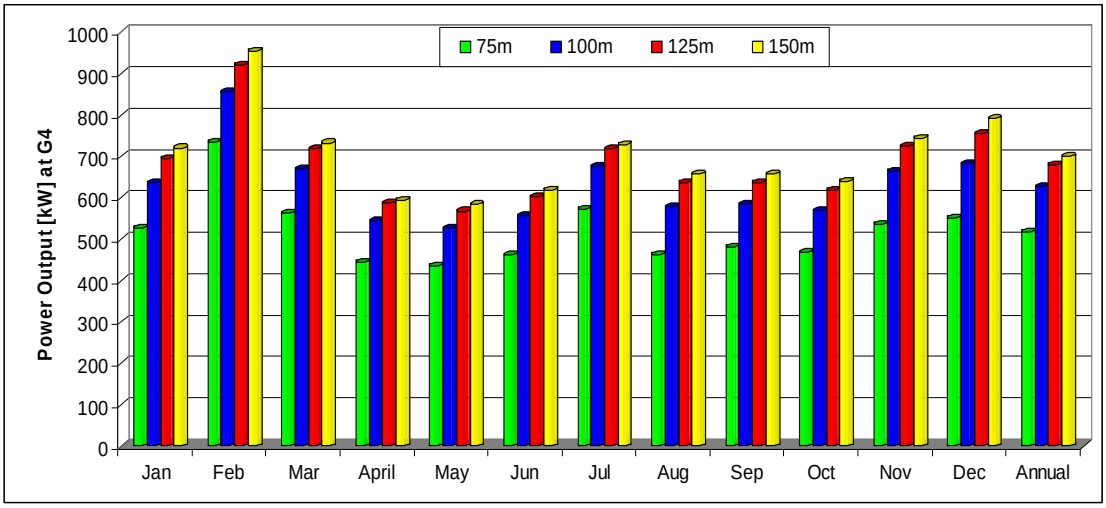

(e)

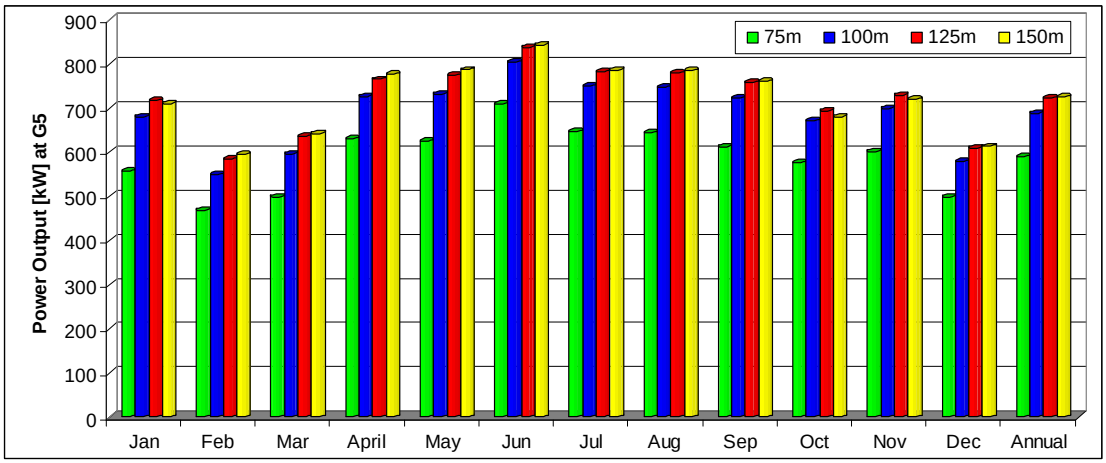

(f)

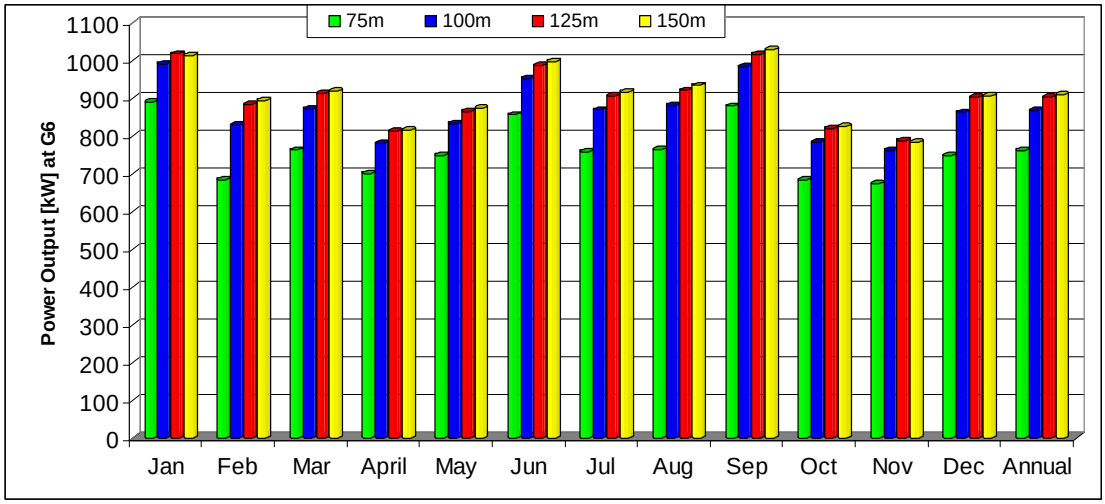

Figure 6.50 (continued): Vertical changes in monthly and annual power outputs [kW] of the G80-1500kW turbine installed at (d) G4, (e) G5, and (f) G6.

Table 6.9: the estimated annual shear exponent for the atmospheric layers over the selected sites.

	G1	G2	G3	G4	G5	G6
10-25m	0.068	0.066	0.049	0.036	0.058	0.083
25-50m	0.096	0.196	0.154	0.16	0.214	0.217
50-75m	0.087	0.351	0.293	0.318	0.382	0.37
75-100m	0.084	0.368	0.333	0.321	0.36	0.384
100-125m	0.087	0.268	0.259	0.216	0.22	0.293
125-150m	0.088	0.193	0.162	0.114	0.074	0.186
Average	**0.085**	**0.240**	**0.208**	**0.194**	**0.218**	**0.255**

Chapter 7

Conclusions and Recommendations

7.1 Overview

The objective of this research was to assess the wind resource of Libya. The study was aimed at the determination of the existence of good wind power potential in the country. The purpose was also to identify areas with good wind power resources that suit prospective wind power generation. Owing to the lack of high-resolution wind observations in Libya, the wind conditions of 2007 were modelled using the WRF-NMM of NCEP.

A series of 3-D real-data high-resolution nested numerical simulations (365 runs) were performed to produce hourly wind velocity data over the country. The coarse domain had a horizontal resolution of 15 km and a temporal resolution of 30 seconds while the fine domain had a horizontal resolution of 5 km and a temporal resolution of 10 seconds.

In addition to 10-m wind data produced directly by the model, the wind velocities at six other heights of 25, 50, 75, 100, 125, and 150 m above the ground were computed at every model grid point using a cubic spline

interpolation between wind data at sigma levels. Hourly wind power densities at these heights were then computed by means of Equation 2.6, using the estimated hourly wind speeds and the calculated 2-m air density. Further, hourly wind power outputs of ten commercially existing wind turbines installed at 100 m were calculated at all model grid points using the actual power curves of these turbines.

Six grid points were also chosen for detailed on-site wind power resource evaluations based on the assumption that these points should provide reasonable representations for the wind conditions in the surrounding regions. The simulation results were presented and analysed in Chapter 6.

7.2 Conclusions

The assessment of wind power resources over Libya has shown that there is a very good potential of wind power generation in the country, especially at heights above 50 m above the ground. Several prospective regions have been identified to be favourable areas for wind-generated electricity.

The eastern coastline of the Mediterranean consisting of Green Mountain, Darnah, Al Bayda, and the neighbouring areas experience very good wind power resources. Tobruk, Imsaad, and Ajdabiya have good wind energy resources as well but their resources are less than previous areas. It is estimated that if wind turbines were installed throughout these regions, they could complement each other so that electricity grids can attain sufficient amounts of power during most of the time of the year.

In addition to the previously mentioned districts, the western coastal regions have high prospective of wind-generated electricity. These areas include the coastline located between Misratah and the Libyan-Tunisian boarder, though the coastal zone from Tripoli along Zuwarah westward to the Libyan-Tunisian boundary possesses better wind power resources.

High potentials of wind power exploitation also exist in the northwestern crescent-shaped mountainous district connecting Al Khums landward along Ghiryan and Yifrin southwards to Dirj. The simulation results have demonstrated that if some wind turbines were installed at these regions, they could yield good electrical power cooperatively as they experience complemented wind power resources.

Better wind energy resources are found in the southern part of the country in the Sahara Desert. The Tibesti Mountains near the Libyan-Chad border and the mountainous region extending from Awbari southwards to the intersection zone of Libya, Algeria and Niger have higher wind speeds and power than coastal areas. Besides, Al Wigh and the northern regions of the Tibesti Mountains have a reasonable wind power generation prospective.

The estimated wind speed and power have shown that wind power resources and the topography of the country are highly correlated, as wind speed is higher at high-altitude areas than low-altitude ones although there are some coastal low-altitude districts having good wind power resources.

The estimates of wind power resources at different heights have indicated that most months see good to very good wind power resources although summer months have the greatest potential of wind-generated electricity over most parts of Libya. Generally, nighttime wind resources are higher than those of daytime. Wind energy resources are low in the morning but during the afternoon through the evening they increase until they peak at night, specifically before midnight.

In addition, it is noted that from 100-m height and above the horizontal sea-land wind speed gradient is small. It is shown that the best improvement of wind power outputs of the used wind turbines would occur when moving the turbines from 75 m up to 100 m above the ground, as the vertical wind shear over most districts peaks in the atmospheric layer of 75-100m. Accordingly, the estimated wind power outputs of considered

turbines have suggested that moving the turbines from 75 m up to 100 m above the ground would make substantial differences in their performance, while increasing the hub height of the turbines to heights above 100 m would not justify the additional power produced. Hence, the height of 100-m above the ground is found to be the optimal elevation for installing wind turbines in the country.

The six turbines discussed in Chapter 6 would do good to very good jobs if they were installed over the identified encouraging areas at 100 m above the ground. Yet, the G58-850kW, G80-1500kW, and V112-3000kW are the most suitable turbines for the wind resource of Libya at this height.

Furthermore, it is estimated that using the standard value of wind shear exponent (0.143) in the $1/7^{th}$ power law to extrapolate the wind speed at most regions in Libya would significantly underestimate the vertical changes of wind speed and power outputs of the turbines, and it can also overestimate wind speed and power outputs in other few areas.

7.3 Recommendations

This study has identified the areas that are favourable for wind power generation. It is suggested that wind towers should be placed in some highlighted potential regions to measure the wind for a period of 1 to 2 years within a temporal resolution of seconds to a minute. This would give an accurate indication about the variations of wind velocity and wind power that can be obtained by electricity grids.

It is also recommended that instead of using the standard value of wind shear exponent to extrapolate wind speed to the hub height at the six investigated locations, the annual shear exponents estimated in this study can be used favourably. The estimated values of wind shear exponents should represent the vertical gradient of wind speed more accurately than the standard value.

References

ACKERMANN, T. (2005) *Wind power in power systems*, John Wiley & Sons,Ltd.

ACKERMANN, T. & SODER, L. (2000) Wind energy technology and status: a review. *Renewable and Sustainable Energy Reviews,* 4**,** 315-374.

ADDIS, T. (2005) An adaptation of the UNSW HIRES numerical weather prediction model for Valencia, Spain. *School of Mathematics & Statistics.* Sydney, University of New South Wales.

AMAR, F. B., ELAMOURI, M. & DHIFAOUI, R. (2008) Energy assessment of the first wind farm section of Sidi Daoud, Tunisia. *Renewable Energy, 33*, 2311–2321.

American Wind Energy Association (AWEA) (2002) The most frequently asked questions about wind energy. Washington, D.C, American Wind Energy Association.

American Wind Energy Association (AWEA) (2005a) Wind energy and wildlife: the three C's. Washington, D.C, American Wind Energy Association.

American Wind Energy Association (AWEA) (2005b) The difference wind makes. *Wind projects provide real energy, economic, and environmental benefits.* Washington, D.C, American Wind Energy Association.

American Wind Energy Association (AWEA) (2009) 10 steps to developing a wind farm. Washington, D.C, American Wind Energy Association, viewed 22 January 2009, <http://www.awea.org/pubs/factsheets/Ten_Steps.pdf>.

ARAKAWA, A. & LAMB, V. R. (1977) Computational design of the basic dynamical processes of the UCLA general circulation model. *Methods in Computational Physics*, 17, 173-265.

ARCHER, C. L. & JACOBSON, M. Z. (2005) Evaluation of global wind power. *Journal of Geophysical Research,* 110.

ARDHUINA, F., BERTOTTIB, L., BIDLOTC, J.-R., CAVALERIB, L., FILIPETTOB, V., LEFEVRED, J.-M. & WITTMAN, P. (2007) Comparison of wind and wave measurements and models in the Western Mediterranean Sea. *Ocean Engineering,* 34**,** 526–541.

Australian Government's Overseas Aid Program (AusAID) (2000) Power for the people: renewable energy in developing countries. Canberra, Commonwealth of Australia.

AVISSAR, R. & PIELKE, R. (1989) A parameterization of heterogeneous land surfaces for atmospheric numerical models and its impact on regional meteorology. *Monthly Weather Review,* 117**,** 2113–2136.

BAILEY, B. (1981) Practical vertical wind profiles as a function of time of the day and surface wind speed. *Proceeding of an International Colloquium on Wind Energy.* Brighton, UK, the British Wind Energy Association.

BAILEY, B. H., MCDONALD, S. L., BERNADETT, D. W., MARKUS, M. J., ELSHOLZ, K. V., BERNADETT, D. W., MARKUS, M. J. & ELSHOLZ, K. V. (1997) Wind resource assessment handbook, AWS Scientific, Inc. & the Utility Wind Resource Assessment Program.

BARRY, R. G. & CHORLEY, R. J. (1998) *Atmosphere, weather & climate,* London Routledge, Seventh edition.

BEAUCAGE, P., GLAZER, A., CHOISNARD, J., YU, W., BERNIER, M., BENOIT, R. & LAFRANCE, G. (2007) Wind assessment in a coastal environment using synthetic aperture radar satellite imagery and a

numerical weather prediction model. *Canadian Journal of Remote Sensing,* 33**,** 368-377.

BELJAARS, A. C. M. (1994) The parameterization of surface fluxes in large-scale models under free convection. *Quarterly Journal of the Royal Meteorological Society,* 121**,** 255–270.

BETTS, A. K. (1986) A new convective adjustment scheme. Part I: Observational and theoretical basis. *Quarterly Journal of the Royal Meteorological Society*, 112, 677-691.

BETTS, A. K. & MILLER, M. J. (1986) A new convective adjustment scheme. Part II: Single column tests using GATE wave, BOMEX, and arctic air-mass data sets. *Quarterly Journal of the Royal Meteorological Society*, 112, 693-709.

BETZ, A. (1966) *Introduction to the theory of flow machines. (D. G. Randall, Trans.),* Oxford, Pergamon Press.

British Wind Energy Association (BWEA) (2000) Noise from wind turbines - the facts, viewed 6 May 2007, <http://www.bwea.com/index.html>.

BURTON, T., SHARPE, D., JENKINS, N. & BOSSANYI, E. (2001) *wind energy handbook,* WEST SUSSEX , England, John WILEY and sons.

CAVALERI, L. & BERTOTTI, L. (2006) The improvement of modelled wind and wave fields with increasing resolution. *Ocean Engineering,* 33**,** 553–565.

CHAPO, R. (2007) The massive Tehachapi wind farm, Article Alley, viewed 12 May 2009, <http://www.articlealley.com/article_124314_22.html>.

CHEN, F. & AVISSAR, R. (1994) The impact of land-surface wetness on mesoscale heat fluxes. *Journal of Applied Meteorology,* 33**,** 1324–1340.

CHEN, F. & DUDHIA, J. (2001a) Coupling an advanced land surface–hydrology model with the Penn State–NCAR MM5 Modeling System. Part I: Model Implementation and Sensitivity. *Monthly Weather Review,* 129**,** 569–585.

CHEN, F. & DUDHIA, J. (2001b) Coupling an advanced land surface–hydrology model with the Penn State–NCAR MM5 Modelling System. Part II: Preliminary Model Validation. *Monthly Weather Review,* 129**,** 587–604.

CHRISTIANSEN, M. B. (2006) Wind energy applications of synthetic Aperture Radar *Wind Energy Department.* Copenhagen, University of Copenhagen.

CHUN, S. (2006) Wind energy in Libya: Combining education, experience and a Pilot Project to Develop a New Market. *Refocus (Renewable Energy Focus),* 7**,** 44-45.

CONTE, A., PAVONE, A. & RATTO, C. F. (1998) Numerical evaluation of the wind energy resource of Liguria. *Journal of Wind Engineering and Industrial Aerodynamics,* 74-76**,** 355-364.

COPPIN, P. A., AYOTTE, K. A. & STEGGEL, N. (2003) Wind resource assessment in Australia – a planners guide. Australia, CSIRO Wind Energy Research Unit.

CRANK, J. N., P. (1947), "A practical method for numerical evaluation of solutions of particial differential equations of the heat conduction type", Proceedings of the Cambridge Philosophical Society 43: 50–50-67.

CRITCHFIELD, H. J. (1983) *Global climatology,* US, Prentice-Hall, Inc., Englewood Cliffs, Fourth edition.

CZISCH, G. & ERNST, B. (2001) High wind power penetration by the systematic use of smoothing effects within huge catchment areas shown in a European example. *Wind Power 2001* Washington, the American Wind Energy Association.

Danish Wind Industry Association (DWIA) (2003) Danish Wind Industry Association website, viewed 1 April 2008, <http://www.windpower.org/en/core.htm>.

Department of Energy (DOE) (2009) Advantages and disadvantages of wind energy, *Energy Efficiency and Renewable Energy,* viewed 18 July 2009, <http://www1.eere.energy.gov/windandhydro/wind_ad.html>.

DODGE, D. M. (2001) *Illustrated history of wind power development*, TelosNet.

DUDHIA, J. (1989) Numerical study of convection observed during the winter monsoon experiment using a mesoscale two-dimensional model. *Journal of the Atmospheric Sciences,* 46**,** 3077–3107.

DURAK, M. & SEN, Z. (2002) Wind power potential in Turkey and Akhisar case study. *Renew Energy,* 25**,** 463–72.

EL-OSTA, W., BELHAG, M., KLAT, M., FALLAH, I. & KALIFA, Y. (1995) Wind farm pilot project in Libya. *Renewable Energy,* 6**,** 639-642.

EL-OSTA, W. & KALIFA, Y. (2003) Prospects of wind power plants in Libya: a case study. *Renewable Energy,* 28, 363–371.

ELAMOURIA, M. & AMARA, F. B. (2008) Wind energy potential in Tunisia. *Renewable Energy,* 33, 758–768.

Energy Information Administration (EIA) (2009a) Libya energy data, statistics and analysis - oil, gas, electricity, coal. *Country Analysis Briefs.* U.S, Energy Information Administration, viewed 7 July 2009, <http://www.eia.doe.gov/>.

Energy Information Administration (EIA) (2009b) Libya energy profile. *Energy Data Series* US, Energy Information Administration, viewed 7 July 2009, <http://www.eia.doe.gov/>.

Energy Information Administration (EIA) (2009c) Short-term energy outlook. *Official Energy Statistics from the US Government, forecasts & analyses,* viewed 7 July 2009, <*http://www.eia.doe.gov/*>.

FERRIER, B. S., LIN, Y., BLACK, T., ROGERS, E. & DIMEGO, G. (2002) Implementation of a new grid-scale cloud and precipitation scheme in the NCEP Eta model, Preprints. *15th Conference on Numerical Weather Prediction.* San Antonio, TX, American Meteor Society, 280-283.

FINARDI, S., TINARELLI, G., FAGGIAN, P. & BRUSASCA, G. (1998) Evaluation of different wind field modeling techniques for wind energy applications over complex topography. *Journal of Wind Engineering and Industrial Aerodynamics,* 74-76**,** 283-294.

FRANDSEN, S. & CHRISTENSEN, C. J. (1992) Accuracy of estimation of energy production from wind power plants. *Wind Energy,* 16**,** 257–267.

GARRATT, J. R. (2004) *the Atmospheric Boundary Layer*, Cambridge University Press, Cambridge.

GASCH, R. & TWELE, J. (2002) *Wind power plants: fundamentals, design, construction and operation,* Berlin, Solarpraxis AG German in association with James & James (Science Publisher) Ltd, UK.

GIPE, P. (2004) *Wind power: renewable energy for home, farm, and business,* Vermont, United States, Chelsea Green Publishing Company, White River Junction, Vermont.

HALTINER, G. J. & WILLIAMS, R. T. (1980) *Numerical prediction and dynamic meteorology,* New York, John Willy & Sons. Second Edition.

HANITSCH, R. & SHATA, A. S. A. (2008) Electricity generation, and wind potential assessment at Hurghada, Egypt. *Renewable Energy,* 33 141–148.

HARTMANN, D. L. (1994) *Global physical climatology,* Washington, Academic Press.

HEIDORN, K. C. (1998) Weather phenomenon and elements*,* the weather doctor, viewed 3 February 2008, *<http://www.islandnet.com/~see/weather/elements/seabrz.htm>.*

HEPBASLI, A. & OZGENER, O. (2004) A review on the development of wind energy in Turkey. *Renewable and Sustainable Energy Reviews,* 8, 257–276.

HERBERTA, G. M. J., INIYANB, S., SREEVALSANC, E. & RAJAPANDIAND, S. (2007) A review of wind energy technologies. *Renewable and Sustainable Energy Reviews,* 11**,** 1117–1145.

HIMRI, Y., REHMAN, S., DRAOUI, B. & HIMRI, S. (2008) Wind power potential assessment for three locations in Algeria. *Renewable and Sustainable Energy Reviews,* 12, 2495-2504.

HOLTON, J. R. (1992) *An introduction to dynamic meteorology,* Third edition, Washington, Academic Press, INC.

HOOGWIJKA, M., VRIESB, B. D. & TURKENBURG, W. (2004) Assessment of the global and regional geographical, technical, and economic potential of onshore wind energy. *Energy Economics,* 26, 889– 919.

HUANG, X., MA, Y. & MILLS, G. (2008) Verification of mesoscale NWP forecasts of abrupt wind changes. Melbourne, Australia, A partnership between the Centre for Australian Weather and Climate Research and the Bureau of Meteorology.

HUBBERT, M. K. (1971) The energy resources of the earth. *Scientific American,* 225**,** 60–84.

Idaho National Laboratory (INL) (2008), Idaho National Laboratory website, viewed 9 June 2008, <http://www.inl.gov/wind/software/>.

IRWIN, J. S. (1978) A theoretical variation of the wind profile power-law exponent as a function of surface roughness and stability. *Atmospheric Environment,* 13**,** 191-194.

JACOBSON, M. Z. (1999) *Fundamentals of Atmospheric Modeling,* Cambridge, UK, Cambridge University Press.

JACOBSON, M. Z. & MASTERS, G. M. (2001) Exploiting wind versus coal. *Science,* 293**,** 1438.

JANJIC, Z. I. (1984) Non–linear advection schemes and energy cascade on semi–staggered grids. *Monthly Weather Review,* 112**,** 1234–1245.

JANJIC, Z. I. (1990) The step-mountain coordinate: physical package *Monthly Weather Review,* 118**,** 1429-1443.

JANJIC, Z. I. (1994) The step–mountain eta coordinate model: further developments of the convection, viscous sublayer and turbulence closure schemes. *Monthly Weather Review,* 122**,** 927–945.

JANJIC, Z. I. (1996a) The Mellor-Yamada level 2.5 scheme in the NCEP Eta Model *Eleventh Conference on Numerical Weather Prediction.* Norfolk, VA,19-23 August 1996, American Meteorological Society, Boston, MA, 333-334.

JANJIC, Z. I. (1996b) The surface layer in the NCEP Eta model. *Eleventh Conference on Numerical Weather Prediction.* Norfolk, VA, American Meteorological Society, 354–355.

JANJIC, Z. I. (2000) Comments on "Development and evaluation of a convection scheme for use in climate models." *Journal of the Atmospheric Sciences,* 57**,** 3686.

JANJIC, Z. I. (2002) Nonsingular implementation of the Mellor-Yamada Level 2.5 scheme in the NCEP Meso model, NCEP Office Note No. 437.

JANJIC, Z. I. (2003) A nonhydrostatic model based on a new approach. *Meteorology and Atmospheric Physics,* 82**,** 271–285.

JANJIC, Z. I., BLACK, T., PYLE, M., CHUANG, H. Y., ROGERS, E. & DIMEGO, G. (2005) High resolution applications of the WRF NMM. *21st Conference on Weather Analysis and Forecasting/17th Conference on Numerical weather Prediction.* Washington DC, American Meteorological Society.

JANJIC, Z. I., BLACK, T. L., ROGERS, E., CHUANG, H. & DIMEGO, G. (2003) The NCEP Nonhydrostatic meso model and first experiences with its applications. *Geophysical Research Abstracts,* 5**,** 04653.

JANJIC, Z. I., GERRITY, J. P. & NICKOVIC, S. (2001) An alternative approach to nonhydrostatic modeling. *Monthly Weather Review,* 129**,** 1164-1178.

JANJIC, Z. I. & PYLE, M. (2009) the WRF NMM Core. National Centers for Environmental Prediction, viewed 3 March 2009, <http://www.mmm.ucar.edu/wrf/users/tutorial/200907/Basic/NMM_Dynamics_jul2009_sent.pdf>.

KARSLI, V. M. & GECIT, C. (2003) An investigation on wind power potential of Nurdag- Gaziantep, Turkey. *Renewable Energy,* 28**,** 823–830.

KRISHNAMURTI, T. N. & BOUNOUA, L. (1996) *An introduction to numerical weather prediction techniques* Florida, CRC Press.

LACKNER, M. A. (2008) The streamlined site assessment methodology: a new approach for wind energy site assessment. ProQuest LLC.

LANDBERG, L., GIEBEL, G., NIELSEN, H. A., NIELSEN, T. & MADSEN, H. (2003a) Short-term prediction—an overview. *Wind Energ,* 6**,** 273–280.

LANDBERG, L., MYLLERUP, L., RATHMANN, O., PETERSEN, E. L., JØRGENSEN, B. H., BADGER, J. & MORTENSEN, N. G. (2003b) Wind resource estimation—an overview. *Wind energy,* 6**,** 261–271.

LAPRISE, R. (1992) The Euler equations of motion with hydrostatic pressure as an independent variable. *Monthly Weather Review,* 120**,** 197–207.

LAYTON, J. (2008) How wind power works, viewed 4 April 2008, *<http://science.howstuffworks.com/wind-power2.htm>.*

LOGAN, J. & KAPLAN, S. M. (2008) Wind power in the United States: Technology, economic, and policy issues. *CRS Report for Congress.* Energy Policy Resources, Science, and Industry Division.

LYNCH, P. (2006) *The emergence of numerical weather prediction: Richardson's dream.* Cambridge, United Kingdom, Cambridge University Press.

LYONS, T. J. & BELL, M. J. (1990) Mesoscale variations in available wind power potential. *Solar Energy,* 45, 149-166.

MARCOS, M. & TSIMPLIS, M. N. (2008) Comparison of results of AOGCMs in the Mediterranean Sea during the 21st century. *Journal of Geophysical Research,* 113.

MATHEW, S. (2006) *Wind energy: fundamentals, resource analysis and economics,* Berline, Springer-Verlag.

MAURIZI, A., PALMA, J. M. L. M. & CASTRO, F. A. (1998) Numerical simulation of the atmospheric flow in a mountainous region of the North of Portugal. *Journal of Wind Engineering and Industrial Aerodynamics,* 74-76**,** 219-228.

MCQUEEN, D. & WATSON, S. (2006) Validation of wind speed prediction methods at offshore sites. *Wind Energy,* 9**,** 75–85.

MELLOR, G. L. & YAMADA, T. (1982) Development of a turbulence closure model for geophysical fluid problems. *Reviews of Geophysics and Space Physics,* 20**,** 851-875.

MESINGER, F. & BLACK, T. L. (1992) On the impact of forecast accuracy of the stepmountain (eta) vs. sigma coordinate. *Meteorology and Atmospheric Physics,* 50**,** 47-50.

MIGLIETTA, M. M. & ROTUNNED, R. (2009) Numerical simulations of conditionally unstable flows over a mountain ridge. *Journal of the Atmospheric Sciences,* 66**,** 1865-1885.

MILLER, S. (2002) New England weather primer. Durham, New Hampshire, the National Oceanic and Atmospheric Administration, the University of New Hampshire, and Plymouth State College, viewed 10 October 2007,<http://ccrc.unh.edu/>.

MLAWER, E. J., TAUBMAN, S. J., BROWN, P. D., IACONO, M. J. & CLOUGH, S. A. (1997) Radiative transfer for inhomogeneous atmosphere: RRTM, a validated correlated-k model for the longwave *Journal of Geophysical Research,* 102, 16663–16682.

MONIN, A. S. & OBUKHOV, A. M. (1954) Basic laws of turbulent mixing in the surface layer of the atmosphere (in Russian). *Contributions of the Geophysical Institute of the Academy of Sciences,* 151**,** 163-187.

NAPPO, C. J. (2002) *An Introduction to atmospheric gravity waves* London, Academic Press, 85.

NAPPO, C. J. & CHIMONAS, G. (1992) Wave exchange between the ground surface and a boundary-layer critical level. *Journal of the Atmospheric Sciences,* 49**,** 1075–1091.

NFAOUI, H., BURET, J. & SAYIGH, A. A. M. (1998) Wind characteristics and wind energy potential in Morocco. *Solar Energy,* 63**,** 51–60.

Non-hydrostatic Mesoscale Model dynamic core of the Weather Research and Forecasting system (WRF-NMM) (2009) The Non-hydrostatic Mesoscale Model dynamic core of the Weather Research and Forecasting system Users Webpage. <*http://www.dtcenter.org/wrf-nmm/users/*>.

OMER, A. M. (2008) On the wind energy resources of Sudan. *Renewable and Sustainable Energy Reviews,* 12, 2117–2139.

OUTHRED, H. (2003) Wind energy and the national electricity market with particular reference to South Australia. *A report for the Australian Greenhouse Office.*

OZERDEM, B. & TURKELI, M. (2003) An investigation of wind characteristics on the campus of Izmir Institute of Technology, Turkey. *Renewable Energy, 28*, 1013–1027.

PASHARDES, S. & CHRISTOFIDES, C. (1995) Statistical analysis of wind speed and direction in Cyprus. *Solar Energy,* 55**,** 405-414.

PATEL, M. R. (1999) *Wind and solar power system,* United States, CRC Press LLC.

Partnership for Renewables (2008) Capacity factor, viewed 13 November 2008, <http://www.pfr.co.uk/pfr>.

PETERSEN, E. L., MORTENSEN, N. G., LANDBERG, L., HOJSTRUP, J. & FRANK, H. P. (1997) Wind power meteorology. Roskilde, Denmark, Riso National Laboratory.

REHMAN, S. & AL-ABBADI, N. M. (2005) Wind shear coefficients and their effect on energy production. *Energy Conversion and Management,* 46, 2578–2591.

RICHARDSON, L. F. (1922) *Weather prediction by numerical process,* Cambridge, Cambridge Univ. Press.

SASHEGYI, K. D. & MADALA, R. V. (1994) Initial conditions and boundary conditions. IN PIELKE, R. A. & PEARCE, R. P. (Eds.) *Mesoscale Modelling of The Atmosphere.* Boston, the American Meteorological Society.

SHATA, A. S. A. & HANITSCH, R. (2006a) Evaluation of wind energy potential and electricity generation on the coast of Mediterranean Sea in Egypt. *Renewable Energy,* 31, 1183–1202.

SHATA, A. S. A. & HANITSCH, R. (2006b) The potential of electricity generation on the east coast of Red Sea in Egypt. *Renewable Energy,* 31, 1597–1615.

SILBERMAN, I. (1954) planetary waves in the atmosphere. *Journal of Meteorology,* 11, 27–34.

SIMMONS, A. J. & BURRIDGE, D. M. (1981) An energy and angular-momentum conserving vertical finite-difference scheme and hybrid vertical coordinates. *Monthly Weather Review,* 109, 758.

SIMPSON, J. E. (1994) *Sea breeze and local winds,* United Kingdom, Cambridge University Press.

SKAMAROCK, W. C., KLEMP, J. B., DUDHIA, J., GILL, D. O., BARKER, D. M., DUDA, M. G., HUANG, X.-Y., WANG, W. & POWERS, J. G. (2008) A description of the advanced research WRF version 3. *NCAR technical notes.* Mesoscale and Microscale Meteorology Division National Center for Atmospheric Research Boulder, Colorado, USA.

SORBJAN, Z. (1989) *Structure of the atmospheric boundary layer,* New Jersey, Prentice Hall.

STEPHENS, G. L. (1978) Radiation profiles in extended water clouds. Part II: parameterization schemes. *Journal of the Atmospheric Sciences,* 35, 2123-2132.

ULIASZ, M. (1994) Subgrid-scale parameterizations. IN PIELKE, R. A. & PEARCE, R. P. (Eds.) *Mesoscale Modelling of the Atmosphere.* Boston, the American Meteorological Society, 25.

Verve Energy (2006) Albany wind farm. *Sustainable Energy* Western Australia, Verve Energy, viewed 15 September 2008, <http://www.verveenergy.com.au/index.html>.

Vestas (2008) Vestas website, viewed 12 January 2008, <http://www.vestas.com/>.

VOGIATZIS, N., SPANOMITSIOS, K. K. S. & STOUKIDES, M. (2004) Analysis of wind potential and characteristics in North Aegean, Greece. *Renewable Energy,* 29, 1193–1208.

World Wind Energy Association (2009) World wind energy report 2008. Bonn,Germany, <http://www.wwindea.org/home/images/stories/worldwindenergyreport2008_s.pdf>.

ZILITINKEVICH, S. S. (1995) Non-local turbulent transport: pollution dispersion aspects of coherent structure of convective flows. In: Air pollution III - Volume I. Air pollution theory and simulation (Eds. H. Power, N. Moussiopoulos and C.A. Brebbia). Computational Mechanics Publications, Southampton Boston, 53-60.